Stefan Weigl *Editor*

Breath Analysis

An Approach for Smart Diagnostics

Springer

4
Bioanalytical Reviews

Series Editors

Frank-Michael Matysik, Institute of Analytical Chemistry, University of Regensburg, Regensburg, Germany

Joachim Wegener, Department of Chemistry, University of Regensburg, Regensburg, Germany

Bioanalytical Reviews is the successor of the former review journal with the same name, and it complements Springer's successful and reputed review book series program in the flourishing and exciting area of the Bioanalytical Sciences.

Bioanalytical Reviews (BAR) publishes reviews covering all aspects of bioanalytical sciences. It therefore is a unique source of quick and authoritative information for anybody using bioanalytical methods in areas such as medicine, biology, biochemistry, genetics, pharmacology, biotechnology, and the like.

Reviews of methods include all modern tools applied, including mass spectrometry, HPLC (in its various forms), capillary electrophoresis, biosensors, bioelectroanalysis, fluorescence, IR/Raman, and other optical spectroscopies, NMR radiometry, and methods related to bioimaging. In particular the series volumes provide reviews on perspective new instrumental approaches as they apply to bioanalysis, and on the use of micro-/nano-materials such as micro- and nanoparticles. Articles on μ-total analytical systems (μ-TAS) and on labs-on-a-chip also fall into this category.

In terms of applications, reviews on novel bioanalytical methods based on the use of enzymes, DNAzymes, antibodies, cell slices, to mention the more typical ones, are highly welcome. Articles on subjects related to the areas including genomics, proteomics, metabolomics, high-throughput screening, but also bioinformatics and statistics as they relate to bioanalytical methods are of course also welcome. Reviews cover both fundamental aspects and practical applications.

Reviews published in BAR are (a) of wider scope and authoratively written (rather than a record of the research of single authors), (b) critical, but balanced and unbiased; (c) timely, with the latest references. BAR does not publish (a) reviews describing established methods of bioanalysis; (b) reviews that lack wider scope, (c) reviews of mainly theoretical nature.

Stefan Weigl

Editor

Breath Analysis

An Approach for Smart Diagnostics

With contributions by

R. Abozaid · M. Aufderhaar · M. Cánovas Díaz ·
T. de Diego Puente · J. Gallego-Jara · M. Hlavatsch ·
S. Karan · S. Klingler · G. Lozano-Terol · A. Meister ·
B. Mizaikoff · M. Müller · R. Myers · K. Nandigam ·
G. Nosovitskiy · P. Nosovitskiy · J. Pangerl · T. Rück ·
D. M. Ruszkiewicz · R. A. Sola-Martínez · P. Sukul ·
P. Trefz · S. Weigl

Springer

Editor
Stefan Weigl
Ostbayerische Technische Hochschule
Regensburg
Regensburg, Germany

I dedicate this book to Prof. Dr. Rudolf Bierl and Prof. Dr. Frank-Michael Matysik. Thank you for your trust, the instructive discussions and your support, not only on my academic path.

Preface

It is the first thing we do upon arrival in this world, the last thing when it is time to leave and just like a person's heartbeat, it is a sign of life—breathing.

But breathing is more than simply the process of moving air in and out of the lungs. Without breathing, we would not be able to speak or even to laugh. Therefore, without the ability to breath, we would be deprived of the expression of many of our emotions. Moreover, breath exhale provides a mirror to the biochemical processes, occurring not only in the lungs but in the whole body, thanks to the gas exchange between lungs and blood taking place at the alveoli. It is therefore not surprising that, since ancient times, analysing breath is a popular diagnostic tool for systemic disorders and diseases.

There is evidence that already the ancient Greeks and the Chinese people analysed breath. Within the fifth and fourth century BC, the period of Hippocrates, breath odour was used to diagnose kidney failure, lung abscess, diabetic ketoacidosis, liver disease and halitosis in Greece. One milestone of breath analysis was reached in 1780, when Antoine Laurent Lavoisier, accompanied by Pièrre Simon de Laplace and Armand Séguin, was able to describe the metabolism of a guinea pig, discovering the metabolization of oxygen to carbon dioxide under the emission of heat. Lavoisier's pioneering work in this field also included the first attempt to describe the human respiratory gas metabolism, thus making an important contribution to the development of respiratory physiology. At the beginning of the nineteenth century, it was A. Nebelthau who invented one of the first colorimetric breath tests. With his test, he was able to detect breath acetone of people suffering from Diabetes Mellitus. In 1874, Francis Edmund Anstie, a British doctor, used an acidic chrome solution changing its colour from red-brown to green upon contact with ethanol, representing the first alcohol breath test. About one century later, in the 1970s, the age of modern breath analysis was heralded by the studies of Linus Pauling. Using gas-liquid partition chromatography, he was able to quantitatively determine about 250 different substances in human breath exhale.

Within the last decades, highly sensitive and selective offline and real-time mass spectrometry emerged and opened new opportunities. Research was mainly focusing

on the discovery of biomarkers, which could be used for early detection of diseases. However, until now, except for nitrogen monoxide, which is an approved biomarker for asthma, no "magic" biomarker or breath print has been discovered. Besides, many resources have been invested in the development of point-of-care devices for potential biomarkers but breath analysis is still failing to proceed from bench to bed and become part of the everyday diagnostic routine in clinics or doctoral offices.

This book therefore addresses the mistakes that have been made in the past and offers answers on how to take breath analysis to the next level. Besides, real-time and offline analysis methods based on spectrometers as well as reviews about different sensing approaches for targeted point-of-care devices are presented. Moreover, this book discusses pulmonary function analysis and its role in modern breath analysis.

The first chapter deals with the physio-metabolic monitoring of breath exhale using real-time mass spectrometry. It describes the complexity of breath analysis since many factors can easily change the composition of breath including different respiratory patterns or rhythms as well as posture or exhaling flow rates. On the one hand, the chapter deals with the challenges and pitfalls coming along with current breath analysis research, but on the other hand highlights its importance and potentials for modern diagnostics.

Within the second chapter, offline breath analysis using gas chromatography coupled with mass spectrometry and the role of standardization of breath sampling as well as data analysis are discussed. Furthermore, the chapter addresses innovative algorithms and how they improve the analytical performance of the measurement device.

In the third chapter, gas chromatography coupled with ion mobility spectrometry for the detection of volatile breath compounds in clinical and emergency settings is presented. It focuses on the potentials of this real-time measurement technique for rapid testing, diagnosis and biomarker discovery. In addition, it addresses the remaining limitations in current applications and how to meet remaining challenges.

The fourth chapter is concerned with the applicability of optical sensing strategies in the infra-red region. Different measurement methods and current applications are reviewed providing an overview on the fundamental principles and recent developments in this emerging field.

The applicability of photoacoustic spectroscopy is addressed in the fifth chapter of this book. The measurement principle is described in detail highlighting the potentials and pitfalls. Besides, the application of innovative algorithms is discussed to employ this technology in complex measurement matrices like breath. Finally, recent applications of photoacoustic spectroscopy in breath analysis are reviewed within the chapter.

Within the sixth chapter of this book, sensor-array-based devices for breath analysis are discussed, highlighting electronic noses. The chapter includes material design advances, material selections and innovative sensor structures. Besides, a discussion of parametric resonance and excitation applied to sensor-based breath analysis devices is presented. An analysis of a review on the development of carbon nanomaterials concludes the chapter by discussing the current challenges related to

sensor array devices, machine-learning algorithms and the application of breath analysis.

The final chapter of the book addresses modern pulmonary function diagnosis highlighting its importance for reliable breath analysis. The techniques described include spirometry, body plethysmography and a variety of other common tests used to assess a patient's respiratory status. Furthermore, the chapter deals with blood gas analysis, capnometry and capnovolumetry and the analysis of nitrogen oxide in human breath exhale for asthma detection.

Although this book covers many aspects of breath analysis, it is not all-encompassing since this would go far beyond the scope of this book. However, it provides a good overview and addresses the most important aspects of modern breath analysis including the advantages and disadvantages of offline and real-time mass spectrometers, the scopes and limits of targeted sensing approaches as well as the importance of pulmonary function diagnostics in the field of breath analysis. Besides, the challenges and pitfalls of breath analysis are addressed and potential solutions like improved standardizations and innovative algorithms are presented.

At this point, I would like to express my deepest gratitude to all authors and co-authors. Without your fine work, this book would not have been possible. I hope you all agree that this big effort and the long hours of work have been worthwhile. The book will be of interest not only for experts in the field but also to students and their teachers in various interdisciplinary research fields encompassed by modern breath analysis.

Regensburg, Germany   Stefan Weigl

Contents

Physio-Metabolic Monitoring via Breath Employing Real-Time Mass Spectrometry: Importance, Challenges, Potentials, and Pitfalls

Pritam Sukul and Phillip Trefz

Contents

Abstract   A tiny fraction of our breath contains trace volatile organics of various chemical classes. Due to their endogenous and/or exogenous origins, these volatiles can denominate many intrinsic and extrinsic effects. Exhaled volatile profiles are super dynamic in nature and their expressions may change from seconds to years. Exhaled volatile concentrations largely depend on normal or abnormal fluctuations in physiological and metabolic attributes. Minute or pronounced alterations in cardiorespiratory and other bronchopulmonary gas-exchange parameters due to simple changes in respiratory patterns, routes, and rhythms, posture, expiratory/inspiratory flow, and upper-airway resistance can immediately affect volatile

P. Sukul (✉) and P. Trefz
Rostock Medical Breath Research Analytics and Technologies (ROMBAT), Department of Anaesthesiology and Intensive Care, University Medicine Rostock, Rostock, Germany
e-mail: Pritam.Sukul@uni-rostock.de

profiles. Similarly, the subject's age, gender, sexual orientation, metabolic state or status, diet, nutrition, therapy, lifestyle habits and habitats, menstrual phases, contraception, pregnancy, menopause, as well as any acute or chronic condition and comorbidities may cause transient or long-lasting differences in breath compositions. Applications of real-time mass spectrometric techniques along with alveolar sampling enabled us to frame fast occurring and continuous changes under diverse physio-metabolic conditions. Physio-metabolic conditions affected breath components more pronouncedly than the differential expression proposed as disease biomarkers in the literature. Investigations of such regulating factors helped us to develop the present state of the art for clinical breath sampling and analysis. Besides, assessments of ventilation and hemodynamics driven changes in exhaled volatiles have depicted potential for physio-metabolic monitoring. Longitudinal personalized analysis of breath profiles may offer unconventional path toward pathophysiological and therapeutic monitoring.

Keywords Pathophysiology · Biomarkers · Breath analysis · Metabolism · Monitoring · Omics · Physiology · Sampling · Standardization · Volatile organic compounds (VOCs)

Abbreviations

COVID-19	Coronavirus disease 2019
FeNO	Fractioned exhaled nitric oxide
IMS	Ion mobility spectrometry
ppbV	Parts per billion by volume
pptV	Parts per trillion by volume
PTR-ToF-MS	Proton transfer reaction–time of flight–mass spectrometry
SARS-CoV-2	Severe acute respiratory distress syndrome – coronavirus 2
SESI-MS	Secondary electrospray ionization–mass spectrometry
SIFT-MS	Selected ion flow-tube–mass spectrometry
VOCs	Volatile organic compounds

1 Introduction

A very tiny fraction ($<1\%$) of our breath contains hundreds of volatile organic compounds (VOCs). These compounds belong to various substance classes and the tracible concentrations of most of these VOCs range between parts per billion and parts per trillion by volume (ppbV–pptV) levels [1]. Many of these volatiles are exogenous – meaning that those are accumulated from our habits, habitats, diet, lifestyle, therapy, etc. For instance, if we smoke a cigarette, we will exhale considerable amounts of acetonitrile and furan [2, 3]. Visiting a fuel station will source

benzene and toluene, whereas entry to a hospital may increase breath isopropanol and formaldehyde concentrations. If we drink orange juice, limonene will become abundant in our breath and a visit to the forest will do the same for alpha-pinene [4]. On the other hand, some other VOCs are potentially endogenous – meaning that those are produced within us via various physiological, metabolic, biochemical, systemic microbial, and/or pathophysiological processes at the cellular/organ levels [5, 6]. For example, acetone is known to originate from cellular and/or hepatic glycolysis and lipolysis [7]. Ammonia, dimethyl, and trimethylamine are linked to protein catabolism [8, 9]. Organosulfur such as dimethyl sulfide, methanethiol, and butanethiol are produced by anerobic methylation by the systemic microbiota of our lower gut [8, 10]. Nonetheless, some substances such as isopropanol, ethanol, acetic acid, acetaldehyde, and acrolein have mixed origins – means that they are sourced within and without. Irrespective of the origin (after being produced in vivo or being accumulated/stored from outside), all VOCs are transported via blood to our lungs, and thereafter, they are released during the bronchopulmonary gas-exchange process and thereby are found in breath. Therefore, profiling of these substances may offer non-invasive, rapid, repeatable, and beyond conventional insights into various systemic phenomena, events, or status [11].

While largely abundant breath gases, e.g., oxygen (O_2) and carbon dioxide (CO_2), are conventionally applied in human medicine for diagnosis and monitoring of certain conditions, nitric oxide (NO) is the only trace gas, which is vividly investigated for point-of-care (PoC) applicability [12–14]. As NO is produced within the proximal airways and inflammation facilitates its production, the fractioned exhaled NO (FeNO) is well attributed to allergic asthma [13, 15]. Nonetheless, the scenario is substantially different in case of other trace VOCs. Same substances were proposed in independent studies as biomarker for different diseases [15–17]. Despite many efforts to find, propose, or establish unique volatile (profiles or patterns) as disease- or event-specific biomarkers in different studies, none of those could pass the independent validation tests [18]. Consequently, the trace volatiles could not enter into routine clinical practice yet.

In fact, almost all the VOCs are present in everyone's breath, and if we simply measure or compare the exhaled compositions of diseased patients with that of an age- and gender-matched healthy cohort, it is very unlikely to come across any unique VOC profile or pattern [19, 20]. After decades of breath analysis, the focus has shifted toward the detection of changes in exhaled VOC concentrations rather than expecting a unique marker. Meanwhile, a series of systematic investigations of immediate, transient, and/or persistent physio-metabolic effects on VOC profiles (mainly from healthy human subjects) helped us to realize the extremely dynamic nature of breath volatiles [21–25]. Changes observed in these physio-metabolic studies turned out to be even more pronounced than those published as biomarkers for diagnosis (even for early detection!) in many cross-sectional (healthy vs. sick) studies. Real-time mapping of such dynamic nature under various conditions along with the available knowledge and fundamental understanding of human physiology, metabolism, and analytical chemistry are the indispensable prerequisites to eventually translate VOCs into clinical applications [5].

2   The Dynamic Nature of Exhaled VOCs

Exhaled VOC concentrations are affected via immediate or precedent extrinsic and intrinsic factors such as environment exposure, diet and lifestyle habits, healthy physiological (respiratory, hemodynamic) and metabolic attributes, systemic microbial activity, as well as any health condition and/or therapy [25–27]. Putative breath markers not only differ interindividually but also may change instantly or over time within the same individual. Even if we succeed to rule out and exclude various extrinsic factors and/or pathological effects, simple and daily life fluctuations in normal and healthy physiology (ventilation and hemodynamics) and/or metabolism may alter our VOC profiles significantly. Besides relying upon our physio-metabolic and health status, such changes and differences are also closely related to the potential origins, physicochemical characters, exhalation kinetics, and compartmental distributions of these VOCs. Thus, while thinking of the dynamic nature of the breath volatiles, a fundamental question does arise. How dynamic are these VOCs or how long does it take to change concentrations?

Well, the actual dynamic timeframe for VOC concentrations ranges from seconds to years.

VOC concentrations can change within seconds simply due to changes in our normal breathing patterns. For example, if we hold our breath for a few seconds, sudden and profound changes are observed after the breath holding phase [21, 28]. Such changes are substance specific and depend on the origin and physicochemical characters such as solubility, volatility, and blood-gas partition coefficients of the VOCs. Concentrations of substances with low aqueous solubility, e.g., isoprene, benzene, furan, and acetonitrile, will increase significantly due to perfusion-limited accumulation during breath holding. In contrast to that, compounds like acetone will remain almost constant due to high solubility – that will allow it to get absorbed within the surrounding lung tissue/compartments. On the other hand, oral microbiota-originated VOCs, e.g., hydrogen sulfide, will decrease via washout due to increased respiratory rate (physiological compensation) after breath holding. The physiological effects due to breath holding of 10–60 s by healthy adults are neutralized to baseline within 8–10 breaths.

VOC concentrations will change within minutes if we just switch our body positions [22]. For instance, if you are reading this book by sitting on a chair, and you suddenly switch to supine posture, your cardiac output and pulmonary perfusion will change immediately resulting in increased exhalation of isoprene and similar substances, whereas compounds like acetone and alike compounds will remain unaffected by hemodynamic effects.

VOC concentrations may reflect metabolic changes taking place within hours or throughout the day [29, 30]. If we continuously measure breath VOCs from early morning till evening, systemic changes will be observed on VOC exhalations. Intake of standard breakfast and lunch will cause systematic postprandial metabolic adaptation via hyperglycemia and corresponding oxidative stress, which will be reflected

in the time profiles of substances such as acetone, 2-propanol, pentanal, dimethyl sulfide, and isoprene.

Changes in VOC concentrations are reported to occur within days, weeks, and also throughout the month. While looking at the natural menstrual cycle in pre-menopausal adult women, exhaled VOC concentrations largely depend on different phases of the monthly endocrine regulation [31]. Endogenous substances such as ammonia, isoprene, acetone, and dimethyl sulfide closely mirror many well-known effects of the female sex hormones on various metabolic pathways [32–35]. Natural interplay between estrogen and progesterone levels at the period, follicular, ovulation, and luteal phases is reflected distinctly on VOC profiles. Such changes differed significantly in adults undertaking daily oral contraceptive pills (i.e., comprised of supplementary female sex hormones). Similarly, longitudinal changes in VOC concentrations take place throughout pregnancy [36, 37]. In pregnant women, various physio-metabolic effects such as gestational endocrine changes, embryonic development, fetal oxygen and nutrient demand-driven increase in cardiac output and respiratory rate, increased cholesterol biosynthesis, and altered breathing pattern via diaphragm upliftment and physiological hyperventilation cause progressive changes in VOC exhalations [37–40].

If we look into the healthy aging process, exhaled expressions of many endogenous and exogenous VOCs differ significantly, based on our biological age. Recent analysis of breath VOCs from a large cohort of healthy females aged between 7 and 80 years has depicted substance-specific changes in breath composition. Breath concentrations of endogenous aldehydes, alcohols, organosulfur, short-chain fatty acids, alkene, ketones, and exogenous nitriles, aromatics, and terpenes have indicated physio-metabolic milieu between endocrine homeostasis, oxidative stress, gut and pulmonary microbial diversity/activity, energy metabolism, and lifestyle habits [41–45].

Due to such dynamic nature, it is utterly critical to trace and translate the actual pathophysiological information from breath VOC expressions – as those are often overridden by the everlasting physio-metabolic effects. Continuous breath-resolved profiling of VOC concentrations under different physio-metabolic conditions may pave the path for framing the complex behavioral dynamics and exhalation kinetics of the potential VOC biomarkers in real time.

3 Mass Spectrometric Methods for Real-Time Breath Analysis

Despite the fact that gas-chromatography and mass spectrometry (GC-MS) has been applied for many years as the gold standard for trace gas analysis [46, 47] at low ppbV–pptV levels, punctual measurements could not provide the actual insight into the dynamic nature of breath VOCs. Further, unavoidable confounding factors related to offline mass spectrometry such as preconcentration steps, sample

collection (e.g., blowing into bags, mixed breath phases), sample storage time/ conditions, and analysis time remained as everlasting challenges. Inception of end-tidal CO_2 controlled manual or automated breath sampling in glass syringes or in micro-extraction-based traps (e.g., needle-trap microextraction) enabled researchers to collect the alveolar fractions of VOCs, which represents the actual systemic/blood concentrations [48, 49]. Nevertheless, fast occurring changes (within seconds or a minute) remained untraceable via offline MS methods.

Development and application of real-time MS techniques, e.g., selected ion flow-tube (SIFT)-MS, proton transfer reaction (PTR)-quadrupole-MS, and PTR-time of flight (ToF)-MS [50], along with online end-tidal/alveolar sampling have eventually overcome various confounding influences [51–53]. In principle, a SIFT and a PTR use alike ionization principles based on various primary/reagent ions such as hydronium (H_3O^+), NO^+, or O_2^+. Both of the instruments allow switching between reagent ions according to diverse analytical requirements. Given the fact that most of the breath VOCs belong to the relatively lower mass range (<500 Da) and have higher proton affinity than water, in the field of breath analysis, soft ionization via H_3O^+ ion is desirable to have minimal fragmentation [21, 23].

PTR-ToF-MS, H_3O^+ ions are produced via cathode discharge on pure (99.99%) water vapor. After production they are pulsed to the next chamber (drift tube) where the proton transfer reaction takes place. The breath sample is introduced to this chamber to react with H_3O^+ ions. Based on the proton affinity, VOCs react with H_3O^+ ions and get protonated (VOC + H_3O^+ → $VOCH^+$ + H_2O). After that, protonated VOCs are detected via a quadrupole-MS or a ToF-MS according to their mass/charge ratio. Introduction of a ToF allows us to achieve mass resolution of 1,000–4,500 m/Δm that can assign volatiles upon their measured mass and corresponding sum formula with high precision as well as enable isobaric separation of VOC masses [54–56]. Unlike GC-MS, no sample preparation, preconcentration steps, and storage are required. Application of constant inlet flows in side-stream mode (in order to avoid interference to the mainstream of breathing) can uniformly introduce samples to the drift tube and measure at high time resolution in milliseconds (ms). For instance, studies have demonstrated application of 200 ms in clinical environment to simultaneously measure rapid changes of VOC concentrations in the ambient air and in the exhaled breath of healthy subjects or ventilated patients [24, 57, 58]. Here, in every 200 ms a data point was recorded and, on each data point, all protonated VOCs were measured as per mass/charge ratio. Thus, the assignment of VOCs at the exhaled alveolar plateau is also possible in real time. Besides continuous measurements, assignment of inspiratory and end-tidal breath phases (via customized data processing algorithms) helps to date the alveolar fraction of VOCs in a breath-resolved manner [21, 54]. For instance, signal intensity of an endogenous and blood-borne VOC (e.g., acetone or isoprene – abundant in exhalation) can be used to denominate the expiratory and inspiratory phases of breath. Based on the area/mass range of interest, mass scale can be recalibrated in desired time intervals. For clinical breath studies, 21.0226 Th (H_3O^+-isotope), 29.9980 Th (NO^+), and 59.049 Th (protonated acetone) can be used for mass scale calibration because of their natural abundances in expired and inspired air [52].

Secondary electrospray ionization-mass spectrometry (SESI-MS) has enabled ambient ionization via nano-electrospray-driven positive (protonated) and negative (deprotonated) ions that collide with sample analytes within the gas phase [59]. Detection of relatively large, semi-volatile, and even nonvolatile molecules is plausible by integrating high-resolution mass spectrometers such as Orbitrap-MS [60]. Nevertheless, the identification of substances with higher molecular weights is extremely challenging – especially where internal standards are not available for such mass ranges [61]. SESI is at an early stage and offers vivid scope for further optimizations and advancements in order to bridge other downstream omics (e.g., metabolomics, proteomics, and lipidomics) with volatolomics and exhaled breathomics.

In contrast to real-time MS techniques for nontargeted screening of VOCs, simpler methods such as electronic noses (eNOSE) or differential ion mobility spectrometry (DMS/IMS) are suitable for targeted approaches [62]. Artificial olfaction is often conducted via chemical, nano-optical sensors as well as via customized laser-based spectroscopy methods. Despite chemical and nano-optical methods being relatively cheap, easy to use, adaptable (e.g., integration of certain gas sensing arrays as per analytical requirements), and PoC applicable [63], they suffer from many demerits. These methods do not allow an unequivocal substance identification due to limited selectivity and specificity but offer promising perspectives for PoC breath tests, once marker substances are defined. Susceptibility to matrix effects, e.g., humidity, temperature, and complex sample compositions, is also an important disadvantage for eNOSEs and IMS.

4 Physiological and Metabolic Effects on Breath Biomarkers

Soon as it was realized that "magic bullet" biomarkers may not exist and pursuing VOC concentration changes under various pathophysiological conditions is more important and realistic than looking for unique biomarkers, the research focus was imposed on framing the factors that are affecting VOC concentrations. Gradually it is realized that "we are our actual challenge/problem." Being human, our own physiology and metabolism affect our VOC profiles more critically than other external factors.

After being produced or stored in vivo, VOCs undergo various metabolic cascades (regulated by our enzyme systems at cellular, systemic microbial, and organ levels, e.g., liver, gut, and muscle) and larger hydrocarbons often break down into smaller molecules. Thereafter, VOCs are carried by blood and pass through other body compartments where they are distributed/redistributed further. For instance, lipophilic substances are absorbed within the fatty compartments [64]. The lung is our blood–gas interface and the alveolar gas-exchange process is largely denominated by pulmonary ventilation-perfusion (VQ) mechanism and the

distributions of blood flow and air in lung compartments. Consequently, VOC exchange is closely relying on the pulmonary ventilation/perfusion (V/Q) ratios, i.e., primarily regulated by cardiac output and minute ventilation [26, 65–67]. After being released in alveolar air, VOCs are further distributed/redistributed within alveolar compartments (due to collateral ventilation between fused alveoli), undergo dilution via airway dead space and substances (e.g., NO and acetone) originating from airway epithelium, and are taken up via extra-alveolar exchange [24, 67]. Mechanisms such as pre-alveolar absorption and post-alveolar revalorization are also playing a crucial role in VOC modifications. Therefore, it is important to achieve a steady state of physio-metabolic interplay, while reproducible breath samples can be collected under minimal and systematic influence from subject's own physiology and metabolism.

Minute muscle movements during sleep or vigorous muscle activity under exercise are well known to reflect physio-metabolic effects on breath VOC profiles in real time [68–71]. The anaerobic threshold under exhaustive exercise (e.g., by following step-wise and incremental ramp protocols) can be determined by means of VOC-based modeling of lactate threshold and ventilatory threshold. Besides the changes during movements, VOC profiles are also affected by normal physio-metabolic effects at rest.

In addition to the aforementioned effects from altered breathing patterns (e.g., breath holding) and/or posture, simple changes in breathing route during breath sampling can also cause substance-specific changes in breath composition at rest. For instance, if you are breathing in and out via mouth and suddenly (even unconsciously) switch to nasal breathing, immediate changes will take place in exhaled VOC concentrations [25]. Substances originating from the nasal cavity bacteria (e.g., methyl-propyl sulfide) will occur and substances originating from the oral cavity (e.g., H_2S and allyl-methyl sulfide) will immediately reduce in concentrations. Effects will be also seen on substances regulated by ventilation and hemodynamics. For example, switching from nasal to oral breathing will significantly reduce isoprene concentrations. Isoprene is negatively correlated to minute ventilation. Therefore, bypassing the nasal cavity dead space (i.e., 70–80 ml) will increase the minute ventilation at oral breathing and thereby will reduce isoprene exhalation.

Similarly, if we simply blow our breath into bags or canisters via small straws (i.e., <1 cm of diameter), the uncontrolled upper-airway resistance from the small breathing orifice will immediately affect our exhaled constituents [72, 73]. Reduction of the breathing mouthpiece diameter has shown substance-specific effects. Such effects depend largely on the breathing resistance-driven changes in respiratory and hemodynamic parameters [72]. Alveolar eliminations of VOCs with relatively higher volatility are increased due to airway resistance-driven negative intrathoracic pressure (at inspiration), which instantly alters the alveolar diffusion gradient and respiratory mechanics.

Spontaneously breathing human subjects (even if healthy) start to hyperventilate once they are asked to breath normally via a mouthpiece or mask [74]. Application of paced breathing (i.e., metronome-controlled via sound beats or via visual guide) can be used for breath sampling in order to keep subjects within the normal

respiratory rate of 10–14 breaths/min. Researchers observed that the intra- and interindividual ventilatory variations in exhaled VOCs increase significantly during paced breathing. On the other hand, switching between spontaneous and paced breathing causes immediate changes in exhaled concentration and variations of endogenous and blood-borne VOCs [75]. Such changes depended on minute ventilation and CO_2 exhalation. Any conscious and voluntary effort of breathing induces autonomic control and momentarily overwrites the natural automatic control of breathing by our respiratory center. Paced breathing, therefore, induces autonomic function that hampers the normal inspiratory:expiratory (I:E) ratio of ~1:2 and increases the minute ventilation. Switching to spontaneous breathing gradually resumes automatic control of breathing and thereby neutralizes the minute ventilation and associated ventilatory variations in CO_2 and VOC exhalations.

Moreover, simple changes in exhalation time and expiratory flow may cause profound effects on VOC exhalations [24, 76]. For instance, if we normally expire our expiratory reserve volume (i.e., maximum exhalation), substances like isoprene, furan, dimethyl sulfide, and allyl-methyl sulfide will increase immediately by mirroring the end-tidal CO_2 profile. This happens mainly due to the change in alveolar slope of exhalation and increased blood-gas contact time which facilitate collateral exchange of gases and VOCs (with low aqueous solubility) between the alveolar compartments [24]. On the other hand, if we perform a forced expiration, those VOCs will decrease instantly due to dilution effects, whereas other substances like acetone will increase significantly as the decelerating flow of exhalation may induce bronchial contribution of such VOC with aqueous miscibility and high blood-gas partition coefficient.

Alongside the above-described immediate and transient effects during sampling, long-term effects and differences due to subject's age, gender, sexual aerosol and orientation, menstrual cycle, pregnancy, menopause, and circadian metabolic rhythms are important attributes for comparison of VOC expressions between cohorts [5, 31, 77, 78]. Such factors increase the overall heterogenicity and randomness in breath data and call for more fundamental investigations to address physio-metabolic crosstalk with VOC exhalations. As physio-metabolic effects are everlasting and unavoidable during breath sampling, a basic understanding of those beyond analytical effects is extremely important for interpreting observations pragmatically.

Therefore, no matter how sophisticated and high end the analytical instrument we may use, if we cannot collect a standardized breath sample, the obvious physio-metabolic effects at the time of sampling may induce unsupervised effects that are sufficient to mislead our clinical interpretations. During the last decade, the importance of standardization of breath sampling came into focus and several taskforces were formed by the *International Association of Breath Research (IABR)* to address the relevant factors and state of the art for clinical breath sampling and analysis [20, 79]. The following section will briefly summarize the lessons learned during the efforts for standardization including the dos and don'ts.

5 Standardization of Real-Time Sampling for Breath Analysis

Around 20 years ago, alveolar sampling came into consideration in order to represent systemic/blood concentrations of VOCs. Thus, confounding effects from mixed-alveolar (i.e., including anatomical dead space of airways, trachea, and mouth/nasal cavity) sampling were minimized significantly reduced. Certainly, the case will be different if airways are of potential interest of a study – such as in obstructive and restrictive tracheobronchial conditions.

During the last 10 years, continuous real-time monitoring of VOCs under various breathing maneuvers at rest have enabled us to knock out the key factors that are essential to collect reproducible breath samples with minimal physio-metabolic influences. Reliable sampling at rest in consciously breathing humans should consider the following crucial aspects:

- *Avoid muscle movements:* During sampling, subjects should maintain relaxed body postures (e.g., sitting or supine) without having any unnecessary muscle movement [22]. These mainly include voluntary or unmindful movements of limbs and other body parts [68]. Even minute and/or involuntary muscle movements must be recorded for data interpretations.
- *Alveolar/end-tidal sampling:* As indicated earlier, if airways are not of the study interest, breath sampling must extract the alveolar phase of the breath [64, 80]. In case of continuous breath-resolved measurements, exhaled alveolar and inspiratory phases should be determined during data analysis for valid interpretations of systematic VOC concentrations.
- *Subjects breathing patterns*: Breathing pattern must remain as spontaneous, constant, and normal as possible during sampling [21]. That means parameters such as respiratory rate, minute ventilation, respiratory flow, and I:E ratio should remain constant throughout the sampling phase. Subjects should not perform prolonged (slow breathing with deeper inhalation and exhalation) or forced expiration or increased respiratory rate [24]. Unusual breathing pattern-driven physiological hyperventilation and cardiorespiratory fluctuations must be avoided to attain steady state of breathing. Prolongation of unusual respiratory rate-driven physiological hyper- and hypoventilation is well known to cause respiratory acidosis and alkalosis, which leads to change in plasma acid–base balance (pH) and affects VOC exhalation [81, 82].
- *Subject's posture*: A particular posture (e.g., sitting or lying on back) must be maintained in order to avoid effects from hemodynamic fluctuations and pulmonary distribution of ventilation and blood flow [22, 83]. If the breath from a sick patient is sampled while he or she was at supine position, during follow-up the same supine posture must be maintained (even if the patient is recovered and can sit on a chair) for valid comparisons of pathophysiological effects beyond normal physiological noise (i.e., posture-driven differences). This is also true for

cross-sectional comparisons between healthy vs. sick cohorts. Sampling should be executed at the same posture in both cohorts.

- *Subject's breathing route*: Either oral or nasal breathing must be maintained without any unconscious switching between both [25]. This is to avoid ventilatory fluctuations and dead space ventilation and to avoid sudden contributions from oral or nasal cavity flora.

- *Applied (instrumental/analytical) upper-airway resistance against breathing*: Any obstruction to the mainstream of breathing must be avoided. In order to overcome unsupervised upper-airway resistance-driven change in pulmonary diffusion gradients and respiratory mechanics, smaller breathing mouthpiece should not be used. The diameter of the breathing mouthpiece should range between 1.5 and 2.0 cm [72]. In case of unavoidable infection safety mandates (e.g., for SARS-CoV-2 and similarly contagious pathogens), mainstream viral/bacterial filters are applied to stop respiratory viral/bacterial transmission to room air [84]. In such cases, effects due to instrumental resistance must be accounted for while evaluating breath data.

- *Precedent effects from wearing face masks*: Researchers have demonstrated pronounced side effects of wearing medical face masks (e.g., COVID-19 protective surgical and FFP2 masks) on respiratory-hemodynamic parameters and exhaled VOC concentrations, at rest. Physiological effects from precedent mask wearing may cause significant hyperventilation (especially in older adults, aged >60 years) as a respiratory compensation process [85]. As such effects may last for minutes to hours based on subject's age and/or health condition, observed breath compositions must account for mask-related effects (where relevant). It is reasonable to allow such subjects to sit without mask for at least 15–30 min prior to breath sampling, in order to minimize precedent physiological effects.

- *Subject's ventilatory variations*: Respiratory rhythms must be meticulously controlled in order to sample breath with minimal ventilatory variations. A recent study has reported that if at least a minute of paced breathing is applied (with fixed respiratory rate of 10–12/min) and then switch to spontaneous breathing, ventilatory variations tend to reduce significantly and attain a steady state after the 2 min of spontaneous breathing and third minute is suitable for collecting/considering reproducible sample without physiological fluctuations [75].

Besides the above-indicated sampling conditions, analysis and interpretation of exhaled VOC markers should incorporate effects from acute ambient conditions and also due to long-term effects from subject's personal attributes. These are mainly associated with subject's age, gender, diet, habits, environment, and lifestyle [5]. Studies have proposed that application of fasting or certain standard diet prior to breath sampling may reduce effects from food intake [86–88]. Nevertheless, such pre-selection is far from the real-life situation and any screening scenario or nontargeted approach [89]. Furthermore, fasting may cause hypoglycemic adaptation and metabolic compensation effects that may induce inseparable effects onto the volatile metabolites [29, 90]. Therefore, it is rather reasonable to carefully consider the attributes from diet, lifestyle habits (e.g., smoking, drinking, nutrition

supplement, and oral contraception), therapy, acute or chronic condition/comorbidity, and living environment as questionnaires during recruitment and retrospectively account for any suspected effects. Most importantly, simultaneous measurements of VOC concentrations in the inspiratory ambient air are extremely important to rule out acute effects.

6 Applications and Potentials of Physio-Metabolic Monitoring in Breath Analysis

Despite the fact that breath research is still in its infancy, the above-mentioned knowhows reflect a steady development toward a state of the art for clinical breath sampling. Nevertheless, the list is rather exhaustive and a lot more effort and time toward standardization of unequivocal confounders related to breath analysis has to be invested.

In principle, a disease/pathophysiological condition is nothing but a disturbed physio-metabolic state. Exhaled VOC profiles may provide rapid information on in vivo physiological or metabolic processes as the time span between marker production and exhalation of VOCs is short. Available knowledge of physiology and metabolism must be translated into disease-driven pathophysiology, for realizing effects on breath compositions. Assessments of physio-metabolic interplay can bridge the gap between our analytical and clinical expertise. Therefore, real-time breathomics holds great promise toward non-invasive monitoring of physiology, metabolism, diseases, and therapy. Screening of a large number of population (e.g., at COVID-19 test center) is also feasible via real-time breathomics. Physio-metabolic and pathobiological effects induced by SARS-CoV-2 and other respiratory pathogens are well addressed in recent studies in hundreds of subjects [89]. Framing of systemic physio-metabolic effects also helped to optimize experimental setups and methods for safe breath analysis and patient monitoring under high safety conditions/mandated at this very time of the global pandemic [84].

As real-time breath analysis can rapidly deliver results directly at the point of care it is especially attractive for personalized monitoring in patients. No risk is imposed on the patient even if the analysis is done frequently or continuously. Physio-metabolic monitoring can be used to follow up substances that were administered to the patient, such as volatile or intravenous anesthetics [26, 47, 91]. Moreover, VOCs enabled continuous monitoring and immediate recognition of therapeutic efforts in intensive care unit patients [57, 58]. Individual monitoring of selected breath VOCs facilitates recognition of metabolic transition without any delay. These findings encourage more research with respect to therapeutic monitoring, longitudinal studies, and follow-up of patients. Besides there is large scope for metabolic monitoring of aging, related life events, and health conditions such as menopause, oxidative stress, endocrine changes, and energy homeostasis. Monitoring of VOC changes during menstrual cycle and pregnancy may reflect phases of healthy natural

cycles, gestation, or any complications based on continuous changes in exhalation profiles [31, 36]. Similarly, physio-metabolic monitoring is applicable to physical fitness tests, exercise training, and various applications in sports science/medicine [70]. Non-invasive assessment of anaerobic threshold, exercise capacity, combined diet, and isotopically labeled substrate interventions are of significant interest. As the putative endogenous origin of most of the VOCs is largely debatable/uncertain and a recent study has even disqualified the long-believed metabolic origin of the second most abundant VOC (i.e., isoprene) in our breath [36], physio-metabolic monitoring under labeled substrate intervention may offer unique insights into the downstream denominators of VOCs and thereby indicate the way to their true systemic sources.

7   Conclusions and Perspective

The dynamic nature of breath VOCs offers a complex but comprehensive spectrum of immediate, transient, and chronic aspects. As breath biomarkers may provide unique and immediate physio-metabolic information on the whole-body status, new insights into normal and pathological processes may be achieved. A fundamental understanding of substance's origins, physicochemical properties, and potential regulating factors such as physiology, metabolism, microbiome, nutrition, lifestyle, and pre-exposure is essential to perceive the VOC expressions case or individual wise. If such knowledge is integrated with state-of-the-art advances in sampling and analytical techniques, observed changes or difference in VOC concentrations may translate actual effects from pathobiological and clinical conditions.

Surprisingly, normal physiology and metabolism-driven changes and variations in VOC concentrations observed in follow-up measurements (where subjects were used as his or her own control) were more pronounced than those reported as unique biomarkers in many published cross-sectional studies. Therefore, cross-sectional comparisons between healthy and ill subjects, in relation to screening or early detection of diseases via breath analysis, are far from our current abilities. In perspective, longitudinal assessments of ventilation and hemodynamics driven changes in breath compositions have depicted excellent potential for physio-metabolic monitoring. Continuous and personalized analysis of breath profiles may serve as an unconventional window for monitoring disease progression and response to therapy that could become a cornerstone toward individualized medicine and therapy.

References

1. de Lacy CB, Amann A, Al-Kateb H, Flynn C, Filipiak W, Khalid T et al (2014) A review of the volatiles from the healthy human body. J Breath Res 8:014001

2. McKee HC, Rhoades JW, Campbell J, Gross AL (1962) Acetonitrile in body fluids related to smoking. Public Health Rep 77:553–554

3. Papaefstathiou E, Stylianou M, Andreou C, Agapiou A (2020) Breath analysis of smokers, non-smokers, and e-cigarette users. J Chromatogr B 1160:122349

4. Filipiak W, Ruzsanyi V, Mochalski P, Filipiak A, Bajtarevic A, Ager C et al (2012) Dependence of exhaled breath composition on exogenous factors, smoking habits and exposure to air pollutants. J Breath Res. [zitiert 29. January 2016];6. Verfügbar unter: http://www.ncbi.nlm.nih.gov/pmc/articles/PMC3863686/

5. Sukul P, Grzegorzewski S, Broderius C, Trefz P, Mittlmeier T, Fischer D-C et al (2022) Physiological and metabolic effects of healthy female aging on exhaled breath biomarkers. iScience 25:103739

6. Kai M, Haustein M, Molina F, Petri A, Scholz B, Piechulla B (2009) Bacterial volatiles and their action potential. Appl Microbiol Biotechnol 81:1001–1012

7. Kalapos MP (2003) On the mammalian acetone metabolism: from chemistry to clinical implications. Biochim Biophys Acta 1621:122–139

8. Pugliese G, Trefz P, Brock B, Schubert JK, Miekisch W (2019) Extending PTR based breath analysis to real-time monitoring of reactive volatile organic compounds. Anal R Soc Chem 144:7359–7367

9. Spacek LA, Strzepka A, Saha S, Kotula J, Gelb J, Guilmain S et al (2018) Repeated measures of blood and breath ammonia in response to control, moderate and high protein dose in healthy men. Sci Rep 8:2554

10. Tangerman A (2009) Measurement and biological significance of the volatile sulfur compounds hydrogen sulfide, methanethiol and dimethyl sulfide in various biological matrices. J Chromatogr B 877:3366–3377

11. Miekisch W, Schubert JK, Noeldge-Schomburg GFE (2004) Diagnostic potential of breath analysis – focus on volatile organic compounds. Clin Chim Acta 347:25–39

12. Alving K, Weitzberg E, Lundberg JM (1993) Increased amount of nitric oxide in exhaled air of asthmatics. Eur Respir J 6:1368–1370

13. Ricciardolo FLM, Sterk PJ, Gaston B, Folkerts G (2004) Nitric oxide in health and disease of the respiratory system. Physiol Rev 84:731–765

14. American Thoracic Society, European Respiratory Society (2005) ATS/ERS recommendations for standardized procedures for the online and offline measurement of exhaled lower respiratory nitric oxide and nasal nitric oxide. Am J Respir Crit Care Med 171:912–930

15. Barnes PJ, Dweik RA, Gelb AF, Gibson PG, George SC, Grasemann H et al (2010) Exhaled nitric oxide in pulmonary diseases: a comprehensive review. Chest 138:682–692

16. Nakhleh MK, Amal H, Jeries R, Broza YY, Aboud M, Gharra A et al (2017) Diagnosis and classification of 17 diseases from 1404 subjects via pattern analysis of exhaled molecules. ACS Nano 11:112–125

17. Amann A, Miekisch W, Schubert J, Buszewski B, Ligor T, Jezierski T et al (2014) Analysis of exhaled breath for disease detection. Annu Rev Anal Chem (Palo Alto, Calif) 7:455–482

18. Amann A, de Lacy Costello B, Miekisch W, Schubert J, Buszewski B, Pleil J et al (2014) The human volatilome: volatile organic compounds (VOCs) in exhaled breath, skin emanations, urine, feces and saliva. J Breath Res 8:034001

19. Miekisch W, Schubert JK, Vagts DA, Geiger K (2001) Analysis of volatile disease markers in blood. Clin Chem 47:1053–1060

20. Miekisch W, Herbig J, Schubert JK (2012) Data interpretation in breath biomarker research: pitfalls and directions. J Breath Res 6:036007

21. Sukul P, Trefz P, Schubert JK, Miekisch W (2014) Immediate effects of breath holding maneuvers onto composition of exhaled breath. J Breath Res 8:037102

22. Sukul P, Trefz P, Kamysek S, Schubert JK, Miekisch W (2015) Instant effects of changing body positions on compositions of exhaled breath. J Breath Res 9:047105

23. Trefz P, Schmidt M, Oertel P, Obermeier J, Brock B, Kamysek S et al (2013) Continuous real time breath gas monitoring in the clinical environment by proton-transfer-reaction-time-of-flight-mass spectrometry. Anal Chem 85:10321–10329

24. Sukul P, Schubert JK, Oertel P, Kamysek S, Taunk K, Trefz P et al (2016) FEV manoeuvre induced changes in breath VOC compositions: an unconventional view on lung function tests. Sci Rep 6:28029

25. Sukul P, Oertel P, Kamysek S, Trefz P (2017) Oral or nasal breathing? Real-time effects of switching sampling route onto exhaled VOC concentrations. J Breath Res 11:027101

26. Kamysek S, Fuchs P, Schwoebel H, Roesner JP, Kischkel S, Wolter K et al (2011) Drug detection in breath: effects of pulmonary blood flow and cardiac output on propofol exhalation. Anal Bioanal Chem 401:2093–2102

27. Trefz P, Kamysek S, Fuchs P, Sukul P, Schubert JK, Miekisch W (2017) Drug detection in breath: non-invasive assessment of illicit or pharmaceutical drugs. J Breath Res 11:024001

28. Lärstad MAE, Torén K, Bake B, Olin A-C (2007) Determination of ethane, pentane and isoprene in exhaled air – effects of breath-holding, flow rate and purified air. Acta Physiol (Oxf) 189:87–98

29. Trefz P, Schmidt SC, Sukul P, Schubert JK, Miekisch W, Fischer D-C (2019) Non-invasive assessment of metabolic adaptation in paediatric patients suffering from type 1 diabetes mellitus. J Clin Med. [zitiert 18. Juli 2020];8. Verfügbar unter: https://www.ncbi.nlm.nih.gov/pmc/articles/PMC6912469/

30. Fink H, Maihöfer T, Bender J, Schulat J (2022) Indole as a new tentative marker in exhaled breath for non-invasive blood glucose monitoring of diabetic subjects. J Breath Res 16

31. Sukul P, Schubert JK, Trefz P, Miekisch W (2018) Natural menstrual rhythm and oral contraception diversely affect exhaled breath compositions. Sci Rep 8:10838

32. Hawkins SM, Matzuk MM (2008) Menstrual cycle: basic biology. Ann N Y Acad Sci 1135:10–18

33. Mumford SL, Dasharathy S, Pollack AZ, Schisterman EF (2011) Variations in lipid levels according to menstrual cycle phase: clinical implications. Clin Lipidol 6:225–234

34. Wilcox AJ, Dunson D, Baird DD (2000) The timing of the "fertile window" in the menstrual cycle: day specific estimates from a prospective study. BMJ 321:1259–1262

35. National Institutes of Health (NIH) (2015) Women's cholesterol levels vary with phase of menstrual cycle. [zitiert 11. April 2018]. Verfügbar unter: https://www.nih.gov/news-events/news-releases/womens-cholesterol-levels-vary-phase-menstrual-cycle

36. Sukul P, Richter A, Schubert JK, Miekisch W (2021) Deficiency and absence of endogenous isoprene in adults, disqualified its putative origin. Heliyon 7:e05922

37. LoMauro A, Aliverti A (2015) Respiratory physiology of pregnancy. Breathe (Sheff) 11:297–301

38. Bartels Ä, O'Donoghue K (2011) Cholesterol in pregnancy: a review of knowns and unknowns. Obstet Med 4:147–151

39. Soma-Pillay P, Catherine N-P, Tolppanen H, Mebazaa A, Tolppanen H, Mebazaa A (2016) Physiological changes in pregnancy. Cardiovasc J Afr 27:89–94

40. Lain KY, Catalano PM (2007) Metabolic changes in pregnancy. Clin Obstet Gynecol 50:938–948

41. Ragonnaud E, Biragyn A (2021) Gut microbiota as the key controllers of "healthy" aging of elderly people. Immun Ageing 18:2

42. Bosco N, Noti M (2021) The aging gut microbiome and its impact on host immunity. Genes & Immunity Nature Publishing Group, pp 1–15

43. Pataky MW, Young WF, Nair KS (2021) Hormonal and metabolic changes of aging and the influence of lifestyle modifications. Mayo Clin Proc 96:788–814

44. Boss GR, Seegmiller JE (1981) Age-related physiological changes and their clinical significance. West J Med 135:434–440

45. Romano AD, Serviddio G, de Mattheis A, Bellanti F, Vendemiale G (2010) Oxidative stress and aging. J Nephrol 23(Suppl 15):S29–S36

46. Intercomparison of infrared cavity leak-out spectroscopy and gas chromatography-flame ioni-zation for trace analysis of ethane. Anal Chem. [zitiert 17. August 2022]. Verfügbar unter: https://pubs.acs.org/doi/10.1021/ac702282q

47. Miekisch W, Fuchs P, Kamysek S, Neumann C, Schubert JK (2008) Assessment of propofol concentrations in human breath and blood by means of HS-SPME-GC-MS. Clin Chim Acta 395:32–37

48. Miekisch W, Trefz P, Bergmann A, Schubert JK (2014) Microextraction techniques in breath biomarker analysis. Bioanalysis 6:1275–1291

49. Trefz P, Rösner L, Hein D, Schubert JK, Miekisch W (2013) Evaluation of needle trap micro-extraction and automatic alveolar sampling for point-of-care breath analysis. Anal Bioanal Chem 405:3105–3115

50. Smith D, Španěl P, Herbig J, Beauchamp J (2014) Mass spectrometry for real-time quantitative breath analysis. J Breath Res 8:027101

51. Smith D, Spanel P (2005) Selected ion flow tube mass spectrometry (SIFT-MS) for on-line trace gas analysis. Mass Spectrom Rev 24:661–700

52. Herbig J, Müller M, Schallhart S, Titzmann T, Graus M, Hansel A (2009) On-line breath analysis with PTR-TOF. J Breath Res 3:027004

53. Lindinger W, Hansel A, Jordan A (1998) On-line monitoring of volatile organic compounds at pptv levels by means of proton-transfer-reaction mass spectrometry (PTR-MS) medical appli-cations, food control and environmental research. Int J Mass Spectrom Ion Process 173:191–241

54. Schwoebel H, Schubert R, Sklorz M, Kischkel S, Zimmermann R, Schubert JK et al (2011) Phase-resolved real-time breath analysis during exercise by means of smart processing of PTR-MS data. Anal Bioanal Chem 401:2079–2091

55. Romano A, Hanna GB (2018) Identification and quantification of VOCs by proton transfer reaction time of flight mass spectrometry: an experimental workflow for the optimization of specificity, sensitivity, and accuracy. J Mass Spectrom 53:287–295

56. Pugliese G, Piel F, Trefz P, Sulzer P, Schubert JK, Miekisch W (2020) Effects of modular ion-funnel technology onto analysis of breath VOCs by means of real-time mass spectrometry. Anal Bioanal Chem 412:7131–7140

57. Löser B, Grabenschröer A, Pugliese G, Sukul P, Trefz P, Schubert JK et al (2020) Changes of exhaled volatile organic compounds in postoperative patients undergoing analgesic treatment: a prospective observational study. Metabolites 10:321

58. Brock B, Kamysek S, Silz J, Trefz P, Schubert JK, Miekisch W (2017) Monitoring of breath VOCs and electrical impedance tomography under pulmonary recruitment in mechanically ventilated patients. J Breath Res 11:016005

59. Singh KD, del Miguel GV, Gaugg MT, Ibañez AJ, Zenobi R, Kohler M et al (2018) Translating secondary electrospray ionization–high-resolution mass spectrometry to the clinical environ-ment. J Breath Res 12:027113

60. Osswald M, Kohlbrenner D, Nowak N, Spörri J, Sinues P, Nieman D et al (2021) Real-time monitoring of metabolism during exercise by exhaled breath. Metabolites 11:856

61. Singh KD, Tancev G, Decrue F, Usemann J, Appenzeller R, Barreiro P et al (2019) Standard-ization procedures for real-time breath analysis by secondary electrospray ionization high-resolution mass spectrometry. Anal Bioanal Chem 411:4883–4898

62. Pereira JAM, Porto-Figueira P, Taware R, Sukul P, Rapole S, Câmara JS (2020) Unravelling the potential of salivary volatile metabolites in oral diseases. Rev Mol 25:E3098

63. Wilson AD, Baietto M (2009) Applications and advances in electronic-nose technologies. Sensors (Basel) 9:5099–5148

64. Miekisch W, Kischkel S, Sawacki A, Liebau T, Mieth M, Schubert JK (2008) Impact of sampling procedures on the results of breath analysis. J Breath Res 2:026007

65. Lumb AB (2016) Nunn's Appl Respir Physiol 8. Aufl. Italy: Elsevier Ltd.; Verfügbar unter: https://www.eu.elsevierhealth.com/nunns-applied-respiratory-physiology-9780702062940.html?dmnum=12449#panel1

66. Anderson JC, Babb AL, Hlastala MP (2003) Modeling soluble gas exchange in the airways and alveoli. Ann Biomed Eng 31:1402–1422

67. Anderson JC, Hlastala MP (2007) Breath tests and airway gas exchange. Pulm Pharmacol Ther 20:112–117

68. King J, Kupferthaler A, Frauscher B, Hackner H, Unterkofler K, Teschl G et al (2012) Measurement of endogenous acetone and isoprene in exhaled breath during sleep. Physiol Meas 33:413–428

69. King J, Mochalski P, Kupferthaler A, Unterkofler K, Koc H, Filipiak W et al (2010) Dynamic profiles of volatile organic compounds in exhaled breath as determined by a coupled PTR-MS/GC-MS study. Physiol Meas 31:1169–1184

70. Pugliese G, Trefz P, Weippert M, Pollex J, Bruhn S, Schubert JK et al (2022) Real-time metabolic monitoring under exhaustive exercise and evaluation of ventilatory threshold by breathomics: independent validation of evidence and advances. Front Physiol. [zitiert 18. August 2022];13. Verfügbar unter: https://www.frontiersin.org/articles/10.3389/fphys.2022.946401

71. Schubert R, Schwoebel H, Mau-Moeller A, Behrens M, Fuchs P, Sklorz M et al (2012) Metabolic monitoring and assessment of anaerobic threshold by means of breath biomarkers. Metabolomics 8:1069–1080

72. Sukul P, Schubert JK, Kamysek S, Trefz P, Miekisch W (2017) Applied upper-airway resistance instantly affects breath components: a unique insight into pulmonary medicine. J Breath Res 11:047108

73. Holsbeke CV, Vos W, Hamilton M, Claes R, Prime D, Vanhevel F et al (2014) Assessment of the effect of mouthpiece design on upper airway geometry using functional respiratory imaging. Eur Respir J 44:P553

74. Cope KA, Watson MT, Foster WM, Sehnert SS, Risby TH (2004) Effects of ventilation on the collection of exhaled breath in humans. J Appl Physiol 96:1371–1379

75. Sukul P, Schubert JK, Zanaty K, Trefz P, Sinha A, Kamysek S et al (2020) Exhaled breath compositions under varying respiratory rhythms reflects ventilatory variations: translating breathomics towards respiratory medicine. Sci Rep 10:14109

76. Bikov A, Paschalaki K, Kharitonov S, Sinclair RL, Horvath I, Usmani O et al (2012) Expiratory flow rate and breath hold affect exhaled volatile organic compounds (VOC) in healthy subjects. Eur Respir J 40:4305

77. Kushch I, Arendacká B, Stolc S, Mochalski P, Filipiak W, Schwarz K et al (2008) Breath isoprene – aspects of normal physiology related to age, gender and cholesterol profile as determined in a proton transfer reaction mass spectrometry study. Clin Chem Lab Med 46:1011–1018

78. Schwarz K, Pizzini A, Arendacká B, Zerlauth K, Filipiak W, Schmid A et al (2009) Breath acetone – aspects of normal physiology related to age and gender as determined in a PTR-MS study. J Breath Res 3:027003

79. Beauchamp J (2015) Current sampling and analysis techniques in breath research – results of a task force poll. J Breath Res 9:047107

80. Birken T, Schubert J, Miekisch W, Nöldge-Schomburg G (2006) A novel visually CO2 controlled alveolar breath sampling technique. Technol Health Care 14:499–506

81. Arbus GS, Hebert LA, Levesque PR, Etsten BE, Schwartz WB (1969) Characterization and clinical application of the significance band for acute respiratory alkalosis. N Engl J Med 280:117–123

82. Cavaliere F, Volpe C, Gargaruti R, Poscia A, Di Donato M, Grieco G et al (2009) Effects of acute hypoventilation and hyperventilation on exhaled carbon monoxide measurement in healthy volunteers. BMC Pulm Med 9:51

83. Moreno F, Lyons HA (1961) Effect of body posture on lung volumes. J Appl Physiol 16:27–29

84. Sukul P, Trefz P, Schubert J, Miekisch W (2022) Advanced setup for safe breath sampling and patient monitoring under highly infectious conditions in the clinical environment. [zitiert 6. Juli 2022]. Verfügbar unter: https://www.researchsquare.com/article/rs-1791972/v1

85. Sukul P, Bartels J, Fuchs P, Trefz P, Remy R, Rührmund L et al (2022) Effects of COVID-19 protective face-masks and wearing durations onto respiratory-haemodynamic physiology and exhaled breath constituents. Eur Respir Soc 60:2200009
86. De Angelis M, Ferrocino I, Calabrese FM, De Filippis F, Cavallo N, Siragusa S et al (2020) Diet influences the functions of the human intestinal microbiome. Sci Rep 10:4247
87. Biagini D, Fusi J, Vezzosi A, Oliveri P, Ghimenti S, Lenzi A et al (2022) Effects of long-term vegan diet on breath composition. J Breath Res 16
88. Ajibola OA, Smith D, Španěl P, Ferns GAA (2013) Effects of dietary nutrients on volatile breath metabolites. J Nutr Sci 2:e34
89. Remy R, Kemnitz N, Trefz P, Fuchs P, Bartels J, Klemenz A-C et al (2022) Profiling of exhaled volatile organics in the screening scenario of a COVID-19 test center. Rochester, NY [zitiert 20. Juni 2022]. Verfügbar unter: https://papers.ssrn.com/abstract=4055638
90. Trefz P, Obermeier J, Lehbrink R, Schubert JK, Miekisch W, Fischer D-C (2019) Exhaled volatile substances in children suffering from type 1 diabetes mellitus: results from a cross-sectional study. Sci Rep 9:15707
91. Ghimenti S, Di Francesco F, Onor M, Stiegel MA, Trivella MG, Comite C et al (2013) Post-operative elimination of sevoflurane anesthetic and hexafluoroisopropanol metabolite in exhaled breath: pharmacokinetic models for assessing liver function. J Breath Res 7:036001

Offline Breath Analysis: Standardization of Breath Sampling and Analysis Using Mass Spectrometry and Innovative Algorithms

Rosa A. Sola-Martínez, Gema Lozano-Terol, Julia Gallego-Jara, Manuel Cánovas Díaz, and Teresa de Diego Puente

Contents

Abstract Over the last decades, breath analysis has been postulated as a useful tool for the noninvasive diagnosis and monitoring of diseases. Specifically, offline breath

R. A. Sola-Martínez, G. Lozano-Terol, J. Gallego-Jara, M. Cánovas Díaz, and
T. de Diego Puente (✉)
Department of Biochemistry and Molecular Biology B and Immunology, University of Murcia, Murcia, Spain

Biomedical Research Institute of Murcia, IMIB-Arrixaca, Murcia, Spain
e-mail: tdp@um.es; https://scholar.google.com/citations?user=FrGSyt4AAAAJ&hl=en

analysis is currently the most common method used for biomarker discovery phase in human exhaled breath. In offline breath analysis, exhaled breath samples are collected in containers and stored prior to analysis, which enables to collect samples from patients at different places. This approach is mainly conducted by analytical platforms with high sensitivity, robustness, and reproducibility, such as technologies based on mass spectrometry. This comprehensive review provides an overview of all aspects of offline breath analysis, including sample collection protocols, challenges of breath sampling standardization, analytical techniques, data preprocessing, and the complex algorithms implemented for data analysis.

Keywords Breath analysis · Exhaled breath · Offline breath analysis · VOCs · Volatile organic compounds · Volatilome · Volatilomics

Abbreviations

|	
ANNs	Artificial neural networks
APCI	Atmospheric pressure chemical ionization
ARDS	Acute respiratory distress syndrome
BAL	Bronchoalveolar lavage
BCA	Breath collecting apparatus
CAR	Carboxen
CI	Chemical ionization
COVID-19	Coronavirus disease-2019
DVB	Divinylbenzene
EBC	Exhaled breath condensate
EI	Electron ionization
EIC	Extracted ion chromatogram
ESI	Electrospray ionization
GC	Gas chromatography
GC-MS	Gas chromatography-mass spectrometry
GCxGC	Two-dimensional gas chromatography
LASSO	Least absolute shrinkage and selection operator
LDA	Linear discriminant analysis
LR	Logistic regression
m/z	mass-to-charge ratio
MS	Mass spectrometry
NTDs	Needle trap devices
PA	Polyacrylate
PCA	Principal component analysis
PCR	Principal component regression
PDMS	Polydimethylsiloxane
PLS	Partial least squares regression
PLS-DA	Partial least squares-discriminant analysis

PTR-MS	Proton transfer reaction-mass spectrometry
PTR-ToF-MS	Proton transfer reaction time-of-flight mass spectrometry
RI	Retention index
ROS	Reactive oxygen species
SESI-HRMS	Secondary electrospray ionization-high resolution mass spectrometry
SESI-MS	Secondary electrospray ionization-mass spectrometry
SIFT-MS	Selected ion flow tube-mass spectrometry
SPME	Solid-phase microextraction
SVM	Support vector machine analysis
TD	Thermal desorption
TIC	Total ion chromatogram
ToF	Time-of-flight
VOCs	Volatile organic compounds

1 Introduction

In the twenty-first century, a major challenge for medicine is the establishment of noninvasive and cost-effective methodologies for early diagnosis and monitoring of highly prevalent chronic diseases, as well as rapid screening for infectious diseases. As a result, improvements in patient prognosis, a reduction in national medical burdens and a decrease in over-saturation of health services could be achieved. In this regard, the analysis of volatile organic compounds (VOCs) in exhaled breath as a diagnostic tool has generated a great expectation in recent years [1, 2].

The whole pool of VOCs in an organism is defined as "volatilome", and "volatilomics" as the new branch of "omics" dedicated to researching it [3]. Even though analysis of human exhaled breath has been used for medical purposes since Classical Antiquity [4], the emergence of the current field of breath analysis dates back to the 1970s thanks to the research of Nobel laureate Linus Pauling who was able to detect about 250 compounds in the air breathed out [5]. Since then, owing to advances in analytical techniques, it has been demonstrated that there are a large number of VOCs of different chemical groups (hydrocarbons, aldehydes, ketones, alcohols, etc.) in human exhaled air. Indeed, Lacy Costello et al. [6] reported 872 VOCs from human breath in 2014. In contrast, these compounds are found in low concentrations and represent a relatively small percentage of exhaled breath, whose main components are nitrogen (N_2), oxygen (O_2), carbon dioxide (CO_2), water vapor, and inert gases [2, 7, 8]. In addition, breath samples also contain nonvolatile compounds (e.g., cytokines, isoprostanes, leukotrienes, etc.), which can be determined by analysis of exhaled breath condensate (EBC) [9, 10].

VOCs detected in exhaled breath can originate from different sources. In fact, it is possible to distinguish VOCs in exhaled breath derived from tobacco, the combustion of fuels or other environmental pollutants. Furthermore, measuring these VOCs allows us to assess human exposure to air pollutants and health risks [11, 12]. In
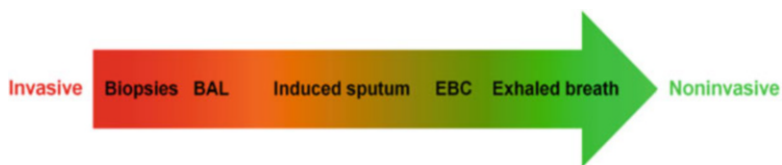
Fig. 1 Techniques for airway inflammation and oxidative stress surveillance. *BAL* bronchoalveolar lavage, *EBC* exhaled breath condensate. Adapted from van de Kant et al. [13] and Ferraro et al. [17]

contrast, many VOCs found in exhaled breath have an endogenous origin and come from both human metabolism and microbiota [4, 9]. In this sense, a lot of hydrocarbons of exhaled air are derived from lipid peroxidation, which increases in inflammatory processes and oxidative stress. In inflammation typical of many disorders, there is an increased production of reactive oxygen species (ROS), which enhances the oxidation of unsaturated fatty acids in cell membranes and the generation of subproducts such as hydrocarbons [13, 14]. Analogously, ROS produced during inflammatory processes and oxidative stress can also damage DNA, proteins, and carbohydrates and generate by-products [15, 16]. For all these reasons, breath analysis has been proposed as a noninvasive alternative for monitoring oxidative stress and airway inflammation in respiratory diseases given that current gold standard methodologies, such as bronchoscopy with bronchoalveolar lavage (BAL) and biopsy, are strongly intrusive (Fig. 1) [13, 17–19].

In addition, among VOCs detected in exhaled breath, there are also by-products of different pathways such as cholesterol biosynthesis (e.g., isoprene), ethanol metabolism (e.g., acetaldehyde), or acetoacetate and acetyl-CoA decarboxylation (e.g., acetone) [4, 9]. Therefore, analysis of volatilome in exhaled breath could be helpful to gain insight into the metabolic processes of the organism in both healthy and pathological states [11, 20]. Consequently, in recent years, a large number of studies have been conducted in order to search for biomarkers in exhaled breath to discriminate between healthy controls and patients with different disorders (e.g., asthma [21, 22], diabetes mellitus [23, 24], lung cancer [25], inflammatory bowel disease [26], infectious diseases [27], etc.), to distinguish between different stages of pathology (e.g., stable asthmatics and asthmatics with exacerbations [28–30]), and to differentiate patients suffering from a disease and subjects with similar symptoms but different illness (e.g., COVID-19 (coronavirus disease 2019) ARDS (acute respiratory distress syndrome) patients and non-COVID-19 ARDS patients [31]).

Nevertheless, the field of breath analysis is still in its infancy. To date, no further progress beyond the biomarker discovery phase has been achieved and introduction into daily clinical practice has not yet occurred [22]. After the biomarker discovery phase, both analytical validation and clinical validation must be carried out before new biomarkers can be used in day-to-day clinical practice [32]. The biomarker discovery phase involves the following steps: study design, breath sampling, exhaled breath analysis, data preprocessing, VOC identification, data analysis, and validation of the putative biomarker in an independent cohort study (Fig. 2). The lack of standardization, especially at the breath sampling step, has been traditionally pointed
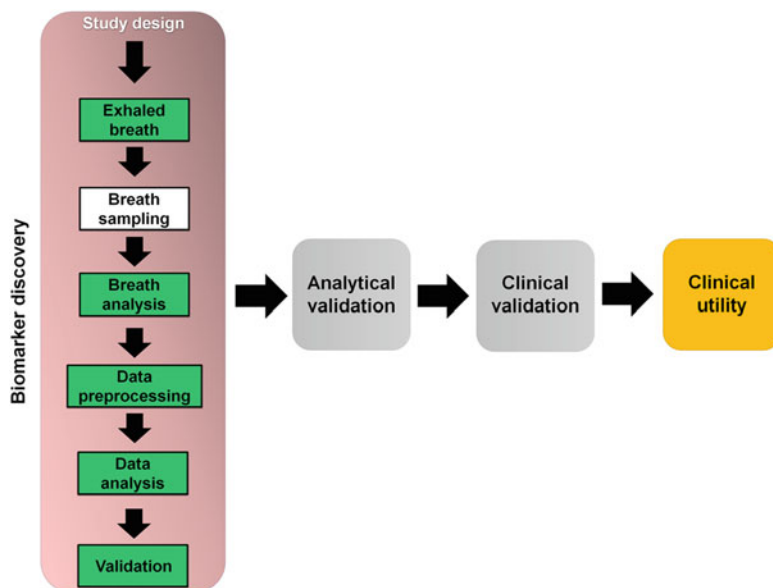
Fig. 2 Process of establishing a biomarker for clinical application: biomarker discovery phase, analytical validation phase, clinical validation phase, and clinical utility phase

out as the main cause of stagnation of this approach [33, 34]. However, it is also essential to integrate well-established metabolomics best practices, such as recruitment of large cohorts of subjects, incorporation of reproducible and transparent workflows for data preprocessing and data analysis, and external validation, among others [35, 36]. Therefore, both the suitable selection of strategies and the right implementation of each of the biomarker discovery steps are mandatory for the successful progress of breath analysis [33, 36].

Another important limitation of the process standardization is the great diversity of organic compounds in strongly varying concentrations that may require a specific protocol for their sampling and subsequent analysis, which are often unknown a priori [37]. The most widely used analytical techniques for the analysis of exhaled breath are technologies based on mass spectrometry and array sensors like the electronic nose (e-nose) [38]. In addition, other methodologies, for example, technologies based on optical spectroscopy, have also been deployed, but not as extensively [39]. In this sense, recent developments in mid-infrared laser spectroscopy have led to the promise of compact optical instruments for the detection of small molecules [40]. On the other hand, array sensors have some strengths for day-to-day clinical settings, such as cheapness, simplicity, and portability. However, there are currently a multitude of mass spectrometry platforms, e.g., gas chromatography-mass spectrometry, that are capable of individual identification of VOCs in a complex gas mixture, sensor arrays can only distinguish patterns or "breath prints." Hence, analytical platforms based on mass spectrometry are useful for the untargeted
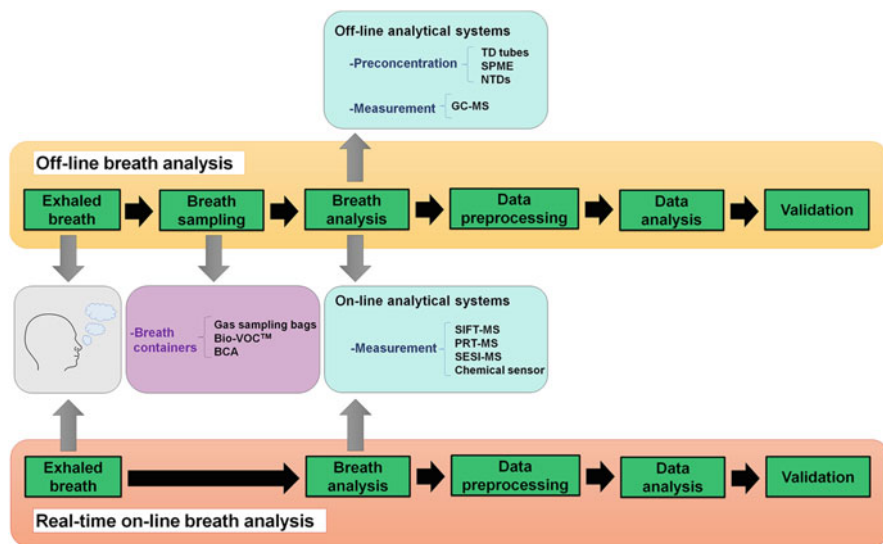
Fig. 3 Main breath analysis approaches: offline breath analysis and real-time online breath analysis. *BCA* breath collecting apparatus, *GC-MS* gas chromatography-mass spectrometry, *TD* thermal desorption, *SPME* solid-phase microextraction, *NTDs* needle trap devices, *SIFT-MS* selected ion flow tube-mass spectrometry, *PTR-MS* proton transfer reaction-mass spectrometry, *SESI-MS* secondary electrospray ionization-mass spectrometry

search for disease biomarkers as they are able to determine the identity of discriminant VOCs and the metabolic pathways related to them [34]. Therefore, mass spectrometry-based technologies may be more appropriate at the current stage of specific biomarker identification compared to targeted or pattern-based sensor systems.

Regarding the procedure for breath sample collection, there are two types of breath analysis (Fig. 3): *offline breath analysis* (the sample is collected in a breath container and stored before analysis) and *real-time online breath analysis* (exhaled breath is analyzed directly) [11, 41]. Over the last years, real-time online breath analysis has gained popularity as it offers numerous advantages for breath analysis implementation in daily clinical practice, for instance, minimal sample manipulation before analysis, continuous monitoring of the volatilome of patients, or fast findings. In spite of these benefits, offline breath analysis remains the preferred method of breath analysis [41, 42]. In offline breath analysis, exhaled breath samples can be easily stored and transported. As a result, samples can be collected at different places and MS analyses can be centralized in a single laboratory, without the patient having to travel to the analytical platform location. It is especially attractive for passive non-cooperative patients (e.g., intensive care patients, elderly, neonates, infants, etc.) [42, 43]. It is also preferable for analytes that require a preconcentration stage for proper detection.

This chapter provides a comprehensive review of the offline breath analysis approach using technologies based on mass spectrometry (MS). This review emphasizes on protocols, challenges for breath sampling standardization, analytical techniques, methods for data preprocessing and data analysis, and the future perspectives of offline breath analysis.

2 Factors Influencing Offline Breath Analysis

Several factors can affect volatilomics studies, ranging from demographic characteristics of subjects to methodologies employed that influence the presence of confounding factors. Concerning the study population, different aspects such as age, gender, comorbidities, smoking habits, physical activity, or medication of subjects should be considered in the study design and results interpretation [8, 21, 25, 44]. In fact, Blanchet et al. [45] determined that age, sex, smoking, and some drugs affected the VOC composition of exhaled breath. Therefore, some studies have focused on specific population groups (children [21, 36], women [46, 47], obes [48], etc.) or tried to estimate the real influence of some of these factors on VOC levels in exhaled breath. For instance, Capone et al. [49] reported differences in some VOCs levels between smokers and non-smokers. On the other hand, breath sampling protocols, containers used for breath collection, time and way of breath storage, or material cleaning protocols are also factors that play a very important role in offline breath analysis. In this sense, quantitative breath measurements depend on a valid, reproducible sampling technique wherefore samples may not be comparable with each other if they have been collected with different protocols. In addition, the choice of the analysis platform and the methods of data preprocessing and data analysis has a great impact on the biomarker searching process increasing its complexity [8, 13, 25, 35, 50].

3 Breath Sampling

Breath sampling is a distinctive aspect of offline breath analysis; thus, it must be carried out correctly in order to avoid introducing bias into sample stability and in breath analysis. In general, the main stages are the selection of the type of exhaled breath collected and the breath container used. In addition, another aspect to consider is either collecting a single or multiple exhalations [2].

3.1 Exhaled Breath Sampling Portions

The human respiratory cycle can be monitored by capnography (measurement of exhaled CO_2). Figure 4 shows a capnogram of the different phases of exhalation. Phase I includes dead space air or air from the airways without gas exchange with the alveoli (low CO_2 levels are observed in the capnogram). Phase II consists of air from both airways and alveoli (an almost linear rise of CO_2 levels is observed in the capnogram). Phase III includes air from the alveoli (a flattening of CO_2 curve can be seen in the capnogram). Finally, a decrease in CO_2 is again observed in the inspiration phase [51–54].

Depending on the exhalation phases collected for breath analysis, the exhaled breath sampling portions are classified into three types [51]:

– *Mixed expiratory breath.* The whole exhaled breath of subject is collected without excluding any of the exhalation phases. Therefore, both dead space air and alveolar air are included. Mixed expiratory breath is widely used because it is simple and easy to collect, being a useful alternative for passive non-cooperative patients. However, it is more susceptible to environmental contaminants. Thus, if
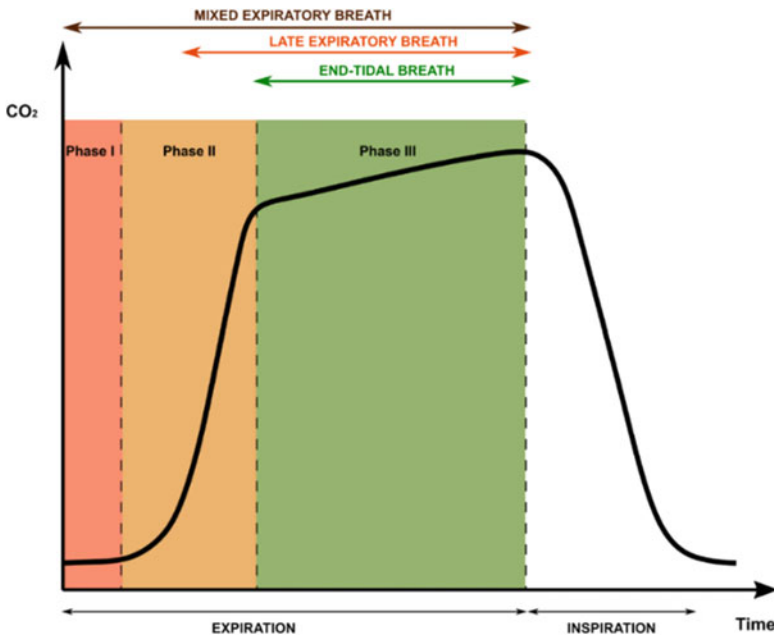
Fig. 4 Schematic representation of a capnogram of the human respiratory cycle. Phases of exhalation (Phase I, Phase II, and Phase III) and exhaled breath portions (mixed expiratory breath, late expiratory breath, and end-tidal breath). Adapted from Lawal et al. [51] and Beauchamp and Miekisch [52]

this option is chosen, room air analysis should be performed to remove the influence of the ambient background [36, 51].

– *Late expiratory breath.* Dead space air is discarded using different strategies, such as excluding the first few seconds of expiration or collecting dead space air in another gas sampling bag. The late expiratory breath includes air from both Phase III and part of Phase II, since these strategies employed cannot accurately determine the time of Phase III beginning [51].

– *End-tidal breath.* Phase III air is collected using the levels of an endogenous VOC as a reference. In general, monitoring of exhaled CO_2 is the most frequent strategy. Thus, exhaled air sampling begins once the capnogram starts to flatten, avoiding Phase I and Phase II air collection. Hence, this is the most accurate and reproducible approach to collect alveolar air [51].

3.2 Breath Containers

From a clinical standpoint, the ideal collector should be inexpensive and easy to use, inert, and most importantly, not allowing VOCs to enter or exit the sample. The most popular breath containers in offline breath analysis are gas sampling bags and other sampler devices such as the Bio-VOC™ sampler or breath collecting apparatus [34, 51, 55].

– *Gas sampling bags.* Gas sampling bags are the most widespread breath containers due to their simplicity and inexpensive cost. Polymer bags such as Tedlar® (polyvinyl fluoride) bags and aluminized Mylar® bags are the most commonly used [34, 51, 56]. They are inert and can be easily incorporated into breath analysis systems. Tedlar® bags can be reused more than once. However, Tedlar® bags have two inherent contaminants (phenol and N,N-dimethylacetamide), so they must be cleaned with pure nitrogen gas before use. In addition, diffusion through the walls of gas sampling bags and condensation issues can compromise the stability of breath samples over long periods of storage. Therefore, it is recommended to use these containers to collect exhaled breath and to use absorbent matrices for sample storage. Other polymer bags used are Teflon® (polytetrafluoroethylene ethylene) bags and Nalophan® (polyethylene terephthalate) bags [34, 56–58].

– *Bio-VOC™ sampler.* The Bio-VOC™ sampler allows the discarding of dead space air, is inert and economical. The Bio-VOC™ sampler consists of three parts: a mouthpiece, a volumetric sampler (a small container with a capacity of 100–150 mL) and a plunger. The Bio-VOC™ sampler has an open side so that air is moved as expiration progresses, in order to collect only the late expiratory breath. One of the main limitations of the Bio-VOC™ sampler is that it is not able to collect a large volume of exhaled breath [34, 51, 59].

– *Breath collecting apparatus (BCA).* The subject breathes into a tubular structure with a mouthpiece. VOCs are retained at the end of the tube by absorbent resins. It

has two different absorbent traps. One is usually used to collect late expiratory breath and the other to capture room air. In addition, it has a heating band to reduce condensation problems [34, 51, 60–62].

Other breath collection devices are reported by White et al. [63], such as the RTubeVOC or the Alveosampler, but are less widespread.

3.3 Standardization of Breath Sampling

In recent years, special emphasis has been placed on the standardization of breath sampling, because the success of the discovery of potential biomarkers in exhaled breath largely depends on this first step. Firstly, it is essential to determine the exhaled breath portion to be collected based on the purpose of the study and to establish a reproducible sampling protocol. Although Phase III air (alveolar air only) provides the most meaningful information for human metabolism and disease research, collection of breath portions that also include dead space air and airway air could be of interest. For example, dead space air may be useful for monitoring exposure to environmental pollutants and in oral health, and airway air collection could be beneficial in studies focusing on asthma for its symptoms. Furthermore, information on smoking habits or daily medication taken by the subjects should be compiled to assess whether they have an impact on their volatilome. In this sense, hours of fasting prior to breath sampling should also be taken into account [1, 8, 64].

On the other hand, it is highly recommended to collect environmental samples during breath sampling, especially if dead space and airway air are not excluded. Thus, it is possible to identify which variations observed in the exhaled breath samples are exclusively due to ambient air, avoiding the determination of incorrect biomarkers. Another alternative approach to minimize the impact of VOCs from ambient air is the use of VOC filters during breath sampling [1, 8, 25, 36]. Furthermore, the season of the year in which breath sampling and analysis was conducted could influence the exhaled breath VOC composition. Therefore, it is another factor to be taken into account [13, 47].

In summary, the variability of breath gas VOC measurements can be affected by many factors during sampling [51], including the physical-chemical properties of the compounds, and must be taken into account for reproducibility of the method applied [65].

# 4 Analytical Platforms Based on Mass Spectrometry

The plethora of analytical platforms based on mass spectrometry can be divided into two main groups: offline analytical systems (samples are preconcentrated before analysis) and online analytical systems (samples do not need pretreatment prior to analysis) [52].

4.1 Offline Analytical Systems

Most studies focusing on offline breath analysis employ gas chromatography coupled to mass spectrometry (GC-MS). GC-MS is a typical offline analytical system, since it requires a previous preconcentration of exhaled breath samples [2, 34, 51]. Nowadays, GC-MS is generally recognized as the gold standard technique in the field of breath analysis. Although it has some drawbacks compared to online analytical systems (e.g., higher time consumption), GC-MS offers high sensitivity, robustness, and reproducibility. In this sense, this methodology allows the identification and quantification of different individual VOCs from exhaled breath samples, including unknowns [33, 34, 38, 66, 67].

Gas chromatography separates VOCs from exhaled breath according to retention time (time required to pass through the capillary GC column), which depends on the interaction between VOCs and column-coating stationary phase [1, 33]. In this regard, an additional gas chromatography column, comprehensive two-dimensional gas chromatography (GCxGC), is used in some studies to improve the separation of co-eluting compounds [61, 68] (Fig. 5). On the downside this method has a higher price and requires more complex data analysis [71].

Once the exhaled metabolites are separated by GC, the compounds are transferred to the mass spectrometer to be analyzed. The main components of a mass spectrometer are an ion source, a mass analyzer and a detector. In the ion source stage, compounds are ionized and fragmented by different types of ionization techniques. Thus, in this stage, different charged fragments are generated depending on which
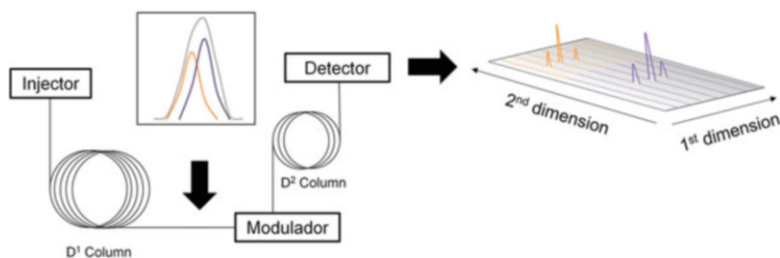
Fig. 5 Schematic diagram illustrating two-dimensional gas chromatography (GCxGC). Adapted from Zanella et al. [69] and Forsythe et al. [70]

compounds are analyzed. Although the use of soft ionization such as atmospheric pressure chemical ionization (APCI) is gaining popularity, electronic ionization (EI) is the most common ionization technique in GC-MS. EI is a high ionization technique and a large number of fragments are generated. Mass analyzer is used to separate these fragments by their mass-to-charge ratio (m/z). The type of mass analyzer determines the characteristics of the mass spectrometer (resolution, sensitivity, accuracy, and mass range) [66, 72–74]. Both low-resolution mass analyzers with unit mass resolution (accuracy of 1 Da) as single quadrupole [75, 76], and high resolution (at least accuracy of 10,000 Da) as time-of-flight (ToF) [33, 77, 78] have been used in breath analysis. GC-MS has the capacity of detecting VOCs within a range of parts per billion, or lower, with good reproducibility and linearity. Finally, signals of the separated fragments are registered in the detector, resulting in a plot called mass spectrum that illustrates the intensity of signals of m/z fragments obtained. In this sense, in hard ionization such as EI, matching of experimental mass spectrum with mass spectral libraries is useful for compound identification [34, 66, 72]. In the case of soft ionization, the molecular ion is generally obtained, so compound identification is based on accurate mass determination rather than on matching with spectral libraries as in hard ionization [73, 74].

4.2   Preconcentration Methods

Preconcentration methods typically involve two stages, whereby VOCs are retained in sorbent traps and then released by thermal desorption (TD). Currently, sorbent traps most commonly used in offline breath analysis are thermal desorption tubes, solid-phase microextraction (SPME), and needle trap devices (NTDs). Preconcentration is a critical step because some VOCs could be diluted during breath sampling as well as removing water vapor from samples, especially when mixed expiratory breath is collected [4, 51, 52].

– *Thermal desorption (TD) tubes*. Nowadays, thermal desorption tubes are the most widespread devices for preconcentration in breath analysis. Exhaled breath collected in gas sampling bags can be transferred to the thermal desorption tubes, where the samples can be stored for a longer period of time. In addition, it is possible to fill the thermal desorption tubes directly or to fill them with ambient air using a syringe, which is useful for monitoring the environmental influence. Another advantage of using thermal desorption tubes is that the samples can be easily transported inter-laboratorily without being altered. Thermal desorption tubes are usually made of stainless steel or glass and packed with sorbent materials such as organic polymers, graphitized carbon, or carbon molecular sieves. Whereas organic polymers (e.g., Tenax TA) present low sensibility of humidity and are indicated to capture hydrocarbons of medium size, tubes of graphitized carbon (e.g., Carbopack X) can trap VOCs with low number of carbons. For this reason, it is recommended to use a combination of different

absorbent beds. Considering the high percentage of water in exhaled breath, the use of organic polymers as sorbents is of great interest [4, 51, 52, 79, 80].

– *Solid phase microextraction (SPME).* It is a methodology commonly used in the preconcentration and storage of exhaled breath samples. The extraction of volatile organic compounds is based on the headspace technique. Thus, a fiber (silica rod coated with different sorbent materials) is exposed to the exhaled breath sample until chemical equilibrium between them is achieved. The type and thickness of the fiber influences the time required to reach equilibrium [51, 81, 82]. Caldeira et al. [57] tested different coating fibers (DVB/CAR/PDMS, PDMS/DVB, PDMS, and PA), obtaining better extraction efficiency with DVB/CAR/PDMS (DVB: divinylbenzene, CAR: carboxen, PDMS: polydimethylsiloxane, PA: polyacrylate). It is important to note that both temperature and extraction time have a great impact on the SPME process.

– *Needle trap devices (NTDs).* Needle trap devices are not as commonly used as TD tubes and SPME in breath analysis, but offer some benefits of both. They consist of needle-shaped devices with absorbent materials inside, where exhaled breath is introduced through a syringe to be captured. Like TD tubes, storage and transport of exhaled breath samples is straightforward [51].

4.3   Online Analytical Systems

The most widespread online analytical systems based on mass spectrometry for VOC measurement in exhaled breath are SIFT-MS (Selected ion flow tube-mass spectrometry), PTR-MS (Proton transfer reaction-mass spectrometry), and SESI-MS (Secondary electrospray ionization-mass spectrometry). Although online analytical systems are used in real-time online breath analysis, these analytical platforms are also implemented in offline breath analysis [41, 83]. Table 1 shows some examples

Table 1 Examples of offline breath analysis by online analytical systems

References	Breath containers	Online analytical systems
Alkhouri et al. [84]	Mylar® bags	SIFT-MS
Boshier et al. [85]	Nalophan® bags	SIFT-MS
Dryahina et al. [86]	Nalophan® bags	SIFT-MS
Wang et al. [87]	Tedlar® bags	SIFT-MS
Alkhouri et al. [48]	Mylar® bags	SIFT-MS
Eng et al. [88]	Mylar® bags	SIFT-MS
Hamilton et al. [89]	Mylar® bags	SIFT-MS
Greiter et al. [90]	Teflon® bags	PTR-MS
Liangou et al. [91]	Tedlar® bags	PTR-ToF-MS
Decrue et al. [43]	Nalophan® bags	SESI-HRMS

SIFT-MS selected ion flow tube-mass spectrometry, *PTR-MS* proton transfer reaction-mass spectrometry, *PTR-ToF-MS* proton transfer reaction time-of-flight mass spectrometry, *SESI-HRMS* secondary electrospray ionization-high resolution mass spectrometry

where online analytical systems have been successfully used in offline breath analysis. Thus, breath containers were used for sample collection prior to breath analysis using online analytical systems.

For both SIFT-MS and PTR-MS, VOCs from exhaled breath are ionized by chemical ionization (CI). Whereas the reagent ions typically used in SIFT-MS are H_3O^+, NO^+ and O_2^+, H_3O^+ is the most popular reagent ion in PTR-MS. In SIFT-MS, the reaction between the reactive ions (produced in a microwave plasma and screened on a quadrupole filter) and the exhaled metabolites is conducted in a drift tube. In general, helium is used as carrier gas. Nevertheless, PTR-MS does not require prior selection of the reagent ions before the reaction in the drift tube; hence, it does not have a quadrupole filter. In PTR-MS, H_3O^+ reagent ions are produced from water vapor using a hollow cathode ion source. Furthermore, PTR-MS is more sensitive than SIFT-MS, as the exhaled breath sample is not diluted because the sample air is used as a carrier gas. On the other hand, the resolution of PTR-MS and SIFT-MS is determined by the mass spectrometer connected to the instrument. Both PTR-MS and SIFT-MS enable the quantification of metabolites. In particular, the quantification of VOCs from breath samples in SIFT-MS is based on kinetic studies of the chemical reactions between these compounds and reagent ions as well as on comparison with kinetic libraries. In this regard, SIFT-MS is mainly used in targeted analysis, focusing on compounds whose chemical reactions with the reagent ions are well-understood. For breath analysis, humidity present in breath samples can interfere with the computation of VOC concentrations due to the generation of hydrates [41, 83, 92].

In recent years, SESI-MS has generated considerable enthusiasm in the field of breath analysis. Secondary electrospray ionization (SESI) is an innovative variant of electrospray ionization (ESI) that allows gaseous sample analysis. Thus, in SESI-MS, VOCs from exhaled breath samples are ionized at ambient pressure by reacting with primary ions formed by an electrospray ionization source from a pure solvent and a conductivity-enhancing additive. The ionization process is efficient and soft, obtaining very often the molecular ion. One of the main strengths of SESI-MS is that SESI can be coupled to any mass analyzer including high-resolution mass spectrometers [41, 93, 94].

5 Data Preprocessing

Raw data obtained from breath analysis by mass spectrometry-based technologies must be processed to obtain a matrix useful for statistical analysis. Proper data preprocessing is key to minimizing potential analytical artifacts and to obtain accurate results in data analysis [95–97]. However, despite the great relevance of this step in the biomarker discovery process, only a few studies provide a comprehensive description of the data preprocessing workflows performed [22, 36]. In contrast, some recent studies focused on breath analysis [98–101] have implemented open-source tools typical of metabolomics such as *xcms* [102]. The use of open-

source tools is essential to overcome the challenges of both metabolomics and volatilomics studies, as it encourages collaboration within the scientific community and the development of reproducible and transparent protocols for data preprocessing [103].

The raw data obtained and the data preprocessing workflows to be conducted depend on the choice of the analytical platform. In the case of GC-MS by EI ionization, raw data involve three dimensions (retention time, m/z value, and intensity) which are represented through chromatograms (retention time on the *x*-axis and intensity on the *y*-axis) and mass spectra (*m/z* value on the *x*-axis and intensity on the *y*-axis) (Fig. 6). TIC (total ion chromatogram) is defined as the sum of intensities of all *m/z* signals or ion peaks in the mass spectrum per unit time or per scan. The gas chromatogram is the total TICs of the scans performed during breath analysis or TIC chromatogram. On the other hand, EICs (extracted ion chromatogram) show the intensities of a particular m/z signal versus the retention time. Therefore, each gas chromatogram peak, which could correspond to one or more volatile organic compounds, has an associated mass spectrum with several *features* (ion peaks characterized by a specific retention time and an *m/z* value) at different intensities [72, 95, 96, 102, 104].

In this sense, there are two main approaches for data preprocessing of raw GC-MS data. Whereas approach 1 is based on peak-picking or determination of ionic peaks in spectra obtained from exhaled breath samples, approach 2 focuses on the detection of compounds present in breath samples by means of spectral deconvolution [104]. Both have benefits and limitations [104–106]; therefore, an interesting strategy could be the integration of both two approaches [97]. Some examples of computational tools are *xcms* [102] or *MetAlign* [107] for approach 1, and *eRah* [104, 108] for approach 2. Regardless of the approach employed, there are some common steps in data preprocessing such as denoising, baseline correction, retention time correction or alignment, missing compounds/*features* recovery and normalization [34, 95, 102, 104].

An important task in data preprocessing, especially in untargeted analysis, is compound identification. In GC-MS using EI, compound identification is mainly based on the similarity of retention times and mass spectra matching with a spectral library. Hence, it is strongly recommended to analyze chemical standards for retention index (RI) calculation and to confirm the identity of the compounds [11, 35, 72, 104].

6 Data Analysis

Once raw data has been transformed into a useful data matrix by data preprocessing, the next step in biomarker discovery is data analysis [33]. A single biomarker is usually not enough to perform an optimal diagnosis and monitoring of complex and heterogeneous diseases. For this reason, in recent years, there has been an increasing interest in finding a set of biomarkers to unravel the metabolic processes related to
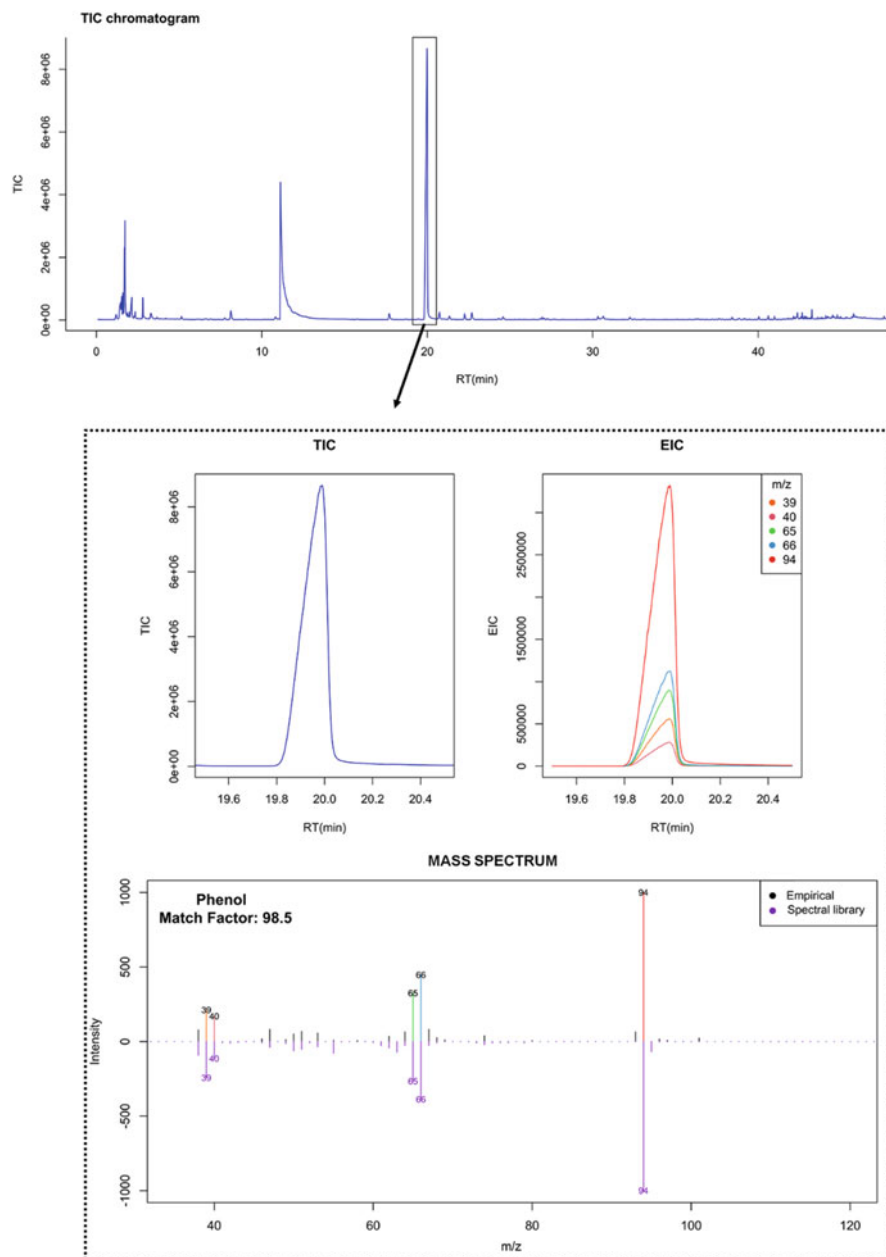
Fig. 6 Outcomes of breath analysis using gas chromatography-mass spectrometry. *TIC* total ion chromatogram, *EIC* extracted ion chromatogram. Plots of this figure were generated by plotChr and plotSpectra functions of the package eRah in R

pathological conditions. This trend has also extended to the field of breath analysis and several studies are focused on searching for profiles of VOCs rather than on a single discriminant VOC. In this sense, multivariate statistical analysis is claimed to be the most suitable approach for VOC profiling. Currently, a wide range of machine learning algorithms are useful for data analysis in breath analysis [2, 35, 109].

6.1 Machine Learning Algorithms

Data obtained in breath analysis shows a high dimensionality. Therefore, volatilome data are characterized by a higher number of VOCs detected than samples available (leading to *fat matrices*), low prevalence of each VOC in all samples and high probability of non-normal distribution. Additionally, multicollinearity, which consists of aleatory correlations of variables, is a typical problem in VOC profiling studies [95, 110]. Multivariate statistical methods are usually classified as: *unsupervised learning methods* (e.g., principal component analysis (PCA)) and *supervised learning methods* (e.g., linear discriminant analysis (LDA), logistic regression (LR), random forest (RF), support vector machine (SVM), or artificial neural networks (ANNs)). Whereas unsupervised learning methods are used to perform exploratory data analysis without previous assumptions and labeled data, supervised learning methods are implemented in order to obtain a discriminant and predictive model through labeled data and prior information (Fig. 7) [95, 105, 111, 112].

Overall, unsupervised methods are used as a first step in data analysis. In this sense, PCA is certainly the most common technique used in studies focused on breath analysis. Mainly, PCA is conducted in order to perform an explorative analysis to observe groups or data tendencies [95, 113]. Then, the next step is usually the implementation of supervised learning methods for model building.
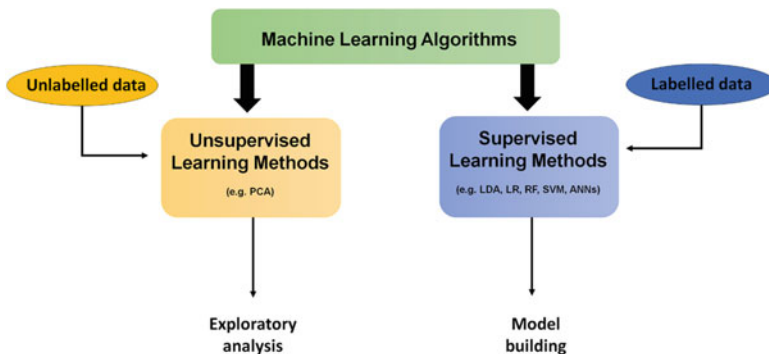
Fig. 7 Machine learning algorithms. *PCA* principal component analysis, *LDA* linear discriminant analysis, *LR* logistic regression, *RF* random forest, *SVM* support vector machine analysis, *ANNs* artificial neural networks

Table 2 Examples of machine learning algorithms used in breath analysis by technologies based on mass spectrometry to obtain a predictive model

Machine learning algorithms	References
PCA + LDA	Zhou et al. [120]
LASSO+LR	Wang et al. [87], Monasta et al. [121], Sola-Martínez et al. [47]
PLS-DA	Caldeira et al. [57], Van Oort et al. [99], Beccaria et al. [122]
SVM	Robroeks et al. [30], Van Berkel et al. [123], Beccaria et al. [122]
Random forest	Beccaria et al. [122], Gashimova et al. [124]
ANNs	Rudnicka et al. [125]

PCA principal component analysis, *LDA* linear discriminant analysis, *LASSO* least absolute shrinkage and selection operator, *LR* logistic regression, *PLS-DA* partial least squares-discriminant analysis, *SVM* support vector machine analysis, *ANNs* artificial neural networks

Supervised learning methods are able to predict the values of outputs or dependent variables, based on the values of inputs or independent variables [111, 114]. Using supervised learning methods is an excellent strategy for biomarker determination [105]. However, any supervised learning method is not adequate for volatilome data, due to the presence of multicollinearity. In this regard, LDA and logistic regression are not the best options for VOC profiling without a prior variable selection [95, 115]. The issue of multicollinearity could be approached mainly from three different perspectives: (1) using an unsupervised learning method before a supervised learning method (e.g., PCA + LDA) [116], (2) data pretreatment by specific techniques such as the shrinkage methods (ridge, LASSO (least absolute shrinkage and selection operator), etc.) or methods using derived input directions (PCR (principal component regression), PLS (partial least squares regression)) [111] and a supervised learning method, or (3) supervised learning methods with tolerance to high-dimensional data (e.g., random forest, SVM, etc.) [117–119]. Table 2 shows some examples of studies focused on breath analysis by technologies based on mass spectrometry that used one of the strategies to obtain a predictive model.

PLS-DA is an algorithm that combines the PLS regression method and a discriminant analysis in order to deal with the multicollinearity problem [95, 126, 127]. Thus, PLS-DA is a widely used supervised learning method in biomarkers discovery [95, 127]. However, Brereton et al. claim that it is possible to achieve similar results with the first strategy (e.g., PCA + LDA) [116]. Nevertheless, a problem of this strategy is that important information may not be considered if it is not compiled by the first principal components [95]. On the other hand, several studies focusing on breath analysis have followed the third strategy and innovative algorithms such as random forest, SVM or ANNs have been implemented. However, these methods have a high computational complexity and their outcomes are often not easy to understand [95].

6.2   Validation of Models

Validation of the models is an essential step in data analysis to assess the performance of the models, the real applicability of the models on unknown data, and the suitability of the selected VOC profiles. However, if model generation and validation are performed on the same data set, which is unfortunately very frequent in volatilomics studies, there is a high risk of overfitting. Accordingly, external validation of models is the best option. In this approach, the model is constructed based on a training set and model validation is carried out over other independent sets (validation set). In this sense, it is frequent to randomly divide exhaled breath samples from subjects into a training set and a validation set. However, it is more desirable that the exhaled breath samples in the validation set belong to a group of new subjects enrolled at a different time or place than those in the training set (real external validation). On the other hand, the sample size in studies focused on breath analysis is sometimes insufficient to provide two independent sets. For this reason, an attractive approach is internal validation of model or resampling techniques such as cross-validation (CV) or bootstrapping. Thus, the most popular cross-validation strategies are "leave-one-out" and "n-fold" cross-validation [35, 36, 95, 105, 112]. The use of resampling methods causes great controversy, since it has been suggested that these techniques could overestimate the predictive power of the models. In this regard, a permutation test can be deployed together with resampling techniques in order to address these challenges. The permutation test evaluates that the performances of the constructed models are significantly better than the performances of predictive models constructed with randomly labeled data [95, 96]. Even though the permutation test is not yet widely used in volatilomics studies, some recent studies have introduced this test [47, 75].

7   Conclusions and Perspective

Since years, exhaled breath has been considered a promising source of potential biomarkers, because it is a noninvasive methodology. In particular, this approach could be especially beneficial for passive non-cooperative patients such as intensive care or pediatric patients. VOC analysis could be extremely useful in the future for the diagnosis and monitoring of prevalent diseases in children such as asthma. In addition, it could also play an important role in monitoring oxidative stress and exposure to environmental pollutants. Specifically, this chapter focuses on offline breath analysis using mass spectrometry-based technologies. This approach provides for easy storage and transport of exhaled breath samples, thereby avoiding unnecessary transit of patients to the location of the analysis platform. Furthermore, the typical analytical techniques used in this approach offer high sensibility, robustness, and reproducibility. The main steps involved in biomarker discovery by offline breath analysis have been reviewed in this chapter. Special emphasis has been

given to protocols and the standardization process of breath sampling since the acquired data are significantly affected by the experimental design and instrumental parameters. The choice of the exhaled breath portion must be based on the main aim of the study. It is also essential to check the influence of the room ambient air where breath sampling is performed. On the other hand, the review has addressed different analytical platforms based on mass spectrometry which have been used in offline breath analysis. In fact, offline analytical systems such as GC-MS with preconcentration methods are clearly the most popular for offline breath analysis. However, this review also shows the emerging use of online systems for this approach. Finally, the innovative strategies and algorithms recommended for data preprocessing and data analysis in the breath analysis field have been reported. Volatilome data has a high dimensionality and often exhibit multicollinearity problems. Therefore, it is crucial to select robust techniques that deal with such issues. By using machine learning algorithms, specifically supervised learning methods, it is possible to obtain predictive models and discriminant VOC profiles. Validation of these models must be rigorously carried out to avoid overfitting and to ensure their universal use.

In summary, exhaled breath analysis is currently an area of intense research that requires a collective effort to move beyond its exploratory stage as it has an immense clinical potential in healthcare in the near future.

References

1. Ibrahim W et al (2021) Breathomics for the clinician: the use of volatile organic compounds in respiratory diseases. Thorax 76:514
2. Pereira J et al (2015) Breath analysis as a potential and non-invasive frontier in disease diagnosis: an overview. Meta 5:3–55
3. Achyuthan KE, Harper JC, Manginell RP, Moorman MW (2017) Volatile metabolites emission by in vivo microalgae – an overlooked opportunity? Meta 7
4. Miekisch W, Schubert JK, Noeldge-Schomburg GFE (2004) Diagnostic potential of breath analysis – focus on volatile organic compounds. Clin Chim Acta 347:25–39
5. Pauling L, Robinson AB, Teranishi R, Cary P (1971) Quantitative analysis of urine vapor and breath by gas-liquid partition chromatography. Proc Natl Acad Sci U S A 68:2374–2376
6. de Lacy Costello B et al (2014) A review of the volatiles from the healthy human body. J Breath Res 8:014001
7. Bos LDJ (2018) Diagnosis of acute respiratory distress syndrome by exhaled breath analysis. Ann Transl Med 6:33–33

8. Davis MD, Fowler SJ, Montpetit AJ (2019) Exhaled breath testing – a tool for the clinician and researcher. Paediatr Respir Rev 29:37–41

9. Buszewski B, Kesy M, Ligor T, Amann A (2007) Human exhaled air analytics: biomarkers of diseases. Biomed Chromatogr 21:553–566

10. Montuschi P (2007) Analysis of exhaled breath condensate in respiratory medicine: methodological aspects and potential clinical applications. Ther Adv Respir Dis 1:5–23

11. Amann A et al (2014) The human volatilome: volatile organic compounds (VOCs) in exhaled breath, skin emanations, urine, feces and saliva. J Breath Res 8:034001

12. Tang Z, Liu Y, Duan Y (2015) Breath analysis: technical developments and challenges in the monitoring of human exposure to volatile organic compounds. J Chromatogr B 1002:285–299

13. van de Kant KDG, van der Sande LJTM, Jöbsis Q, van Schayck OCP, Dompeling E (2012) Clinical use of exhaled volatile organic compounds in pulmonary diseases: a systematic review. Respir Res 13:117

14. Ratcliffe N et al (2020) A mechanistic study and review of volatile products from peroxidation of unsaturated fatty acids: an aid to understanding the origins of volatile organic compounds from the human body. J Breath Res 14:034001

15. Zuo L, Otenbaker NP, Rose BA, Salisbury KS (2013) Molecular mechanisms of reactive oxygen species-related pulmonary inflammation and asthma. Mol Immunol 56:57–63

16. Calenic B et al (2015) Oxidative stress and volatile organic compounds: interplay in pulmonary, cardio-vascular, digestive tract systems and cancer. Open Chem 13:1020–1030

17. Ferraro V, Carraro S, Bozzetto S, Zanconato S, Baraldi E (2018) Exhaled biomarkers in childhood asthma: old and new approaches. Asthma Res Pract 4:9

18. Tenero L, Zaffanello M, Piazza M, Piacentini G (2018) Measuring airway inflammation in asthmatic children. Front Pediatr 6:196

19. Sola-Martínez RA et al (2022) Relationship between lung function and exhaled volatile organic compounds in healthy infants. Pediatr Pulmonol 57:1282–1292

20. Kim KH, Jahan SA, Kabir E (2012) A review of breath analysis for diagnosis of human health. TrAC Trends Anal Chem 33:1–8

21. Neerincx AH et al (2017) Breathomics from exhaled volatile organic compounds in pediatric asthma. Pediatr Pulmonol 52:1616–1627

22. Azim A, Barber C, Dennison P, Riley J, Howarth P (2019) Exhaled volatile organic compounds in adult asthma: a systematic review. Eur Respir J 54:1900056

23. Wang W et al (2021) Accuracy of breath test for diabetes mellitus diagnosis: a systematic review and meta-analysis. BMJ Open Diabetes Res Care 9:e002174

24. Dixit K, Fardindoost S, Ravishankara A, Tasnim N, Hoorfar M (2021) Exhaled breath analysis for diabetes diagnosis and monitoring: relevance, challenges and possibilities. Biosensors 11:476

25. Marzorati D et al (2019) A review of exhaled breath: a key role in lung cancer diagnosis. J Breath Res 13:034001

26. Kurada S, Alkhouri N, Fiocchi C, Dweik R, Rieder F (2015) Review article: breath analysis in inflammatory bowel diseases. Aliment Pharmacol Ther 41:329–341

27. Ahmed WM, Lawal O, Nijsen TM, Goodacre R, Fowler SJ (2017) Exhaled volatile organic compounds of infection: a systematic review. ACS Infect Dis 3:695–710

28. Brinkman P et al (2017) Exhaled breath profiles in the monitoring of loss of control and clinical recovery in asthma. Clin Exp Allergy 47:1159–1169

29. van Vliet D et al (2017) Can exhaled volatile organic compounds predict asthma exacerbations in children? J Breath Res 11:016016

30. Robroeks CM et al (2013) Exhaled volatile organic compounds predict exacerbations of childhood asthma in a 1-year prospective study. Eur Respir J 42:98–106

31. Grassin-Delyle S et al (2021) Metabolomics of exhaled breath in critically ill COVID-19 patients: a pilot study. EBioMedicine 63:103154

32. Mazzone PJ et al (2017) Evaluating molecular biomarkers for the early detection of lung cancer: when is a biomarker ready for clinical use? An official American Thoracic Society policy statement. Am J Respir Crit Care Med 196:e15–e29

33. Boots AW et al (2012) The versatile use of exhaled volatile organic compounds in human health and disease. J Breath Res 6:027108

34. Rattray NJW, Hamrang Z, Trivedi DK, Goodacre R, Fowler SJ (2014) Taking your breath away: metabolomics breathes life in to personalized medicine. Trends Biotechnol 32: 538–548

35. Boots AW, Bos LD, van der Schee MP, van Schooten FJ, Sterk PJ (2015) Exhaled molecular fingerprinting in diagnosis and monitoring: validating volatile promises. Trends Mol Med 21: 633–644

36. Sola Martínez RA et al (2021) Exhaled volatile organic compounds analysis in clinical pediatrics: a systematic review. Pediatr Res 89:1352–1363

37. Herbig J, Beauchamp J (2014) Towards standardization in the analysis of breath gas volatiles. J Breath Res 8:037101

38. Kaloumenou M, Skotadis E, Lagopati N, Efstathopoulos E, Tsoukalas D (2022) Breath analysis: a promising tool for disease diagnosis – the role of sensors. Sensors 22:1238

39. Metsälä M (2018) Optical techniques for breath analysis: from single to multi-species detection. J Breath Res 12:027104

40. Selvaraj R, Vasa NJ, Nagendra SMS, Mizaikoff B (2020) Advances in mid-infrared spectroscopy-based sensing techniques for exhaled breath diagnostics. Molecules 25:2227

41. Bruderer T et al (2019) On-line analysis of exhaled breath. Chem Rev 119:10803–10828

42. Zhang J et al (2021) Breath volatile organic compound analysis: an emerging method for gastric cancer detection. J Breath Res 15

43. Decrue F et al (2021) Combination of exhaled breath analysis with parallel lung function and FeNO measurements in infants. Anal Chem 93:15579–15583

44. Skelly AC, Dettori JR, Brodt ED (2012) Assessing bias: the importance of considering confounding. Evid Based Spine Care J 3:9

45. Blanchet L et al (2017) Factors that influence the volatile organic compound content in human breath. J Breath Res 11:016013

46. Sukul P, Schubert JK, Trefz P, Miekisch W (2018) Natural menstrual rhythm and oral contraception diversely affect exhaled breath compositions. Sci Rep 8:10838

47. Sola-Martínez RA et al (2021) Exhaled volatilome analysis as a useful tool to discriminate asthma with other coexisting atopic diseases in women of childbearing age. Sci Rep 11:13823

48. Alkhouri N et al (2015) Breathprints of childhood obesity: changes in volatile organic compounds in obese children compared with lean controls. Pediatr Obes 10:23–29

49. Capone S et al (2018) Chromatographic analysis of VOC patterns in exhaled breath from smokers and nonsmokers. Biomed Chromatogr 32

50. Van Der Schee MP et al (2015) Breathomics in lung disease. Chest 147:224–231

51. Lawal O, Ahmed WM, Nijsen TME, Goodacre R, Fowler SJ (2017) Exhaled breath analysis: a review of 'breath-taking' methods for off-line analysis. Metabolomics 13:110

52. Beauchamp JD, Miekisch W (2020) Breath sampling and standardization. In: Beauchamp J, Davis C, Pleil J (eds) Breathborne biomarkers and the human volatilome. Elsevier, pp 23–40

53. Verscheure S, Massion PB, Verschuren F, Damas P, Magder S (2016) Volumetric capnography: lessons from the past and current clinical applications. Crit Care 20:184

54. Pham YL, Beauchamp J (2021) Breath biomarkers in diagnostic applications. Molecules 26: 5514

55. Zhou J, Huang ZA, Kumar U, Chen DDY (2017) Review of recent developments in determining volatile organic compounds in exhaled breath as biomarkers for lung cancer diagnosis. Anal Chim Acta 996:1–9

56. Mochalski P, Wzorek B, Śliwka I, Amann A (2009) Suitability of different polymer bags for storage of volatile sulphur compounds relevant to breath analysis. J Chromatogr B 877:189–196

57. Caldeira M et al (2011) Profiling allergic asthma volatile metabolic patterns using a headspace-solid phase microextraction/gas chromatography based methodology. J Chromatogr A 1218: 3771–3780

58. Beauchamp J, Herbig J, Gutmann R, Hansel A (2008) On the use of Tedlar® bags for breath-gas sampling and analysis. J Breath Res 2:046001

59. Kwak J et al (2014) Evaluation of bio-VOC sampler for analysis of volatile organic compounds in exhaled breath. Meta 4:879

60. Phillips M et al (2013) Detection of volatile biomarkers of therapeutic radiation in breath. J Breath Res 7:036002

61. Phillips M et al (2013) Detection of an extended human volatome with comprehensive two-dimensional gas chromatography time-of-flight mass spectrometry. PLoS One 8:e75274

62. Phillips M (1997) Method for the collection and assay of volatile organic compounds in breath. Anal Biochem 247:272–278

63. White IR, Fowler SJ (2019) Capturing and storing exhaled breath for offline analysis. In: Pennazza G, Santonico M (eds) Breath analysis. Academic Press, pp 13–31

64. Ratiu IA, Ligor T, Bocos-Bintintan V, Mayhew CA, Buszewski B (2020) Volatile organic compounds in exhaled breath as fingerprints of lung cancer, asthma and COPD. J Clin Med 10: 1–41

65. Di Gilio A et al (2020) Breath analysis: comparison among methodological approaches for breath sampling. Molecules 25:5823

66. Belizário JE, Faintuch J, Malpartida MG (2021) Breath biopsy and discovery of exclusive volatile organic compounds for diagnosis of infectious diseases. Front Cell Infect Microbiol 10:564194

67. Shende P, Vaidya J, Kulkarni YA, Gaud RS (2017) Systematic approaches for biodiagnostics using exhaled air. J Control Release 268:282–295

68. Caldeira M et al (2012) Allergic asthma exhaled breath metabolome: a challenge for comprehensive two-dimensional gas chromatography. J Chromatogr A 1254:87–97

69. Zanella D, Focant J-F, Hill JE, Stefanuto P-H (2020) Comprehensive gas chromatography-mass spectrometry. In: Beauchamp J, Davis C, Pleil J (eds) Breathborne biomarkers and the human volatilome. Elsevier, pp 239–251

70. Forsythe JC et al (2017) Integrating comprehensive two-dimensional gas chromatography and downhole fluid analysis to validate a spill-fill sequence of reservoirs with variations of biodegradation, water washing and thermal maturity. Fuel 191:538–554

71. de Carvalho F, Rocha W, Schantz MM, Sheen DA, Chu PM, Lippa KA (2017) Unsupervised classification of petroleum certified reference materials and other fuels by chemometric analysis of gas chromatography-mass spectrometry data. Fuel 197:248–258

72. Smith JS, Thakur RA (2010) Mass spectrometry. In: Suzanne Nielsen S (ed) Food analysis. Springer, pp 457–470

73. Li DX, Gan L, Bronja A, Schmitz OJ (2015) Gas chromatography coupled to atmospheric pressure ionization mass spectrometry (GC-API-MS): review. Anal Chim Acta 891:43–61

74. Beale DJ et al (2018) Review of recent developments in GC-MS approaches to metabolomics-based research. Metabolomics 14:152

75. Neerincx AH et al (2016) Detection of Staphylococcus aureus in cystic fibrosis patients using breath VOC profiles. J Breath Res 10:046014

76. Grabowska-Polanowska B, Skowron M, Miarka P, Pietrzycka A, Śliwka I (2017) The application of chromatographic breath analysis in the search of volatile biomarkers of chronic kidney disease and coexisting type 2 diabetes mellitus. J Chromatogr B 1060:103–110

77. Pizzini A et al (2018) Analysis of volatile organic compounds in the breath of patients with stable or acute exacerbation of chronic obstructive pulmonary disease. J Breath Res 12:036002

78. Smolinska A et al (2014) Profiling of volatile organic compounds in exhaled breath as a strategy to find early predictive signatures of asthma in children. PLoS One 9:e95668

79. Woolfenden E (2021) Thermal desorption gas chromatography. In: Poole CF (ed) Gas chromatography. Elsevier, pp 267–323

80. Dharmawardana N, Woods C, Watson DI, Yazbeck R, Ooi EH (2020) A review of breath analysis techniques in head and neck cancer. Oral Oncol 104:104654
81. Sun X, Shao K, Wang T (2016) Detection of volatile organic compounds (VOCs) from exhaled breath as noninvasive methods for cancer diagnosis. Anal Bioanal Chem 408:2759–2780
82. Nerín C, Salafranca J, Aznar M, Batlle R (2009) Critical review on recent developments in solventless techniques for extraction of analytes. Anal Bioanal Chem 393:809–833
83. Španěl P, Smith D (2020) Quantification of volatile metabolites in exhaled breath by selected ion flow tube mass spectrometry, SIFT-MS. Clin Mass Spectrom 16:18
84. Alkhouri N et al (2014) Analysis of breath volatile organic compounds as a noninvasive tool to diagnose nonalcoholic fatty liver disease in children. Eur J Gastroenterol Hepatol 26:82–87
85. Boshier PR et al (2015) Breath metabolite response to major upper gastrointestinal surgery. J Surg Res 193:704–712
86. Dryahina K et al (2017) Pentane and other volatile organic compounds, including carboxylic acids, in the exhaled breath of patients with Crohn's disease and ulcerative colitis. J Breath Res 12:016002
87. Wang MH et al (2016) Use of a least absolute shrinkage and selection operator (LASSO) model to selected ion flow tube mass spectrometry (SIFT-MS) analysis of exhaled breath to predict the efficacy of dialysis: a pilot study. J Breath Res 10:046004
88. Eng K et al (2015) Analysis of breath volatile organic compounds in children with chronic liver disease compared to healthy controls. J Breath Res 9:026002
89. Hamilton BK et al (2019) Breath analysis in gastrointestinal graft-versus-host disease after allogeneic hematopoietic cell transplantation. Blood Adv 3:2732
90. Greiter MB et al (2010) Differences in exhaled gas profiles between patients with type 2 diabetes and healthy controls. Diabetes Technol Ther 12:455–463
91. Liangou A et al (2021) A method for the identification of COVID-19 biomarkers in human breath using proton transfer reaction time-of-flight mass spectrometry. EClinicalMedicine 42
92. Smith D, Španěl P, Herbig J, Beauchamp J (2014) Mass spectrometry for real-time quantitative breath analysis. J Breath Res 8:027101
93. Singh KD et al (2018) Translating secondary electrospray ionization–high-resolution mass spectrometry to the clinical environment. J Breath Res 12:027113
94. Casas-Ferreira AM, del Nogal-Sánchez M, Pérez-Pavón JL, Moreno-Cordero B (2019) Non-separative mass spectrometry methods for non-invasive medical diagnostics based on volatile organic compounds: a review. Anal Chim Acta 1045:10–22
95. Smolinska A et al (2014) Current breathomics – a review on data pre-processing techniques and machine learning in metabolomics breath analysis. J Breath Res 8:027105
96. Stavropoulos G, Salman D, Alkhalifah Y, van Schooten F-J, Smolinska A (2020) Preprocessing and analysis of volatilome data. In: Beauchamp J, Davis C, Pleil J (eds) Breathborne biomarkers and the human volatilome. Elsevier, pp 633–647
97. Sola Martínez RA et al (2020) Data preprocessing workflow for exhaled breath analysis by GC/MS using open sources. Sci Rep 10:22008
98. Bos LDJ et al (2014) A simple breath sampling method in intubated and mechanically ventilated critically ill patients. Respir Physiol Neurobiol 191:67–74
99. Van Oort PMP et al (2017) Exhaled breath metabolomics for the diagnosis of pneumonia in intubated and mechanically-ventilated intensive care unit (ICU)-patients. Int J Mol Sci 18:449
100. Koureas M et al (2021) Comparison of targeted and untargeted approaches in breath analysis for the discrimination of lung cancer from benign pulmonary diseases and healthy persons. Molecules 26:2609
101. Phillips M, Cataneo RN, Lebauer C, Mundada M, Saunders C (2017) Breath mass ion biomarkers of breast cancer. J Breath Res 11:016004
102. Smith CA, Want EJ, O'Maille G, Abagyan R, Siuzdak G (2006) XCMS: processing mass spectrometry data for metabolite profiling using nonlinear peak alignment, matching, and identification. Anal Chem 78:779–787

103. Barnes S (2020) Overview of experimental methods and study design in metabolomics, and statistical and pathway considerations. Methods Mol Biol 2104:1–10
104. Domingo-Almenara X et al (2016) eRah: a computational tool integrating spectral deconvolution and alignment with quantification and identification of metabolites in GC/MS-based metabolomics. Anal Chem 88:9821–9829
105. Ren S, Hinzman AA, Kang EL, Szczesniak RD, Lu LJ (2015) Computational and statistical analysis of metabolomics data. Metabolomics 11:1492–1513
106. Domingo-Almenara X, Siuzdak G (2020) Metabolomics data processing using XCMS. Methods Mol Biol 2104:11–24
107. Lommen A (2009) MetAlign: interface-driven, versatile metabolomics tool for hyphenated full-scan mass spectrometry data preprocessing. Anal Chem 81:3079–3086
108. Domingo-Almenara X (2015) An introduction to erah package. J Chromatogr A 1409:226–233
109. van Mastrigt E, de Jongste JC, Pijnenburg MW (2015) The analysis of volatile organic compounds in exhaled breath and biomarkers in exhaled breath condensate in children – clinical tools or scientific toys? Clin Exp Allergy 45:1170–1188
110. Broadhurst DI, Kell DB (2007) Statistical strategies for avoiding false discoveries in metabolomics and related experiments. Metabolomics 2:171–196
111. Hastie T, Tibshirani R, Friedman J (2009) The elements of statistical learning: data mining, inference, and prediction. Springer
112. Leopold JH et al (2015) Comparison of classification methods in breath analysis by electronic nose. J Breath Res 9:046002
113. Paleczek A, Rydosz A (2022) Review of the algorithms used in exhaled breath analysis for the detection of diabetes. J Breath Res 16:026003
114. Peng J, Jury EC, Dönnes P, Ciurtin C (2021) Machine learning techniques for personalised medicine approaches in immune-mediated chronic inflammatory diseases: applications and challenges. Front Pharmacol 12:2667
115. Huang, J., Ma, S. & Zhang, C.-H. The iterated Lasso for high-dimensional logistic regression. (2008)
116. Brereton RG, Lloyd GR (2014) Partial least squares discriminant analysis: taking the magic away. J Chemom 28:213–225
117. Breiman L (2001) Random forests. Mach Learn 45:5–32
118. Amato F et al (2013) Artificial neural networks in medical diagnosis. J Appl Biomed 11:47–58
119. Lê Cao K-A, Boitard S, Besse P (2011) Sparse PLS discriminant analysis: biologically relevant feature selection and graphical displays for multiclass problems. BMC Bioinformatics 12:253
120. Zhou M et al (2019) Rapid breath analysis for acute respiratory distress syndrome diagnostics using a portable two-dimensional gas chromatography device. Anal Bioanal Chem 411:6435
121. Monasta L et al (2017) Inflammatory bowel disease and patterns of volatile organic compounds in the exhaled breath of children: a case-control study using ion molecule reaction-mass spectrometry. PLoS One 12:e0184118
122. Beccaria M et al (2018) Exhaled human breath analysis in active pulmonary tuberculosis diagnostics by comprehensive gas chromatography-mass spectrometry and chemometric techniques. J Breath Res 13:016005
123. Van Berkel JJBN et al (2008) Development of accurate classification method based on the analysis of volatile organic compounds from human exhaled air. J Chromatogr B 861:101–107
124. Gashimova E et al (2021) Exhaled breath analysis using GC-MS and an electronic nose for lung cancer diagnostics. Anal Methods 13:4793–4804
125. Rudnicka J, Kowalkowski T, Buszewski B (2019) Searching for selected VOCs in human breath samples as potential markers of lung cancer. Lung Cancer 135:123–129
126. Szymańska E, Saccenti E, Smilde AK, Westerhuis JA (2012) Double-check: validation of diagnostic statistics for PLS-DA models in metabolomics studies. Metabolomics 8:3–16

127. Lee LC, Liong C-Y, Jemain AA (2018) Partial least squares-discriminant analysis (PLS-DA) for classification of high-dimensional (HD) data: a review of contemporary practice strategies and knowledge gaps. Analyst 143:3526–3539

Ion Mobility Spectrometry in Clinical and Emergency Setting: Research and Potential Applications

Dorota M. Ruszkiewicz, Austin Meister, and Renelle Myers

Contents

Abstract Interest in the use of GC-IMS for the detection of volatiles has seen a rapid expansion over the last decade. The following chapter will focus on classical GC-IMS and its research applications in the potential for diagnosis, rapid testing and biomarker discovery, with an emphasis on breath testing. Breath analysis via GC-IMS has enormous potential in many clinical areas including screening for pulmonary diseases, infections and toxins. Due to the technology's small footprint, robustness in various environments and ease of use, there have been many studies looking at its potential utility in the clinical field, including its use as a screening tool for SARS-CoV-2 infections. There remain limitations to the device usage and data processing which are discussed throughout the chapter. An introduction to its

————————————

D. M. Ruszkiewicz and A. Meister
Department of Integrative Oncology, BC Cancer Research Institute, Vancouver, BC, Canada

R. Myers (✉)
Department of Integrative Oncology, BC Cancer Research Institute, Vancouver, BC, Canada

Department of Medicine, University of British Columbia, Vancouver, BC, Canada
e-mail: renelle.myers@vch.ca

fundamentals, standardisation, breath collection methods and active areas of research and development will be covered.

Abbreviations

AI	Artificial intelligence
AUROC	Area under the receiver operator curve
CBRN	Chemical, biological, radiation and nuclear
CI	Confidence interval
CPAP	Continuous positive airway pressure
DMS	Differential mobility spectrometry
FAIMS	Field asymmetric waveform ion mobility spectrometry
FDA	Federal drug administration
FID	Flame ionising detector
FTX	Field technical exercise
GC	Gas chromatography
HC	Healthy controls
HEPA	High-efficiency particulate air
HS	Headspace
IMS	Ion mobility spectrometry
KD	Klinikum Dortmund
MCC	Multi-capillary column
MS	Mass spectrometry
ms	Milliseconds
PDAC	Pancreatic ductal adenocarcinoma
ppb	Parts per billion
ppbV	Parts per billion by volume
ppt	Parts per trillion
pptV	Parts per trillion by volume
PTR	Proton transfer reaction
RI	Respiratory tract infection
RIE	Royal infirmary of Edinburgh
RIP	Reactant ion peak
ROC	Receiver operating characteristic curve
SIFT	Selected ion flow tube
VOC	Volatile organic compound
μ-TD	Micro thermal desorption

1 Introduction

Ion mobility spectrometry (IMS) is a trace gas detection technique, developed through the 1960s and 1970s, now widely used commercially for security, military and industrial process applications. One of the most widely used applications is the use of IMS in airport security for the detection of explosives and illicit drugs. It has also been an important tool for chemical warfare detection in military applications [1, 2]. The technology offers multiple benefits including high sensitivity (ppb/ppt trace detection), portability, ease of use, relatively low cost and detection times on the milliseconds scale. By coupling an IMS to a chromatographic or multicapillary column (GC/MCC), the analysis of complex matrices was enabled; including biological samples, allowing the technology to merge into the clinical research field. This technique combines the ultra-sensitivity of the device with the high efficiency of GC – separation, improving selectivity and providing an additional information dimension for compound characterisation and identification. There are currently several types of IMS, which differ in the way they identify ions. The most important among them are classical time-of-flight IMS, but other methods such as differential mobility spectrometry (DMS) or high-field asymmetric waveform ion mobility spectrometers (FAIMS) are also available. However, their main use is exploited as a mobility filter, when coupled to other detectors such as mass spectrometers. Commercially available GC-IMS/MCC-IMS systems now offer a platform for the analysis of volatiles from bacterial cultures, blood, urine, saliva and breath, promising bedside testing. Research is ongoing with this application for diagnostic and rapid screening in community settings. This device may bridge the gap between current mass spectrometry platforms and clinical needs. Current platforms for analysis of Volatile Organic Compounds (VOCs) are either laboratory-based and resource intensive such as mass-spectrometric methods (GC, GCxGC – MS) and stand-alone Proton Transfer Reaction Mass Spectrometry (PTR-MS), or, point-of-care but less selective sensors/sensor arrays (metal oxides, semiconductor metal oxides, conducting polymers or functionalised nanoparticles). It would be cost, labour and workflow prohibitive to deploy large numbers of mass spectrometers for point-of-care, large cohort settings. Conversely, while sensor arrays are often cited as providing high-discrimination power between cohorts they do not identify biomarkers; their data is difficult to verify and cannot really be used in synoptic or meta-studies. Chemically specific sensors can be used most effectively for targeted analysis, exhaled NO being a case-in-point; however, a different sensor will be needed for each potential analytical target; not a sustainable solution. GC/MCC-IMS devices can easily be adapted for multiple and newly developed applications. In the area of rapid testing of VOCs, it is breath analysis that drew the most interest in recent years, thanks to its many advantages. It is the least invasive of all sampling techniques, the sample is easy to obtain and unlimited in amount. It is not a surprise then that a large part of the clinical studies with GC/MCC-IMS focus on the development of such a test. In this chapter, we will strongly focus on such applications, specifically with GC-IMS.

The chemical information obtained from the GC-IMS generated data: ion intensity, retention time, and drift time allow for both targeted and untargeted analysis in research settings. For example, in biomarker discovery, studies on drug kinetics and metabolomic profiling by GC-IMS are becoming a powerful tool due to the use of modern Artificial Intelligence (AI) technology. However, when it comes to identification there are still challenges to overcome. Currently, the identification of compounds is based on drift time and retention times libraries, which are limited, and the information provided do not include structural information. Though, there is ongoing development in this research field.

Within this chapter, we will focus on the classical GC-IMS, and its applications in diagnosis, rapid testing and biomarker discovery, with an emphasis on breath testing and will provide some recent examples of research and development in this area.

2 Ion Mobility Spectrometry Fundamentals

Ion mobility spectrometry is a gas phase detection technique that uses differences in ion velocities in an electrostatic field as a means to characterise and separate compounds typically under atmospheric pressure. The fundamentals of IMS date from the late nineteenth century with Thomson's studies on ionised air via X-ray radiation. The discovery was followed by further explorations on ion behaviour in the gas phase, development of a drift tube and apparatus that ultimately reached its modern form in the 1970s [3]. The basis of the technique lay in the proportional relationship between velocity of ions with an electric field, and mobility constant K, which is unique for an ion (Eq. 1).

$$V_d = KE \tag{1}$$

where: V_d is ion drift velocity in cm s^{-1}; K is mobility in cm^2 V^{-1} s^{-1}; E is electric field strength in V cm^{-1}.

Ions have different mobilities under a constant electric field due to differences in their structures. A version of the Mason–Schamp equation (Eq. 2) describes mobility in relation to the structural parameters of the species [4].

$$K = \frac{3ze}{16N} \times \sqrt{\frac{2\pi}{\mu k_B T_{\text{eff}}}} \times \frac{1}{\Omega} \tag{2}$$

where: z is an ion charge, e is an electronic charge, N is gas density number, μ is reduced mass of ion, Ω is cross-sectional area of ion cluster, T_{eff} is effective temperature, k_B is Boltzmann constant; and $= \frac{mM}{m+M}$, where m is mass of the ion and M is the mass of drift gas molecules.

Note: If the ratio of the electric field strength (E) to gas number density (N) exceeds the low-field limit ($\frac{E}{N} > 2$ Townsend) such as in DMS, which oscillates

between high and low electric fields, then the gas phase mobility of an ion, K, is no longer independent of the electric field gradient and additional laws apply [3].

IMS measures the drift time (t_D); the time it takes for the ion to traverse through a drift cell (from the ion shutter to the Faraday plate detector) of known length (L) and in linear fashion under a uniform electric field. The time is inversely proportional to the ion velocity under the applied conditions; and it is one of the measurements used to characterise the ion. The typical time for an ion swarm to travel through the drift tube is on the order of milliseconds.

$$V_d = \frac{L}{t_D} \tag{3}$$

However, this value only represents the specific conditions used. The velocity of the ion is certainly mostly affected by the field but pressure and temperature also play an important role; therefore, the use of t_D values has limited power in transferring the results across different devices.[1]

To reduce the effect of the instrument conditions, researchers often report the relative drift time (t_{Dr}), which provides its normalised value towards the drift time of the reactant ion peak (RIP), protonated water H + $(H_2O)_n$ cluster in most cases (Eq. 4).

$$t_{Dr} = \frac{t_{D(i)}}{t_{D(RIP)}} \tag{4}$$

However, the most accurate and universal way used to characterise/identify ions is by using the reduced form of the mobility constant K_0. This value is used in most of the existing mobility data bases, and is in principle transferable. The K_0 coefficient normalises the constant K to the standard conditions of temperature and pressure, by using the expression shown in Eq. 5.

$$K_0 = K \times \frac{273.15}{T} \times \frac{P}{760} \tag{5}$$

where: T is temperature and P is the pressure of the buffer gas.

The operational schematic of a typical IMS system is shown in Fig. 1.

Another important aspect of working with IMS-based systems is understanding the underlying ionisation processes, which lie at the heart of the technique. This includes the ionisation potential of the analytes and the ionisation type and regime used.

---

[1]Note: The extensive review on the studies of those effects and the IMS principles in general, its history and applications and future perspective can be found in "Ion Mobility Spectrometry" by G.A. Eiceman, Z. Karpas, and Herbert H. Hill, Jr. [5] an important and complete reference on GC-IMS technique.
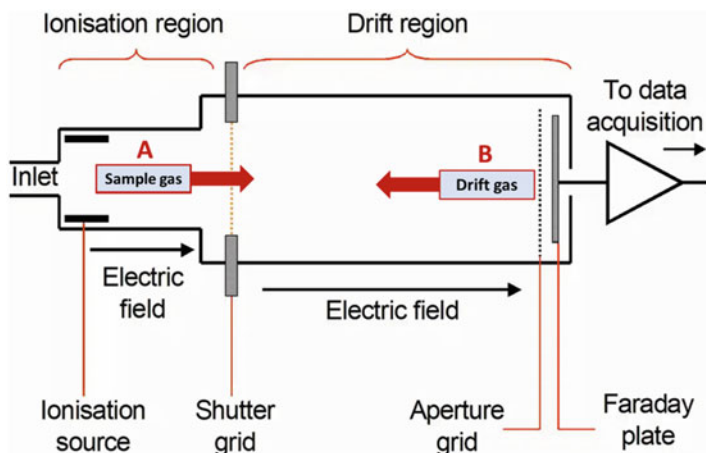
Fig. 1 Schematic of the IMS system working principle, where the sample is introduced into an ionisation region to become charged mainly via proton-transfer reactions (PTR) process and moved towards a shutter grid, which will regularly inject an ion swarm into the drift region. In this region, the separation of the ions takes place, on the basis of ion differences in their mobilities under the electric field, when passing through a neutral buffer gas, also called drift gas. The aperture grid focuses the ions as they move towards the detector (Faraday plate), producing an electric signal which is then acquired and provides the results in a form of the IMS spectrum (See Fig. 2)

In IMS common ionisation sources include beta emitters: Nickel (^{63}Ni) or Tritium (^{3}H), non-radioactive sources: corona discharge, photo- and electrospray-ionisation are also available. In pure nitrogen or air (most common transport gases used in IMS), the energy emitted from the radioactive source generates positively charged nitrogen cation radicals [4] from reactions with thermalised electrons. The ionised buffer gas (nitrogen or air) then reacts with traces of water present in the gas at and through a series of ion–molecule reactions, reactant ion species such as $H + (H_2O)_n$ (with up to six water molecules, n, in the typical atmosphere) are formed. Finally, the ionisation of the analyte molecules (M) happens in the ionisation region of the IMS via ion-molecule reactions based on proton transfer and driven by the affinity of the compound to accept the proton. The proton affinity of water is equal to 691 ± 3 kJ mol^{-1}, so molecules with higher potential will be ionised and form the product ion (Eq. 6).

$$H^+(H_2O)_n + M = H^+M(H_2O)_{n-1} + (H_2O) \tag{6}$$
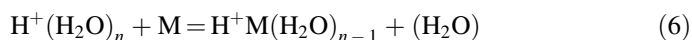
If the concentration of the analyte is high enough, higher clusters such as dimers or trimers can be formed, via the reaction shown in Eq. 7.

$$H^+M(H_2O)_{n-1} + M = H^+M_2(H_2O)_{n-2} + (H_2O) \tag{7}$$
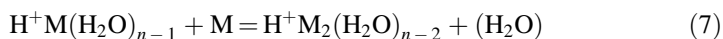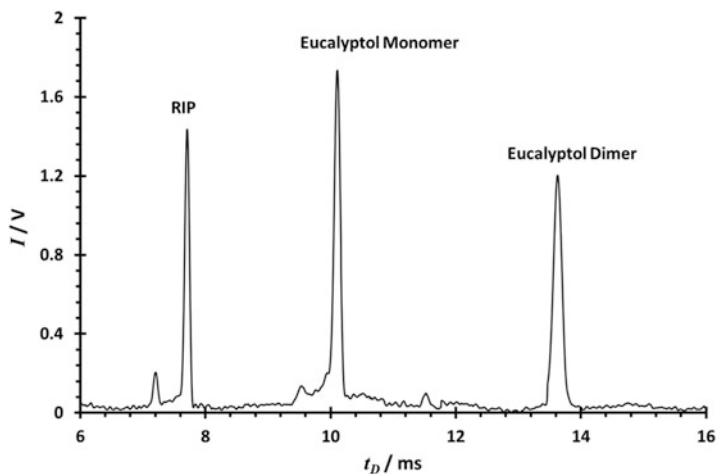
Fig. 2 Example of typical ion mobility spectrum with reactant ion peak (RIP) present 7.7 ms drift time, and product ions of eucalyptol: monomer ion at 10.1 ms and the dimer peak at further drift time of 13.6 ms. Traces of ammonia present in the atmosphere are also detected (peak to the left of the RIP), often seen in the IMS systems

Example of a typical IMS spectrum, showing the RIP and product ions: monomer and dimer of eucalyptol in this case, is shown in Fig. 2.

It needs to be understood that in complex systems, there may be competitive ionisation happening at the same time between other compounds or impurities present; therefore, pre-separation is essential for the analysis of such matrixes. To fulfill its application potential as a fast clinical screening tool, the systems used in clinical research have been interfaced with chromatographic columns (GC-IMS), which provide an additional dimension to the analysis and compound characterisation via retention times (Fig. 3).

As explained above, the parameters such as temperature and pressure affect the velocity of the ions and must be carefully monitored on a daily basis as a part of quality assurance procedures. The humidity level in the system also has an ability to alter the results, and although the influence of humidity has been known for decades, it has not been largely documented. What is known is that changes in water levels may affect sensitivity, quantification of an analyte and may alter ion composition. The best way to tackle this challenge is to monitor its level or incorporate changing/conditioning moisture filters on a regular basis, in accordance with manufacturer specifications. Humidity commonly causes changes in RIP drift times and its intensity as well as peak broadening and in extreme cases complete loss of sensitivity in the system. Monitoring of the RIP signal is essential for the successful use of IMS technology.
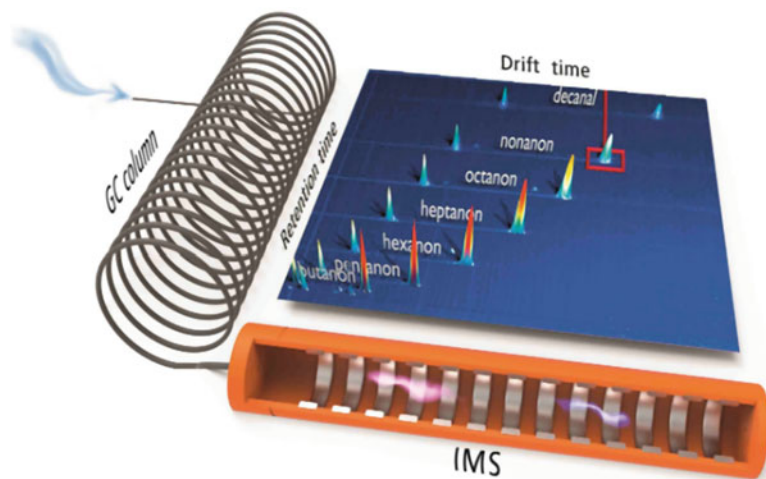
Fig. 3 Example of 3D GC-IMS chromatograph, obtained from analysing a homologous mixture of ketones, where separation in both directions: chromatographic elution (retention times in seconds) and mobility (drift times in ms) is highlighted, used to characterise an analyte. On the Z axis, the intensity is shown (V) used for quantification. Copyrights: G.A.S Dortmund

3 Sampling Methods

Rapid analysis with GC-IMS devices has the potential to be revolutionary for clinical practice. One of the most important aspects is the sample collection process. Ideally, sampling is reproducible, fast, easy to use by both patient and operator and above all safe. Volatiles are complex matrixes and proper, consistent sample collection is paramount. The amount of an analyte is often present at part per billion (ppb) or part per trillion (ppt) levels; therefore, any slight change in the system can potentially introduce significant error. There is also active chemistry with absorption, and reactions along the entire sampler device, as well as artefacts that can be introduced during collection. A comprehensive review on all physicochemical processes happening during the transfer of biochemical signals from the body to an analyser and details on VOC sampling can be found in the ion mobility spectrometry section of "Breath borne Biomarkers and the Human Volatilome" (Second Edition) [6].

Many sampling techniques commonly used for the analysis of VOCs can be adapted for use with GC-IMS. However, since the main advantage of GC-IMS devices comes from rapid detection, direct sample introduction methods are commonly implemented without further enhancement. For solid and liquid samples such as urine, blood, sputum or microbiological analysis, headspace (HS) sampling is most widely used. Samples are either transferred into an inert, thermally resistant container and subsequently agitated and heated prior to analysis to release volatiles or a volume of headspace is collected directly from above the sample without

Fig. 4 Commonly used with IMS sampling devices: (**a**) FlavourSpec® (G.A.S/Imspex), (**b**) polymer bags, (**c**) Haldane sampler, (**d**) Loccioni® sampler with CO_2 monitor, (**e**) direct online sampling, (**f**) SpiroScout® (B&S Analytics)

additional heating [7–11]. This technique is commonly used in in-vitro bacterial studies. The collected volume of HS is then either injected or withdrawn into the analyser. Commercially available HS autosamplers are now available, for example, Flavourspec® from G.A.S Dortmund/IMSPEX (Fig. 4a), which allows for faster sample processing. For gas analysis such as breath, both online and offline approaches are common. Online techniques are most often used with disposable mouthpieces and a heated transfer line, connected directly to the instrument. In many cases additional sensors are implemented such as CO_2 sensors, allowing for the collection of the end-tidal portion of breath (SpiroScout spirometer from B&S Analytics or Loccioni® Sampler – See Fig. 4d, f) [12]. These methods however are often fitted with either pre-built or attached bio-filters to protect against infectious pathogens, reducing the risk of person-to-person transmission. The use of a bio-filter may introduce condensation and adsorption artefacts into analysis. This has been demonstrated recently with GC-MS studies by Myers et al. [13]. A similar effect was also observed within the breath standardisation study by GC-IMS, using peppermint oil. In the group of participants, where a High-Efficiency Particulate Air (HEPA) filter was used the number of compounds detected from ingestion of the capsule was also reduced [14]. BreathSpec from G.A.S/IMSPEX have an option for direct sampling and is not employed with a filter, but has the option to attach one into the sampling line (Fig. 4e). Offline techniques have gained much more popularity recently, especially during the emergence of the COVID-19 pandemic. With such approaches, the risk of patient-to-patient transmission is greatly minimised. The two commonly used methods for sample collection are: polymer bags and Haldane-type samplers (Fig. 4b, c). The bags are hermetically sealed and fitted with a valve, allowing for the bag to be filled in with breath, using a required volume. The sample is then drawn into an analyser or adsorbent tube. The bags are made from different

materials (Tedlar$^®$ (Dupont™), Nalophan$^®$, Cali-5-Bond™, FlexFoil$^®$ and Teflon$^®$, ALTEF$^®$) which may introduce contaminant VOCs and are prone to condensation artefacts; they also have different storage performance [15]. It is important to note at this stage that with this type of sampling technique, mixed exhaled breath is collected. Sometimes, a practice of exhaling the first part of the breath into the room, followed by exhalation of the remaining part into the bag, is applied, to concentrate the end-tidal portion of breath. This, however, could reduce the reproducibility of the sampling techniques, and studies standardising this approach are non-existent. An advantage of using polymer bags is their simplicity and relatively low cost. The bags can be reused in theory, but re-conditioning protocols, especially in the era of COVID-19, would have to be carefully studied first. The second type of offline sampler, known as Haldane-type samplers, captures a small volume of end-tidal breath. A participant exhales through a small inert tube (10–20 cm^3), fitted with one-way valves, to completely empty their lungs. The last part of the breath (1–5 cm^3) is captured within the tube and withdrawn and injected into the analyser. The sampler is cheap and disposable but its main limitation is the small volume of sample and the possibility of condensation artefacts.

Regardless of the sampling method used for the analysis of biological matrixes with IMS, due to the small volume of sample required to provide fast analysis, it is extremely rare to see more than 100 features detected in a sample. This limits the detectable concentration levels of compounds to tens of ppbV, despite instrument sensitivity. Therefore, depending on the requirement of the analysis it may be worth considering the use of the adsorption techniques, such as adsorption tubes or needle traps, followed by thermal desorption.

The use of needle-trap and GC-IMS was shown with controlled study of breath, demonstrating that the method can be used for appropriate quantification when the adsorbent and the sample volume are adapted properly to the required concentration range of the targeted compounds of interest and humidity of the sample. Depending on the sample volume used the detectable concentration levels were reduced to: pptV with 20 cm^3 and low ppbV for 10 cm^3 of sample volume [16]. Enhancement using adsorbent tubes with GC-IMS is also being explored, for example, with the use of a µ-Thermal Desorption system (µ-TD) developed for use with GC-IMS systems from AIRSENSE Analytics. The power of the enhancement delivered is truly impressive, with full analysis times below 20 min and 100 cm^3 of collected sample (Fig. 5).

Each method has its advantages and disadvantages, and one size will most likely not fit all. Regardless of the method, for the technique to find a place in routine clinical use, sampling procedures will need to be standardised and quality control measures developed. In the next section, we will look at work done with IMS systems in this context.
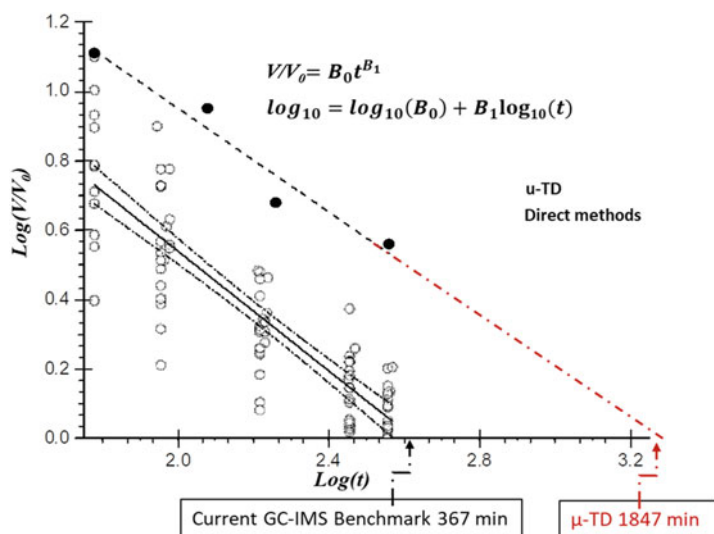
Fig. 5 Logarithmic plots of the eucalyptol washout curves of the fold-change change in peak volume versus time, for current benchmark, based on GC-IMS studies from three different centres, two direct analysis methods versus sampling using 100 cm³ volume of breath and application of μTD

3.1 Breath Sampling Standardisation

The need for standardisation of breath sampling approaches has been highlighted by the European Respiratory Society and described within recommendation for breath analysis [17]. This need has also been realised by the breath research community, resulting in the formation of the "Peppermint Initiative", which aims to provide standardised methods that allow comparison of breath sampling techniques in an evidential manner [18]. The protocol has been developed using an MCC-IMS system. So far, 17 partners from eight countries have joined the effort to run the experiment, using eight analytical techniques. The proposed experiment involves ingesting a peppermint oil capsule (200 mg, Boots, UK) and collecting of series of breath samples at baseline and at +60, +90, +165, +285 and +360 min post capsule ingestion. The teams seek to establish a current benchmark value – the time for the compound measurement to return to baseline levels – for each comparable analytical technique, as a measure of sensitivity of the analytical process. The linear regression analysis of the washout profile also allows for the reproducibility of the sampling approach to be evaluated and the analytical process monitored. So far, the results from three analytical techniques and various sampling methods have been published: GC-MS, PTR/SIFT-MS and most recently with GC-IMS [14, 18, 19]. Within the GC-IMS studies, a single IMS system has been used by three international teams – BreathSpec G.A.S/IMSPEX – with two sampling methods: offline Haldane tube and online sampling with Loccioni sampler. An average extrapolated from the regression
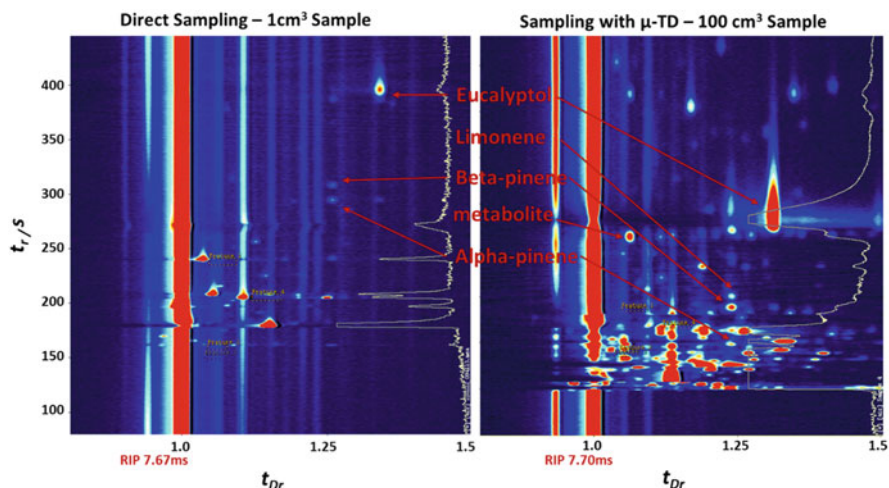
Fig. 6 A cut-out section of GC-IMS contour plots of breath samples collected 60 min post-peppermint oil digestion, using direct (1 cm^3 volume, left) and μ-TD sampling (100 cm^3 volume, right) techniques, where t_r is the retention time and t_{Dr} is relative drift time. The graph shows impressive enhancement in the number of features detected with the pre-concentration method

analysis time, taken for exhaled eucalyptol (the main constituent of the peppermint oil capsule) level to return to baseline was 429 ± 62 min (±95% confidence-interval). The Benchmark value, set on the lower 95% Ci band, was 367 min. This means that, if such time cannot be reached, the system operates below the current standard, and the analyst needs to seek improvements. On the other hand, if higher values of time are reached, then it should certainly be reported, for continuous improvement of the technique. The performance of the μTD-GC-IMS for breath analysis is currently being studied, and preliminary results demonstrate the baseline time for the eucalyptol washout to be over 1,800 min, an enhancement of nearly five times, what is comparable with results obtained with GC-MS using 1 L of sample volume (Fig. 5).

Moreover, the number of peppermint-related features detected also demonstrates significant improvement. For example, when sampling with a Loccioni sampler, on average two to three peppermint-related compounds were detected, most likely due to HEPA filter involvement. All five targeted compounds: eucalyptol, limonene, alpha and beta pinene and eucalyptol metabolite, and in some cases their dimer peaks are seen (Fig. 6).

The peppermint experiment can be used to evaluate breath samplers, but it can be implemented within routine quality control protocols for monitoring system performance and as a means to train clinical staff with sampling procedures. The ability to measure the consistency of sampling proficiency is important for international multicentre trials. It provides an excellent layer of quality control and especially in clinical applications where chemists are not on-site.

4   Applications

Due to the small footprint, ease of use and fast analysis time of IMSs, they make for ideal point-of-care devices that have the potential to be added to any clinical practice. They are also extremely simple to operate and sample introduction methods can be automated for faster processing. IMS devices can also be programmed with automated methods that give simple positive or negative results back to the operator without the need for interpretation by trained staff. Over the past 5 years, there have been three main areas of clinical and research usage for GC-IMS: (a) the determination of drugs and drug volatile metabolites; (b) rapid detection for medical diagnoses; and (c) identification of micro-organisms with in-vitro studies.

4.1   *CBRN and Mass Casualty Triage*

A promising development is being made in utilising GC-IMS in fields where fast diagnostic, bed side and field testing are most required. This includes toxicology and forensic testing, but also triage in mass casualty incidents, such as those with the use of CBRN (chemical, biological, radiological, nuclear) agents.

One such example was demonstrated in a large European Union Horizon 2020 project called Toxi-triage (http://toxi-triage.eu). Eighteen partners from seven countries developed technologies and procedures that were integrated to provide situational awareness at the level of an individual casualty for a mass casualty event, secondary to a CBRN agent. One of the goals was to develop a biomarkers database and test preparedness of dual-use devices which would have the capacity to assist doctor's decision-making but also being able to identify VOCs indicative of CBRN exposure, in the event of an attack. Within this chapter, some detailed examples of the results from those studies are provided, which demonstrated high compatibility of the GC-IMS with the needs of the medical emergency services, targeted toxins detection and untargeted biomarker discovery.

One of the clinical applications demonstrated in the project was on the detection of toxic alcohols, such as methanol. Diagnosing methanol poisoning is difficult, since the presentation is similar to intoxication with ethanol, and laboratory analyses for toxic alcohols are frequently unavailable in smaller medical centres or take hours to get results secondary to samples being sent to reference laboratories [20, 21]. With clinical suspicion of toxic alcohol poisoning, but no proof of exposure from blood sample analysis, patients must be treated with an expensive antidote (fomepizole) or an antidote with complex dosing regimens and a high risk of adverse reactions (ethanol) until the diagnosis can be confirmed [22]. This is a major issue, especially in developing countries, which report the highest number of deadly methanol poisonings. GC-IMS devices were set in a University Hospital in Oslo (Norway) and in a General Hospital in Jakarta (Indonesia). A sample of breath was collected (volume 0.5 cm^3) and analysed with a 10 min long analysis method
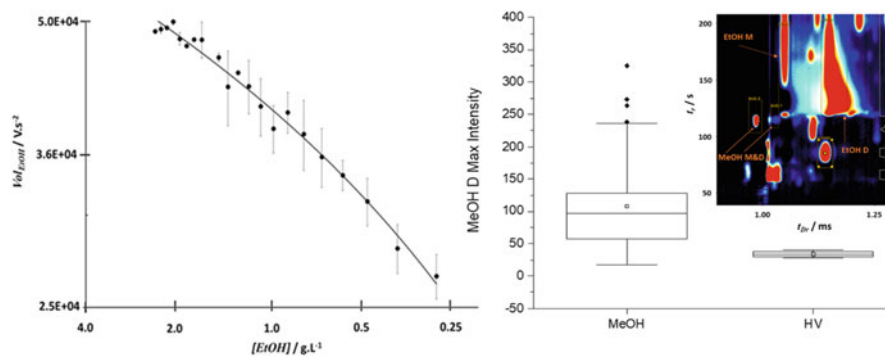
Fig. 7 Left: ethanol breath/blood level correlation obtained from 19 ethanol intoxicated participants. Right: example of GC-IMS chromatograph showing detection of methanol in breath in presence of elevated ethanol level

[23]. Simultaneous blood samples were collected and sent for analysis in a reference laboratory. Thirty-seven participants were recruited, 19 from participants with elevated ethanol levels and 18 from patients with suspected methanol poisoning. High correlation between breath and blood ethanol levels was demonstrated, within 0.3 and 2 g L^{-1} concentration range (Fig. 7, left), and elevated methanol levels were observed in all suspected methanol poisoned patients (Fig. 7, right).

The methanol levels in blood were below the detection limits of the GC-FID instrument used in the reference laboratory, which was at 0.2 g L^{-1}. The results showed greater sensitivity of the IMS for methanol detection from breath, in comparison to the current clinical approach, even in samples where the methanol level was below the cut-off on the GC-FID. Further studies are still needed to correctly determine the correlation between breath and blood levels using a more appropriate method for analysing blood.

A second application of GC-IMS in the project was the detection of radiation exposure biomarkers, related to CBRN. Recent studies indicate that the damage caused by radiotherapy to tissues can be detected in breath [24, 25]. This offers the opportunity for detecting in real-time the quantity of injury produced during radiotherapy. This may allow rapid revision of radiotherapy protocols according to an individual's response to radiotherapy, allowing for personalised treatment. In this study, participants undergoing radiation treatment were recruited and breath collection/assessment was completed after the participants' first dose to further develop the methodology for repeated radiation treatment. The study was set in a Western Edinburgh Hospital. Breath samples were collected from 23 participants using a Haldane tube sampler, before radiotherapy and at 1, 3 and 6 h post-exposure. 0.5 cm^3 of breath was immediately analysed with GC-IMS using a 10-min-long analysis method to evaluate its feasibility as a point-of-care device and to compare the results with previously described radiation markers. The device was able to detect four radio-sensitive compounds, including tentatively assigned methylated furaldehyde and 3-methylthiopropanal [23]. Those findings were in line with those observed with
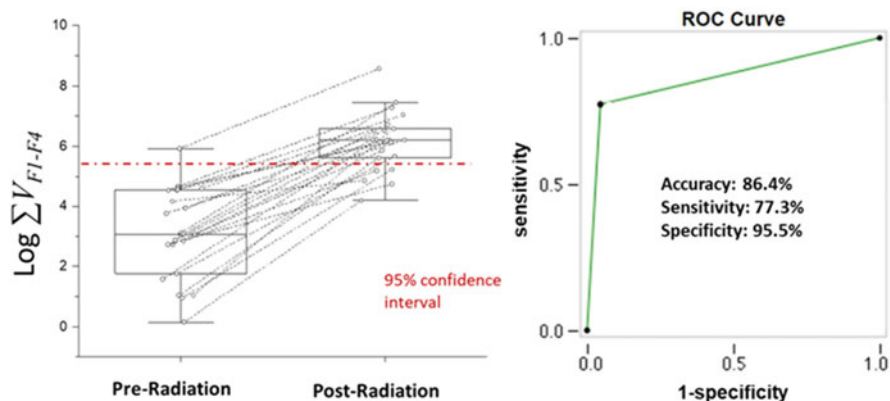
Fig. 8 Left: Box-Whisker plots of pre- and post-radiation summary score of 23 participants, based on peak volume of four features selected in the GC-IMS study. 95% confidence interval was used to provide classification cut-off value used to produce a receiver operating characteristic curve (right)

GC-MS. The Receiver Operating Characteristic (ROC) curve based on the summary score (summary of the Log(10) GC-IMS peak volumes of the four compounds) for each participant gave an accuracy of 84.6% in distinguishing pre- and post-radiation exposure participants (Fig. 8).

It is important to note that the study targeted one of the previously described VOC (3-methylthiopehene), found in the study by TD-GC-MS, and reported its breath concentration to be between 80 and 790 ng m^{-3}. Its detection limit was assessed with GC-IMS and was estimated to be 210 fg s^{-1}, showing its full capability to detect it in breath [25]. However, the feature was only found in 8/28 participants with GC-IMS (Note: TD-GC-MS generates a 104 enrichment from a 1 L of breath sample while the GC-IMS only used volume of 0.5 cm^3 sample of end-tidal breath without enrichment). What this means is that even though the instrument detection limit is sufficient the method detection limit is not. This demonstrates how the choice of sampling device, sampling volume and method optimisation will play an important role in full translation of the findings but demonstrates feasibility.

4.1.1 Mass Casualty Triage

The operational capacity for mass triage with breath testing was evaluated during two field technical (FTX) exercises simulating a chemical weapon attack [26]. Chemical weapon attacks, as occurred in 1995 in Tokyo [27] and more recently in Syria [28], are an ongoing global threat [29]. The current war in Ukraine makes this threat even more likely to happen in Europe. Rapid identification of the agent involved is difficult and currently only patients who develop symptoms are easily triaged [30]. Health care systems can be overwhelmed with unexposed but worried individuals after an attack becomes widely known [31]. Multiple detection, security, clinical

Fig. 9 FTX-disperse: left: a complicated and dynamic environment in FTX Disperse. Number of casualties awaiting decontamination, triage and treatment. Right: a paramedic analysing a breath sample for the presence of peppermint simulant. A sensitive analytical procedure detecting pictogram levels of eucalyptol in exhaled breath tested from the cargo area of an emergency response vehicle

and information technologies were tested during the exercises, to increase preparedness, management capability and situational awareness. The larger scale exercise, FTX DISPERSE, took place in the Finish city of Mikkili and closely reflected a civilian CBRN crises response as it was run by multi-agencies involving the: Fire and Rescue Service; Emergency Medical Services, military CBRN specialists, Police Service, and the local hospital. Two IMS-based technologies were tested, one for the detection of a nerve agent simulant (methyl salicylate) which alarmed at the presence of methyl salicylate in the attack centre point (Hot-Zone) and was used by CBRN services at the casualty's decontamination lines; second device BreathSpec GC-IMS was used to detect the signs of poisoning with chemical agent in breath (simulated by eucalyptol from peppermint oil) and inform triage of casualties.

BreathSpec GC-IMS was installed and used in an emergency medical vehicle (Fig. 9, right) in the marketplace city centre. The device was supplied with external power supply (battery life of over 1 h) to avoid a re-start with movement of the instrument, so it can be brought to the patient and casualty to provide fast breath profiling at point of care. A second device was set at the emergency department of the local hospital. The medical service teams were ready to perform breath tests and operating the device, after just half a day of a training. The use of Peppermint test safely provided a controlled trace metabolite profile in the breath of participants enabling a robust operational performance and training evaluation of breath analysis to be undertaken in close to operational conditions.

One hundred and thirteen volunteer participants undertook the role of casualties. Throughout the crisis, emergency service paramedics were instructed to "tag" each target they interacted with. The information was collected on triage status, contamination status, and the result of any breath analysis. This allowed monitoring of the

casualty journey through the exercise, from the Hot-Zone, where the attack took place, through decontamination and triage (Fig. 9) prioritising treatment, based on a positive breath test. There were 39 casualties, who showed signs of exposure and qualified for the breath test. The test took less than a minute from sample collection to results, allowing all 39 casualties to be triaged within the first hour of the exercise. The test showed 83% sensitivity and 100% specificity. The results of this exercise demonstrated convincingly, how this technology was compatible with emergency medical service operations and simple enough to use in austere conditions.

4.2   Breath as a Screening Tool for COVID-19

Since the emergence of the pandemic, much attention was given to identifying breath biomarkers to detect SARS-CoV-2 infections for screening purposes, but also to study the biology of the disease through the metabolites and shed light on the disease mechanisms. There have been several prospective trials published. Ruszkiewicz et al. provided the first evidence that distinguishing SARS-CoV-2 infection from other respiratory disorders using breath testing in an emergency room setting may be possible with portable GC-IMS [32]. Although breath sampling via GC-IMS has not been accepted as a clinical COVID-19 screening tool to date, there have been over 10 published research papers prospectively designed using VOC-based analysis to distinguish COVID-19 in various clinical settings. Recently the FDA approved a portable GC-MS machine for screening COVID-19 via breath, allowing for this technique to be used as a clinical screening tool. Subali et al. present a detailed review on existing studies with exhaled breath and provided its cumulative diagnostic evaluation, with sensitivity and specificity values of 98.2% (97.5% CI 93.1–99.6%) and 74.3% (97.5% CI 66.4–80.9%), respectively [33]. This demonstrates the potential for further development of the breath test for clinical use. In recently presented work by Myers et al., the breath profile of patients was repeated through active infection to recovery, allowing for differentiation of symptomatic SARS-CoV-2 positives vs. SARS-CoV-2 negatives patients presenting with upper respiratory tract infection [34]. They included a longitudinal study following patients through recovery; an important subgroup to study for potential screening applications and more importantly the potential to understand the biology of the disease and long COVID.

In April 2022 the FDA approved the first clinical breath test for screening of SARS CoV-2 infections in the USA based on 2409 subjects, 102 were RT-PCR SARS-CoV-2 positives. The sensitivity and specificity of the test was 91.2% (90% CI: 85.4, 94.8) and 99.3% (95% CI: 98.8, 99.5%), respectively. Additionally, a small cohort of 12 people were tested during the emergence of the Omicron variant (11 were RT-PCR SARS-CoV-2 positives). The test showed high sensitivity of 90.9%. The study had limitations in both design and practicality. The data set was unbalanced and demonstration of the applicability to the newly emerging variants needs further testing. The mass spectrometer used is a substantial size and requires

trained operators supervised by health care professionals, limiting its applicability; however, this is an exciting step forward for the breath analysis field as it is the first breath test permitted for clinical use in the pandemic.

4.2.1 COVID-19 Studies with GC- IMS

Three GC-IMS volatolomic papers have been published so far using IMS technology to study COVID-19 detection.

The first study demonstrating the ability to find differences in the VOC profiles between SARS-CoV-2 positive participants and SARS CoV-2 negative patients was carried out using GC-IMS. The work involved two independent studies in the UK and Germany [32]. The studies were set up rapidly and early on in the emergence of the pandemic with first patients being recruited at the end of March 2020. The devices were set in two Hospitals: Royal Infirmary of Edinburgh (RIE) and in Klinikum Dortmund (KD), to study whether patients with COVID-19 can be distinguished from those admitted with other respiratory symptoms. Both teams used the same GC-IMS device with disposable Haldane tube breath sampler and 10-min-long analytical method with slightly different chromatographic conditions. The simplicity of the device and sampling procedures allowed for efficient set-up. The clinical teams went through 2 days of training and finished with proficiency testing using the peppermint proficiency protocol. In this pilot study, data from 28 and 65 patients admitted to RIE and KD, respectively, was analysed. Twenty-seven were RT-PCR SARS-CoV-2 positive and 66 were RT-PCR SARS-CoV-2 negative (respectively). Two different and independent data processing approaches were applied to the data to extract candidate markers (data mining – KD and vectorising peak volume – RIE), before combined sets were assessed with principal component analysis (PCA-X) model. The compounds distinguishing COVID-19 from other upper respiratory tract infections were increased levels of ketones (acetone and 2-butanone) suggesting ketosis, aldehydes, specifically heptanal and octanal which are known inflammatory and oxidative stress markers as well as ethanal and reduced methanol production. The models produced for each centre provided AUROC curves of 0.87 (RIE) and 0.91 (KD), with sensitivity of 82.4% (RIE) and 90.0% (KD) and specificity of 75.0% (RIE) and 80% (KD). The results were assessed without a need for specialised software and complicated algorithms, using simple ratio-metric scoring (C19) based on the peak volumes used in each model shown in Fig. 10. The classification based on that assessment provided comparable AUROCs. To fully explore the potential of a screening breath test with GC-IMS, a much larger study is needed based on different populations and cohorts. This is underway with a partnership including COVID-19 clinics in the tropics (Sri Lanka) and community COVID-19 test centres in British Columbia, Canada as well as clinics in the UK including Leicester and Glenfield University Hospital. The consortium also includes researchers from Warwick University who will lead the data processing. It is a prospective study design with breath collection from symptomatic patients presenting for RT-PCR COVID-19 testing. Breath is
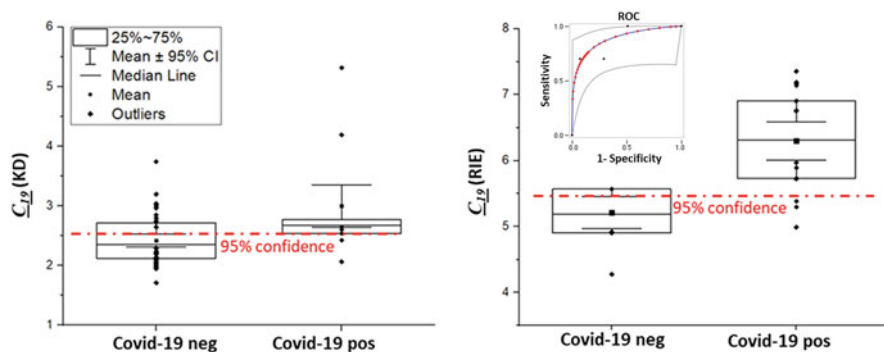
Fig. 10 Box-Whisker plots derived from ratio-metric studies with a 95% confidence limit highlighted, based on the group of COVID-19 negative patients. Left: Dortmund data (KD), right: Edinburgh data (RIE) with ROC curve

collected at the time of presentation with respiratory illness symptoms and all participants will have a gold standard RT-PCR for COVID-19. There is concurrent development of a data pipeline for uniform processing of the data and creation of single model from the different data sets from all study sites.

Additional data published from a UK cooperation between Leicester Glenfield hospital, Leicester University Hospital and Warwick University, evaluated 113 participants from highly diverse populations, via breath test after admission to the hospital [35]. One hundred and fifteen participants were evaluated with 72 participants RT-PCR SARS-CoV-2 positive (COVID-19), 20 were RT-PCR SARS-CoV-2 negative but symptomatic with a respiratory tract infection (RI). An additional, 21 healthy controls were included (HC). The team used an automated method for analysis of the data, with the pipeline published elsewhere [36]. The extracted (by ten-fold cross-validation) features were used to produce a model using different classifiers such as Gaussian Process and Neural Network. The relation between variables including white cell count and urea levels at admission, number of comorbidities and duration of symptoms was also investigated using multivariable logistic regression to test the ability of GC-IMS to distinguish COVID-19 from other Respiratory infections and predict the requirement for subsequent Continuous Positive Airway Pressure (CPAP) treatment. The study provided similar discrimination power for the breath test to distinguish between acute COVID-19 infection and other respiratory infections, as those previously reported by Ruszkiewicz et.al (Table 1). There was a high correlation between breath and subsequent need for CPAP in hospitalised patients with COVID-19; however, it was independent for predicting outcomes. More studies need to be done to fully explore the potential of breath VOCs analysis via GC-IMS to not only detect SARS CoV-2 infections but also predict disease outcome.

Challenges remain with deploying GC-IMS at multiple centres and combining the data, as even though individual studies were run using the same chromatographic

Table 1 Characteristics of the GC-IMS performance in distinguishing COVID-19 participants from healthy controls (HC) and participants with other respiratory infections (RI) as well as its ability to predict the need for subsequent CPAP in SARS-CoV-2 positives

Characteristic	COVID-19 vs HC (neural network)	COVID-19 vs RI (Gaussian process)	*Subsequent CPAP No subsequent CPAP (neural network)
AUROC (95% ci)	0.85 (0.74–0.96)	0.89 (0.81–0.96)	0.70 (0.53–0.87
Sensitivity	80% (56–94%)	85 (76–91%)	62% (32–86%)
Specificity	88% (79–94%)	90 (68–99%)	80% (69–89%)
p-value	<0.001	<0.001	<0.01

Table 2 Breakout of participants' SARS-CoV-2 status, from three sites taking part in breath test COVID-19 query

Testing centre	RT-PCR SARS-CoV-2 positives	RT-PCR SARS-CoV-2 negatives with RI	Cohort description
Vancouver	16	85	Community testing site
Leicester	91	20	Admitted to hospital
Sri Lanka	83	48	Admitted to hospital
Total/312	167	148	

column there were differences in chromatographic conditions and aligning the data sets (retention times and drift times), required compensation. Researchers from Warwick University produced a data processing pipeline for GC-IMS data collected at different sites from the global partnership of the COVID-19 query. This was achieved by selecting a single master file from one site and aligning all the data to that master file. This included RIP alignment of all the samples to the master file and then undertaking manual re-alignment of the drift and retention times for chemical peak alignment, until all the key peaks aligned in all the data. It required moving peaks in the drift and retention axes and re-scaling the axes. In addition, all the data was scaled so that the RIP magnitude was the same in all the samples. Three hundred and twelve samples from a mixed cohort with participants from Sri Lanka, Leicester and Vancouver were processed via this pipeline (Table 2). The participants were symptomatic and either admitted to hospital or recruited from community test sites. Seventy percent of the data was used as a training set to construct the predictive model, using different classifiers (Gaussian Process, Sparse Logistic Regression and Neural Network) and 30% was used as a validation set.

The results are impressive (Fig. 11), with average AUROCs for the validation data set of 0.85 (95% ci 0.86–0.79), The combination of data science with AI methods demonstrates an attractive way of combining different GC-IMS data sets
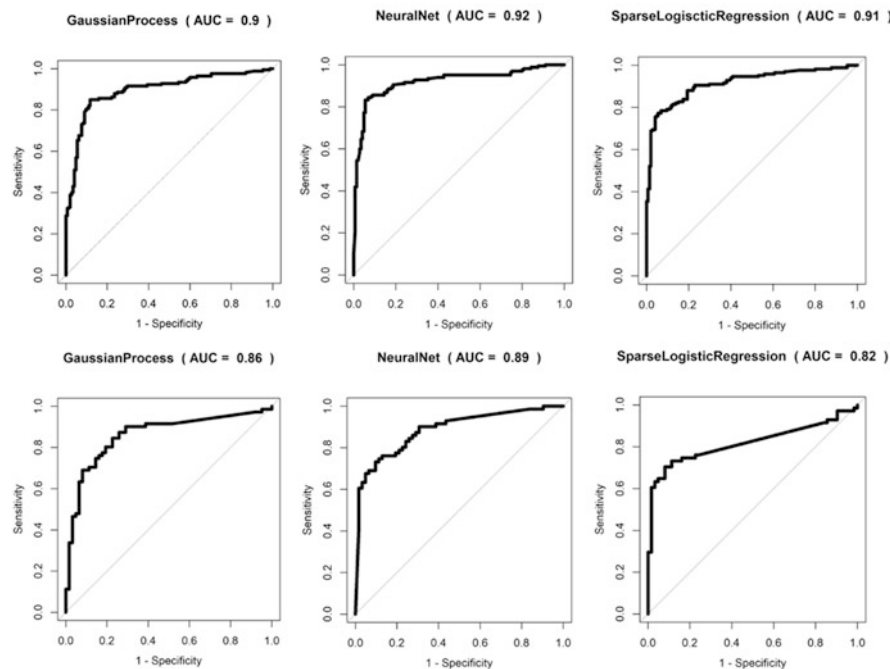
Fig. 11 Receiver operating characteristic curves obtained from combined models, produced using three different classifiers and based on three data sets from Global COVID-19 query (312 samples). Top: training set (70% of the samples), bottom: validation set (30% of the samples)

to increase the statistical power of the test. Work is ongoing to identify the VOCs produced in the above models and apart from this, only one other study performed by Chen et al. reports identified VOCs determined by GC-IMS [37]. The study included 191 subjects recruited in Beijing, including 74 RT-PCR SARS-CoV-2 positive (COVID-19) patients and 30 RT-PCR SARS-CoV-2 negative patients with respiratory infection symptoms, and 87 healthy controls, RT-PCR negative.

The samples were collected into small ALTEF bags, attempting to capture end tidal breath, then immediately transferred into the instrument for analysis. 12 features were selected as significant based on differences between cohorts. Five of those were identified including acetone, acetic acid, acetaldehyde, and 1- and 2-propanol. The common compound between GC-IMS COVID detection studies is acetone and possibly acetic acid. 2-propanol is a common disinfectant, and high background levels were observed in clinical areas, often overwhelming this part of the GC-IMS chromatographs; therefore, it was excluded from the analysis. They reported a high level of specificity and selectivity of the method and used different modelling approaches summarised in Table 3.

The environmental surroundings in clinical settings need to be carefully considered when working with GC-IMS. The presence of elevated alcohol levels in the environment such as iso-propanol (common sanitiser) may change the chemistry of

Table 3 The AUOC for COVID-19 detection in symptomatic patients with respiratory illness via three different modelling approaches

Model	COVID-19 vs RI AUROC (95% ci)	COVID-19 vs controls AUROC (95% ci)
Random forest	1.00 (1.00–1.00)	0.99 (0.97–1.00)
Support vector machine	0.93 (0.90–1.00)	1.00 (1.00–1.00)
Gradient boosting machine	1.00 (1.00–1.00)	0.97 (0.92–1.00)

proton transfer reactions producing a mixed cluster of the compound and contaminant, changing the desired response and making data much more variable. Certain precautions should be taken to avoid contamination including: careful attention to instrument set-up location, minimising number of chemicals used in its proximity and frequent glove changes.

In summary, GC- IMS technology truly proved itself as a valuable clinical research device, throughout the pandemic, which can be rapidly deployed into health care settings and provide reliable data in extreme conditions, from the tropical heat and humidity of Sri Lanka to the biting winter cold of the Canadian Rockies. Although not yet incorporated in the clinical field, recent studies have demonstrated a strong foundation for the technology to be potentially adapted as a rapid screening test showing both: low burden on participants and operators, as well as a possible economic impact. Further validation studies are required.

4.3 Potential Clinical Point of Care Applications for GC-IMS

As seen in the previous section on sampling, breath samples for GC-IMS are non-invasive and simple to collect. The smaller footprint of the machine allows for easy portability and integration into busy clinical settings. Since breath is already in the gas phase, the sample is directly transferred to the GC-IMS device with an online or offline sampler. Breath is a rich matrix that is being studied for possible insight into screening and detection of diseases such as lung cancer, COVID-19 infection, COPD, asthma, etc. [35, 37, 38]. GC-IMS devices can also provide real-time data of anaesthetic states of patients during surgery. There have been several studies investigating the real-time concentration of propofol in exhaled breath compared to the concentration in blood during surgeries [39, 40]. This has been demonstrated to be comparable and could greatly help an anaesthesiologist during surgery to accurately dose anaesthetics.

Urine is a very common and easily collected bio-specimen from patients as it is non-invasive and quick to collect. In order to analyse the VOCs released from urine, an autosampler such as Flavorspec® is needed to heat and introduce the sample into the GC-IMS. Current studies have shown urine to discern pancreatic ductal adenocarcinoma (PDAC) cancer from healthy participants using logistic regression with

an AUC of 0.88 with a sensitivity of 0.84 and specificity of 0.94. This study completed by Daulton et al. collected 123 urine samples from participants who were diagnosed with PDAC, chronic pancreatitis, and healthy controls [9]. The urine samples were analysed using GC-IMS as well as TD-GC-MS and compared to one another. The results from the GC-IMS data performed as well, and in some cases better than the TD-GC-MS data when comparing different cohorts to one another. Urine has also been shown to be able to distinguish the presence of bladder or prostate cancer with good sensitivity and specificity.

Blood is also being actively studied; it is typically a sample matrix that contains many VOCs; however, most of them are unable to be detected by GC-IMS due to their low proton affinities. There are certain use cases for analysing blood with GC-IMS devices for specific scenarios such as detecting infections of the blood due to pathogens such as *Escherichia coli*, *Staphylococcus aureus* and *Pseudomonas aeruginosa* [11]. Routine medical microbiological tests for these pathogens are relatively slow and can take anywhere from 24 to 48 h to complete. Drees et al. were able to demonstrate that they could detect and differentiate a blood-borne infection in just 6 h using a GC-IMS. This reduced the analysis time of 75% compared to conventional methods with good sensitivity and specificity. This remains an area that is actively being researched.

GC-IMS devices have the potential to be used as screening tools to group patients in risk categories and can help guide clinical treatment courses. Although IMS devices have shown the potential to distinguish multiple disease states from multiple clinical matrices, further standardisation of methods is needed along with external validation and multi-centred studies. It also needs to be said that most published IMS research papers do not necessarily identify their discovered biomarkers and instead use names such as "Peak Area 2" or "Molecular Feature 2". Regulators such as the FDA may not be satisfied with this level of identification routinely performed and may require better identification levels before these devices make the move into clinical practice. The future for the use of IMS devices in clinical settings is promising; however, there is still a great deal of work to be done to move the IMS from a research centre to an emergency room.

5   Future Perspective

Interest in the use of GC-IMS for the detection of volatiles has seen a rapid expansion over the last decade. This is reflected in the number of published papers, book chapters and review articles on the subject. According to the Science Direct journal database, nearly a quarter of all published GC-IMS work describes its potential use in clinical applications, which has more than tripled in size within the last 10 years (Fig. 12). This trend is expected to carry on into the next decade.

This successful decade allowed for the GC-IMS to become an established analytical tool used by researchers in many fields, including clinical with VOC markers discovery, study on drug intervention and rapid triage. The technique is also
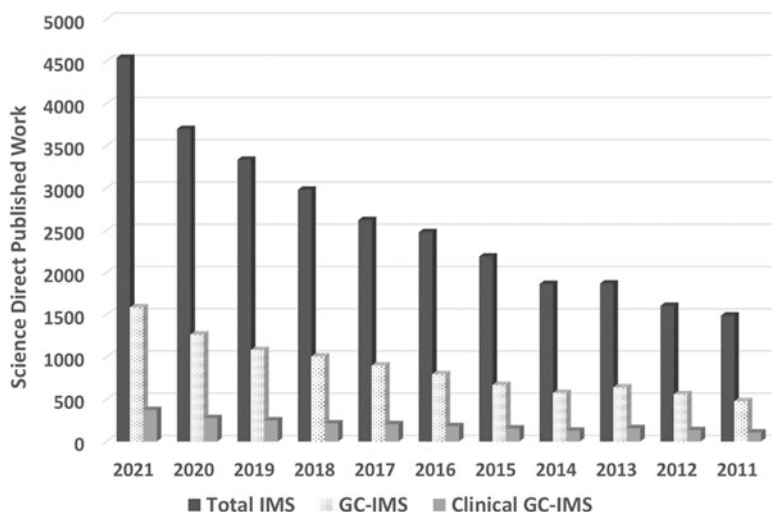
Fig. 12 Number of published work (research papers, review papers and book chapters) found by search of following keywords: IMS, GC-IMS and Clinical GC-IMS, using ScienceDirect Database

succeeding in certain industries, for example, in quality control of the food sector, demonstrating that when working with targeted analytes, fast analysis times and reliability can be achieved.

Despite the demonstrated potential, expansion of the GC-IMS into the clinical field for routine analysis of VOCs will depend on large robust clinical trials to overcome its main challenges and limitations.

The first challenging aspect is the complexity of the GC-IMS data, processing is laborious and requires highly skilled analysts to extract the required information. The work in this sector has already started in recent years (for example, as presented in the example of the COVID-19 application) with the employment of AI algorithms and the automation of processing workflows. This sector is expected to rapidly develop, allowing a wider use of pre-concentration sampling techniques and a richer spectrum of information to be extracted from biological samples.

The second challenge lies in the continued use of radio-active sources, which the technique largely relies on. The sources are highly regulated, increasing the burden on the organisation and transportation. It is expected that a less or non-radioactive source (based on photoionisation or corona discharges) will be adapted for clinical GC-IMS instrumentation, as has happened in the case of IMS field detectors for security applications.

Finally, IMS technology does not provide enough structural information for the compound to be identified; therefore, the identification relies on limited libraries of mobility coefficients and retention indexes when coupled to a chromatographic column. If such information could be provided, the device would truly compete with the golden standard technology for the analysis of VOCs, which currently is GC-MS. Tandem IMS with a Field Induced Fragmentation stage is at its early stage

of development but shows that different chemical classes provide specific fragmentation patterns, which could be used for ion identification in the way that mass spectrometry identifies ions. Active work on this on this subject is especially exciting [41, 42] and is certainly expected to grow in the next decade, to provide the next generation of IMS technology.

References

1. Cohen MJ, Karasek FW (1970) Plasma chromatographytm – a new dimension for gas chromatography and mass spectrometry. J Chromatogr Sci 8:330
2. Kanu AB, Hill Jr HH (2007) Identity confirmation of drugs and explosives in ion mobility spectrometry using a secondary drift gas. Talanta 73(4):692–699
3. Cohen MJ, Karasek FW (1970) Plasma chromatography™ – a new dimension for gas chromatography and mass spectrometry. J Chromatogr Sci 8(6):330–337
4. Revercomb HE, Mason EA (1975) Theory of plasma chromatography/gaseous electrophoresis. Review. Anal Chem 47(7):970–983
5. Eiceman GA, Karpas Z (2005) Ion mobility spectrometry. CRC Press
6. Davis C, Pleil J, Beauchamp J (eds) (2020) Breathborne biomarkers and the human volatilome
7. Daulton E et al (2021) Volatile organic compounds (VOCs) for the non-invasive detection of pancreatic cancer from urine. Talanta 221:121604
8. Tyagi H et al (2021) Urinary volatiles and chemical characterisation for the non-invasive detection of prostate and bladder cancers. Biosensors 11(11):437
9. Daulton E et al (2020) The detection of wound infection by ion mobility chemical analysis. Biosensors 10(3):19
10. Lacey L et al (2020) Detection of group B Streptococcus in pregnancy by vaginal volatile organic compound analysis: a prospective exploratory study. Transl Res 216:23–29
11. Drees C, Vautz W, Liedtke S et al (2019) GC-IMS headspace analyses allow early recognition of bacterial growth and rapid pathogen differentiation in standard blood cultures. Appl Microbiol Biotechnol 103:9091–9101
12. Fabio DF et al (2008) Implementation of Fowler's method for end-tidal air sampling. J Breath Res 2(3):037009
13. Myers R et al (2022) Breath collection protocol for SARS-CoV-2 testing in an ambulatory setting. J Breath Res 16(2):027105
14. Ruszkiewicz DM et al (2022) Peppermint protocol: first results for gas chromatography-ion mobility spectrometry. J Breath Res 16(3):036004
15. Ghimenti S et al (2015) Comparison of sampling bags for the analysis of volatile organic compounds in breath. J Breath Res 9(4):047110
16. Vautz W et al (2014) GC/IMS and GC/MS analysis of pre-concentrated medical and biological samples. Int J Ion Mobil Spectrom 17(1):25–33

17. Horváth I et al (2017) A European Respiratory Society technical standard: exhaled biomarkers in lung disease. Eur Respir J 49:4
18. Henderson B et al (2020) A benchmarking protocol for breath analysis: the peppermint experiment. J Breath Res 14(4):046008
19. Wilkinson M et al (2021) The peppermint breath test: a benchmarking protocol for breath sampling and analysis using GC–MS. J Breath Res 15(2):026006
20. Hovda KE, Urdal P, Jacobsen D (2005) Increased serum formate in the diagnosis of methanol poisoning. J Anal Toxicol 29(6):586–588
21. Helge Hunderi O, Hovda KE, Jacobsen D (2006) Use of the osmolal gap to guide the start and duration of dialysis in methanol poisoning. Scand J Urol Nephrol 40(1):70–74
22. Kraut JA, Mullins ME (2018) Toxic alcohols. N Engl J Med 378(3):270–280. https://doi.org/10.1056/NEJMra1615295. Erratum in: N Engl J Med. 2019 Jan 10;380(2):202
23. "Ion mobility spectrometry in clinical setting" – talk given on 16th of February 2022 at RSC molecular spectroscopy group meeting
24. Phillips M et al (2013) Detection of volatile biomarkers of therapeutic radiation in breath. J Breath Res 7(3):036002
25. Salman D et al (2020) Breath markers for therapeutic radiation. J Breath Res 15(1):016004
26. Toxi-Triage. http://toxi-triage.eu
27. Okumura T et al (1996) Report on 640 victims of the Tokyo subway sarin attack. Ann Emerg Med 28(2):129–135
28. John H et al (2018) Fatal sarin poisoning in Syria 2013: forensic verification within an international laboratory network. Forensic Toxicol 36(1):61–71
29. (2018) Organisation for the prohibition of chemical weapons. Fact sheet 4. What is a chemical weapon? OPCW, The Hague
30. Tomassoni AJ, French RNE, Walter FG (2015) Toxic industrial chemicals and chemical weapons: exposure, identification, and management by syndrome. Emerg Med Clin 33(1):13–36
31. North CS, Pfefferbaum B, Vythilingam M, Martin GJ, Schorr JK, Boudreaux AS, Spitznagel EL, Hong BA (2009) Exposure to bioterrorism and mental health response among staff on Capitol Hill. Biosecur Bioterror: Biodefense Strat Pract Sci 7
32. Ruszkiewicz DM et al (2020) Diagnosis of COVID-19 by analysis of breath with gas chromatography-ion mobility spectrometry – a feasibility study. EClinicalMedicine 29:100609
33. Subali AD et al (2022) The potential of volatile organic compounds-based breath analysis for COVID-19 screening: a systematic review & meta-analysis. Diagn Microbiol Infect Dis 102(2):115589
34. Myers R (2022) Detection of mild SARS-CoV2 infection in out-patients. IABR breath summit 2022 Pisa, Italy
35. Nazareth J et al (2022) Discriminatory ability of gas chromatography-ion mobility spectrometry to identify patients hospitalised with COVID-19 and predict prognosis. medRxiv
36. Bannaga AS et al (2021) Exploratory study using urinary volatile organic compounds for the detection of hepatocellular carcinoma. Molecules 9:2447
37. Chen H et al (2021) COVID-19 screening using breath-borne volatile organic compounds. J Breath Res 15:047104
38. Ratiu IA et al (2020) Volatile organic compounds in exhaled breath as fingerprints of lung cancer, asthma and COPD. J Clin Med 10(1):32

39. Jiang D et al (2021) Breath-by-breath measurement of intraoperative propofol by unidirectional anisole-assisted photoionization ion mobility spectrometry via real-time correction of humidity. Anal Chim Acta 1150:338223
40. Heiderich S et al (2021) Correlation of exhaled propofol with Narcotrend index and calculated propofol plasma levels in children undergoing surgery under total intravenous anesthesia-an observational study. BMC Anesthesiol 21(1):1–9
41. Shokri H et al (2020) Field induced fragmentation (Fif) spectra of oxygen containing volatile organic compounds with reactive stage tandem ion mobility spectrometry and functional group classification by neural network analysis. Anal Chem 92(8):5862–5870
42. Shokri H et al (2021) Successive reactions in field induced fragmentation spectra from tandem ion mobility spectrometry at ambient pressure and their influence on classification by neural networks. Int J Mass Spectrom 470:116701

Infrared Sensing Strategies: Toward Smart Diagnostics for Exhaled Breath Analysis

Michael Hlavatsch, Sarah Klingler, and Boris Mizaikoff

Contents

Abstract To date, the most commonly applied method for detecting constituents in exhaled breath is gas chromatography (GC) coupled with mass spectrometry (GC-MS). Despite the ability to accurately detect a wide range of volatile organic

Michael Hlavatsch and Sarah Klingler contributed equally to this work.

M. Hlavatsch and S. Klingler
Institute of Analytical und Bioanalytical Chemistry, Ulm University, Ulm, Germany

B. Mizaikoff (✉)
Institute of Analytical und Bioanalytical Chemistry, Ulm University, Ulm, Germany

Hahn-Schickard, Ulm, Germany
e-mail: boris.mizaikoff@uni-ulm.de

compounds (VOCs), GC-MS-based instruments are frequently large and expensive, and the analysis is time consuming. Modern exhaled breath analysis requires on-line sampling and real-time selective biomarker detection with high sensitivity, precision, and accuracy. Therefore, optical sensing strategies are increasingly adopted and have emerged as a promising alternative method to meet these requirements. In particular, the mid-infrared wavelength regime has substantial potential, as almost any biomedically relevant gaseous molecule has species-characteristic vibrational, ro-vibrational, and rotational transitions in this frequency range. This chapter provides an overview on the fundamental principles and recent developments in this emerging field with a focus on technological and application examples in the infrared regime, as these sensing devices have already demonstrated their potential serving as a smart diagnostic tool in exhaled breath analysis.

Keywords Exhaled breath analysis · Mid-infrared sensing techniques · Optical sensing techniques

Abbreviations

ATR	Attenuated total reflection
CEAS	Cavity-enhanced absorption spectroscopy
CKD	Chronic kidney disease
COPD	Chronic obstructive pulmonary disease
CRDS	Cavity ring-down spectroscopy
CW	Continuous wave
DFB	Distributed feedback diode laser
DFG	Difference frequency generation
DLATGS	Deuterated L-alanine triglycine sulfate
DTGS	Deuterated triglycine sulfate
EB	Exhaled breath
ECL	External cavity laser
EM	Electromagnetic
FC	Frequency comb
FIR	Far-infrared
FT-IR	Fourier transform infrared
GC	Gas chromatography
GC-MS	Gas chromatography coupled with mass spectrometry
HOT	High operating temperature
HWG	Hollow-core waveguide
ICAS	Intracavity absorption spectroscopy (or ICLAS)
ICL	Interband cascade laser
ICLAS	Intracavity laser absorption spectroscopy
ICLED	Interband cascade light emitting diode (or IR-LED)
ICLS	Intracavity laser spectroscopy

ICOS   Integrated cavity output spectroscopy
iHWG   Substrate-integrated hollow-core waveguide
IR   Infrared
IR-LED   Infrared light emitting diode
IRMS   Isotope ratio mass spectrometry
LSL   Lead-salt laser
MCT   Mercury cadmium telluride (or HgCdTe)
MIR   Mid-infrared
MPC   Multi-pass cell
MQW   Multi-quantum well
MS   Mass spectrometry
NDIR   Non-dispersive infrared
NIR   Near-infrared
OFC   Optical frequency comb
OF-CEAS   Cavity-enhanced absorption spectroscopy
QCL   Quantum cascade laser
QD   Quantum dot
QDL   Quantum dot laser
QW   Quantum well
SNR   Signal-to-noise ratio
T1D   Type 1 diabetes
T2D   Type 2 diabetes
TDLAS   Tunable diode laser absorption spectroscopy
TLAS   Tunable laser absorption spectroscopy
UV   Ultraviolet
VAP   Valproic acid (drug for therapy of epilepsy patients)
VIS   Visible
VOC   Volatile organic compound
WMS   Wavelength modulation spectroscopy

1   Introduction

The current state of the art in breath analysis for clinical use requires on-line sampling, real-time detection, and quantification of selective biomarkers in small sample volumes with high accuracy, precision, and selectivity. Fast measurement times allow high sample throughput ideally providing direct results and enabling statistics for extended clinical/epidemiological studies. Continuous measurements over extended periods of time can provide information on the uptake and excretion of biomarkers, such as volatile organic compounds (VOCs), from the body or provide information on the body's response to interventions.

Analysis of the exhaled breath matrix immediately after exhalation without preconcentration and storage simplifies sample handling and minimizes the risk of

contamination or analyte loss. Ideally, several different VOCs should be detected simultaneously to provide a reliable diagnostic panel of a person's health status. However, this exhibits a major challenge for the main analytical techniques currently in use, especially mass spectrometry (MS). MS techniques are very sensitive in the low concentration range (i.e., ppb – ppt) of larger VOCs in exhaled air, but quantification remains difficult, and the need for large and expensive equipment and highly skilled personnel, as well as long measurement times renders direct clinical applications cumbersome. Optical sensing techniques offer a viable alternative. In particular, the infrared wavelength range – more specifically the near-infrared (0.78–2.5 μm) and mid-infrared (2.5–20 μm) regime – are of great importance for the detection of gaseous molecules in environmental analysis, process monitoring, and especially biomedical diagnostics. In the infrared region, many relevant gases such as ammonia (NH_3), methane (CH_4), hydrogen chloride (HCl), nitrous oxide (N_2O), sulfur dioxide (SO_2), carbon dioxide (CO_2), and carbon monoxide (CO) have molecule-specific vibrational, oscillatory, and rotational transitions [1]. Other optical techniques based on alternative wavelength ranges or using different techniques such as Raman spectroscopy, ultraviolet (UV), and visible (VIS) spectroscopy, and mm-wave/THz spectroscopy should be mentioned here as well, but will not be discussed in detail in this chapter.

The main advantages of optical sensing are reasonable cost, compact size, potential for miniaturization, and the possibility of on-line and real-time analysis combined with easy quantification, high sensitivity, and selectivity for small molecules and isotope effects. Although MS is better suited for the identification and fingerprinting, optical methods complement rather than replace MS-based methods and hold promise for integrating breath analysis into routine clinical practice, especially in on-line and in-line monitoring scenarios.

1.1 Basic Principles

Optical spectroscopy takes advantage of the fact that different properties of molecules can be investigated depending on the energy used, i.e. the wavelength range. The electronic structure of a molecule can be probed by using UV/Vis light, whereby the infrared (IR) range is sensitive toward the intermolecular band vibrations and rotations. Transitions involving both, changes in vibrational and rotational quantum number are called ro-vibrational transitions.

Generally, excitation of either valence electrons or resonant vibrations and rotations are caused by absorption of photons with the respective energy equal or higher than the energy gap (i.e., the energy levels are quantized). Electronic transitions are predominantly excited by photons with higher energy (electromagnetic (EM) radiation with lower wavelength) which is used in fluorescence spectroscopy as well as ultraviolet, visible, and near-infrared (NIR) absorption spectroscopy. Photons with lower energy (longer wavelength) are too low in energy to address electronic transitions but provide sufficient energy for transitions between the much

closer vibrational and rotational molecular states. Frequently, the mid-infrared range (MIR; 2–20 μm, 4,000–400 cm^{-1}) is used for identification, as in this spectral regime the basic vibrational and mixed ro-vibrational modes of molecules with a change in dipole moment during the vibration occur and are therefore considered the most pronounced IR transitions. Within this region, also the so-called fingerprint region is located giving rise to distinctive spectral patterns resulting from combination vibrations that are characteristic for each molecule.

The wavelength range from 20 to 100 μm (500–100 cm^{-1}) is known as the far-infrared (FIR) regime, while the range above 100 μm (3 THz) to 1 mm (0.3 THz) is considered as THz radiation. To date, the terahertz region is the most less researched area, because the needed light sources, light-guiding structures, and suitable detectors have only recently emerged. As the typical photon energies are only a few meV, this area is feasible for the study of macromolecules like proteins or DNA with regard to low-energy vibrational modes (i.e., for example, protein folding or receptor binding) [2].

Raman spectroscopy – the complementary technique to the aforementioned IR spectroscopy – has also matured into a commonly applied optical technique for medical diagnosis. In general, Raman spectroscopy is based on the absorption of EM radiation in the UV/Vis/NIR spectral range and relaxation from these excited states by elastically and inelastically scattering. The optical response is mainly located in the MIR spectral range, as the relaxation from higher energy states results in molecular vibrations at much longer wavelengths.

Each interaction between molecules and photons of different energy leads to specific information about organic or inorganic compounds, i.e. identification, quantification, determination of functional groups or electronic structure. Thereby, it is obvious that all the different optical spectroscopic techniques support and complement each other rather than compete with each other and should be selected depending on the analytical questioning.

1.2 Fundamentals of Infrared Spectroscopic Analysis

Infrared spectroscopy relies on the absorption of IR photons by a sample placed in the path of an IR light source. Therefore, if the frequency of a particular vibration of a molecule is equal to the frequency of the IR radiation directed at the molecule, that molecule absorbs the radiation and undergoes the corresponding motion. A stretching motion resulting from absorption is caused by the movement of the two atomic nuclei toward and away from each other. During the motion, the distance between the two atoms decreases, which leads to an increase in energy due to the repulsion of the atomic nuclei. Again, as the distance between the atoms of the molecule increases, the potential energy approaches its equilibrium. If further stretching of the bond leads to an increase in the atomic spacing, again the potential energy may increase to the point of dissociation energy, thus breaking the molecular bond. In the simplest way, neglecting the repulsion of the nuclei and the possibility

of dissociation, this periodic molecular motion is described by a classical harmonic oscillator:

$$\nu = \frac{c_0}{\lambda} = \frac{1}{2\pi} \sqrt{k/\mu}$$

with ν the frequency of the motion, c_0 the speed of light, λ the wavelength, k the spring constant of the imaginary spring mass connecting the two atoms, and μ the reduced mass of the molecular atoms.

In addition to vibrational motions, molecules can undergo rotational motion perpendicular to the bond axis. In the case of linear molecules, the energy associated with rotational transitions can be described by the rigid rotation model. Excitation of the rotational energy levels usually requires much less energy than energy available at room temperature. As a result, many different rotational levels can be occupied at room temperature and just as many different energy transitions can occur. In particular, small gaseous diatomic molecules have a large number of absorption lines corresponding to energy transitions between rotational and vibration. These spectral lines are only resolved in spectra of gas molecules, because in the condensed phase, due to the smaller degrees of freedom, molecular collisions often occur.

Since molecules have more than one fundamental IR vibration, they are divided into two classes. These are classified by whether or not the fundamental vibration occurs at the same frequency in many molecules. Furthermore, the absorption of molecules with the same functional group is called group frequency, which are typically in the spectral range of 4,000–1,300 cm^{-1} (2.5–7.7 μm). On the other hand, in the range of 1,300–400 cm^{-1} (7.7–25 μm) absorptions can be found, which result from the combination and superposition of absorptions of the whole molecule. In this range, absorbances of organic molecules are predominantly observed, and this regime is therefore called the "fingerprint region," as it uniquely identifies basically any molecular species.

Lambert-Beer's law can be used to quantitatively analyze the IR absorption data of gases. It describes the linear relationship between the sample concentration c and the proportion of IR light A_λ absorbed by the sample at a given wavelength, measured in wavenumbers:

$$A_\lambda = -\log\left(\frac{I_1}{I_0}\right) = \varepsilon_\lambda \cdot c \cdot d$$

where I_0 is the intensity of the incident radiation, I_1 is the intensity of the transmitted radiation, ε_λ is the frequency-dependent absorption coefficient, and d the optical path length.

Although theory suggests a linear relationship between the two quantities, in practice linearity depends on the concentration range and other instrumental factors such as background noise, stray light, and instrument bandpass. For this reason, the absorbance is determined empirically for a given sample, concentration range, and operating conditions.

1.3   Infrared Waveguides

For the guidance of photons from a light source to an optical detector, many sensors use optical fibers [3, 4]. Infrared optical fibers can be categorized into three main types: glass, crystalline, and hollow waveguides, guiding wavelengths >2 μm [5]. In addition, a further subdivision of these broad categories can be made based on the fiber structure and material [6].

Rayleigh was the first one, describing the principle of propagating electromagnetic radiation through a hollow tube in 1897 [7]. Because the requirements in the microwave range (especially for optical communication technologies [4]) in the 1930s increased, there was a need for the further development of optical waveguides leading to the invention of the waveguides for the IR region. In the 1960s, the first IR fibers were manufactured from chalcogenide glasses. In the following, around 1975 they were complemented by a variety of other materials like heavy metal fluoride glass, polycrystalline fibers, and hollow-core waveguides (HWG) [6, 8].

For application in gas sensing, it is of great advantage if the light-guiding channel can also function as a gas cell, which is fulfilled by HWGs. Mostly, HWGs are hollow tubes with a high-reflective coating made out of plastic, metal, or glass, enabling to be filled via an in- and outlet with different media such as gases [5, 9].

Hollow waveguides can be divided into two different major classes by the way how they are guiding light through their structure – (1) attenuated total reflection (ATR) HWGs, and (2) leaky-type HWGs [5]. Because HWGs are frequently coated silica or glass tubes, they are fragile, not resistant against mechanical vibrations, influenced by temperature changes and of limited utility for compact sensing devices (see Fig. 1d) [10]. That is due to the fact that the sensitivity is proportional to the optical light path, i.e., for obtaining sufficient sensitivity, there is the need of relatively long HWGs ideally avoiding bending or coiling for the resulting attenuation/outcoupling losses.

A significant improvement was the introduction of the so-called substrate-integrated HWGs (iHWG) as a new generation of robust HWGs by the research team of Mizaikoff [4]. As evident in Fig. 1a, b, the straight or meandered light-guiding channel is integrated into a robust, solid-state substrate (e.g., brass, aluminum, etc.) with a mirror-like polished inner wall. Thereby, sufficient robustness yet design flexibility is ensured, and via different geometries the optical path length may be tailored while maintaining a compact size. At the same time, the hollow core also serves as an efficient gas cell for probing minute gas volumes (usually a few hundred microliters), allowing fast transient times and thus excellent temporal resolution [11].

Another light-guiding structure, also able to function as gas sample chamber while enabling the achievement of very long optical path lengths, are the so-called multi-pass cells (MPCs), which are frequently used in conventional IR gas spectroscopy (see Fig. 1c). The use of a series of spherical mirrors leads to multiple reflections in between these devices thereby "folding" the IR beam multiple times in a wide variety of configurations (e.g., White cell already introduced in 1942, etc.)
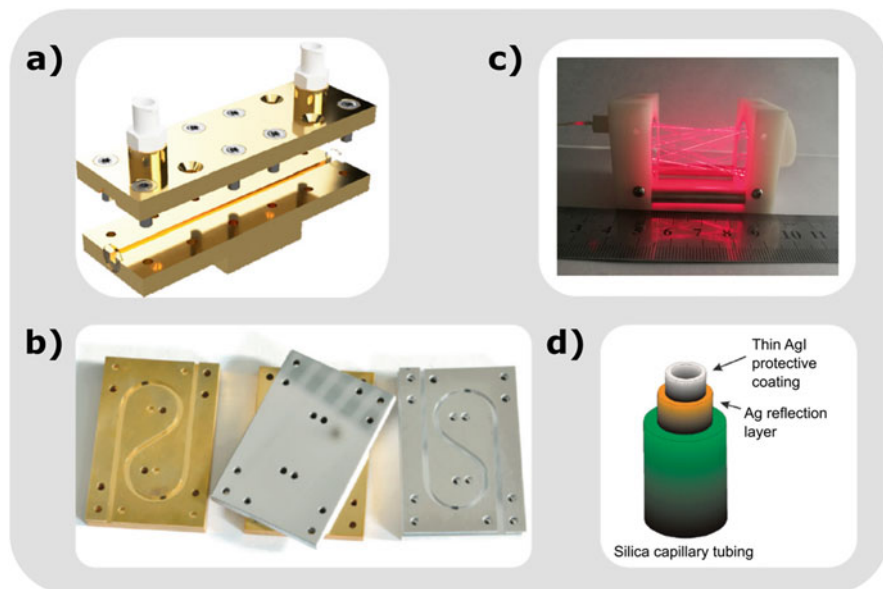
Fig. 1 Substrate-integrated hollow waveguide (iHWG) with straight (**a**) and meandered (**b**) light-guiding channel, multi-pass cell (MPC) (**c**) and exemplary silica hollow waveguide (HWG) structure (**d**). (**a**), (**b**), and (**d**) reprinted and modified from [4]: Copyright © Royal Society of Chemistry 2013; (**c**) reprinted and modified from [12]: Copyright © American Chemical Society 2020

[13]. Thereby, extended absorption path lengths of up to several tens to hundreds of meters can be achieved greatly enhancing the sensitivity, while maintaining a compact configuration. However, the probed gas volume ranges from few hundreds of milliliters up to several liters, which is often a limiting factor in selected applications. Nowadays, the most used geometry is the so-called Herriott cell, which comprises two concave mirrors with the same radius of curvature R and separated by a distance $L < 2R$ [14, 15]. Besides, also circular cells are commercially sold and already used in a variety of gas sensing applications [16–20].

1.4 Infrared Light Sources

One of the fundamental components determining the overall performance of an optical setup is the light source. Therefore, their evolution has played an important role in the development of optical sensing technologies in recent decades. Traditionally, the most commonly used IR light sources are broadband thermal light sources. Broadband IR radiation is usually generated by a heated material (e.g., a silicon carbide (SiC) or tungsten (W) filament), which respectively covers the entire NIR or MIR spectral range. These thermal light sources typically require operating

temperatures of ~200–1,400 K and follow the emission behavior of the black body radiator. However, due to the nature of broadband blackbody radiators, the energy density per wavelength is limited. In addition, such radiation sources are inefficient in terms of optical power and are not compatible with applications that require either low-power consumption or highly directional, narrowband, or coherent IR radiation.

As an alternative to broadband light sources, semiconductor light sources combined with a distributed feedback (DFB) element or with an external cavity configuration enable narrowband or even single-mode emission. Such sources include lead-salt lasers (LSL), diode lasers (DL), interband cascade lasers (ICL), quantum cascade lasers (QCL), and quantum dot lasers (QDL). These advanced light sources allow to selectively tune and thus detect defined absorption lines even of low molecular weight constituents thanks to their narrow bandwidth, wavelength tunability, and emissive power (i.e., energy density) in a narrow frequency band.

The two most prominent representatives of single-mode semiconductor light sources are QCLs and ICLs [21, 22]. QCLs were first experimentally reported in 1994 [23] and are based on intersubband transitions between engineered conduction band states in multilayer semiconductor heterostructures instead of conventional electron-hole recombination within a semiconductor bandgap [24, 25]. However, QCLs were limited to wavelengths $\lambda > 5$ μm due to the common use of the InGaAs/InAlAs material system. When materials like InP substrates [26, 27], III-nitride [28], or II-Vi material systems [29] were introduced, wavelengths smaller than 5 μm were achieved.

At about the same time as QCLs, ICLs were proposed and realized [30, 31]. Unlike QCLs, ICLs are based on electron-hole recombination of type-II interfaces. Their design allows the ICL to operate at room temperature in continuous-wave (cw) mode in a spectral window of 3–6 μm.

Alternative light sources that combine the advantages of narrowband lasers and broadband light sources are optical frequency comb (OFC) light sources [32]. Optical frequency comb light sources have an optical spectrum consisting of equidistant lines, i.e., featuring equidistant optical frequency components, while the intensity of the frequencies can vary considerably. Typically, these frequency components are generated by a regular sequence of ultrashort pulses (i.e., synchronized coherent modes) with a fixed pulse repetition rate. Utilizing interferometers, OFCs provide spectrally resolved information over a broad spectral window, which makes them an attractive light source for sensitive, broadband, and high-resolution spectroscopy.

In recent years, increasing research efforts have been dedicated to light sources beyond today's established and proven laser systems with the goal of developing low-cost, low-power, narrowband IR sensors for diagnostics. In particular, thermal emitters based on metamaterial structures and interband cascade light emitting diodes (ICLED, or IR-LED) with a heterostructure similar to ICLs are the most promising device strategies. For this purpose, thermal emitters use structures such as microelectromechanical systems, plasmonic nanostructured arrays, or photonic crystals in combination with metal-semiconductor compounds such as SiO_2 doped with SnO_2:Sb or Ag/SiO_2/Ag, Au/SiO_2/Au [33–39].

In IR-LEDs, the recombination of electrons and holes in heterostructures is achieved using a type-II interface. In a "W"-element structure, electrons in the so-called quantum wells (QWs) in the conduction band recombine with holes in the QWs in the valence band. As a result, the fractional bandgap type-II alignment enables emission energies below the bulk bandgap of the two components via controlling the QW thickness and thus the position of the electron and hole energy states in the active region where electron-hole recombination occurs. Using multi-quantum well (MQW), superlattice structures as well as quantum dots (QD) and based on organic solutions, various IR-LEDs are fabricated in the wavelength range from 780 nm to 8 μm [40–47].

1.5 Infrared Detectors

Besides light sources, the sensitivity of the detection device plays a crucial role in the analysis of trace amounts of analytes with small absorption cross sections. For infrared imaging, detector materials are needed that have high quantum efficiency and suitable absorption band gaps.

Common broadband IR detector materials for room temperature analysis in the NIR range are systems based on InAs, InAsSb, or InGaAs. Therefore, they are also called uncooled or high operating temperature (HOT) detectors and commercially available. Whereas, for the MIR range detectors based on deuterated triglycine sulfate (DTGS) or deuterated L-alanine triglycine sulfate (DLATGS) are found. For both – NIR and MIR – in order to achieve even better detectability, materials are mostly used that reach their maximum sensitivity at temperatures of liquid nitrogen (77 K). Therefore, semiconductor detector elements and structures such as InSb or type-II superlattices (consisting, for example, of InAs and GaSb layers) for NIR detectors, or mercury cadmium telluride (MCT or HgCdTe) for MIR are mainly used. It is worth mentioning that detectors of the respective IR ranges can also detect radiation of the other range with a lower sensitivity.

As an alternative to the conventional infrared detectors, various type-II materials such as indium arsenide/indium arsenide antimonide (InAs/InAsSb) [48, 49], and type III-V such as GaAsSb [50, 51] or InGaAs [52] have been reported in recent years. However, detector models based on surface structure modification have also been developed, e.g., with quantum dots [53–55] or by structural etching and deposition of graphene monolayers [56, 57].

2 Measurement Techniques

Absorption spectroscopy is the most commonly used optical method in breath analysis. Thanks to its simplicity and high sensitivity, it is possible to determine analyte concentrations in real-time without additional time-consuming sample
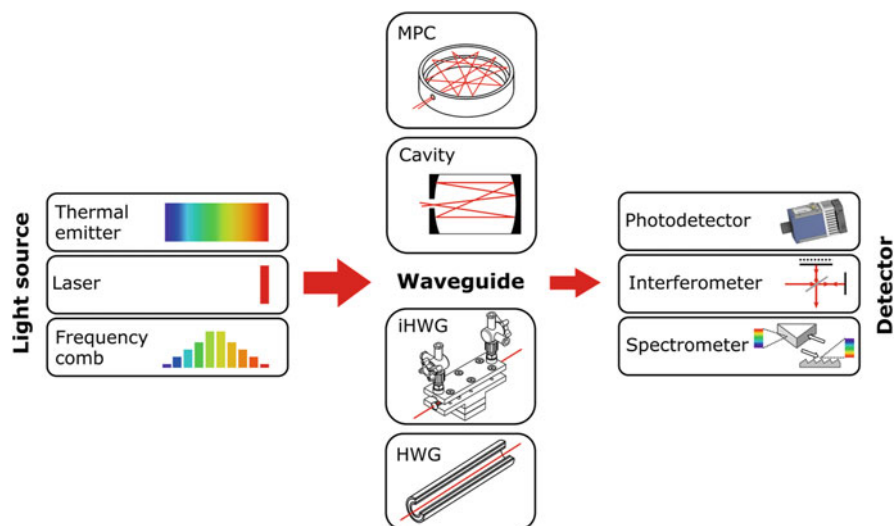
Fig. 2 Schematic overview on IR light sources, waveguide types and gas cells, and detection strategies used in photonic exhaled breath diagnostics

preparation and enrichment. Based on the optical elements described in the previous chapter, an overview of the most important device components is summarized in Fig. 2. In the following, the most established and emerging measurement techniques will be discussed focusing primarily on methodologies in the MIR regime.

2.1 NDIR and FT-IR Spectroscopy Using Thermal Light Sources

One application of IR spectroscopy is the non-dispersive infrared (NDIR) gas measurement, which has its beginnings in the 1930s [58]. An NDIR setup consists of a broadband IR radiation source, a gas cell, a photodetector, and optionally, an optical filter. The analyte concentration is determined by the extent of attenuation of a certain wavelength, while the wavelength filter transmits only a narrow spectrum of the light source. Ideally, the analyte molecules absorb effectively at this wavelength, while other molecules of the gas matrix do not absorb this light. NDIR devices can be constructed in a very robust and compact way, because they profit from the small number of components. However, there are mainly two drawbacks: (1) the lack of selectivity (i.e., interference with other molecules absorbing at the same wavelength), and (2) the high detection limits, as the absorption path length is usually short. Consequently, NDIR sensors are more likely applicable for the highly abundant breath constituents such as water vapor and carbon dioxide [59–63], but also usable for breath biomarker in lower quantities [64–69].
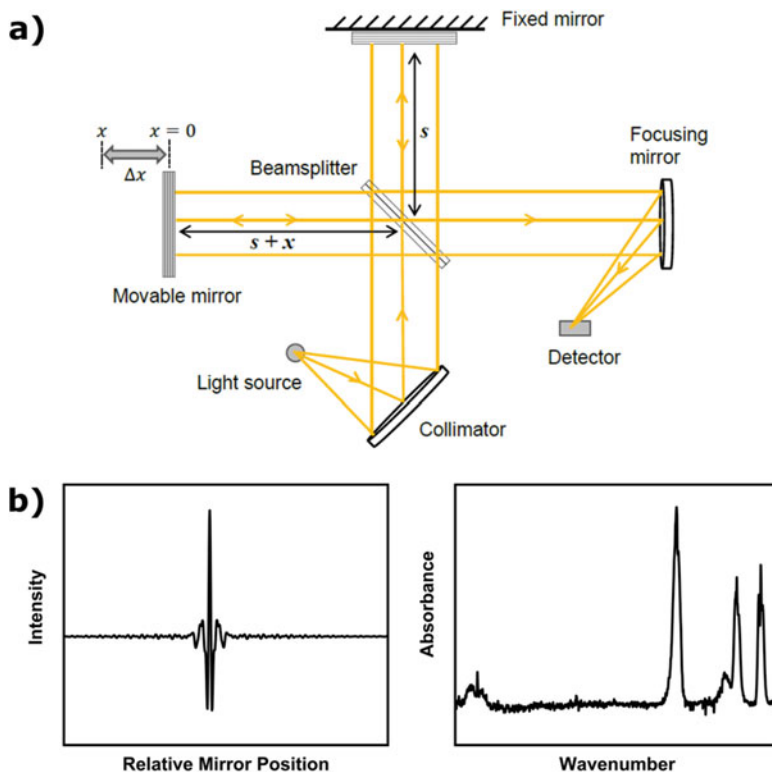
Fig. 3 Schematic of a Michelson interferometer (**a**), an interferogram recorded for a 200 ppm acetone gas sample (left) (**b**), and the corresponding band spectrum after Fourier transformation (right) (**b**)

Fourier transform infrared (FT-IR) spectroscopy is another commonly used spectroscopic technique utilizing broadband thermal light sources but splitting the light through an interferometer before hitting the detector [70]. Mostly, a Michelson interferometer is utilized in a conventional FT-IR spectrometer, as illustrated in Fig. 3a). The emitted light is focused to a parallel light beam by a collimator and hits the beam splitter. The IR beam is separated into two beams with half of the initial intensity. One part of the beam reaches a fixed mirror after a distance s and is reflected back. The other beam part is incident at a movable mirror, which can be moved by the distance x resulting in the total light path $2(s + x)$. At the beam splitter, the two waves recombine after reflection off the stationary and the moving mirror with an optical difference of $2x$. If this distance $2x$ is an integer multiple of the wavelength of a particular wave, constructive interference occurs and the full light intensity is incident at the detector. If there is a difference of a multiple of $\lambda/4$, the distance difference is a multiple of $\lambda/2$ and a minimum (i.e., destructive interference) is occurring. To every position of the movable mirror, one wavelength can be related that causes maximum constructive interference. This modulated signal passes the

sample and is incident at the detector, where the so-called interferogram is recorded as function of the intensity of the radiation depending on the position of the movable mirror [71, 72]. As shown in Fig. 3b), the interferogram collected by the photodetector may then be converted numerically from a function of position or time into a function of spectral frequency – respectively, wavenumber – via a so-called Fourier transformation [70].

2.2 Direct Laser Absorption Spectroscopy

The most commonly used method among direct laser absorption spectroscopy is tunable laser absorption spectroscopy (TLAS), in which the absorption characteristics of sample molecules are measured by scanning their respective central absorption peak. Here, the laser light with a narrow linewidth, which is the limiting factor of spectral resolution, is tuned to a specific wavelength and the absorption of the light by a sample is measured as a function of this wavelength. However, TLAS is subject to low-frequency laser noise and is therefore limited in its sensitivity.

Other methods related to TLAS that use tunable, narrowband semiconductor diode lasers include tunable diode laser absorption spectroscopy (TDLAS) and wavelength modulation spectroscopy (WMS). These systems have the ability to be miniaturized and can be designed to be compact and robustly optimized for targeted detection of a few biomarkers with high selectivity and temporal resolution. This enables real-time detection of respiratory biomarkers in the ppb to ppm range with TDLAS [20, 73–77].

2.3 Cavity-Enhanced Laser Absorption Spectroscopy

Cavity-enhanced absorption spectroscopy (CEAS) uses an optical cavity comprising two or more highly reflective mirrors enclosing the gas sample. As the sensitivity strongly depends on the absorption path length, CEAS provides a substantial improvement of the sensitivity by several orders of magnitude from multiple reflections of light essentially "trapped" between the reflective mirrors inside the cavity for few tens of microseconds. Thereby, depending on the reflectivity of the mirrors, the effective absorption path length can reach tens of kilometers, while maintaining a compact size. The reflectivity is determined by the mirror coating which is the highest in the NIR spectral region, since the coating technology is the most advanced in this region. For the MIR range, the reflectivity is lower but sufficient for being compensated through the stronger absorption line strengths of the exited fundamental vibrational transitions.

The CEAS can be used in different configurations, whereby the so-called cavity ring-down spectroscopy (CRDS) is one of the most common approaches [78–87]. In CRDS, the time evolution of the laser intensity inside the optical cavity is recorded

by a fast-response photodetector and the decay time constant is extracted, which is directly dependent on the level of absorption, i.e. the molecular species, inside the cavity. Therefore, the direct quantitative analysis of the molecular species is accessible without secondary calibration, if the absorption cross-section of the molecule is known at a certain wavelength.

Another strategy is to measure the total amount of transmitted light, leaking out of the cavity, which is called integrated cavity output spectroscopy (ICOS). By scanning rapidly and repetitively with the laser wavelength across the spectral range of the analyte molecule and then averaging the scans, high-quality spectra with improved signal-to-noise ratio (SNR) can be obtained within a few seconds [88, 89]. Depending on how the laser light is coupled into the optical resonator, a distinction is made between optical feedback cavity-enhanced absorption spectroscopy (OF-CEAS) [90] and off-axis cavity-enhanced absorption spectroscopy (OF-CEAS) [91–93].

Besides, there is the intracavity absorption spectroscopy (ICAS; *a.k.a.*, intracavity laser spectroscopy (ICLS) or intracavity laser absorption spectroscopy (ICLAS)). As the name implies, in ICAS the sample is placed inside the laser resonator whereby the laser light passes through the sample many times [94].

All the different variants of CEAS have in common, that the effective absorption length is significantly enhanced, leading to a very high detection sensitivity, enough for the detection of almost all small breath VOCs at trace quantities.

2.4   Frequency Comb Spectroscopy

A variety of analytical applications require a compromise between broadband and narrowband light sources that provide sensitive, fast, and versatile detection for IR absorption spectroscopy studies to investigate sufficiently complex samples with a limited number of compounds. This requirement can be met by using frequency combs (FCs). With the equidistant frequencies within the FC, this technique can be used for narrowband absorption of molecules to obtain spectrally resolved, high-resolution information. Thus, it is possible to distinguish and characterize both narrow- and broad-band absorbers with FC spectroscopy.

Radiation in the mid-infrared with such spectral properties can be generated by various techniques. Mode-locked lasers in the mid-infrared are similar to known sources in the near-infrared. Typically, approaches using mode-locked lasers in the MIR are similar to established sources in the NIR. Typical approaches in combination with lasers include difference frequency generation (DFG), femtosecond lasers, optical parametric oscillation, and Kerr comb generation [32, 95–97]. An FC spectrometer is more complicated compared to spectrometers using single-mode lasers because the broadband spectrum must be spectrally analyzed to generate an absorption spectrum. It is possible to perform this spectral analysis using a diffraction grating or FT-IR, both of which have a disadvantage in terms of selectivity, measurement speed, and sensitivity.

3 Selected Applications of IR Sensing Technologies in Exhaled Breath Diagnostics

Over the last few years, research has focused on VOCs and their prevalence/role in disease detection. In the following chapter, the importance and application of optical sensor technologies for respiratory gas analysis will be highlighted using selected examples based on relevant biomarker molecules.

3.1 Acetone as Biomarker for Diabetes

Diabetes mellitus is one of the best known and most common metabolic disorders, in which the body's blood glucose level either exceeds 11.1 mml/L [98] (hyperglycemia) or falls below 3.9 mmol/L [99] (hypoglycemia). In this case, affected individuals are unable to produce or properly use the hormone insulin, which regulates blood glucose levels and consequently allows cells to take up glucose as an energy source. Long-term, chronic consequences of diabetes include heart disease, kidney disease, stroke, vision loss, and damage to the nervous system [100].

In general, diabetes can be divided into two groups: Type 1 diabetes (T1D) and Type 2 diabetes (T2D). In T1D, beta cells are destroyed by an autoimmune reaction, resulting in glucose not being recognized and insulin not being released into the bloodstream. In T2D, on the other hand, the body of affected does not respond properly to insulin production, which is caused by damaged or desensitized insulin receptors.

For both diabetes types, acetone can be used as an indicator molecule. Acetone is a ketone that is more highly expressed in diabetic patients due to insulin deficiency and lack of conversion. Consequently, diabetics have an acetone concentration > 1 ppm, while healthy people have an acetone level between 0.3 and 0.9 ppm [101–103]. In addition to diabetes, acetone is also used as an indicator molecule of other medically relevant processes such as fat burning during weight loss [104, 105], monitoring of ketogenic diets in children with epileptic seizures [106, 107], testing of anaerobic limits in sports [108], and heart failure [109, 110].

In the last decade, a wide variety of research groups have been able to detect and quantify acetone in the low ppm range, mainly on the combination of QCLs and multi-pass cells or with cavity-enhanced setups [111–116]. Among these, it is worth mentioning the study by Reyes-Reyes et al. [113], who compared the measured acetone concentration of T1D patients and a control group with their blood glucose levels. They showed that the acetone content in exhaled air was significantly higher in adults than in healthy subjects, although this did not apply to minors. However, in the case of a repeat measurement in an underage subject when ketosis was under control after injecting insulin, they saw that blood glucose and acetone concentrations in exhaled air were higher than in the first measurement. This confirmed that excretion of acetone via the respiratory air is a slow process, which is responsible for

acetone being present in the respiratory air long after ketosis has been controlled. The measurements by Reyes-Reyes and colleagues have shown that measurement of acetone can be helpful in detecting diabetes, although the question of correlation between acetone in respiratory gases and blood glucose levels is still hotly debated and studied.

As an alternative to the expensive and complex laser-based setups, Xing et al. [117] have presented NDIR measurements based on a plasmon enhanced emitter. In their measurements of acetone in dry air and 25% relative humidity, they were able to detect concentrations as low as 50 ppm. While this detection limit is significantly higher compared to laser-based sensors, such a sensor would be significantly less expensive, more compact, and simpler.

These optical sensors offer the possibility of real-time analysis and have the potential to develop wearable and mobile devices. However, for practical use, they require sensitivity and are currently limited by available technology to achieve sufficient species selectivity. In addition, IR-based research has shown that tailored studies are required for more accurate detection of acetone by such sensors.

3.2 Ammonia Detection in Exhaled Breath

Ammonia (NH_3) is one of the simplest and smallest molecules and can therefore be forced into the blood–lung barrier and thus occur in exhaled breath (EB). There are different causes of elevated ammonia concentration in the exhaled breath, like asthma, *Helicobacter pylori*, oral cavity disease, and epilepsy. Most commonly, the ammonia (fishy) odor is associated with renal disorder (e.g., chronic kidney disease (CKD)), dysfunction or failure causing high levels of blood urea nitrogen. Normally, ammonia and ammonia ions are converted into urea through the urea cycle by the liver and then excreted by the kidneys. In case of disorders, the urea amount cannot be sufficiently removed leading to an excessive build-up of ammonia [118, 119]. As alternative to blood analysis, the development of optical sensors for the non-invasive detection and quantification of ammonia in EB is a current field of research.

The relationship between chronic kidney disease, epilepsy, and the NH_3 concentration in the breath was investigated by Bayrakli et al. [120]. Here, the breath ammonia content of 15 healthy volunteers, 10 epilepsy patients before and after taking valproic acid (VAP; drug for therapy of epilepsy patients), and 27 patients with different stages of CKD was evaluated. They used external cavity laser (ECL-) based off-axis cavity-enhanced absorption spectroscopy and determined ammonia levels of 120–530 ppb for healthy and 710–10,400 ppb for CKD patients and found that VAP led to increasing ammonia levels in the exhaled breath.

In another study, Luo et al. [93] used near-infrared OF-CEAS for the detection of ammonia in human exhaled breath, while eliminating the main interference of the gases CO_2 and H_2O. A fibered DFB diode laser with an emission wavelength of 1531.6 nm was coupled to the V-shaped cavity using an appropriate optical

feedback. For their study, exhaled breath was collected into a 10 L Tedlar bag through a disposable mouthpiece. Thereby, a detection limit of 17 ppb for NH_3 in breath gas was achieved for a single scan and could be improved by averaging over 16 scans down to 4.5 ppb, showcasing the detection of very low NH_3 concentrations in human breath.

3.3 CO & NO: Biomarkers for Inflammatory Diseases

Some other small and light molecules that have received attention due to their medical relevance are CO and NO. Most notably, these two molecules stand out for their potential as biomarkers of inflammation or disease, and as possible candidates as inhalation gases for therapeutic use in lung disease [20, 73, 77, 121–127]. Both CO and NO have been implicated as potential indicators of pulmonary and/or systemic inflammation or oxidative stress. In this context, both exhaled CO (eCO) and exhaled NO (eNO) have been extensively studied as putative inflammatory markers for diseases, with applications in respiratory diseases such as asthma, chronic obstructive pulmonary disease (COPD), and cystic fibrosis. In addition, eCO has been shown to be useful in screening for smoking status in the form of a breath test [20, 77, 125].

Several groups performed initial eNO studies in volunteers with cavity-enhanced TDLAS with the background of NO as a potential biomarker for asthma and COPD [123, 124, 128]. With a sensor measurement accuracy in the low ppb range, it was possible to prove that an increased NO concentration is present in asthma and COPD disease in numbers of probands between 170 and 2,500.

In a more recent study to improve sensitivity, Ventrillard et al. [122] demonstrated OF-CEAS for NO trace gas analysis using a QCL at room temperature that achieves a detection limit of 60 ppt.

In contrast to NO, primarily CO studies have been conducted using tunable (diode) laser absorption spectroscopy, examining the effect of smoking as well as various exhalation flow rates and breath-holding durations in the low CO ppb range to provide a reliable sampling method for future medical investigations [20, 77, 125, 127]. Most notably, Ghorbani and Schmidt's [20, 77] studies using their QCL multipass cell sensor showed a clear dependence on exhalation flow rate and breath-hold time for the eCO exhalation profiles. Figure 4 illustrates the setup used for their eCO experiments. Furthermore, for the smokers they found increased eCO values after smoking. Their subsequent analysis of the isotopic ratio of $e^{13}CO$ and $e^{12}CO$ revealed a depletion of $e^{13}CO$ in all breath samples after smoking compared to the natural abundance.
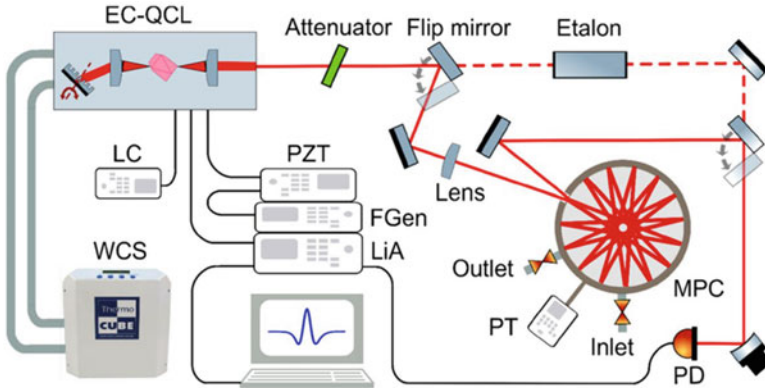
Fig. 4 Schematic of an experimental TDLAS setup for CO measurements including PZT piezo amplifier, FGen function generator, LiA lock-in amplifier, WCS water cooling system, MPC multi-pass cell, PT pressure transducer, and PD photodetector. Copyright © 2017, Optica Publishing Group. Reprinted and modified with permission from [77]

3.4 $^{12}CO_2/^{13}CO_2$ Isotope Ratio Analysis and Its Use in Medical Diagnosis

As optical spectroscopy is very sensitive to distinguish between isotopes it is a fast and low-cost alternative to the commonly used isotope ratio mass spectrometry (IRMS). Especially the ratio between $^{12}CO_2$ and $^{13}CO_2$ has been already used in various studies for the diagnosis of bacterial overgrowth, liver malfunction, fat absorption, the diagnosis of *Helicobacter pylori* infection, and the monitoring of glucose metabolism [63, 129]. The latter is in particular an important parameter in the monitoring of animal experiments in preclinical research or for diagnosis in veterinary medicine. To meet the special requirements such as very small pore volumes (as is the case for mice, for example), on-line and in-situ analysis and real-time results, Tütüncü et al. [130] developed TDLAS gas sensors based on interband cascade lasers and iHWGs and used the mid-infrared spectral window around 2,293–2,295 cm^{-1} (~4.35–4.37 μm) for the distinction between $^{12}CO_2$ and $^{13}CO_2$. Within this study, a 4.35 μm DFB-ICL single-mode IR radiation source was coupled into a straight dual-channel iHWG (75 mm) with 50/50 beam splitter for simultaneous reference measurement. Two pyroelectric infrared detectors were used to evaluate the sample and reference signals synchronously to the oxygen concentrations, evaluated by electron spun oxygen sensors based on luminescence quenching of an immobilized dye. The designed sensor was applied for the routine on-line breath monitoring of 14 ventilated and instrumented mice, illustrated in Fig. 5. The device was able to monitor important metabolic parameters, i.e. total CO_2 amount, $^{13}CO_2$ isotope enrichment, and O_2 in the mice EB, in a sample volume of 315 μL.
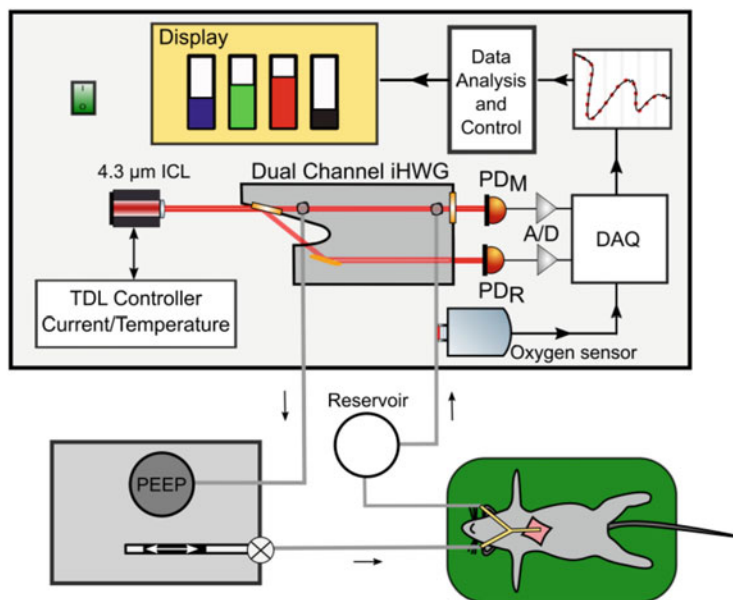
Fig. 5 Mouse breath analyzer: PEEP peep positive and expiratory pressure system, ICL interband cascade laser, PD pyroelectric detector (m measurement, r reference), A/D AD converter, DAQ data acquisition system. Copyright © 2018 American Chemical Society. Reprinted and modified from [130]

Another study showed the versatility of FT-IR-iHWG-based gas sensors to monitor the ^{13}C-enriched carbon dioxide in the same measurement scenario, i.e. in metabolic monitoring via mouse breath analysis. Seichter et al. [131] used an FT-IR-iHWG-sensor to monitor metabolic parameters such as the contribution of protein, carbohydrate, or fat oxidation. The test mice got a ^{13}C glucose stable isotope infusion and the exhaled breath measurements were performed on-line during murine experiments to investigate the reaction of mice to thorax trauma and hemorrhagic shock, using a conventional and compact FT-IR spectrometer combined with a straight-channel iHWG (7.5 cm). For the monitoring of oxygen, a luminescence-based flow-through sensor was integrated into the ventilation equipment in the mouse intensive care unit.

Zhou and co-workers [132, 133] have focused in two studies on the real-time monitoring of ^{13}C and [18]O isotopes in CO_2 with an HWG (1 m)-based mid-infrared gas sensor. In the first study, a 2.73 μm DFB laser was used for simultaneous measurement of concentration changes of the three isotopologues $^{13}CO_2$, $^{12}CO_2$ and $^{18}OC^{16}O$ via direct absorption spectroscopy. In a second study, the results were compared with calibration-free WMS and calibration-needed WMS. The sequences of three CO_2 isotope expirograms of tidal breathing in healthy volunteer and the ratios of $^{13}C/^{12}C$ and $^{18}O/^{16}O$ were evaluated using the same setup as in their previous work, demonstrating the potential for clinical respiratory monitoring.

4   Summary and Outlook

Optical sensors and especially mid-infrared sensing technologies are a powerful and smart approach for the analysis of exhaled breath. Provided that the chemical identity of the biomarker(s) in exhaled air is known and the molecule has well-defined absorption characteristics, robust, user-friendly, and relatively inexpensive optical sensing and analysis devices are readily made available. It has been shown that based on the wide variety of optical breath gas sensing strategies, a large number of biomedically relevant analytes could be detected with concentrations in the diagnostically relevant ppm-to-ppb concentration range. Ultimately, the cost, size, and complexity of the device will depend on the sensitivity required for the desired application scenario. For example, NDIR-based sensors for analyzing CO_2 are significantly cheaper than laser-based systems with, e.g., cavity enhancement, which in comparison have significantly better spectral resolution and sensitivity albeit at higher cost.

Conversely, optical sensors also have remaining challenges to overcome. For example, the sensitivity of an optical absorption measurement depends linearly on the linewidth of the optical transition of the analyte under investigation. Another important aspect is that advanced data analysis strategies (i.e., multivariate statistics; also known as chemometrics) are used in obtaining broadband – i.e., often highly convoluted – IR data from breath samples containing a large variety of absorbing molecules at a variety of concentrations. In addition, the analysis of diagnostically relevant low-concentrated molecules (i.e., usually sub-ppm concentrations) such as frequently encountered for NO, CO, NH_3, and acetone, their signatures may be overlapped by the relatively high-concentrated molecules such as H_2O and CO_2. A third limitation of current optical gas analyzers may be the number of analytes that can be addressed with a single light source. Most optical analyzers are designed to determine one up to maybe three or four analytes simultaneously, while frequently only one of them may be analyzed with high sensitivity.

In conclusion, optical sensor technology with its outstanding ability for real-time analysis and monitoring represents a viable strategy for the accurate quantification of volatile biomarkers at low concentration levels within complex exhaled breath matrices. In particular, the mid-infrared region is the most information-rich segment of the electromagnetic spectrum, which is therefore ideally suited for the development of non-invasive and label-free sensing devices and diagnostic technologies. Especially due to the revolution – and ongoing evolution – of IR light sources, waveguides, and detectors, a new generation of exhaled breath analyzers and sensing tools will be emerging. Their inherent molecular selectivity, robustness, and ease of implementation and handling combined with appropriated automated data evaluation, mining, and classification algorithms render them ideally suited for routines use in daily clinical practice, intensive care scenarios, and – once available in a hand-held format – even in medical emergencies and first responder scenarios.

Author Contribution M.H. and S.K. contributed equally and B.M. has proofread, prepared, and edited the final manuscript for submission and publication. All authors have read and agreed to the published version of the manuscript.

References

1. Gordon IE, Rothman LS, Hill C, Kochanov RV, Tan Y, Bernath PF, Birk M, Boudon V, Campargue A, Chance KV, Drouin BJ, Flaud J-M, Gamache RR, Hodges JT, Jacquemart D, Perevalov VI, Perrin A, Shine KP, Smith M-AH, Tennyson J, Toon GC, Tran H, Tyuterev VG, Barbe A, Császár AG, Devi VM, Furtenbacher T, Harrison JJ, Hartmann J-M, Jolly A, Johnson TJ, Karman T, Kleiner I, Kyuberis AA, Loos J, Lyulin OM, Massie ST, Mikhailenko SN, Moazzen-Ahmadi N, Müller HSP, Naumenko OV, Nikitin AV, Polyansky OL, Rey M, Rotger M, Sharpe SW, Sung K, Starikova E, Tashkun SA, Auwera J v, Wagner G, Wilzewski J, Wcisło P, Yu S, Zak EJ (2017) The HITRAN2016 molecular spectroscopic database. J Quant Spectrosc Radiat Transf 203:3–69. https://doi.org/10.1016/j.jqsrt.2017.06.038
2. Kim SS, Mizaikoff B (2014) Miniaturized optical sensors for medical diagnostics. In: Handbook of spectroscopy: second, enlarged edition 4–4, pp 1557–1584. https://doi.org/10.1002/9783527654703.ch46
3. Marazuela MD, Moreno-Bondi MC (2002) Fiber-optic biosensors – an overview. Anal Bioanal Chem 372:664–682. https://doi.org/10.1007/s00216-002-1235-9
4. Mizaikoff B (2013) Waveguide-enhanced mid-infrared chem/bio sensors. Chem Soc Rev 42:8683–8699. https://doi.org/10.1039/c3cs60173k
5. Tong XC (2013) Advanced materials for integrated optical waveguide.1st edn. Springer
6. Harrington JA (2000) A review of IR transmitting, hollow waveguides. Fiber Integr Opt 19:211–227. https://doi.org/10.1080/01468030050058794
7. Rayleigh L (1897) XVIII. On the passage of electric waves through tubes, or the vibrations of dielectric cylinders. Lond Edinb Dublin Philos Mag J Sci 43:125–132. https://doi.org/10.1080/14786449708620969
8. Kapany NS, Simms RJ (1965) Recent developments in infrared fiber optics*. Infrared Phys 5:69–80. https://doi.org/10.1016/0020-0891(65)90009-6
9. Haas J, Pleyer M, Nauschütz J, Koeth J, Nägele M, Bibikova O, Sakharova T, Artyushenko V, Mizaikoff B (2019) iBEAM: substrate-integrated hollow waveguides for efficient laser beam combining. Opt Express 27:23059. https://doi.org/10.1364/OE.27.023059
10. Wilk A, Chance Carter J, Chrisp M, Manuel AM, Mirkarimi P, Alameda JB, Mizaikoff B (2013) Substrate-integrated hollow waveguides: a new level of integration in mid-infrared gas sensing. Anal Chem 85:11205–11210. https://doi.org/10.1021/ac402391m
11. Fortes PR, Da Silveira Petruci JF, Wilk A, Cardoso AA, Raimundo IM, Mizaikoff B (2014) Optimized design of substrate-integrated hollow waveguides for mid-infrared gas analyzers. J Opt 16:094006. https://doi.org/10.1088/2040-8978/16/9/094006
12. Cui R, Dong L, Wu H, Ma W, Xiao L, Jia S, Chen W, Tittel FK (2020) Three-dimensional printed miniature fiber-coupled multipass cells with dense spot patterns for ppb-level methane detection using a near-IR diode laser. Anal Chem 92:13034–13041. https://doi.org/10.1021/acs.analchem.0c01931
13. White JU (1942) Long optical paths of large aperture. J Opt Soc Am 32:285. https://doi.org/10.1364/josa.32.000285

14. Hanna M, Guichard F, Daher N, Bournet Q, Délen X, Georges P (2021) Nonlinear optics in multipass cells. Laser Photonics Rev 15:1–14. https://doi.org/10.1002/lpor.202100220

15. Herriott D, Kogelnik H, Kompfner R (1964) Off-axis paths in spherical mirror interferometers. Appl Opt 3:523. https://doi.org/10.1364/ao.3.000523

16. Rothbart N, Schmalz K, Hubers HW (2020) A compact circular multipass cell for millimeter-wave/terahertz gas spectroscopy. IEEE Trans Terahertz Sci Technol 10:9–14. https://doi.org/10.1109/TTHZ.2019.2950123

17. Manninen A, Tuzson B, Looser H, Bonetti Y, Emmenegger L (2012) Versatile multipass cell for laser spectroscopic trace gas analysis. Appl Phys B Lasers Opt 109:461–466. https://doi.org/10.1007/s00340-012-4964-2

18. Tuzson B, Mangold M, Looser H, Manninen A, Emmenegger L (2013) Compact multipass optical cell for laser spectroscopy. Opt Lett 38:257. https://doi.org/10.1364/ol.38.000257

19. Zou M, Yang Z, Sun L, Ming X (2020) Acetylene sensing system based on wavelength modulation spectroscopy using a triple-row circular multi-pass cell. Opt Express 28:11573. https://doi.org/10.1364/oe.388343

20. Ghorbani R, Schmidt FM (2017) ICL-based TDLAS sensor for real-time breath gas analysis of carbon monoxide isotopes. Opt Express 25:12743. https://doi.org/10.1364/oe.25.012743

21. Yao Y, Hoffman AJ, Gmachl CF (2012) Mid-infrared quantum cascade lasers. Nat Photonics 6:432–439. https://doi.org/10.1038/nphoton.2012.143

22. Vurgaftman I, Weih R, Kamp M, Meyer JR, Canedy CL, Kim CS, Kim M, Bewley WW, Merritt CD, Abell J, Höfling S (2015) Interband cascade lasers. J Phys D Appl Phys 48:123001. https://doi.org/10.1088/0022-3727/48/12/123001

23. Faist J, Capasso F, Sivco DL, Sirtori C, Hutchinson AL, Cho AY (1994) Quantum cascade laser. Science 264:553–556. https://doi.org/10.1126/science.264.5158.553

24. Köhler R, Tredicucci A, Beltram F, Beere HE, Linfield EH, Davies AG, Ritchie DA, Iotti RC, Rossi F (2002) Terahertz semiconductor-heterostructure laser. Nature 417:156–159. https://doi.org/10.1038/417156a

25. Williams BS (2007) Terahertz quantum-cascade lasers. Nat Photonics 1:517–525. https://doi.org/10.1038/nphoton.2007.166

26. Semtsiv MP, Ziegler M, Dressler S, Masselink WT, Georgiev N, Dekorsy T, Helm M (2004) Above room temperature operation of short wavelength ($\lambda=3.8\mu m$) strain-compensated In0.73Ga0.27As–AlAs quantum-cascade lasers. Appl Phys Lett 85:1478–1480. https://doi.org/10.1063/1.1789246

27. Bandyopadhyay N, Slivken S, Bai Y, Razeghi M (2012) High power, continuous wave, room temperature operation of $\lambda \sim 3.4\,\mu m$ and $\lambda \sim 3.55\,\mu m$ InP-based quantum cascade lasers. Appl Phys Lett 100:212104. https://doi.org/10.1063/1.4719110

28. Machhadani H, Kandaswamy P, Sakr S, Vardi A, Wirtmüller A, Nevou L, Guillot F, Pozzovivo G, Tchernycheva M, Lupu A, Vivien L, Crozat P, Warde E, Bougerol C, Schacham S, Strasser G, Bahir G, Monroy E, Julien FH (2009) GaN/AlGaN intersubband optoelectronic devices. New J Phys 11:125023. https://doi.org/10.1088/1367-2630/11/12/125023

29. Franz KJ, Charles WO, Shen A, Hoffman AJ, Tamargo MC, Gmachl C (2008) ZnCdSe/ZnCdMgSe quantum cascade electroluminescence. Appl Phys Lett 92:121105. https://doi.org/10.1063/1.2903135

30. Yang RQ (1995) Infrared laser based on intersubband transitions in quantum wells. Superlattice Microst 17:77–83. https://doi.org/10.1006/spmi.1995.1017

31. Yang RQ, Bruno JD, Bradshaw JL, Pham JT, Wortman DE (2000) Interband cascade lasers: progress and challenges. Physica E 7:69–75. https://doi.org/10.1016/S1386-9477(99)00280-5

32. Schliesser A, Picqué N, Hänsch TW (2012) Mid-infrared frequency combs. Nat Photonics 6:440–449. https://doi.org/10.1038/nphoton.2012.142

33. Kazemi Moridani A, Zando R, Xie W, Howell I, Watkins JJ, Lee J-H (2017) Plasmonic thermal emitters for dynamically tunable infrared radiation. Adv Opt Mater 5:1600993. https://doi.org/10.1002/adom.201600993

34. Sha J, Chen W, Yan K, Luo J, Xu R, Yao D, Liao S, Zhong J, Yang S, Yu Y, Tong Y, Xu Z, Liu X, Lin Y-S (2018) Tunable metamaterial ir emitter by using MEMS microheater. In: 2018 international conference on optical MEMS and nanophotonics (OMN). IEEE, pp 1–2

35. Spannhake J, Schulz O, Helwig A, Krenkow A, Müller G, Doll T (2006) High-temperature MEMS heater platforms: long-term performance of metal and semiconductor heater materials. Sensors 6:405–419. https://doi.org/10.3390/s6040405

36. Takahara J, Ueba Y (2013) Thermal infrared emitters by plasmonic metasurface. In: Mackay TG, Lakhtakia A, Jen Y-J, Suzuki M (eds) Nanostructured thin films VI, p 88180X

37. Tsai M-W, Chuang T-H, Meng C-Y, Chang Y-T, Lee S-C (2006) High performance midinfrared narrow-band plasmonic thermal emitter. Appl Phys Lett 89:173116. https://doi.org/10.1063/1.2364860

38. Yang Z, Ishii S, Yokoyama T, Dao TD, Sun M, Nagao T, Chen K (2016) Tamm plasmon selective thermal emitters. Opt Lett 41:4453. https://doi.org/10.1364/ol.41.004453

39. Hlavatsch M, Mizaikoff B (2022) Advanced mid-infrared lightsources above and beyond lasers and their analytical utility. Anal Sci 38:1125. https://doi.org/10.1007/s44211-022-00133-3

40. Briggs AF, Nordin LJ, Muhowski AJ, Petluru P, Silva D, Wasserman D, Bank SR (2020) Mid-infrared electroluminescence from type-II In(Ga)Sb quantum dots. Appl Phys Lett 116: 061103. https://doi.org/10.1063/1.5134808

41. Das NC (2011) Effect of indium mole fraction on infrared light emitting diode (LED) device performance. Phys Status Solidi A 208:191–194. https://doi.org/10.1002/pssa.201026350

42. Gong X, Yang Z, Walters G, Comin R, Ning Z, Beauregard E, Adinolfi V, Voznyy O, Sargent EH (2016) Highly efficient quantum dot near-infrared light-emitting diodes. Nat Photonics 10: 253–257. https://doi.org/10.1038/nphoton.2016.11

43. Han X, Bai Q, Yao L, Liu H, Gao Y, Li J, Liu L, Liu Y, Li X, Lu P, Yang B (2015) Highly efficient solid-state near-infrared emitting material based on triphenylamine and diphenylfumaronitrile with an EQE of 2.58% in nondoped organic light-emitting diode. Adv Funct Mater 25:7521–7529. https://doi.org/10.1002/adfm.201503344

44. Tuong Ly K, Chen-Cheng R-W, Lin H-W, Shiau Y-J, Liu S-H, Chou P-T, Tsao C-S, Huang Y-C, Chi Y (2017) Near-infrared organic light-emitting diodes with very high external quantum efficiency and radiance. Nat Photonics 11:63–68. https://doi.org/10.1038/nphoton.2016.230

45. Montealegre DA, Schrock KN, Walhof AC, Muellerleile AM, Prineas JP (2021) High-power mid-wave infrared LED using W-superlattices and textured surfaces. Appl Phys Lett 118: 071105. https://doi.org/10.1063/5.0039269

46. Pradhan S, di Stasio F, Bi Y, Gupta S, Christodoulou S, Stavrinadis A, Konstantatos G (2019) High-efficiency colloidal quantum dot infrared light-emitting diodes via engineering at the supra-nanocrystalline level. Nat Nanotechnol 14:72–79. https://doi.org/10.1038/s41565-018-0312-y

47. Schäfer N, Scheuermann J, Weih R, Koeth J, Höfling S (2019) High efficiency mid-infrared interband cascade LEDs grown on low absorbing substrates emitting >5 mW of output power. Opt Eng 58:1. https://doi.org/10.1117/1.OE.58.11.117106

48. Rogalski A, Martyniuk P, Kopytko M (2017) InAs/GaSb type-II superlattice infrared detectors: future prospect. Appl Phys Rev 4:031304. https://doi.org/10.1063/1.4999077

49. Soibel A, Ting DZ, Rafol SB, Fisher AM, Keo SA, Khoshakhlagh A, Gunapala SD (2019) Mid-wavelength infrared InAsSb/InAs nBn detectors and FPAs with very low dark current density. Appl Phys Lett 114:161103. https://doi.org/10.1063/1.5092342

50. Ma L, Zhang X, Li H, Tan H, Yang Y, Xu Y, Hu W, Zhu X, Zhuang X, Pan A (2015) Bandgap-engineered GaAsSb alloy nanowires for near-infrared photodetection at 1.31 μm. Semicond Sci Technol 30:105033. https://doi.org/10.1088/0268-1242/30/10/105033

51. Li Z, Yuan X, Fu L, Peng K, Wang F, Fu X, Caroff P, White TP, Hoe Tan H, Jagadish C (2015) Room temperature GaAsSb single nanowire infrared photodetectors. Nanotechnology 26:445202. https://doi.org/10.1088/0957-4484/26/44/445202

52. Tan H, Fan C, Ma L, Zhang X, Fan P, Yang Y, Hu W, Zhou H, Zhuang X, Zhu X, Pan A (2016) Single-crystalline InGaAs nanowires for room-temperature high-performance near-infrared photodetectors. Nano-Micro Lett 8:29–35. https://doi.org/10.1007/s40820-015-0058-0

53. Pettersson H, Trägårdh J, Persson AI, Landin L, Hessman D, Samuelson L (2006) Infrared photodetectors in heterostructure nanowires. Nano Lett 6:229–232. https://doi.org/10.1021/nl052170l

54. Downs C, Vandervelde T (2013) Progress in infrared photodetectors since 2000. Sensors 13: 5054–5098. https://doi.org/10.3390/s130405054

55. Zavvari M, Ahmadi V (2013) Quantum-dot-based mid-IR single-photon detector with self-quenching and self-recovering operation. IEEE Electron Device Lett 34:783–785. https://doi.org/10.1109/LED.2013.2258396

56. Cao R, Wang H, Guo Z, Sang DK, Zhang L, Xiao Q, Zhang Y, Fan D, Li J, Zhang H (2019) Black phosphorous/indium selenide photoconductive detector for visible and near-infrared light with high sensitivity. Adv Opt Mater 7:1900020. https://doi.org/10.1002/adom.201900020

57. Luo L-B, Chen J-J, Wang M-Z, Hu H, Wu C-Y, Li Q, Wang L, Huang J-A, Liang F-X (2014) Near-infrared light photovoltaic detector based on GaAs nanocone array/monolayer graphene schottky junction. Adv Funct Mater 24:2794–2800. https://doi.org/10.1002/adfm.201303368

58. Dinh TV, Choi IY, Son YS, Kim JC (2016) A review on non-dispersive infrared gas sensors: improvement of sensor detection limit and interference correction. Sensors Actuators B Chem 231:529–538. https://doi.org/10.1016/j.snb.2016.03.040

59. Chowdhury MF, Hopper R, Ali SZ, Gardner JW, Udrea F (2016) MEMS infrared emitter and detector for capnography applications. Procedia Eng 168:1204–1207. https://doi.org/10.1016/j.proeng.2016.11.415

60. Fleming L, Gibson D, Hutson D, Ahmadzadeh S, Waddell E, Song S, Reid S, Clark C, Baker JS, Overend R, MacGregor C (2021) Breath emulator for simulation and modelling of expired tidal breath carbon dioxide characteristics. Comput Methods Prog Biomed 200:105826. https://doi.org/10.1016/j.cmpb.2020.105826

61. Hartmann A, Strzoda R, Schrobenhauser R, Weigel R (2014) CO2 sensor for mainstream capnography based on TDLAS. Appl Phys B Lasers Opt 116:1023–1026. https://doi.org/10.1007/s00340-014-5791-4

62. Prokopiuk A, Bielecki Z, Wojtas J (2021) Improving the accuracy of the Ndir-based Co2 sensor for breath analysis. Metrol Meas Syst 28:803–812. https://doi.org/10.24425/mms.2021.138578

63. Modak AS (2007) Stable isotope breath tests in clinical medicine: a review. J Breath Res 1: 014003. https://doi.org/10.1088/1752-7155/1/1/014003

64. Esfahani S, Tiele A, Agbroko SO, Covington JA (2020) Development of a tuneable NDIR optical electronic nose. Sensors 20:1–16. https://doi.org/10.3390/s20236875

65. Rey J, Atxaerandio R, Ruiz R, Ugarte E, González-Recio O, Garcia-Rodriguez A, Goiri I (2019) Comparison between non-invasive methane measurement techniques in cattle. Animals 9:1–9. https://doi.org/10.3390/ani9080563

66. Zhu Z, Xu Y, Jiang B (2012) A one ppm NDIR methane gas sensor with single frequency filter denoising algorithm. Sensors 12:12729–12740. https://doi.org/10.3390/s120912729

67. Kim J, Lee K, Yi S (2016) NDIR ethanol gas sensor with two elliptical optical structures. Procedia Eng 168:359–362. https://doi.org/10.1016/j.proeng.2016.11.122

68. Fujitsuka N, Yonemura M, Sakakibara K, Taguchi T, Wakita T (2014) Alcohol detection in exhaled air using NDIR absorption method. R&D Rev Toyota CRDL 45:29–34

69. Xing Y, Urasinska-Wojcik B, Gardner JW (2018) Plasmonic enhanced CMOS non-dispersive infrared gas sensor for acetone and ammonia detection. In: I2MTC 2018 – 2018 IEEE international instrumentation and measurement technology conference: discovering new horizons in instrumentation and measurement, proceedings, pp 1–5. https://doi.org/10.1109/I2MTC.2018.8409745

70. Bienz S, Bigler L, Fox T, Meier H (2016) Spektroskopische Methoden in der organischen Chemie.7th edn. Thieme
71. Bell RJ (1972) Introductory Fourier transform spectroscopy. Academic Press
72. Helmut G, Hans-Ulrich G (2003) IR-Spektroskopie: eine Einführung.4th edn. Wiley-VCH, Weinheim
73. Roller C, Namjou K, Jeffers J, Potter W, McCann PJ, Grego J (2002) Simultaneous NO and CO_2 measurement in human breath with a single IV–VI mid-infrared laser. Opt Lett 27:107. https://doi.org/10.1364/ol.27.000107
74. Vaittinen O, Manfred Schmidt F, Metsala M, Halonen L (2013) Exhaled breath biomonitoring using laser spectroscopy. Curr Anal Chem 9:463–475. https://doi.org/10.2174/1573411011309030016
75. Wang C, Sahay P (2009) Breath analysis using laser spectroscopic techniques: breath biomarkers, spectral fingerprints, and detection limits. Sensors 9:8230–8262. https://doi.org/10.3390/s91008230
76. Jahjah M, Ren W, Stefański P, Lewicki R, Zhang J, Jiang W, Tarka J, Tittel FK (2014) A compact QCL based methane and nitrous oxide sensor for environmental and medical applications. Analyst 139:2065–2069. https://doi.org/10.1039/c3an01452e
77. Ghorbani R, Schmidt FM (2017) Real-time breath gas analysis of CO and CO2 using an EC-QCL. Appl Phys B Lasers Opt 123:1. https://doi.org/10.1007/s00340-017-6715-x
78. Ai Y, Li J, Li Q, Sun M, Li Y, Wang C (2020) Cavity ringdown spectroscopy of nitric oxide in the ultraviolet region for human breath test. J Breath Res 14:037101. https://doi.org/10.1088/1752-7163/ab8184
79. Chen W, Metsälä M, Vaittinen O, Halonen L (2014) The origin of mouth-exhaled ammonia. J Breath Res 8:036003. https://doi.org/10.1088/1752-7155/8/3/036003
80. Keppler F, Schiller A, Ehehalt R, Greule M, Hartmann J, Polag D (2016) Stable isotope and high precision concentration measurements confirm that all humans produce and exhale methane. J Breath Res 10:016003. https://doi.org/10.1088/1752-7155/10/1/016003
81. Larracy R, Phinyomark A, Scheme E (2022) Infrared cavity ring-down spectroscopy for detecting non-small cell lung cancer in exhaled breath. J Breath Res 16:026008. https://doi.org/10.1088/1752-7163/ac5e4f
82. Maithani S, Mandal S, Maity A, Pal M, Pradhan M (2018) High-resolution spectral analysis of ammonia near 6.2 μm using a cw EC-QCL coupled with cavity ring-down spectroscopy. Analyst 143:2109–2114. https://doi.org/10.1039/c7an02008b
83. Maity A, Pal M, Banik GD, Maithani S, Pradhan M (2017) Cavity ring-down spectroscopy using an EC-QCL operating at 7.5 μm for direct monitoring of methane isotopes in air. Laser Phys Lett 14:115701. https://doi.org/10.1088/1612-202X/aa8584
84. Neri G, Lacquaniti A, Rizzo G, Donato N, Latino M, Buemi M (2012) Real-time monitoring of breath ammonia during haemodialysis: use of ion mobility spectrometry (IMS) and cavity ring-down spectroscopy (CRDS) techniques. Nephrol Dial Transplant 27:2945–2952. https://doi.org/10.1093/ndt/gfr738
85. Schmidt FM, Metsälä M, Vaittinen O, Halonen L (2011) Background levels and diurnal variations of hydrogen cyanide in breath and emitted from skin. J Breath Res 5:046004. https://doi.org/10.1088/1752-7155/5/4/046004
86. Schmidt FM, Vaittinen O, Metsälä M, Lehto M, Forsblom C, Groop PH, Halonen L (2013) Ammonia in breath and emitted from skin. J Breath Res 7:017109. https://doi.org/10.1088/1752-7155/7/1/017109
87. Zhou S, Han Y, Li B (2018) Pressure optimization of an EC-QCL based cavity ring-down spectroscopy instrument for exhaled NO detection. Appl Phys B Lasers Opt 124:1–8. https://doi.org/10.1007/s00340-018-6898-9
88. Banik GD, Mizaikoff B (2020) Exhaled breath analysis using cavity-enhanced optical techniques: a review. J Breath Res 14:043001. https://doi.org/10.1088/1752-7163/abaf07

89. Mandal S, Mukhopadhyay P, Ghosh C, Pal M, Banik GD, Chatterjee T, Ghosh S, Pradhan M (2018) Isotope-specific breath analysis to track the end-stage renal disease during hemodialysis. J Breath Res 12:036019. https://doi.org/10.1088/1752-7163/aab84d

90. Ventrillard-Courtillot I, Gonthiez T, Clerici C, Romanini D (2009) Multispecies breath analysis faster than a single respiratory cycle by optical-feedback cavity-enhanced absorption spectroscopy. J Biomed Opt 14:064026. https://doi.org/10.1117/1.3269677

91. Ciaffoni L, O'Neill DP, Couper JH, Ritchie GAD, Hancock G, Robbins PA (2016) In-airway molecular flow sensing: a new technology for continuous, noninvasive monitoring of oxygen consumption in critical care. Sci Adv 2:1–10. https://doi.org/10.1126/sciadv.1600560

92. Maignan M, Briot R, Romanini D, Gennai S, Hazane-Puch F, Brouta A, Debaty G, Ventrillard I (2014) Real-time measurements of endogenous carbon monoxide production in isolated pig lungs. J Biomed Opt 19:047001. https://doi.org/10.1117/1.jbo.19.4.047001

93. Luo Z, Tan Z, Long X (2019) Application of near-infrared optical feedback cavity enhanced absorption spectroscopy (OF-CEAS) to the detection of ammonia in exhaled human breath. Sensors 19:1–11. https://doi.org/10.3390/s19173686

94. Fjodorow P, Frolov MP, Korostelin YV, Kozlovsky VI, Leonov SO, Schulz C, Skasyrsky YK (2021) Intracavity absorption spectroscopy of CO_2, CO and N_2O using a Fe:ZnSe laser tunable in the range of 3.7-5.3 μm. Opt InfoBase Conf Pap 29:12033–12049. https://doi.org/10.1364/es.2021.eth1a.6

95. Eisele M, Cocker TL, Huber MA, Plankl M, Viti L, Ercolani D, Sorba L, Vitiello MS, Huber R (2014) Ultrafast multi-terahertz nano-spectroscopy with sub-cycle temporal resolution. Nat Photonics 8:841–845. https://doi.org/10.1038/nphoton.2014.225

96. Holzwarth R, Udem T, Hänsch TW, Knight JC, Wadsworth WJ, St Russell PJ (2000) Optical frequency synthesizer for precision spectroscopy. Phys Rev Lett 85(11):2264

97. Liang Q, Chan YC, Bryan Changala P, Nesbitt DJ, Ye J, Toscano J (2021) Ultrasensitive multispecies spectroscopic breath analysis for real-time health monitoring and diagnostics. Proc Natl Acad Sci U S A 118:1–6. https://doi.org/10.1073/pnas.2105063118

98. American Diabetes Association (2017) 2. Classification and diagnosis of diabetes. Diabetes Care 40:S11–S24. https://doi.org/10.2337/dc17-S005

99. Seaquist ER, Anderson J, Childs B, Cryer P, Dagogo-Jack S, Fish L, Heller SR, Rodriguez H, Rosenzweig J, Vigersky R (2013) Hypoglycemia and diabetes: a report of a workgroup of the American diabetes association and the endocrine society. J Clin Endocrinol Metab 98:1845–1859. https://doi.org/10.1210/jc.2012-4127

100. Roglic G, World Health Organization (2016) Global report on diabetes. WHO, Geneva

101. Jiang C, Sun M, Wang Z, Chen Z, Zhao X, Yuan Y, Li Y, Wang C (2016) Portable real-time ringdown breath acetone analyzer: toward potential diabetic screening and management. Sensors 16:1199. https://doi.org/10.3390/s16081199

102. Deng C, Zhang J, Yu X, Zhang W, Zhang X (2004) Determination of acetone in human breath by gas chromatography–mass spectrometry and solid-phase microextraction with on-fiber derivatization. J Chromatogr B 810:269–275. https://doi.org/10.1016/j.jchromb.2004.08.013

103. Saasa V, Malwela T, Beukes M, Mokgotho M, Liu C-P, Mwakikunga B (2018) Sensing technologies for detection of acetone in human breath for diabetes diagnosis and monitoring. Diagnostics 8:12. https://doi.org/10.3390/diagnostics8010012

104. Anderson JC (2015) Measuring breath acetone for monitoring fat loss: review. Obesity 23:2327–2334. https://doi.org/10.1002/oby.21242

105. Toyooka T, Hiyama S, Yamada Y (2013) A prototype portable breath acetone analyzer for monitoring fat loss. J Breath Res 7:036005. https://doi.org/10.1088/1752-7155/7/3/036005

106. Musa-Veloso K (2002) Epilepsy and the ketogenic diet: assessment of ketosis in children using breath acetone. Pediatr Res 52:443–448. https://doi.org/10.1203/01.PDR.0000030717.77598.40

107. Musa-Veloso K, Likhodii SS, Rarama E, Benoit S, Liu YC, Chartrand D, Curtis R, Carmant L, Lortie A, Comeau FJE, Cunnane SC (2006) Breath acetone predicts plasma ketone bodies in

children with epilepsy on a ketogenic diet. Nutrition 22:1–8. https://doi.org/10.1016/j.nut.2005.04.008

108. King J, Kupferthaler A, Unterkofler K, Koc H, Teschl S, Teschl G, Miekisch W, Schubert J, Hinterhuber H, Amann A (2009) Isoprene and acetone concentration profiles during exercise on an ergometer. J Breath Res 3:027006. https://doi.org/10.1088/1752-7155/3/2/027006

109. Gouzi F, Ayache D, Hédon C, Molinari N, Vicet A (2022) Breath acetone concentration: too heterogeneous to constitute a diagnosis or prognosis biomarker in heart failure? A systematic review and meta-analysis. J Breath Res 16:016001. https://doi.org/10.1088/1752-7163/ac356d

110. Marcondes-Braga FG, Gutz IGR, Batista GL, Saldiva PHN, Ayub-Ferreira SM, Issa VS, Mangini S, Bocchi EA, Bacal F (2012) Exhaled acetone as a new biomarker of heart failure severity. Chest 142:457–466. https://doi.org/10.1378/chest.11-2892

111. Ciaffoni L, Hancock G, Harrison JJ, Van Helden JPH, Langley CE, Peverall R, Ritchie GAD, Wood S (2013) Demonstration of a mid-infrared cavity enhanced absorption spectrometer for breath acetone detection. Anal Chem 85:846–850. https://doi.org/10.1021/ac3031465

112. Reyes-Reyes A, Hou Z, van Mastrigt E, Horsten RC, de Jongste JC, Pijnenburg MW, Urbach HP, Bhattacharya N (2014) Multicomponent gas analysis using broadband quantum cascade laser spectroscopy. Opt Express 22:18299. https://doi.org/10.1364/oe.22.018299

113. Reyes-Reyes A, Horsten RC, Urbach HP, Bhattacharya N (2015) Study of the exhaled acetone in type 1 diabetes using quantum cascade laser spectroscopy. Anal Chem 87:507–512. https://doi.org/10.1021/ac504235e

114. Nadeem F, Mandon J, Khodabakhsh A, Cristescu SM, Harren FJM (2018) Sensitive spectroscopy of acetone using a widely tunable external-cavity quantum cascade laser. Sensors 18:2050. https://doi.org/10.3390/s18072050

115. Schwarm KK, Strand CL, Miller VA, Spearrin RM (2020) Calibration-free breath acetone sensor with interference correction based on wavelength modulation spectroscopy near 8.2 μm. Appl Phys B Lasers Opt 126:1–10. https://doi.org/10.1007/s00340-019-7358-x

116. Centeno R, Marchenko D, Mandon J, Cristescu SM, Wulterkens G, Harren FJM (2014) High power, widely tunable, mode-hop free, continuous wave external cavity quantum cascade laser for multi-species trace gas detection. Appl Phys Lett 105:261907. https://doi.org/10.1063/1.4905281

117. Xing Y, Urasinska-Wojcik B, Gardner JW (2018) Plasmonic enhanced CMOS non-dispersive infrared gas sensor for acetone and ammonia detection. In: 2018 IEEE international instrumentation and measurement technology conference (I2MTC). IEEE, pp 1–5

118. Krishnan ST, Devadhasan JP, Kim S (2017) Recent analytical approaches to detect exhaled breath ammonia with special reference to renal patients. Anal Bioanal Chem 409:21–31. https://doi.org/10.1007/s00216-016-9903-3

119. Mochalski P, King J, Haas M, Unterkofler K, Amann A, Mayer G (2014) Blood and breath profiles of volatile organic compounds in patients with end-stage renal disease. BMC Nephrol 15:1–14. https://doi.org/10.1186/1471-2369-15-43

120. Bayrakli I, Turkmen A, Akman H, Sezer MT, Kutluhan S (2016) Applications of external cavity diode laser-based technique to noninvasive clinical diagnosis using expired breath ammonia analysis: chronic kidney disease, epilepsy. J Biomed Opt 21:087004. https://doi.org/10.1117/1.jbo.21.8.087004

121. McCurdy MR, Bakhirkin YA, Tittel FK (2006) Quantum cascade laser-based integrated cavity output spectroscopy of exhaled nitric oxide. Appl Phys B Lasers Opt 85:445–452. https://doi.org/10.1007/s00340-006-2365-0

122. Ventrillard I, Gorrotxategi-Carbajo P, Romanini D (2017) Part per trillion nitric oxide measurement by optical feedback cavity-enhanced absorption spectroscopy in the mid-infrared. Appl Phys B Lasers Opt 123:1–8. https://doi.org/10.1007/s00340-017-6750-7

123. Shorter JH, Nelson DD, McManus JB, Zahniser MS, Sama SR, Milton DK (2011) Clinical study of multiple breath biomarkers of asthma and COPD (NO, CO2, CO and N2O) by infrared laser spectroscopy. J Breath Res 5:037108. https://doi.org/10.1088/1752-7155/5/3/037108

124. Namjou K, Roller CB, McMillen G (2007) Breath-analysis using mid-infrared tunable laser spectroscopy. In: Proceedings of IEEE sensors, pp 1337–1340. https://doi.org/10.1109/ICSENS.2007.4388658

125. Ghorbani R, Schmidt FM (2019) Fitting of single-exhalation profiles using a pulmonary gas exchange model – application to carbon monoxide. J Breath Res 13:026001. https://doi.org/10.1088/1752-7163/aafc91

126. Thorpe MJ, Balslev-Clausen D, Kirchner MS, Ye J (2008) Cavity-enhanced optical frequency comb spectroscopy: application to human breath analysis. Opt Express 16:2387. https://doi.org/10.1364/oe.16.002387

127. Pakmanesh N, Cristescu SM, Ghorbanzadeh A, Harren FJM, Mandon J (2016) Quantum cascade laser-based sensors for the detection of exhaled carbon monoxide. Appl Phys B Lasers Opt 122:1–9. https://doi.org/10.1007/s00340-015-6294-7

128. Namjou K, Roller CB, Reich TE, Jeffers JD, McMillen GL, McCann PJ, Camp MA (2006) Determination of exhaled nitric oxide distributions in a diverse sample population using tunable diode laser absorption spectroscopy. Appl Phys B Lasers Opt 85:427–435. https://doi.org/10.1007/s00340-006-2301-3

129. Barreto DN, Kokoric V, da Silveira Petruci JF, Mizaikoff B (2021) From light pipes to substrate-integrated hollow waveguides for gas sensing: a review. ACS Meas Sci Au 1:97–109. https://doi.org/10.1021/acsmeasuresciau.1c00029

130. Tütüncü E, Nägele M, Becker S, Fischer M, Koeth J, Wolf C, Köstler S, Ribitsch V, Teuber A, Gröger M, Kress S, Wepler M, Wachter U, Vogt J, Radermacher P, Mizaikoff B (2018) Advanced photonic sensors based on interband cascade lasers for real-time mouse breath analysis. ACS Sens 3:1743–1749. https://doi.org/10.1021/acssensors.8b00477

131. Seichter F, Vogt J, Tütüncü E, Hagemann LT, Wachter U, Gröger M, Kress S, Radermacher P, Mizaikoff B (2021) Metabolic monitoring via on-line analysis of 13C-enriched carbon dioxide in exhaled mouse breath using substrate-integrated hollow waveguide infrared spectroscopy and luminescence sensing combined with Bayesian sampling. J Breath Res 15:026013. https://doi.org/10.1088/1752-7163/ab8dcd

132. Zhou T, Wu T, Wu Q, Chen W, Wu M, Ye C, He X (2020) Real-time monitoring of 13C- and 18O-isotopes of human breath CO2 using a mid-infrared hollow waveguide gas sensor. Anal Chem 92:12943–12949. https://doi.org/10.1021/acs.analchem.0c01586

133. Zhou T, Wu T, Wu Q, Ye C, Hu R, Chen W, He X (2020) Real-time measurement of CO2 isotopologue ratios in exhaled breath by a hollow waveguide based mid-infrared gas sensor. Opt Express 28:10970. https://doi.org/10.1364/oe.385103

Scopes and Limits of Photoacoustic Spectroscopy in Modern Breath Analysis

Stefan Weigl, Max Müller, Jonas Pangerl, and Thomas Rück

Contents

Abstract Photoacoustic spectroscopy is a viable tool for trace gas detection in various application fields. In recent years, this technique has been exploited more and more for modern breath analysis as well. Within this chapter, a holistic overview of photoacoustic spectroscopy is presented, while maintaining the relationship to breath analysis. Therefore, a concise description of the fundamentals of photoacoustic spectroscopy is provided. This is essential for understanding the

S. Weigl (✉), M. Müller, J. Pangerl, and T. Rück
Sensorik-ApplikationsZentrum (SappZ), Regensburg University of Applied Sciences, Regensburg, Germany
e-mail: stefan.weigl@oth-regensburg.de

scopes and limits of this outstanding measurement technique being described within this chapter. In the past several different types of photoacoustic measurement setups for trace gas detection have emerged, including different light sources, modulation techniques, and detection schemes. These are described shortly and advantages as well as disadvantages, especially in relation to breath analysis, are highlighted. Though being a promising sensor principle, measurement devices based on photoacoustic spectroscopy are still rare on the sensor market, especially when it comes to trace gas detection in complex gas matrices, e.g., human breath exhale. One main reason is due to possible molecular interactions influencing the relaxational behavior of the analyte altering the sensor signal. Recent results shedding light on the intricate relaxational processes within complex gas matrices are discussed in detail, providing approaches to overcome this issue. Finally, various applications of photoacoustic spectroscopy in breath analysis are described demonstrating the great potential of this technology.

Keywords Breath analysis · Cross-sensitivities · Photoacoustic cell design · Photoacoustic spectroscopy · Relaxational effects

Abbreviations

AC	Alternating current
ACS	Absorption cross-section
AM	Amplitude modulation
AS	Absorption spectroscopy
BA	Breath analysis
BF	Beat frequency
CF	Cystic fibrosis
COVID-19	Coronavirus SARS-CoV-2
cw	Continuous wave
DFB	Distributed feedback laser
DOF	Degrees of freedom
FFT	Fast Fourier transform
FT-PAS	Fourier transform photoacoustic spectroscopy
FWHM	Full width at half maximum
GC	Gas chromatography
HITRAN	High-resolution transmission molecular absorption database
IC	Internal conversion
ICL	Interband cascade laser
IR	Infrared
ISC	Inter-system crossing
LD	Laser diode
LDC	Laser diode controller
LED	Light emitting diode
LOD	Limit of detection
LP	Lipid peroxidation

MEMS	Micro-electro-mechanical-system
MEPS	Microextraction by packed sorbent
MIR	Mid-infrared
MLR	Multi-linear regression
MOCAM	Modulation cancelation methods
MPI	Max Planck Institute
MS	Mass spectrometry
MVA	Multivariate analysis
NICE	National Institute for Health and Care Excellence
NIR	Near infrared
NNEA	Normalized noise equivalent absorption
NTD	Needle trap device
OPO	Optical parametric oscillator
OS	Oxidative stress
PA	Photoacoustic
PAC	Photoacoustic cell
PAS	Photoacoustic spectroscopy
PCA	Principal component analysis
PLS	Partial least square
PLSR	Partial least square regression
PNNL	Pacific Northwest National Laboratory
POC	Point-of-care
PTR	Proton transfer reaction
PTS	Photothermal spectroscopy
QCL	Quantum cascade laser
QEPAS	Quartz enhanced photoacoustic spectroscopy
QTF	Quartz tuning fork
RT	Resonance tracking
SC	Super continuum
SESI	Secondary electrospray ionization
SIFT	Selected-ion flow-tube
SM	Sugar malabsorption
SNR	Signal-to-noise ratio
SPME	Solid phase microextraction
UV/Vis	Ultraviolet and visible
VOC	Volatile organic compound
VR	Vibronic relaxation
VT	Vibrational-translational
VV	Vibrational-vibrational
WM	Wavelength modulation
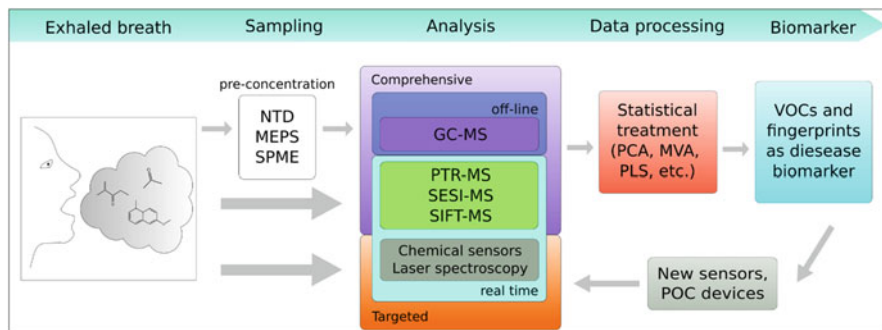
Fig. 1 Generic overview of the different steps with regard to sensor development for breath analysis after [2]. *NTD* needle trap device, *MEPS* microextraction by packed sorbent, *SPME* solid phase microextraction, *GC* gas chromatography, *MS* mass spectrometry, *PTR* proton transfer reaction, *SESI* secondary electrospray ionization, *SIFT* selected ion flow tube, *PCA* principal component analysis, *MVA* multivariate analysis, *PLS* partial least-square, *VOC* volatile organic compound, *POC* point of care

1   Introduction

Nowadays, the need for innovative and smart diagnostics is omnipresent. Especially the COVID-19 pandemic has once more demonstrated the importance of fast, sensitive, and selective diagnostic tools. In the last decades, breath analysis (BA) has emerged as a promising diagnostic tool contributing to mastering these challenges by fulfilling these requirements and furthermore representing a non-invasive and easily repeatable diagnostic procedure.

Linus Pauling's human breath examinations from 1971, using a gas chromatograph coupled with a flame ionization analyzer, mark the beginning of modern breath analysis [1]. Pauling detected about 250 different analytes though at this time an identification was not yet possible. Today, more than 50 years after Pauling's pioneering work, BA is considered a multidisciplinary research field consisting of different elements, which are depicted in Fig. 1 [2].

In general, for the development of a new medical device for diagnosis, it is mandatory to define the target analytes also known as biomarkers. Therefore, depending on the molecules of interest pre-concentration methods combined with a comprehensive analysis of the human breath exhale must be performed. This allows the detection of a huge number of molecules, including volatile organic compounds (VOC) and other volatile substances like ammonia or carbon monoxide to name only a few. The analysis tools of choice are usually either offline methods like gas chromatography combined with mass spectrometry (MS) [3] or online techniques like proton transfer reaction (PTR) MS or selected-ion flow-tube (SIFT) MS [4]. The measured spectra are then post-processed using different statistical treatments, e.g., multivariate analysis (MVA), revealing the biomarkers. Changes of the concentration of these biomarkers in the exhaled breath can hence be used to detect diseases or abnormalities. This is usually done by a targeted sensor

device, forming the heart of a point of care (POC) device, and it is regarded as the final research and development stage toward a breath analysis diagnostic tool. Targeted sensors based on optical spectroscopy, electronic noses, or other sensor principles are considered superior to expensive and bulky MS systems for a POC. However, for fundamental research those MS systems are essential.

Although photoacoustic spectroscopy (PAS) could be treated as a subcategory of absorption spectroscopy (AS), the fact that an acoustic transducer is used as a sensor element clearly distinguishes PAS from common AS, which is discussed within the chapter *Infrared Sensing Strategies: Toward Smart Diagnostics for Exhaled Breath Analysis* of this book. Though discovered already in 1880 by Alexander Graham Bell [5], the photoacoustic effect and photoacoustic spectroscopy can be considered a quite novel research field. Using the database *dimensions.ai* Müller et al. highlighted that between the years 2000 and 2020 the number of publications dealing with photoacoustic spectroscopy, excluding photoacoustic imaging, rose from 140 to about 800 [6]. In recent years, PAS has proven a highly sensitive tool for a plethora of target analytes in various application fields. These areas include atmospheric and environmental monitoring, production monitoring, facility maintenance, the detection of chemical warfare agents and explosives, agricultural applications and, of course, medical applications like non-invasive breath analysis to name a few [7–9]. At this point, it must be mentioned that this chapter will not cover medical applications of the photoacoustic effect by means of photoacoustic imaging, photoacoustic tomography, photoacoustic microscopy, or other photothermal sensor principles.

Within this chapter, the sensor principle of photoacoustic spectroscopy will be presented in detail as it is a promising, yet rarely mentioned candidate for future POC devices in human breath analysis. The following sections describe the physical fundamentals from light absorption to the creation of an acoustic signal. Concepts of acoustic amplification as well as attenuation effects will be described, too. Furthermore, it covers a variety of different photoacoustic sensor setups pointing out their advantages and disadvantages. Since BA can be certainly considered a complex gas matrix, it is important to take measures to ensure a reliable analyte quantification. Therefore, this work discusses these measures in detail based on recent findings. Finally, selected applications of PAS in breath analysis will be described demonstrating the potential and future perspective of this technique in BA.

2 Theory

This section presents the physical derivation of the photoacoustic signal along with an explanation of fundamental concepts like absorption, absorption bands, and various relaxation paths. This description of theory is intended to facilitate subsequent discussion of problems and potential solutions, respectively.

2.1   Molecular Absorption of Light and Relaxation of Excited States

Absorption of light is a phenomenon of interaction between electromagnetic radiation and matter, that is based on energy transfer processes. Among atoms and molecules in the gas phase, the energy components consist of kinetic E_{kin} and internal energy E_{int}. The internal energy in turn is stored in descending order in *electronic*, *vibrational*, and *rotational* states, while the respective energy components are denoted as E_{el}, E_{vib} and E_{rot}

$$E_{total} = E_{kin} + \underbrace{E_{el} + E_{vib} + E_{rot}}_{E_{int}} \tag{1}$$

According to Beer–Lambert, a light beam of intensity I_0 penetrating a homogenous, isotropic medium of thickness d is absorbed to a certain extent yielding an attenuated intensity I_1.

$$I_1 = I_0 e^{-\alpha d} \tag{2}$$

Herein the absorption coefficient α is a measure of reduction in intensity at a certain wavelength in cm^{-1} when passing through a medium. The energy of the absorbed photon converts into internal energy by stimulating transitions between discrete energy states of the sample. Therefore, the wavelength of the light determines the energy level of the transition, i.e., infrared (IR) radiation excites rotational and vibrational transitions, whereas ultraviolet and visible (UV/Vis) light additionally induces electronic transitions. Those modes can also be superimposed yielding *ro-vibrational* (rotational + vibrational), *vibronic* (vibrational + electronic), and *ro-vibronic* (rotational + vibrational + electronic) excitation, respectively. The stimulation of vibrations can be approximated by a harmonic oscillator model considering the atoms in the molecule as masses connected by springs. The energy stored in the spring-mass oscillator thus corresponds to the energy of the absorbed light quantum, which equals the energy difference between excited and ground state of a molecule in the gas phase for example. The first excited state of a vibration describes the fundamental oscillation, any additional excited state represents a harmonic of this fundamental mode. However, the energy differences between the fundamental mode and harmonics are not equidistant but decrease with ascending order. This results from the potential distribution in the molecule, which does not correspond to the idealized one of a parabola, but to that of the Morse potential.

Each molecule exhibits characteristic *absorption bands*, where photons of the respective energy are absorbed with the probability of the *absorption cross-section* (ACS) σ in cm^2/molecule. Since the absorption coefficient is defined as the product of the absorption cross-section and the volume number density of a gas sample, the concentration of the sample can be quantified by measuring the intensity attenuation. In an idealized view, absorbing or emitting systems only show line spectra.

However, real spectra are affected by broadening mechanisms, causing the absorption bands to not only correspond exactly to the actual energy transitions in the molecule. These broadening effects can be assigned to three different phenomena:

- *Natural line broadening:* Since the lifetime τ_e of excited states is subject to an uncertainty, a range of possible frequencies results in showing a Lorentz profile. The resulting frequency broadening amounts to ~30 MHz in case of electronic excitation, ~10 kHz in case of vibrational excitation, and only to ~10^{-4} Hz in case of rotational excitation [10, p. 11]. In comparison, natural line broadening has only a minor effect compared to Doppler and collision broadening, which are discussed below. Consequently, it can be neglected in terms of excited rotational, vibrational, and ro-vibrational states [11, p. 35].

- *Doppler broadening:* This inhomogeneous type of line broadening can be attributed to the Doppler effect, i.e., when a molecule exhibits the same velocity component as the propagation of the photon, causing a frequency shift. Line broadening resulting from the Doppler effect is approximately two orders of magnitude more pronounced compared to that one of natural line broadening in the visible range and dominates in gaseous samples at low pressure [12, p. 49]. Typical values of Doppler broadening in the NIR region are 100–300 MHz and 20–40 MHz in the IR region at about 10 μm, respectively [10, p. 12].

- *Collision broadening:* Collision broadening results from the collision of atoms or molecules while absorbing a photon. Similar to natural line broadening, collision broadening is a homogeneous effect yielding a Lorentzian distribution. When atoms or molecules approach each other, their potential wells deform, causing the energy states to shift, which is directly related to a change in frequency by $E = h\nu_{Ph}$. This type of line broadening thus depends on the mean free path length between the collision partners, which is statistically scattered around a mean value influenced by both, pressure and temperature [12, p. 52]. Typically, collision broadening accounts for approximately 2 GHz of line broadening [10, p. 13].

Altogether, the Lorentzian distribution dominates at atmospheric conditions due to fast molecular movement, whereas natural broadening as well as Doppler broadening can be neglected. In case of both, collision and Doppler broadening, the Gaussian and Lorentz profile are convoluted to the so-called Voigt profile. The different profiles, Gaussian (black), Lorentz (blue), and Voigt (red) are plotted in Fig. 2.

In terms of relaxation processes, after a certain lifetime τ_e of an excited state, different decay mechanisms exist to restore energetic equilibrium. In case of higher energetic photon absorption, e.g., in the UV or visible wavelength range, *photodissociation* can occur, too, i.e., the breaking of covalent bonds within a molecule. This phenomenon mitigates toward lower energetic photons, e.g., in the IR region. Here, the entire absorbed energy is released by relaxation either radiatively as an emission (rarely occurring) or non-radiatively as heat, returning the molecule to its ground state, which is also known as *deactivation*. In other words, interrupting the illumination of a gas sample restores the initial energy distribution after the time τ_e. The radiative relaxation processes are referred to as the luminescence processes
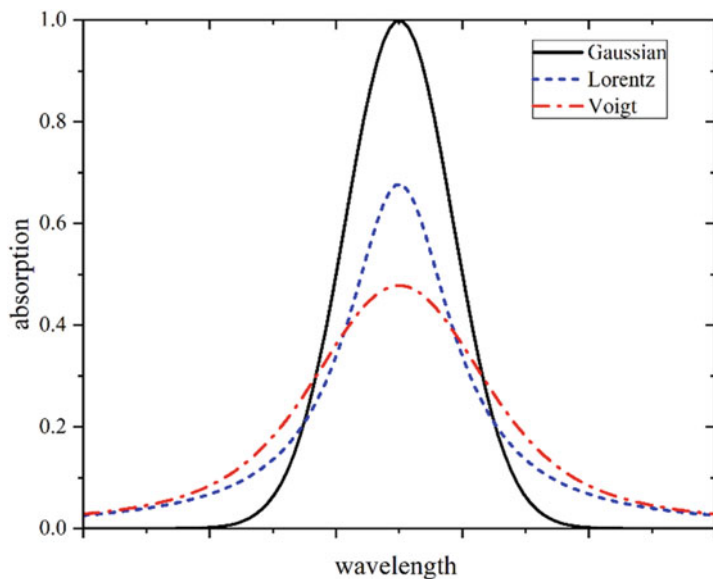
Fig. 2 Surface normalized Gaussian, Lorentz, and Voigt profiles within absorption spectra

fluorescence and *phosphorescence*. In terms of PAS, collision-induced *vibrational-vibrational (VV)* and *vibrational-translational (VT)* relaxations are crucial non-radiative deactivation processes. Besides, photodissociation causes a redistribution of the kinetic and internal energy of the resulting fragments. The released energy due to further relaxation or recombination of the fragments with themselves or surrounding molecules causes an increase of kinetic energy and thus a local heat input into the medium. Photophysical processes, e.g., *internal conversion*[1] (IC) and *inter-system crossing*[2] (ISC) are non-radiative processes changing isoenergetic electronic states into vibrational and rotational states. A visualization of all transitions between ground state and the excited singlet and triplet states is provided by the Jablonski diagram in Fig. 3.

2.2 Photoacoustic Spectroscopy

PAS is based on the photoacoustic effect, discovered by Alexander Graham Bell (1847–1922) in 1880. During experiments with a photophone, he noticed an audible

---

[1] Isoenergetic, non-radiative transition of an electronically excited state into a highly excited vibrational state of the next lower electronic state, e.g., $S_1 \rightarrow S_0$.

[2] Isoenergetic, non-radiative transition from one electronic excited state to another excited state, e.g., $S \rightarrow T$ and $T \rightarrow S$ transitions, respectively.
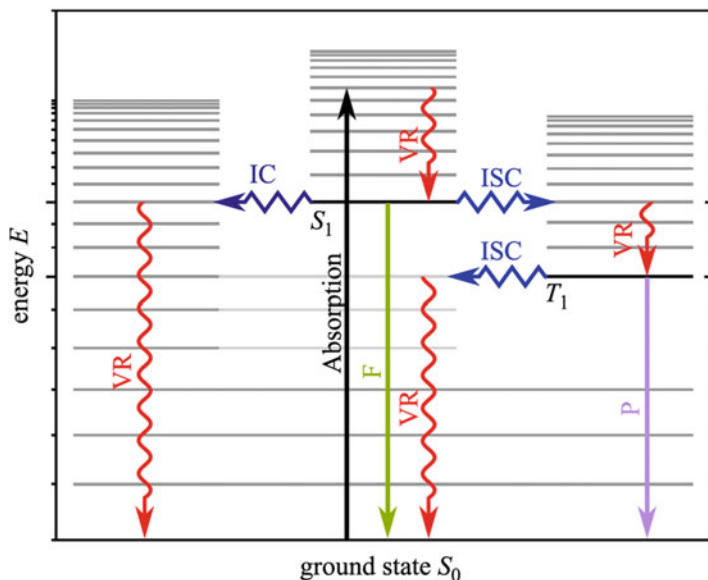
Fig. 3 Jablonski diagram of the electronic ground state So, excited singlet – S_1 and triplet state T_1: *F* fluorescence, *P* phosphorescence, *IC* internal conversion, *ISC* inter-system crossing, *VR* vibronic relaxation

sound, when a rapidly interrupted (chopped), focused ray of sunlight hit a solid substance [5]. The application of the photoacoustic effect on gases started already one year after Bell's discovery by Tyndall. In collaboration with Wilhelm Conrad Röntgen (1845–1926), Bell discovered that the photoacoustic effect also occurs in liquids. Due to a lack of instrumentation, like suitable light sources, microphones, and electronics, the photoacoustic effect did not apply in analytical methods right after its discovery. Only half a century later, in 1938, Viegerov [13] developed the first systematic application of photoacoustics in analytics, based on a blackbody infrared source and a microphone. He constructed a photoacoustic spectroscope, named spectrophone, that succeeded in producing absorption spectra of molecules in the gas phase. In the 1960s an important breakthrough was achieved by the first use of a laser source in PA gas detection [14] and the actual development of PAS began.

Compared to AS, PAS offers certain advantages, especially in the field of trace gas analysis, although both principles are based on the absorption of light. Both have advantages like fast response time or high selectivity and sensitivity; however, PAS additionally offers an offset-free and direct measurement. Here, in contrast to AS, not the transmission of light is monitored (optical transducer) as a measure of absorption but an acoustic signal, that is proportional to the concentration of the absorbing species (acoustic transducer). By inelastic collisions, the energy stored due to photon absorption is transferred to translational (kinetic) energy, which yields a local heat input with heat production rate $\dot{H}$. As a consequence of modulation, sequences of dilatation and contraction generate a periodic pressure oscillation,
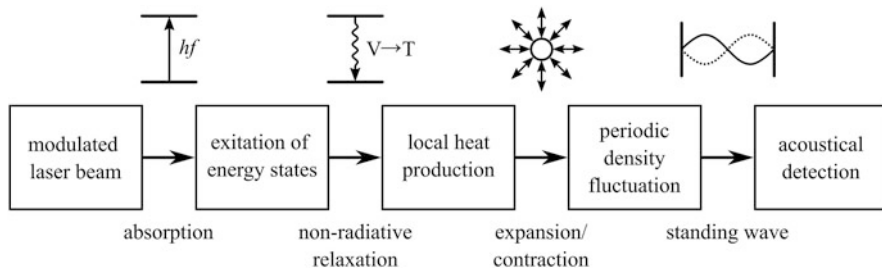
Fig. 4 Schematic drawing of the photoacoustic principle

which stimulates the generation of an acoustic wave. Modulating techniques of the light source include mainly amplitude modulation (AM) or wavelength modulation (WM) by an overlaid sine on the laser current. The resulting sound wave can now be detected as an acoustic signal with an amplitude directly proportional to the present analyte concentration. Figure 4 illustrates the functional principle of PA signal generation.

2.2.1 Heat Production Rate at Thermal Equilibrium

A simplified scenario of heat production can be modeled as a two-level system. Within this derivation, the absorbing gas concentration is expressed as the volume number density $[\rho] = \frac{molecules}{m^3}$, which is defined as the dimensionless volume ratio $[N] = $ ppmV[3] multiplied by the ratio of Avogadro-constant N_A and molar volume V_{mol}:

$$\rho = N \frac{N_A}{V_{mol}} \tag{3}$$

The volume number density ρ can be considered separately as the population density of ground state ρ and excited state ρ', respectively. The rate equation in (4) calculates the density of the excited analyte molecules ρ' in thermal equilibrium:

$$\frac{d\rho'}{dt} = (\rho - \rho')\sigma(\tilde{\nu}_{Ph})\psi - \rho'\sigma(\tilde{\nu}_{Ph})\psi - \frac{\rho'}{\tau_e} \tag{4}$$

---

[3] Due to the dependence on temperature and pressure, concentrations of gaseous samples cannot be described as ratio of weights as it is carried out for solids and liquids [15]. Therefore, gas concentrations are expressed as the ratio of two volumes, e.g., ppm → ppmV (parts per million by volume).

where $\sigma(\tilde{\nu}_{Ph})$ is the absorption cross-section in m^2 and ψ the photon flux in $s^{-1}\,m^{-2}$. The total lifetime of the excited state τ_e can be expressed by the reciprocal sum of the time constants of non-radiative τ_n and radiative relaxation τ_r.

$$\tau_e^{-1} = \tau_n^{-1} + \tau_r^{-1} \tag{5}$$

The first term of the right-hand side in Eq. (4) expresses the absorption of photons at a frequency $\nu_{Ph} = \frac{E_1 - E_0}{h}$. The second term represents stimulated emission, and the third term combines the phenomena of spontaneous emission of photons and non-radiative relaxation. At atmospheric pressure τ_e can be approximated by τ_n within the IR region, since the relaxation time of radiative deactivation is significantly higher compared to non-radiative relaxation [16]. Therefore, a major part of the energy absorbed by the molecule is released as heat. If the excitation rate $\sigma(\tilde{\nu}_{Ph})\psi$ is small, the population density of the excited state is also considerably lower than the total volume number density of the absorbing species, i.e., $(\rho' \gg \rho)$. Accordingly, the stimulated emission can be neglected and Eq. (4) simplifies to:

$$\frac{d\rho'}{dt} = \rho\sigma(\tilde{\nu}_{Ph})\psi - \frac{\rho'}{\tau_e} \tag{6}$$

In case of harmonic modulating the light with angular frequency $\omega = 2\pi f$, e.g., AM or WM, the photon flux ψ can be calculated by

$$\psi = \psi_0\left(1 + e^{i\omega t}\right) \tag{7}$$

with

$$\psi_0 = \frac{I_0}{h\nu_{Ph}} = \frac{P_0}{hc_0\tilde{\nu}_{Ph}\pi\left(\frac{d_b}{2}\right)^2} \tag{8}$$

where ψ_0 is the photon flux without modulation. In calculating ψ_0, h is the Plank constant, ν_{Ph} the frequency and $\tilde{\nu}_{Ph}$ the wavenumber of the photon, respectively. P_0 represents the intensity expressed as optical power per cross-section area of the light beam $\left(I_0 = \frac{P_0}{A}\right)$ with diameter d_b. By applying Eq. (7) to Eq. (6), the rate equation yields

$$\frac{d\rho'}{dt} = \rho\sigma(\tilde{\nu}_{Ph})\psi_0(1 + e^{i\omega t}) - \frac{\rho'}{\tau_e} \tag{9}$$

having only one time-dependent term contributing to the PA signal. In consequence, the solution of the type $\rho' = \rho'_0 e^{i\omega t}$ can be obtained by

$$\rho'_0 = \frac{\rho\sigma(\tilde{\nu}_{Ph})\tau_e\psi_0}{\sqrt{1 + (\omega\tau_e)^2}} e^{i\varphi} \tag{10}$$

where $\varphi = \arctan(\omega\tau_e)$ describes the phase lag between the number density ρ' of the excited state and the photon flux ψ_0. Then, the solution of the rate Eq. (9) can finally be written as

$$\rho'(t) = \frac{\rho\sigma(\tilde{\nu}_{Ph})\tau_e\psi_0}{\sqrt{1 + (\omega\tau_e)^2}} e^{i(\omega t - \varphi)} \tag{11}$$

The heat production rate $\dot{H}$ is related to $\rho'(t)$ by multiplying with the average thermal energy released due to VT-relaxation of the excited state $hc_0\tilde{\nu}_{Ph}$ and divided by its relaxation time τ_n. In consequence, a time-dependent power density with unit J s^{-1} m^{-3} results as the heat production rate at thermal equilibrium.

$$\dot{H}(t) = \rho'(t)\frac{hc_0\tilde{\nu}_{Ph}}{\tau_n} = \dot{H}_0 e^{i(\omega t - \varphi)} \tag{12}$$

with

$$\dot{H}_0 = \rho\sigma(\tilde{\nu}_{Ph})I_0\underbrace{\frac{1}{\sqrt{1 + (\omega\tau_n)^2}}}_{\epsilon_{relax}} \tag{13}$$

with $I_0 = \psi_0 hc_0\tilde{\nu}_{Ph}$ being the incident light intensity and ϵ_{relax} denominates the total efficiency of non-radiative relaxation (refer to Sect. 4.3.2).

2.2.2 Acoustic Wave Generation

Sound describes a pressure or deflection wave, which propagates as a longitudinal wave in gases as well as in liquids. In solids, however, the wave propagates with an additional transverse component. In gases, the static pressure is superimposed by the sound pressure wave, which can be detected by an acoustic transducer, e.g., microphone, quartz tuning fork (QTF), or cantilever (refer to Sect. 3.3). In terms of PAS, the absorption of a modulated light beam and subsequent conversion into thermal energy causes the generation of such a sound wave. This section aims to shortly describe the development of an expression for the PA signal derived from the physical quantities temperature T, pressure p, volumetric mass density $\tilde{\rho}$, and the three components of the particle velocity vector $\vec{v}$. To determine these six quantities, the same number of independent linear equations is necessary, which are all derived from classical physics, i.e., fluid mechanics, thermodynamics, the conservation laws

of energy (heat diffusion), momentum (Navier–Stokes), and mass (continuity), as well as the thermodynamic equation of state. As this is a complex problem, no general solution can be found, and simplifications need to be made. For instance, the changes in T, p, and $\tilde{\rho}$ induced by the light absorption are very small compared to their equilibrium values (index 0) so that new variables can be introduced indicating the changes through absorption (index a). By coupling and solving the initial different equations for the absorption-induced sound pressure $p_a(\vec{r},t)$, a damped wave equation can be obtained which leads to

$$\Delta p_a(\vec{r},t) - \frac{1}{c_s^2}\left[\frac{\partial^2}{\partial t^2}p_a(\vec{r},t) + \underbrace{\gamma\mu_k\frac{\partial}{\partial t}\Delta p_a(\vec{r},t)}_{\text{loss term}}\right] = \underbrace{-\frac{\gamma-1}{c_s^2}\frac{\partial}{\partial t}\dot{H}(\vec{r},t)}_{\text{source term}} \qquad (14)$$

where γ is the heat capacity ratio, μ_k the kinematic viscosity of the medium, and c_s the speed of sound. The loss term corresponds to the damping caused by the viscosity of the medium. Since a detailed derivation of this equation is beyond the scope of this chapter, the interested reader may find more information elsewhere [17, pp. 80–83]. Furthermore, this loss term prevents an analytical solution of (14) wherefore this part is neglected in the first approximation and added again later as an excess term [18, 19]. The solution of the resulting non-damped inhomogeneous equation can be obtained by taking the Fourier transformation on both sides, which yields to [20]

$$\left(\Delta + \frac{\omega^2}{c_s^2}\right)p_a\left(\vec{r},\omega\right) = \left(\frac{\gamma-1}{c_s^2}\right)i\omega\dot{H}\left(\vec{r},\omega\right) \qquad (15)$$

with

$$p_a(\vec{r},t) = \int d\omega\, p_a(\vec{r},\omega)e^{-i\omega t} \qquad (16)$$

and

$$\dot{H}(\vec{r},t) = \int d\omega\, \dot{H}(\vec{r},\omega)e^{-i\omega t} \qquad (17)$$

Equation (15) links the frequency-dependent heat production rate derived from the absorption of photons with the generation of an acoustic wave.
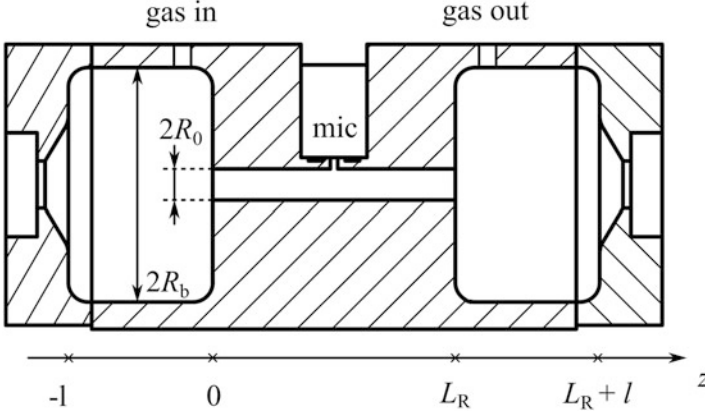
Fig. 5 Cross-section of an H-shaped photoacoustic cell

2.3 Signal Amplification by Resonant Geometries

The solution of the inhomogeneous wave Eq. (15) depends directly on the geometry of the photoacoustic cell (PAC). Within this section, a commonly used approach of signal amplification based on an acoustic resonator tube with diameter R_R, length L_R and open ends is introduced (see Fig. 5). Sections 3.2.1 and 3.3 give an overview of alternative PAC geometries as well as alternative acoustic transducers that have been reported in literature.

The PAC shown in Fig. 5 is composed of an acoustic resonator tube that is enclosed by two buffer volumes with radius R_b. Halfway through the resonator tube, there is a small opening, which is connected to a microphone (mic). In this section, however, only the actual resonator is considered. Later, the approximation made within this section is compared with experimentally determined values. Using cylindrical coordinates, the resonances of the PAC are given by the solutions of the homogeneous wave equation in (14) disregarding the source term and loss term.

$$\Delta p_a(r,\phi,z,t) - \frac{1}{c_s^2} \frac{\partial^2}{\partial t^2} p_a(r,\phi,z,t) = 0 \tag{18}$$

Applying the approach $p_a(r,\phi,z,t) = p_a(r,\phi,z)p_a(t) = p_a(r,\phi,z)e^{-i\Omega_{kmn}t}$, Ω_{kmn} is the resonance angular frequency depending on longitudinal (k), azimuthal (m), and radial (n) modes. By introducing the wavenumber of acoustical modes κ_j with

$$\kappa_j = \frac{\Omega_{kmn}}{c_s} \tag{19}$$

Equation (18) yields to the well-known *Helmholtz equation*:
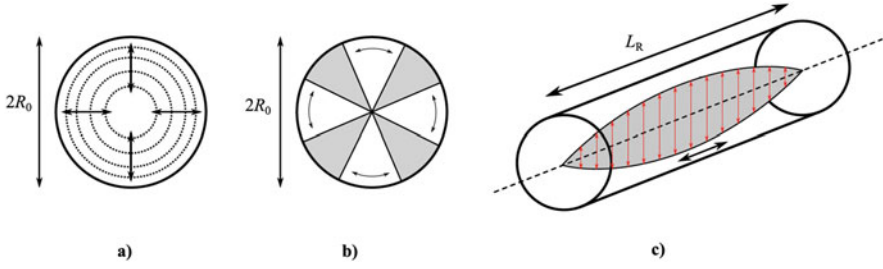
Fig. 6 Different acoustic modes within a cylindrical, both-side-opened resonator. (**a**) Radial mode, (**b**) azimuthal mode, (**c**) longitudinal mode

$$[\Delta + \kappa_j^2]p_a(r,\phi,z,t) = 0 \tag{20}$$

The boundary conditions for resonance amplification must be selected according to the geometry of the photoacoustic cell in order to obtain the oscillation modes of this acoustic wave [21]. Therefore, the walls of the resonator are considered rigid and the openings are assumed to constitute zero acoustic impedance [10, p. 21].

$$\frac{\partial}{\partial r}p_a(r,\phi,z)\Big|_{r=R_0} = 0 \tag{21}$$

$$p_a(r,\phi,z=0,L_R) = 0 \tag{22}$$

By separation of variables, $p_a(r, \phi, z)$ can be written as a product of solutions to the uncoupled differential equations representing radial, azimuthal, and longitudinal modes, i.e., $p_a(r, \phi, z) = R(r)\Phi(\phi)Z(z)$. By solving the Helmholtz Eq. (20) applying the separation ansatz and substitution, respectively, we obtain expressions for the respective modes, which are visualized in Fig. 6.

- *radial dependence $R_{mn}(r)$*

$$R_{mn}(r) = J_m\left(\alpha_{mn}\frac{\pi r}{R_0}\right) \tag{23}$$

where J_m is a *Bessel function* of index m and α_{mn} is the nth root of the derivative of an mth order Bessel function.

- *azimuthal dependence $\Phi_m(\phi)$*

$$\Phi_m(\phi) = \cos(m\phi) \tag{24}$$

- *longitudinal dependence $Z_k(z)$*

$$Z_k(z) = \sin\left(\frac{k\pi z}{L_R}\right) \tag{25}$$

From the relations $\sqrt{\kappa_j^2 - \left(\frac{k\pi}{L_R}\right)^2} = \alpha_{mn}\frac{\pi}{R_0}$ and $\kappa_j = \frac{2\pi f_j}{c_s}$, the discrete frequencies (eigenfrequencies) for transverse pressure modes f_{kmn} can be determined via

$$f_j = \frac{c_s}{2}\sqrt{\left(\frac{\alpha_{mn}}{R_0}\right)^2 + \left(\frac{k}{L_R}\right)^2} \tag{26}$$

However, the great majority of the PACs are based on tube-shaped resonators, thus most often longitudinal pressure modes at low frequencies are of interest. In doing so, $m = n = 0 \rightarrow \alpha_{mn} = 0$ and (26) simplifies to

$$f_k = \frac{kc_s}{2L_R} \tag{27}$$

Using the relation $c = \lambda f$, Eq. (27) transforms into the resonance criteria for longitudinal resonance amplification within a two-sided open tube

$$L_R = k\frac{\lambda_s}{2} \tag{28}$$

Generally, the theoretical value of the longitudinal resonance frequency is higher than the experimentally determined value. This discrepancy can be explained by a phenomenon called *node shifting*. Literature already provides plenty of phenomena that cause elongation of the longitudinal mode, e.g. the assumption of a one-dimensional resonator, the assumption of infinite buffer volumes, the neglected out-coupling hole in the tube at half-length, classical attenuation effects, or non-perfectly adiabatic behavior of real gases [22, p. 42]. By disregarding this node shifting effect for the moment we can express the pressure wave $p_a(\vec{r}, \omega)$, which is a complete orthonormal system of linear combinations of the orthonormalized functions $p_j(\vec{r})$, since the acoustic pressure is the sum over all normal modes.

$$p_a(\vec{r}, \omega) = \sum_j A_j(\omega)p_j(\vec{r}) \tag{29}$$

where $A_j(\omega)$ is the amplitude of the jth mode and $p_j(\vec{r})$ its dimensionless spatial distribution. Since the normal modes are orthogonal, they obey the relationship [23, p. 7]

$$\frac{1}{V_R} \langle p_i | p_j \rangle = \delta_{ij} \tag{30}$$

normalized by the resonator volume V_R. Substituting (29) in (15) and making use of (20) and (30) we obtain an expression for the amplitude of this pressure wave [23, p. 8]

$$A_j(\omega) = -\underbrace{\frac{i\omega}{\omega_j^2 \left(1 - \frac{\omega^2}{\omega_j^2}\right)}}_{\substack{\text{resonance} \\ \text{condition}}} \underbrace{\frac{\gamma - 1}{V_R} \int p_j^*(\vec{r}) \dot{H}(\vec{r}, \omega) dV}_{\substack{\text{coupling of heating} \\ \text{and pressure normal mode}}} \tag{31}$$

While the integral in Eq. (31) represents the heat production rate $\dot{H}\left(\vec{r}, \omega\right)$ and the (complex conjugate) normal mode $p_j^*\left(\vec{r}\right)$. If the angular frequency ω approaches the resonance angular frequency ω_j, the amplitude of the photoacoustic signal $A_j(\omega)$ would become infinite. This ideal scenario results from the previously neglected losses (the loss term was excluded from this derivation in Eq. (14)). Including a mode damping term caused by losses from fluid viscosity and heat conduction [23, p. 8], Eq. (31) yields to

$$A_j(\omega) = -\frac{i\omega}{\omega_j^2 \left(1 - \frac{\omega^2}{\omega_j^2} + i\underbrace{\frac{\omega}{\omega_j Q_j}}_{\text{loss term}}\right)} \frac{\gamma - 1}{V_R} \int p_j^*(\vec{r}) \dot{H}(\vec{r}, \omega) dV \tag{32}$$

where Q_j is the quality factor of the jth normal mode. The quality factor describes the ratio of accumulated and dissipated energy during one period of acoustic oscillation.[4] Another method to determine the quality factor empirically is to take the ratio of f_j and the half-power bandwidth Δf. Since generally root mean square values are taken, this point is at $\sqrt{2}$ of the measured output voltage, i.e.,

$$Q_j = \frac{f_j}{\Delta f_{\sqrt{2}}} \tag{33}$$

Continuing with the derivation of the connection between cell illumination and acoustic pressure, there are several steps that are skipped here for reasons of

---

[4]The energy dissipation of the acoustic amplitude is caused by numerous different factors, which are treated in detail in Sect. 4.

simplicity but evaluated in detail in [17, pp. 90–92]. Assuming the resonant case, i.e., ($\omega \to \omega_j$) the PA amplitude with unit Pa results in

$$A_j(\omega_j) = (\gamma - 1) \frac{Q_j}{\omega_j} \frac{L_R}{V_R} p_j \epsilon_{relax} \alpha P_0 e^{-\mu_j} \tag{34}$$

where μ_j is the reciprocal light-to-sound coupling factor of the jth normal mode. Provided the modulation angular frequency ω is equal to the resonator's eigenfrequencies ω_j, the energy of multiple modulation cycles is accumulated in a standing acoustic wave and the system operates as an acoustic amplifier. In order to find an expression of the photoacoustic signal, combining (34) and (29) finally yields to

$$p_a(\vec{r}, \omega_j) = \underbrace{(\gamma - 1) \frac{Q_j}{\omega_j} \frac{L_R}{V_R} p_j}_{\text{cell constant } C_{cell}} \epsilon_{relax} \alpha P_0 e^{-\mu_j} p_j(\vec{r}) \tag{35}$$

Here, the amplitude of the PA signal is directly proportional to the absorption coefficient α, i.e., the product of volume number density ρ and absorption cross-section $\sigma(\tilde{\nu}_{Ph})$ of the absorbing molecules, as well as to the optical power P_0, used for the excitation of analyte molecules. Besides, the PA amplitude is also determined by cell constant C_{cell} consisting of parameters that are independent of light and analyte, namely:

- The ratio of the quality factor Q_j and angular frequency ω_j of acoustic resonance amplification.
- The length-to-volume ratio in terms of a tube-shaped PACs[5].
- The decremented heat capacity ratio ($\gamma - 1$.)
- The dimensionless normalization coefficient p_j, which depends on the detected mode

$p_j(\vec{r})$ is the only factor that depends on spatial coordinates. However, in the case of first longitudinal mode excitation in a tube-shaped resonator (using cylindrical coordinates), the acoustic pressure only varies in z-direction and remains constant with respect to the tube radius r and spatial angle ϕ. In this case the normalization coefficient $p_j = \sqrt{2}$ [19, 24] and the scale factor $p_j(\vec{r})$ can be expressed as sinusoidal half-wave ranging from 0 to 1 [24]

---

[5] In terms of calculations, also the node shifting phenomenon has to be considered here. For this reason $L_R \to L_{R, eff}$.

$$p_j(\vec{r}) \equiv p_{100}(z) = \sin\left(z\frac{\pi}{L_{R,eff}}\right) \qquad (36)$$

Assuming optimal light-to-sound coupling, i.e. $\mu_j \to 0$ together with a microphone position in the middle of the resonator as depicted in Fig. 5, i.e., $\vec{r} \to \vec{r}_{mic} = (R_0, 0, \frac{L_R}{2})$, then $e^{-\mu_{100}}p_{100}(z) \to 1$ and Eq. (35) reduces to

$$p_a(\vec{r}_{mic}, \omega_{100}) = \underbrace{(\gamma - 1)\frac{Q_{100}}{\omega_{100}}\frac{L_{R,eff}}{V_R}\sqrt{2}}_{\text{cell constant } C_{cell}}\, \epsilon_{relax}\underbrace{\rho\sigma(\tilde{\nu}_{Ph})}_{\alpha}P_0 \qquad (37)$$

Regarding breath gas detection with low volume number densities ρ of the analyte in the sub-ppmV range some suggestions for achieving a higher PA signal and therefore a higher sensitivity and limit of detection can be derived from Eq. (37) after [22, p. 52]:

- Choose a wavelength to excite molecular transitions with a large absorption cross-section $\sigma(\tilde{\nu}_{Ph})$ in order to achieve a high absorption coefficient α, but avoid spectral cross sensitivities to other components within the gas matrix.
- Use a light source with high optical power in the wavelength region of interest.
- Apply resonant PAC designs with a quality factor $Q_j \gtrsim 20$ and maintain constant pressure and temperature during measurements to ensure a constant resonance frequency.
- Use small tube diameters $2R_0$ but consider the beam collimation and the resulting PA background signal caused i.a. by interactions between beam and inner cell walls.
- Focus illumination to regions with pressure maxima in order to achieve a high light-to-sound coupling ($\mu_j \to 0$).

3 Overview of Different Photoacoustic Setups and Techniques

In Sect. 1, the general interest in the photoacoustic technique for trace gas analysis was already highlighted to have rapidly increased within the last two decades. As an ongoing trend, this interest on the part of academia but also on the part of sensor manufacturers is also reflected in the diversity of different setups and approaches that are reported. With reference to the path of PA signal generation (refer to Fig. 4 in 2.2), this diversity is based on the application of various light sources, modulators, cell designs, and signal transducers, but also on the development and implementation of innovative concepts for acoustic resonance amplification, noise reduction, optical power amplification or self-calibration of the sensor system. This section is

meant to give a good overview of the state of the art of photoacoustic setups and highlights obvious advantages and disadvantages for breath analysis. It is intended to be a guide for the non-expert reader to decide which technique or setup might be best for a specific application. However, it is recommended that the references provided be explored further, as this overview does not claim to be all-inclusive.

3.1 Electromagnetic Signal Stimulation

Developing PA gas sensors should always start with choosing an appropriate light source. This requires research and simulation of suitable internal energy states of the analyte molecules as well as potential spectral interference with other species on the one hand, and the availability and characteristics of suitable emitters such as wavelength, optical output power, spectral bandwidth, optical divergence, tuneability, modulation capability, size, and cost on the other hand. The references within the following sections identify PA sensors to take advantage of exciting ro-vibronic states using most commonly near-infrared (NIR), middle infrared (MIR), or visible radiation, though also the exploitation of ultraviolet [25, 26] and Terahertz [27] radiation is viable.

3.1.1 Light Sources

Nowadays, *laser diodes* (LD) are most used to excite internal analyte states by photon absorption for PA signal stimulation. Whether standard Fabry–Perot lasers (0.4–3 μm) [28–33] interband cascade lasers (ICL) (3–6 μm) [6, 24, 34] or quantum cascade lasers (QCL) (6–14 μm) [35–37] are utilized, LDs combine the advantages of narrow bandwidth, high output power, small size, and simple operation, current modulation, and cooling. Once very narrow bandwidth single mode emission (≤ 5 cm^{-1}) is required in order to scan distinct narrow-band absorption features applying wavelength modulation for example (refer to Sect. 3.1.3), Bragg gratings can be integrated into the light source to achieve distributed feedback (DFB) aiming for DFB-LDs [38–49], DFB-ICLs [50], or DFB-QCLs [51–55]. Regarding their price, those three types of emitters roughly scale with the wavelength of emission; hence, it is recommended to choose a rather low wavelength if the spectral properties of the sample allow it. In case ultra-narrow-band emitters are required, Pan et al. reported the use of sub-attometer bandwidth whispering-gallery-mode diode lasers [56]. However, standard PA applications, which do not take advantage of special techniques for background signal reduction, optical amplification, or self-calibration such as the use of Brewster windows (Sect. 3.2.4) optical cavities (Sect. 3.2.2) or beat frequency methods (Sect. 3.2.5), do not necessarily rely on single mode emitters.

For this reason, low-cost applications based on *thermal light sources* [57, 58] or *light emitting diodes* (LED) [25, 59, 60] have recently been described more

frequently. While thermal emitters and LEDs are rather inexpensive compared to laser sources, both share the disadvantages of highly divergent and spectrally broadband radiation, which entails elaborate beam shaping and excludes wavelength modulation. Further disadvantages of thermal sources are the necessity of narrow-band optical filters and separate modulators,[6] which drastically attenuate the optical power that is available for PA signal generation and increase the error susceptibility of the sensor system, respectively. Nevertheless, in 2019 the first miniaturized photoacoustic CO_2 sensors based on broadband infrared excitation have been announced to be commercially available by Sensirion AG[7] and Infineon Technologies AG.[8] Recently, Gaßner et al. reported another thermal emitter-based concept that, however, rather exploits standard optical absorption according to Beer–Lambert Law with an analyte-filled photoacoustic detector cell [61]. Although beam shaping using LEDs is more complex than LDs, they provide an additional pathway of high-energy electronic excitation, as the development of UV LEDs has increased significantly in recent years [26]. Another alternative for generating broadband radiation is the use of supercontinuum (SC) sources [62]. Compared to thermal emitters or LEDs, SC beams can be more easily focused or collimated, but they are also more expensive as they additionally require a pump source.

The tunability of light sources becomes important with respect to multi-component monitoring. Provided extensive research of the absorption spectra of all matrix components, Fabry–Perot LDs [48], ICLs [24] or QCLs [52] may be used to monitor multiple species, since laser diodes often can be tuned up to about $10 \, \text{cm}^{-1}$ by adjusting the operation temperature and current. Besides common QCLs, external cavity QCLs provide even wider tuning range ($>100 \, \text{cm}^{-1}$) [63]. Albeit thermal sources and broadband LEDs may also be used to monitor several species by integrating appropriate optical filters [57, 64], *optical parametric oscillators* (OPO) still offer the most degrees of freedom for monitoring multiple components with a single light source, since signal- and idler-emission can be tuned over several microns each. Although OPO radiation in PAS is usually modulated by means of mechanical choppers [65], further concepts are reported that base upon amplitude modulating the pump source [66] or even applying a WM/AM double-modulation technique [67]. *CO_2 lasers* also enable multi-component monitoring between 9.4 and 10.6 μm [68, 69]; however, they are now being used less frequently in PAS, because preferable alternatives became available.

3.1.2   Amplitude Modulation

According to Sect. 2.2, PA signal generation relies on modulating the light to trigger periodic heating. The simplest way to achieve this is called amplitude modulation

---

[6] At least when exploiting acoustic resonance amplification in the kHz range.

[7] https://sensirion.com/products/catalog/SCD40/ visited 28.08.2022.

[8] https://www.infineon.com/cms/en/product/sensor/co2-sensors/pasco2v01/ visited 28.08.2022.

(a.k.a. intensity modulation), in which the light is periodically turned on and off. Resonance amplification then is accomplished once this periodicity matches an Eigenfrequency of the sensor module comprising photoacoustic cell (see Sect. 3.2.1) and signal transducer (see Sect. 3.3). Regarding LDs, LEDs, or in case of low-frequency modulation even thermal emitters [61], AM can be accomplished without the need of additional hardware by modulating the operating current of the light source. Most common alternatives to realize AM are choppers [53, 58, 64, 69] that might, however, produce interfering acoustic noise, be prone to jitter inaccuracies in particular at kHz frequencies and are more susceptible to mechanical vibrations. Further, albeit rather uncommon parts that were reported to be used for AM in photoacoustics are fiber-coupled electro-optic [56] and acousto-optic modulators [70] or micro-electro-mechanical-system (MEMS) based scanning mirrors [71, 72].

In some references that apply AM, the duty cycle, i.e., the temporal ratio of illumination and shading, was optimized as it is associated with certain characteristics of the source, such as the modulation frequency of LEDs [26] or the emission linewidth of DFB-QCLs [53]. Regarding the latter reference, pulsed photoacoustic spectroscopy is utilized as a special case of AM, where the duty cycle is far lower than 50% [62]. Such a regime is based on pulsed emitters with a certain repetition rate instead of continuous wave (cw) sources. This drastically boosts the pulse energy, and thus the optical power which scales linearly with the PA magnitude. Whether amplitude modulating a cw source or using pulsed emitters, it should be considered that the off-time, i.e., the period without illumination, might affect the efficiency of energy relaxation and therefore the PA signal (refer to Sect. 4) [6]. Finally, a general disadvantage of amplitude modulation has to be mentioned, namely spectral interferences with other species in the gas sample and periodic heating of the inner walls or the windows of the PAC, respectively, which both might contribute to the PA signal. Provided that the concentrations of absorbing non-analyte species and the absorption properties of the PAC do not change, this causes a background signal, which can be subjected to an offset correction according to Eqs. (38) and (39), respectively, otherwise the PA sensor has to undergo complex calibration before it is used in the field.

3.1.3   Wavelength Modulation

Figure 7 illustrates an alternative technique that is mainly applied to diode lasers, namely wavelength modulation. In this process, periodic heating is not achieved by periodically turning on and off illumination but by modulating a sinusoidal alternating current (AC) of low amplitude onto a constant offset laser diode current, which is fine-tuned, thus the emission spectrally coincides with the maximum of an absorption peak of the analyte. The AC modulation causes the wavelength to be swept approximately over the full width at half maximum (FWHM) of the absorption feature yielding a maximum symmetric sound pressure signal, which is doubled in frequency compared to the initial AC modulation. In terms of WM-based photoacoustic spectroscopy, these two currents often are further superimposed
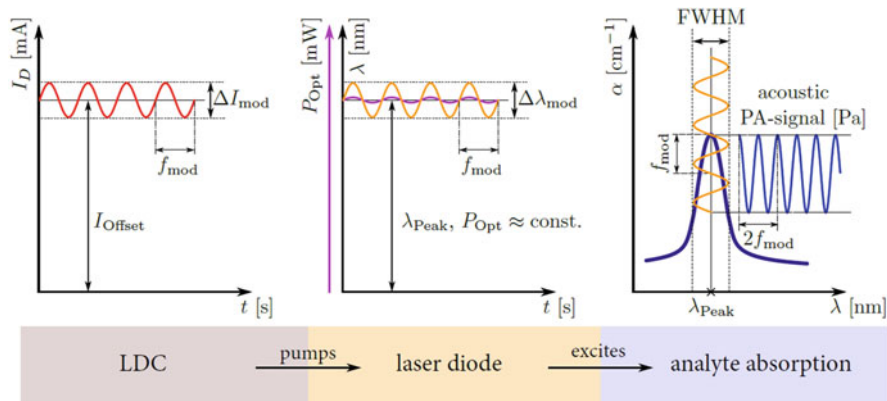
Fig. 7 Principle of wavelength modulated PAS and 2*f*-signal generation. *LDC* laser diode controller, *FWHM* full width at half maximum, *PA* photoacoustic

with a ramped current signal that is considerably lower in frequency compared to the sinusoidal alternating current. In order to scan across the entire absorption feature, the current must be ramped over a certain range, which, besides a distinct modulation of the emission wavelength, might also result in a minor residual amplitude modulation [37].

The key advantage of WM is that no spectrally overlapping absorption profiles of PAC components or other species in the gas sample contribute to the PA signal, as long as this overlapping absorption remains rather constant within the range of wavelength modulation. In view of breath analysis, applying WM might reduce cross-sensitivities toward varying amounts of CO_2 and H_2O in the sample, once an appropriate analyte feature has been chosen. However, non-constant interfering absorption as well as varying ambient parameters, especially changing the pressure of the gas sample, may cause distinct peak deformations which in turn might affect the PA magnitude, thus falsifying the analyte concentration reading. One approach to face this problem of peak deformation is to simulate the superimposed absorption of the sample in real-time using the HITRAN (High-resolution transmission molecular absorption database) API known as HAPI. However, this requires to separately monitor the concentrations of the interfering species that cause peak deformation. Moreover, some absorption features especially of electronic transitions such as the $n \to \pi^*$ transition of acetone between 220 and 330 nm [26] or the excitation of electronic $^2B_2$ and $^2B_1$ states of nitrogen dioxide between 300 and 500 nm [73] cannot be excited by means of WM as they are simply too broad.

3.2 Techniques and Photoacoustic Cell Designs

Apart from the variety of different light sources to initiate PA signal generation, literature provides a multitude of photoacoustic cell designs as well as innovative

concepts to increase the signal-to-noise ratio (SNR) or to facilitate the self-calibration of sensor systems.

3.2.1 Acoustic Resonance Amplification

In principle, the frequency of light modulation, which corresponds to the frequency of the resulting acoustic signal, can be freely selected when designing a PA trace gas sensor. Only under the condition that resonant signal amplification is aimed at, the frequency of modulation must be adapted to the corresponding natural resonance frequency of the system. Hence, *non-resonant PA setups* are usually operated at low frequencies between 20 and 300 Hz in order to facilitate data acquisition and signal processing as well as to assure maximum relaxation efficiency (refer to Sect. 4) [62, 74, 75]. The photoacoustic cell design is not related to the principle of modulation, thus non-resonant PACs have been described to be operated in amplitude modulation mode [57, 58] or wavelength modulation mode accompanied by 2*f*-demodulation [43, 46, 47]. By utilizing an LED-based non-resonant setup that was operated in AM mode, for example, Karhu et al. achieved a remarkable limit of NO_2 detection in the sub-ppbV range [59].

However, Hofstetter et al. identified the exploitation of acoustic resonance amplification to further improve the SNR by a factor of 70 compared to non-resonant cell designs [53]. In detail, they compared the PA signal of a PAC by modulating the light source out of resonance with the equivalent signal after matching the frequency of modulation with the frequency of the first mode of longitudinal resonance amplification, which is derived in Sect. 2.3, Eq. (27). Most commonly, PACs exploiting longitudinal resonances are designed as open cylinders that are accompanied by two buffer volumes, a.k.a. *H-type resonators* [24, 37, 69, 70]. In view of optimizing the dimensions of H-type cell designs, literature provides a variety of references, where the length of the buffer volumes was identified to affect the frequency and quality factor of resonance amplification [73] or the diameter of the resonator tube and the diameter of one buffer volume were enlarged, respectively, in order to enhance light-to-sound coupling [25, 60, 67].

A common alternative PAC design is based on so-called *T-type resonators*, where the resonator tube is not open on both sides surrounded by buffer volumes, but only on one side, while the second one is closed and equipped with an acoustic transducer [38, 64]. Unlike H-type resonators, where the length of the resonator tube must correspond to a multiple of half the length of the amplified standing sound wave with sound pressure nodes at the open ends of the tube (refer to Eq. (28) in Sect. 2), T-type resonators must correspond to an odd multiple of a fourth of the standing sound wave with a sound pressure anti-node at the closed end of the tube. Gong et al. performed sophisticated research comparing T-type with H-type resonators and identified the former one to show a limit of C_2H_2 detection enhanced by 17% compared to H-type PACs, further accompanied by a faster response of the sensor system [39]. Besides, literature provides alternative, albeit less common approaches of acoustic resonance amplification, namely the exploitation of *Helmholtz*

resonances [40] or acoustic *azimuthal and radial modes* according to Eqs. (24) and (23), respectively [41].

In general, but not limited to applications for breath analysis, acoustic resonance amplification should only be utilized once it is needed to achieve certain sensitivity specifications, as it requires acoustic resonance tracking (refer to Sect. 3.2.5). Moreover, it increases the probability of relaxational losses (refer to Sect. 4), since acoustic amplification is usually operated at higher modulation frequencies; otherwise, the dimensions of the PAC would become too large.

3.2.2 Optical Power Amplification

According to Eq. (35), the PA signal scales linearly with the optical power of illumination, thus, various concepts of optical power amplification have been reported in order to accomplish photoacoustic trace gas monitoring. The most common one of these concepts is referred to as *multi-pass photoacoustics*, where the light beam passes the PAC several times causing optical power enhancement. Multi-pass regimes can be used in most PA applications, regardless the applied modulation technique is amplitude [28, 62] or wavelength [43, 46, 47, 51, 76] modulation as well as regardless of whether acoustic resonance amplification is exploited [28, 51, 67] or not [43, 46, 47, 57]. While the majority of multi-pass absorption cells in photoacoustics are designed as Herriott cells [46, 47, 62, 76] or without any pre-defined beam path [43, 46, 57], also sphere tube designs [28] and White cells [51] are reported. However, White cells on the one hand are less stable and more complex to manufacture than Herriott cells, but on the other hand, they allow for higher numerical aperture beams. Based on a sphere tube design, Li et al. determined the SNR to be enhanced by a factor of 5 by exploiting multi-pass reflection [28]. While in most PA multi-pass setups the reflecting mirrors are employed within the PAC, Mikkonen et al. reported an approach where external mirrors were positioned outside next to the windows of the PAC [62]. Finally, multi-pass regimes are not restricted to the usage of microphones as sound transducers, but also quartz enhanced (refer to Sect. 3.3) photoacoustic (QEPAS) multi-pass applications have been reported, both using bare QTF [49, 77] or exploiting the on-beam QEPAS technique [45].

An even more sophisticated approach to enhance the radiative flux density within the PAC is called *cavity-enhanced photoacoustic spectroscopy*, where external mirrors are used to form an optical cavity in order to gain optical resonance amplification. As already mentioned in case of multi-pass techniques, cavity enhancement can be applied to microphone-based photoacoustic setups [56] and QEPAS applications [52, 54, 78]. More specific, combining optical cavities with QEPAS is even less complex than combining multi-pass with QEPAS, because the focal point halfway through the optical resonator can be more easily adjusted to pass between the prongs of a QTF than multiple beam reflections. While Wojtas et al. [54] and Borri et al. [79] employed an optical bow-tie cavity with bare QTF detection, Hayden et al. [52] and Wang et al. [78] utilized on-beam QEPAS and determined the

optical cavity to cause an at least 600 times SNR improvement and a remarkable limit of C_2H_2 detection in the sub-pptV range, respectively. To the best of the authors' knowledge, cavity-enhanced PAS is the most sensitive photoacoustic technique that has been reported so far. However, as in the case of multi-pass technology, a decision must be made as to whether such sensitivity is necessary and whether the expense and complexity of optics is justified.

An alternative option of optical power amplification is the usage of optical fibers together with Erbium-doped fiber amplifiers [76, 80] or the installation of a fiber-ring-cavity using a pump laser and a Bragg grating [70]. However, concluding these approaches of optical power amplification, it must be noted that the derivation of the photoacoustic formula in Sect. 2 assumes the population of the excited analyte state to be considerably lower than the population of the ground state [22, pp. 35–36]. By pronounced optical amplification, this assumption may not be valid anymore, causing non-linear effects to gain influence, which may result in non-linear calibration characteristics of the sensor system.

3.2.3 Fourier Transform and Frequency Comb Photoacoustic Spectroscopy

Fourier Transform PAS (FT-PAS) and frequency comb PAS are two rather seldomly used techniques for photoacoustically detecting trace gases. Both approaches have in common, that the resulting measurement provides a whole photoacoustic absorption spectrum within a comparatively short period of time.

As in common FT spectroscopy, usually broadband emitters are employed for FT-PAS and combined with an interferometer to create an optical interferogram. This interferogram illuminates a gas-filled cell, which is equipped with an acoustic transducer as well as a photodiode for later signal normalization. The resulting photoacoustic signal consists of a superposition of acoustic waves originating from the periodic interaction between optical interferogram and analyte gas. The acoustic signal is then Fourier transformed and normalized providing a photoacoustic absorption spectrum of the analyte illuminated within the gas sample. Besides, each absorption line can be assigned to its respective acoustic frequency after the Fourier transformation of the photoacoustic signal [62].

Mikkonen et al. [62] used FT-PAS with a supercontinuum light source to detect several hydrocarbons (methane, ethane, ethene, propene in N_2) in a multi-pass setup with a non-resonant Herriot cell and a cantilever as an acoustic transducer. The ten beam-pass in the Herriot cell allowed for compensation of the rather low incident spectral power density of $15\,\mu W\,cm^{-1}$ leading to a detection limit of 32 ppb (1 s) for methane after 40 s signal averaging. Instead of a broadband emitter, a frequency comb can be employed as well, which was demonstrated by Sadiek et al. [81] and Karhu et al. [82].

A further technique exploiting frequency combs for rapid broadband photoacoustic scanning is dual comb PAS. Compared to FT-PAS, instead of an optical interferogram, a frequency comb is illuminating the gas sample directly. This

novel approach was recently published by Wildi et al. [83]. In their proof-of-concept study, they estimated a minimal noise equivalent acetylene concentration of 10 ppm for a 1,000 s averaging time.

3.2.4   Noise and Background Reduction

The key parameter of a trace gas monitoring system is its limit of detection (LOD), a.k.a. noise equivalent concentration, i.e., the ratio of sensor noise and sensor sensitivity (see Sect. 3.4.1). While optical amplification yields a sensitivity enhancement, an alternative way to improve the LOD is to reduce the sensor noise. An elementary approach of *noise reduction* that is applied in almost every PA application is the implementation of *lock-in amplification* in terms of signal processing [84]. Without going into detail, the lock-in technique can be considered as a very narrow bandpass, only observing the acoustic signal with respect to the frequency of light modulation. This technique can therefore be used to detect photoacoustic signals that are significantly below the actual broadband acoustic noise that is recorded by a microphone for example. Alternative yet less common methods of signal processing are the usage of standard soundcards with Fast Fourier Transform (FFT) analysis [85] or the implementation of the so-called Goertzel algorithm [86].

Another term, that is sometimes confused with the noise level of a PA sensor in literature, is the photoacoustic background signal. Generally, photoacoustic spectroscopy is an offset-free technique, i.e., zero sensor signal if no analyte is present in the gas sample. However, even if no other species in the sample shows an absorption feature in the wavelength range of illumination, photoacoustic background signals might result from interactions of intensity modulated light with the windows or the inner walls of the PAC for example, thus causing periodic heating, i.e., PA signal generation. Besides, purely acoustic background signal components may originate from environmental noise or gas flowing through the PAC. Once such a background signal can be assumed to be constant over a certain measuring period without calibration, a zero-point measurement with a magnitude $\widehat{u}_0$ and phase ϕ_0 can be performed beforehand in the absence of an analyte. Afterward, every PA signal reading $(\widehat{u}_i, \phi_i)$ can be *offset corrected* (index *oc*) in vector space according to [22, p. 65].

$$\phi_{i,\mathrm{oc}} = \left| \tan^{-1} \left[\frac{\widehat{u}_i \, \sin \phi_i - \widehat{u}_0 \, \sin \phi_0}{\widehat{u}_i \, \cos \phi_i - \widehat{u}_0 \, \cos \phi_0} \right] \right| \tag{38}$$

$$\widehat{u}_{i,\mathrm{oc}} = \left| \frac{\widehat{u}_i \, \cos \phi_i - \widehat{u}_0 \, \cos \phi_0}{\cos \phi_{i,\mathrm{oc}}} \right| \tag{39}$$

However, as soon as it can no longer be ensured that the background signal is constant, a new zero-point calibration must be performed. A further common approach of *background reduction* is to incorporate *acoustic filters* into the PAC design in order to proactively tone down acoustic background signals [33, 87, 88]. In

view of reducing light-initiated background signals, various options such as mounting *Brewster windows* [31, 69] or implementing *modulation cancelation methods* (MOCAM) have been reported [59, 89, 90].

Beyond that, a more comprehensive approach of background and noise reduction entails the utilization of *differential PA* concepts. Liu et al., for example, applied the most obvious differential concept by assembling two identical PACs, while each of them was equipped with a condenser microphone and the analog microphone signals were pre-processed by a mixing unit prior to lock-in amplification [64]. With both, the sample cell and the reference cell being filled with an analyte-containing gas sample and ambient air in advance, respectively, they achieved a remarkable normalized noise equivalent absorption (NNEA) of 4.1×10^{-10} W cm^{-1} Hz$^{-0.5}$ (refer to Sect. 3.4.1). By implementing this technique, noise and background originating from environmental acoustic noise or interactions of the modulated light with parts of the PAC can be drastically reduced. However, this concept precludes flow-through operation and requires a reference equivalent to the actual gas sample, but with only the analyte species removed. In view of breath analysis, this concept has the disadvantage that the bulk composition of different samples from different test persons, especially the H_2O and CO_2 content, cannot be assumed to be constant, thus no universal reference can be provided. Therefore, most differential PA designs are based on an alternative concept that allows for flow-through operation. More precisely, these designs employ two parallel tubes for amplifying the longitudinal acoustic resonance, both equipped with a microphone and being continuously flushed with sample gas while only one of the tubes is illuminated [56, 66, 73, 80]. By mixing both microphone signals using a differential amplifier, noise and background signals resulting from environmental acoustic noise and gas flow can be significantly reduced. In order to additionally account for background signals due to light-with-PAC interaction, this concept may be complemented by implementing Brewster windows or the MOCAM technique. Alahmari et al. demonstrated that differential PA cell designs cannot only be adopted to concepts that are based on longitudinal resonance amplification, but also on Helmholtz resonance amplification [40]. An extensive comparison of various differential PA setups can be found in [91].

3.2.5 Resonance Tracking for Self-calibration

As already discussed in Sect. 3.2.1, exploiting acoustic resonance amplification entails the modulation frequency to be adjusted to the dimensions of the acoustic resonator, but also to the actual speed of sound within the gas sample. Since temperature and bulk composition of the gas sample affect the speed of sound, field applications require knowledge about that, to either adjust the frequency of modulation or to apply different calibrations, that must be recorded in laboratory beforehand. However, in case there is no knowledge about the actual speed of sound, resonance tracking techniques have been reported. In common microphone-based PA setups, these techniques use an additional speaker, which is integrated in the

PAC and allows for recording the frequency response of the acoustic module [73, 92]. Regarding bare QTF-based PA setups, such *resonance tracking systems* can be implemented even more easily, as simple circuit designs allow to switch between measuring mode and electronic QTF excitation, respectively [93], which is not that important for real-time resonance adjustment though, since the frequency of QTF resonance rather depends on the viscosity than of the speed of sound of the sample.

However, bulk composition and temperature may not only affect the frequency but also the quality factor of resonance amplification, which in turn affects the PA signal (see Eq. (37)). Therefore, an alternative approach of simultaneously determining analyte concentration, as well as frequency and quality of resonance is the application of *beat frequency* (BF) photoacoustics, which, however, requires the utilization of a resonant acoustic signal transducer, e.g., a quartz tuning fork. Comparing BF-QEPAS with standard QEPAS, the frequency of light modulation is slightly detuned from the natural frequency of the signal transducer, and illumination rather triggers an acoustic pulse than a continuous acoustic wave. This subsequently causes free instead of forced vibrations of the signal transducer, which are demodulated at the frequency of light modulation. The demodulated signal will thus oscillate at a frequency equal to the difference of light modulation frequency and QTF resonance frequency. The benefit of such transient signal analysis is the simultaneous identification of analyte concentration, quality factor and frequency of the transducers' resonance by evaluating its peak value, ring-down time and period of oscillation, respectively (see Sect. 4.2, Fig. 11). In view of bare QTF setups [94], this technique avoids calibration and improves the sensor response time. Finally, Li et al. recently adapted the BF technique for real-time ammonia measurement at pptV-level with regard to breath analysis [35]. A major drawback of the BF technique is that a fast wavelength scan does not allow coverage of a broad spectrum, making its applicability infeasible for the analysis of overlapping absorption features, which is, however, the most common situation in breath analysis.

3.3 Acoustic Signal Transducers

Standard photoacoustic setups use *condenser microphones* that may be micromechanically fabricated, e.g., MEMS microphones that were originally intended to be used in mobile phones or hearing aids [24, 25, 31, 36, 37, 66, 70]. The most common alternative signal transducers in PA setups are *quartz tuning forks* [33, 44], which were basically designed as clock generators for electronic watches. The major advantages of QTFs over microphones are a superior immunity to ambient acoustic noise due to their quadrupole transducer characteristics [95] and their small size and low-cost allowing for miniaturization and mass production. On the other hand, their small size requires elaborate beam focusing between the prongs of the fork, and the SNR of bare QTF setups is known to be about at least one magnitude of order inferior compared to sophisticated microphone-based PA setups

exploiting acoustic resonance amplification [96]. To compensate the disadvantage of lower sensitivity, QTFs also are often combined with acoustic resonators, which are either arranged as *on-beam QEPAS* configuration with two resonator tubes being placed in front and behind the prong spacing of the QTF or as *off-beam QEPAS* configuration, resembling a standard microphone-based setup, where only the microphone is replaced by a tuning fork. The latter of these configurations facilitates beam shaping, as the light does not have to be focused between the prongs. Moreover, Shang et al. identified the SNR of off-beam QEPAS to exceed the SNR of bare QTF QEPAS by at least a factor of 5 [29] and based on a literature research, Hu et al. further reported the off-beam regime to outperform on-beam QEPAS as well [45]. In order to compensate for the disadvantage of difficult optical alignment in terms of bare QTF or on-beam QEPAS as well as to enhance the SNR, the scientific community spent a lot of effort in designing and fabricating *custom QTFs* in recent years [97]. This has resulted in a large number of publications, introducing custom QTFs with flexural modes that are lower than the 32.8 kHz natural frequency of common QTFs that are commercially available, namely 28 kHz [48], 15.2 kHz [30, 34], 12.5 kHz [55], or even below 3 kHz [27, 49]. By customizing a QTF with a fundamental frequency at 2.9 kHz and a first overtone mode at 17.8 kHz, Elefante et al. introduced an inventive technique of dual-gas on-beam QEPAS, that allows to simultaneously exploit the fundamental mode for water monitoring and the overtone mode for CH_4 or N_2O detection, using two laser sources but only one signal transducer [98]. However, regardless of their natural frequency, combining mechanically resonant signal transducers with acoustic resonance amplification yields *double-resonant systems*, that are more difficult to calibrate than systems, which solely exploit single resonance amplification, as they may be prone to detuning. Detuning may result from changes in the speed of sound, e.g., by variations in temperature or in the composition of the gas sample, which severely affects acoustic resonance, but influences mechanical resonance only to a small degree. As it was investigated in [32] in detail, changes in air humidity of less than 2%V might cause 25% signal deviations due to changes in the speed of sound causing detuning of a double-resonant off-beam QEPAS application.

Another way to increase the SNR of a photoacoustic setup is the application of multiple transducers, e.g., an *array of microphones*. By using three MEMS microphones, for example, Mitrayana et al. were able to detect noise equivalent concentrations of 6, 11, and 31 ppbV of ethylene, acetone, and ammonia in the breath of patients with lung diseases such as lung cancer [69]. To further increase the sensitivity, Hofstetter et al. [53] and Romann et al. [74] even employed arrays of 16 and 80 microphones, respectively. Because sensitivity scales with n and noise scales with $\sqrt{n}$, the SNR is known to be improved by $\sqrt{n}$ when operating a number of n microphones in parallel [99]. By cascading two tuning forks, Ma et al. verified that the concept of multiple signal transducers can also be transferred to an *array of QTFs* [42]. Although the electronic noise is not expected to increase by cascading multiple forks at all, they only observed a 70% instead of 100% SNR improvement due to minor mismatching of the resonance frequencies of both QTFs. However, they were able to compensate for those frequency deviations by means of

temperature or pressure regulation in later studies [44]. Further alternatives for acoustic signal detection in PA applications are the utilization of *fiber-optic* [38, 39, 47] or *cantilever-based* acoustic transducers with optical readout [58, 59, 62, 75]. Concluding this section, Zhang et al. published a comprehensive review article, summing up the most used detectors in PA gas-phase analysis [96].

3.4 Selecting the Most Suitable Setup for Your Requirements

To summarize Sect. 3, there is an enormous variety of different methods and concepts available, when it comes to photoacoustic trace gas detection. This provides the opportunity to customize PA applications in order to adapt it to specific needs, but the multitude of possibilities also requires an in-depth study of the subject and the available literature. This section is intended to assist in selecting the appropriate methods for photoacoustic breath analysis applications.

3.4.1 Limit of Detection and Normalized Noise Equivalent Absorption Coefficient

Since biomarkers for recognizing diseases in human breath are only present in very low volume ratios, ranging from about 1 ppbV to several ppmV [9], the most important parameter of a suitable measuring device might be its limit of detection, which is the ratio of sensor noise and sensor sensitivity. However, in order to be able to compare the multitude of different approaches and concepts in PA trace gas analysis, the scientific community introduced a physical quantity, namely the normalized noise equivalent absorption coefficient. The NNEA in units $W\,cm^{-1}\,Hz^{-0.5}$ is a uniform way to express the performance of a photoacoustic setup, as it takes into account:

- The minimum detectable dimensionless volume ratio $N_{i,\,min}$ (i.e., the detection limit), calculated by using n-times the standard deviation as the sensor noise.
- The absorption cross-section of the analyte at a given wavelength $\sigma(\lambda)$ in units $[cm^2]$.
- The optical power of the light P_0 [W] that contributes to PA signal generation.
- The equivalent noise bandwidth Δf [Hz], which depends on the lock-in time constant as well as on the filter roll-off

$$\text{NNEA} = \frac{N_{i,\,min}\,N_A\,\sigma(\lambda)\,P_0\,p}{n\,\sqrt{\Delta f}\,R\,T} \tag{40}$$

In Eq. (40), N_A in mol^{-1} denominates the Avogadro constant, R in $J\,mol^{-1}\,K^{-1}$ is the universal gas constant, and T and p are the given temperature in K and pressure in

Pa, respectively. The NNEA lacks only one parameter, namely the time of sensor data averaging that had been taken for LOD determination, which must not be confused with the integration time of lock-in amplification. Without providing a detailed comparison, non-resonant multi-pass designs, concepts that exploit solely acoustic resonance amplification as well as acoustically double-resonant quartz-enhanced techniques usually are characterized by NNEAs in the order of 10^{-9} to 10^{-10}, when averaging the sensor data over 1 s. Increasing the data acquisition and averaging time can significantly suppress sensor noise, thus improving the LOD. Many publications, therefore, provide an Allan–Werle deviation plot in order to characterize the sensor noise as well as to quantify noise suppression as a function of averaging time [100]. While single-resonant bare QTF sensors may rather be one magnitude of order inferior in terms of performance, optical cavity-enhanced methods, on the contrary, may perform 2–3 magnitudes of order better.

3.4.2   Assessment Criteria

As it has already been briefly touched upon in Sect. 3.1, conceptualizing a PA application should always start with choosing an appropriate analyte absorption feature together with a suitable emitter. In this regard, the product of optical power and cross-section of the absorption feature must be ensured to meet the requirements of sensitivity. The easiest way to verify this is to browse references that specify these quantities together with the limit of detection, the authors achieved. This theoretical study must also take into account potential spectral cross-sensitivities toward components, which you may expect to be part of the gas sample. Furthermore, it has to be considered if emitter as well as absorption feature allow for wavelength modulation, which might be preferable to that of amplitude modulation, especially if the non-analyte components must be assumed to significantly vary in concentration or if light-with-PAC interactions are expected to generate a non-neglectable background signal. Cost is also a decisive factor with regard to the development of a respiratory gas sensor, and it scales with complexity. Accordingly, while for example a bare QTF setup or a LED-based non-resonant multi-pass approach can meet the requirements of a simple sensor for private self-administration, systems for qualitative pre-diagnosis in a family doctor's office or quantitative high-end clinical analysis may rather necessitate sophisticated resonant PAC designs or even optical cavity-enhanced approaches.

In terms of calibration and sensor resilience, changes of temperature as well as of water or carbon dioxide concentrations in the exhaled breath have to be considered. Once these parameters are not kept constant by application, e.g., by temperature control, humidification or de-humidification, resonant or especially acoustically double-resonant systems require sophisticated calibration. If, in addition, relaxation-induced signal changes must be suspected due to concentration changes of the main components of the mixture (refer to Sect. 4), acoustically double-resonant systems must be supported by a robust multivariate data analysis as discussed in [101]. Besides calibration intervals, maintenance and ease of use are

further criteria, that must be regarded when comparing simple non-resonant designs with complex optics in cavity-enhanced approaches, for example. A final and yet very important property is the long-term stability of the sensor and its drift behavior. As PA sensor drifts often correlate with the light that is used for PA signal generation, e.g., by emitter aging or contamination and de-alignment of the optical path, respectively, a reliable monitoring of the optical power inside the PAC is recommended. All things considered, an all-including comparison of different PA techniques culminating in a perfect hardware concept proposal is hardly possible, as it depends heavily on the application and the targeted specifications, such as LOD, selectivity, ambient noise, analyte species, measuring interval, target size of the sensor, importance of cost factor, static or varying bulk composition, maintenance interval and so forth. A comprehensive review of NIR PA applications for human breath analysis can also be found in [9].

4 Photoacoustic Spectroscopy in Complex Gas Matrices

Based on the very first experimental studies carried out by Pauling in 1971 [1], it has been demonstrated that human exhaled breath represents a complex gas matrix. In the following years, various components of exhaled air could be identified, see Table 1. Some of those molecules, called biomarkers could be linked to correlate with various diseases or metabolism anomalies. However, since until today only nitrogen monoxide has been accepted as a unique biomarker for asthma it is more appropriate to refer to these molecules as "potential" biomarkers. A more detailed discussion on biomarkers in breath analysis is provided in the chapter *Physio-Metabolic Monitoring via Breath Employing Real-Time Mass Spectrometry: Importance, Challenges, Potentials and Pitfalls* within this book.

Medical POC devices need to be capable of reliably measuring the low concentration ranges and changes of the respective analytes of interest in human breath exhale. Photoacoustic sensors already proved their potential for ultra-sensitive trace gas analysis in many fields of application, e.g. monitoring of environmental relevant trace gases [24, 31, 32, 48, 119–121], industrial process control [122, 123] or exhaled breath diagnostics [9, 25, 26, 69, 124, 125].

Utilizing low-cost and miniaturized components, photoacoustic-based sensors provide a suitable technique for mobile and affordable breath diagnostics. Nevertheless, the inherent disadvantages of PAS, such as the dependency of the measurement signal on environmental parameters, i.e., pressure p, temperature T, and gas composition $\sum \chi$ should not be neglected, when developing reliable medical diagnostic tools.

Variations in ambient conditions may affect the measurement signal due to spectral effects, e.g., additional photon absorption of interfering molecules or spectral peak deformation. The generation of the acoustic wave within the PAC may be also influenced, as the speed of sound changes and potential attenuation effects might occur. Furthermore, the overall efficiency of photoacoustic signal generation

Table 1 List of selected compounds in healthy human breath exhale adapted from [17, pp. 23–24]

Exhale breath component	Concentration range (healthy, ***altered***) in ppmV	Reference
Nitrogen (N_2)	740,000	
Oxygen (O_2)	140,000–160,000	
Carbon dioxide (CO_2)	40.000–50.000	[102, 103]
Water (H_2O)	29.000–50.000	[104]
Argon (Ar)	10.000	[102]
Carbon monoxide (CO)	0.4–0.8 1.14–1.37; ***13.6–19.3***	[105, 106]
Methane (CH_4)	3–8	[105, 107]
Hydrogen (H_2)	ppmV range	[107, 108]
Ammonia (NH_3)	0.43–1.8; ***14.7*** 0.05–0.15 0.628	[105, 109, 110]
Isoprene (C_5H_8)	0.12; ***<0.014*** 0.04 0.02–0.23	[110–113]
Methanol (CH_3OH)	0.46	[114, 115]
Ethanol (C_2H_5OH)	0.26	[110]
Carbonly sulfide (OCS)	0.1; ***0.64***	[116, 117]
Acetone (C_3H_6O)	0.3–0.9; ***128*** (The concentration has been converted from 5,063 nmol L^{-1} to 128 ppmV using $V_{mol} = 25.28$ L mol^{-1} and $T = 308$ K)	[113, 118]

The typical healthy concentration range is displayed in normal font numbers, the altered concentrations for non-healthy conditions are highlighted in bold and italic numbers

ϵ_{relax} via non-radiative relaxation is also strongly dependent on environmental conditions. In general, the photoacoustic signal is prone to three major categories of cross-sensitivities:

- *Spectral cross-sensitivities:* Since PAS is an optical measurement technique, i.e., stimulating certain energy transitions of the analyte, possible spectral influences pose a major challenge. Detailed investigation, e.g., utilizing well-known spectral databases like HITRAN, PNNL, or MPI-Mainz UV/Vis Spectral Atlas can minimize the risk of such cross-influences a priori. Nevertheless, in complex gas mixtures containing multiple gases it cannot be guaranteed that a completely cross-influence-free wavelength or wavelength region can be found. Section 4.1 discusses various approaches to cope with spectral cross-influences. The application of wavelength-adjustable light sources (refer to Sect. 3.1.1) and statistical evaluation methods, such as partial least squares regression (PLSR), can compensate for interfering spectral effects for a major part, or even allow reliable multicomponent detection in highly overlapping spectral regions [101].

- *Classical acoustic attenuation effects:* In PAS, the periodic local heat input via non-radiative relaxation of the excited molecules is detected. This periodic heat input results in compression and subsequent dilatation of the gas, which is per definition a sound wave. Several acoustic effects influence the propagation of this sound wave. Typically, an acoustic resonator is employed in PA setups to amplify the generated sound wave (refer to Sects. 2.3 and 3.2.1). The resonant properties of such an acoustic resonator and its attenuation effects due to several loss mechanisms can be described by its quality factor (Q-factor). For cylindrical acoustic resonators, the photoacoustic signal is directly proportional to the Q-factor (see Eq. 37). Section 4.2 discusses real-time capable compensation approaches regarding acoustic attenuation effects for different PA setups.
- *Non-radiative relaxational effects:* The periodic heat input results from non-radiative relaxation via molecular collisions. When an excited molecule collides with another molecule, three possible energy transition may occur. The first possibility describes no exchange of internal energy, only a change in the direction of translational motion of the respective collisional partners. Vibrational-translational relaxation on the contrary considers the possibility of converting internal energy of an excited molecule into translational energy of motion, in turn generating heat. Vibrational energy transfer from one collisional partner to another is labeled vibrational-vibrational relaxation. Those VV processes increase the complexity of the overall relaxation path and tend to become more influential with regard to complex multi-component gas mixtures. The example of methane is used to illustrate the challenge of calibrating photoacoustic sensors with respect to relaxational effects. A special case of non-radiative relaxational effects is a phenomenon called *kinetic cooling*. Concluding Sect. 4.3, an algorithmic model is briefly introduced, which increases the resilience of the PA signal against relaxational effects.

A further effect that might influence the photoacoustic signal is the effect of photodissociation. This effect has been discussed in detail regarding photoacoustic acetone [25, 26] and ozone detection [126, 127] in the UV/Vis range.

Spectral and relaxational cross-effects on the photoacoustic signal apply to all PA setups, as they are inherent in the basic physics behind the photoacoustic effect. However, from this point, only a longitudinally excited cylindrical resonator is considered. Other PAC designs that exploit different ways of acoustic amplification are described in Sect. 3.2.1 and will be neglected for further consideration.

The photoacoustic pressure of the first longitudinal mode can be represented by Eq. (37). Besides geometrical factors of the cylindrical measurement cell $(L/V)_R$ and the light-to-sound coupling factor μ_j, which both can be assumed constant for a given setup, the photoacoustic pressure depends on the resonance condition $(Q/\omega)_{res}$, the non-radiative relaxation efficiency ϵ_{relax} and the absorption coefficient α of the gas matrix at the wavelength of emission.

The complex correlations between the non-spectral, non-constant photoacoustically relevant parameters and environmental conditions, i.e., temperature T, pressure p, and gas composition $\sum \chi$, are schematically illustrated in Fig. 8.
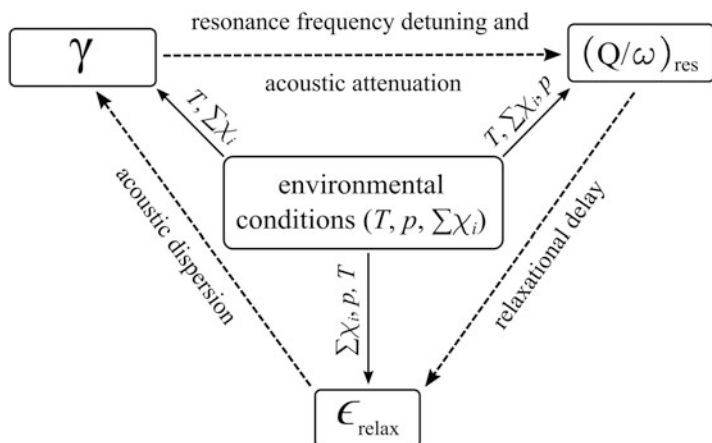
Fig. 8 Schematic representation of the circular dependencies of different environmental parameters, i.e., temperature T, pressure p, and gas composition $\sum \chi_i$ on certain PA parameters. The environmental influences are arranged in descending order of influence

Variations in ambient conditions (solid arrows) affect the heat capacity ratio of the measurement gas, the resonance parameters and ϵ_{relax}. The circular dependencies between these PA parameters are indicated by the dashed arrows labeled with the respective underlying physical effects. The absorption coefficient α likewise depends on pressure, temperature and measurement matrix, but is excluded from these circular relationships.

In the following sections, the challenges for PAS in complex and varying gas matrices, such as human exhaled breath are discussed. Experimental as well as mathematical approaches to cope with different cross-influences on the photoacoustic signal are provided to conclude this section.

4.1 Spectral Cross-Sensitivities

The photoacoustic pressure results from initial photon absorption of analyte molecules and subsequent non-radiative relaxation of the excited molecules. Spectral cross-sensitivities pose a major challenge in any photon absorption-based measurement technique, especially in complex gas matrices, such as human breath exhale. Due to spectral overlap with the analyte molecules, even low concentrated breath components in the ppbV to ppmV range might have a significant influence on the photoacoustic signal. Figure 9 illustrates the problem of overlapping absorption features in human breath exhale. The spectral region from 3,500 to 7,500 cm^{-1} is completely dominated by the high concentration breath components water and carbon dioxide. In this region, a reliable analyte detection in the ppmV or
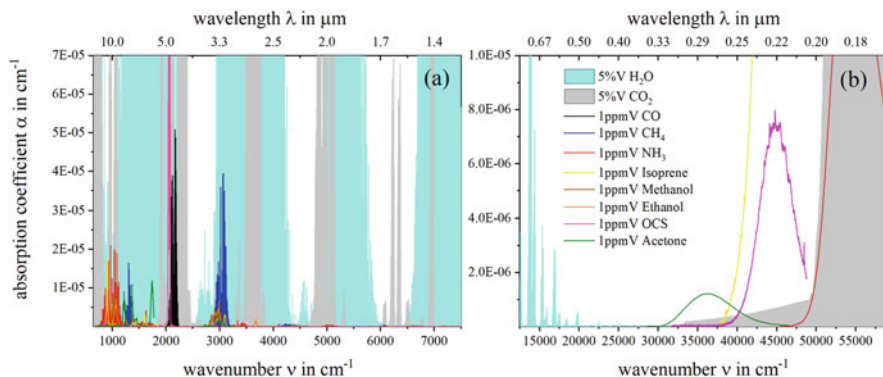
Fig. 9 Absorption coefficients of the endogenous exhale breath components listed in Table 1 in the infrared (**a**) and ultraviolet/visible (**b**) – region. The data was taken from HITRAN and the MPI-Mainz UV/Vis Spectral Atlas. For better visual clarity the spectra of water and carbon dioxide were filled

sub-ppmV range by means of PAS is hardly feasible. For the IR region at around 3,000 cm^{-1} and lower, some of the trace gas breath components exhibit relatively strong absorption, thus providing an interesting area for optical breath analysis. In the ultraviolet region (Fig. 9b) the spectral overlap is less pronounced. While not all analytes present in human exhale breath show noticeable absorption in the UV region, some, such as acetone, can be detected without significant spectral cross-sensitivities at approximately 0.28 μm [25, 26].

In regions where spectral interference from other molecules cannot be avoided, the employment of tunable light sources, e.g., ICL and QCL, provide a possible approach for reliably determining the target analyte concentration [123, 128–130]. Utilizing the tunability of those light sources, the PA response can be recorded for multiple wavelengths. Consequently, the individual contribution of interfering molecules to the overall PA signal can be determined, thus allowing to retrieve the desired analyte concentration. A simple hypothetical example regarding the effect of overlapping absorption spectra is illustrated in Fig. 10. While molecules A and B show gaussian distributed absorption characteristics with center wavelengths λ_A and λ_B, molecule C exhibits constant absorption over the whole displayed spectral region. Due to the strong overlap of the individual absorption characteristics, the actual concentration of molecule B cannot be determined by recording the PA signal of the mixture at a single wavelength.

The PA signals $\widehat{S}_{ij}$ of the individual components i in a gas sample containing multiple species K, scanned over a wavelength region from λ_j to λ_n can be represented as a $(K \times n)$ matrix of linear equations
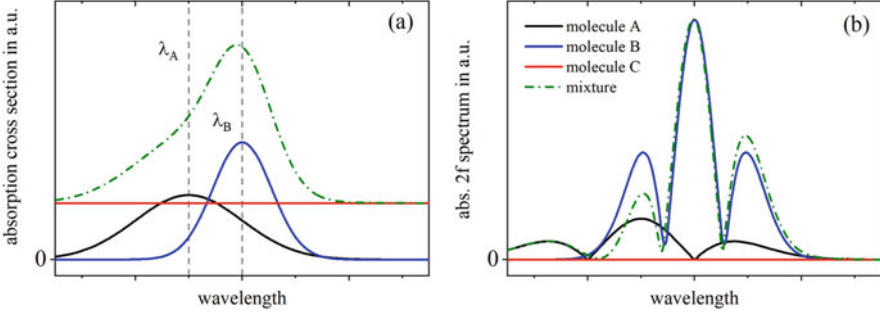
Fig. 10 Schematic representation of multicomponent analysis, with overlapping spectra of the individual components (A, B, C) resulting in a cumulative spectrum of the gas mixture (**a**). The graphs on the right side (**b**) display the absolute resulting $2f$ spectra

$$\widehat{S}_{ij} = \begin{pmatrix} S_{11} = P_1(\lambda_1)N_1R_{11}(\lambda_1) & \cdots & S_{1n} = P_n(\lambda_n)N_1R_{1n}(\lambda_n) \\ \vdots & \ddots & \vdots \\ S_{K1} = P_1(\lambda_1)N_KR_{K1}(\lambda_1) & \cdots & S_{Kn} = P_n(\lambda_n)N_KR_{Kn}(\lambda_n) \end{pmatrix} \quad (41)$$

Each element of the matrix is a function of emitted optical power P_j at wavelength λ_j, the unknown volume ratio N_i of molecule i and the respectively measured response R_{ij} of the PA sensor [131]. The photoacoustic signal of the gas matrix $\widehat{S}_j$ at wavelength λ_j is defined as the sum of the individual responses R_{ij}

$$\widehat{S}_j = P_j(\lambda_j) \sum_{i=1}^{K} N_i R_{ij} \quad (42)$$

Solving Eq. (42) for the unknown volume ratio N_i of component i results in

$$N_i = \sum_{j=1}^{K} R_{ji}^{-1} \frac{\widehat{S}_j}{P_j(\lambda_j)} \quad (43)$$

where R_{ji}^{-1} represents the inverse of the matrix R_{ij}. In order to deduce the concentrations of the individual species within a gas sample, an unambiguous solution for the set of linear Eq. (42) must be found. This requires the photoacoustic signal to be measured at a minimum of K different wavelengths [131]. It is obvious that appropriate wavelengths should be selected based on the absorption characteristics of the individual components. Utilizing wavelength modulation of the light source the effect of constant absorbers, such as molecule C can be avoided in terms of PA signal generation, see Fig. 10b. When dealing with complex gas mixtures, a combination of WM and AM may be an appropriate approach.

In recent literature, several examples can be found that successfully apply the approach of spectra reconstruction in complex gas mixtures utilizing PAS. Zifarelli et al. employed a QCL to reconstruct the spectra of mixtures diluted in N_2 containing traces of N_2O and CO_2 from 2,188.8 to 2,191.2 cm^{-1} as well as CH_4, C_2H_2, and N_2O from 1,295.5 up to 1,296.5 cm^{-1} by means of WM-QEPAS [129]. With an overlap Z of the individual absorption features of up to 97.4% ($Z_{CO-N_2O} = 7.3\%$, $Z_{CH_4-N_2O} = 79.8\%$, $Z_{CH_4-C_2H_2} = 97.4\%$) spectral cross-sensitivities pose a significant challenge. The approach in this study was to combine the spectral measurements with statistical evaluation algorithms, i.e., multi linear regression (MLR) and PLSR, to retrieve the desired analyte concentrations. In principle, both MLR and PLSR are suitable for retrieving individual concentrations from highly overlapping gas mixtures. However, Zifarelli et al. demonstrated that PLSR improves the root mean squared error of calibration by up to a factor of 5 compared to MLR [129]. The work of Loh et al. [132] and Saalberg et al. [133] represent further examples of the successful implementation of PLSR in multi-component gas mixtures. In [132], PLSR allowed to accurately quantify individual short-chained ^{12}C, ^{13}C hydrocarbon isotopologues from CH_4, C_2H_6, and C_3H_8 in the region from 2,998.8 to 3,005.1 cm^{-1} and from 2,944.0 to 2,964.5 cm^{-1}. Volatile organic compounds, such as 2-butanone, 1-propanol, isoprene, ethylbenzene, styrene, and hexanal exhibit strong spectral overlap in the range from 2,817 to 3,077 cm^{-1}. Despite these strong cross-influences, Saalberg et al. were able to quantify the individual concentrations in mixtures with excellent relative accuracy of 2.6%, emphasizing the potential of PLSR for spectral measurements [133].

4.2 Acoustic Attenuation Effects and Resonance Monitoring

While regarding spectral interferences even trace gases could potentially cause a significant impact on the PA signal, due to overlapping absorption features, acoustic attenuation and relaxational effects more likely occur at higher concentrations. Formula (37) describes the photoacoustic pressure p_a of the first longitudinal mode. Referring to Fig. 8 changes in environmental conditions, i.e., temperature, gas composition, or pressure, will affect the standing wave formation within the acoustic resonator. This in turn influences the resonance parameters $(Q/\omega)_{res}$. Referring to Eq. (27) changes in the speed of sound result in a shift of acoustic resonance frequency. In microphone-based PA setups, the resonance frequency of the system can be determined by the acoustic resonator, since microphones generally feature a rather flat frequency response between 1 and 20 kHz. When using resonant acoustic transducers instead, e.g., QTF or cantilever, the resonance frequency of the system is predetermined by the transducer properties. Utilizing beat frequency photoacoustics the resonance frequency f_{res}, Q-factor and analyte concentration can be determined in real-time. In BF-PAS the modulation frequency of the laser f_{laser} is set slightly different to the actual resonance frequency of the PA system f_{res}.
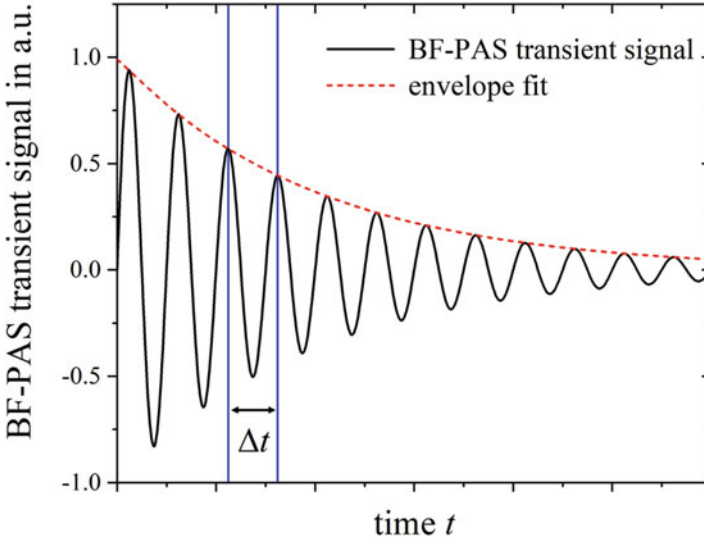
Fig. 11 Typical demodulated BF-PAS (beat frequency – photoacoustic spectroscopy) signal (black solid line) with frequency $f = \Delta t^{-1}$ and the resulting envelope fit (red dashed line) to determine the ringdown time τ

$$f_{\text{laser}} = f_{\text{res}} \pm f \tag{44}$$

Demodulating the measured BF-PAS signal at f_{laser} results in the transient signal of the setup, as displayed in Fig. 11. The frequency $f = \Delta t^{-1}$ of the demodulated transient signal corresponds to the difference between laser modulation f_{laser} and resonance frequency of the transducer, thus allowing simple f_{res} tracking. The Q-factor depends on the ringdown time τ and f_{res}, according to classical damped oscillator theory [50].

$$Q = \tau \pi f_{\text{res}} \tag{45}$$

The ringdown time τ is defined as the time required for the system to drop to $1/e$ of the initial vibration amplitude and can be determined by exploiting the envelope of the BF-PAS transient signal.

Regarding microphone-based PA setups, Schindler et al. presented a simple approach to determine the resonance frequency of acoustic resonators by integrating a miniaturized speaker within the PA sensor [134]. In this work, the resonance frequency was quantified by frequency sweeping the speaker and recording the resulting microphone response. Moreover, substituting the frequency sweeps with pulsed, periodic excitation of the speaker and analyzing the FFT of the microphone signal allows for real-time resonance frequency tracking (RT) [135]. Furthermore, the FFT of the microphone signal contains information about the Q-factor of the PA

system [135]. Utilizing this could potentially yield a real-time monitoring system for all relevant resonance properties.

Implementing an RT technique guarantees the photoacoustic signal to match the Eigenfrequency of the system. This avoids signal losses provided that the system is not based on the exploitation of multiple acoustic resonators, that are affected differently by varying ambient conditions, such as changing temperature. Additionally, utilizing BF-PAS or Q-factor monitoring the influence of acoustic attenuation on the photoacoustic signal might be compensated by determining the resonance parameters $(Q/\omega)_{\text{res}}$. This would increase the reliability of PA gas sensors in case of varying environmental parameters. In [26] the effect of temperature on the Q-factor for a microphone-based PA sensor was investigated. A temperature shift of 30 K from 20 to 50°C of the PAC resulted in a 3.4% decrease in the Q-factor. Considering that the PA amplitude is directly dependent on the Q-factor, this effect, if not taken into account, would result in a 3.4% deviation of the sensor reading from the calibrated value.

As an alternative approach to avoid signal deviation that might occur due to changes in bulk composition, several PA-based sensor concepts for breath analysis successfully include dehumidifiers or CO_2 scrubbers to avoid potential cross-sensitivities [66, 69]. However, these approaches are accompanied with an increase in apparatus complexity as well as an increase in sensor dimensions. By combining a multi-wavelength approach (see Sect. 4.1) with the concept of acoustic resonance monitoring, the reliability of the sensor system can be improved without increasing its mechanical complexity.

4.3 Molecular Effects in Photoacoustic Spectroscopy

4.3.1 Heat Capacity Ratio γ in Gaseous Media

Referring to Eqs. (14) and (37) the heat capacity ratio γ is directly correlated to the source term of photoacoustic signal generation and the resulting photoacoustic pressure p_a. In gaseous media, this ratio can generally be expressed as a function of the sum over all degrees of freedom (DOF) $\sum f$.

$$\gamma = 1 + \frac{2}{\sum f} \tag{46}$$

The sum $\sum f$ includes three categories of molecular motion. Linear motion in three-dimensional space (x-, y-, z-direction) is described by the translational degrees of freedom $f_{\text{trans}} = 3$. Rotational and vibrational states of the molecules are summarized in f_{rot} and f_{vib}, respectively. Linear molecules, e.g., CO_2 exhibit two possibilities of rotational motion $f_{\text{rot}} = 2$, while for non-linear molecules $f_{\text{rot}} = 3$. The vibrational DOF equal $(3N - 5)$ in case of linear and $(3N - 6)$ in case of non-linear molecules, consisting of N atoms. However, since temperature and frequency affect

which DOF are thermally activated and exhibit sufficiently fast relaxation to contribute to sound propagation, respectively, T and f_{sound} have to be considered. At moderate temperatures and moderate acoustic frequencies in the lower kHz range, all rotational and translational degrees of freedom can be assumed to completely contribute to sound propagation. However, this assumption cannot be applied generally to vibrational DOF. The ratio of thermally excited f_{vib} can be calculated according to Eq. (47), which considers the temperature T of the sample, as well as the degeneracy n and the temperature Θ_{vib} of the vibration, respectively.

$$f_{\text{vib}}(T) = 2n \left(\frac{\Theta_{\text{vib}}}{T}\right)^2 \left(\frac{\exp\left(-\frac{\Theta_{\text{vib}}}{2T}\right)}{1 - \exp\left(-\frac{\Theta_{\text{vib}}}{T}\right)}\right)^2 \tag{47}$$

The temperature of vibration Θ_{vib} is a function of the related wavenumber $\tilde{\nu}$, the speed of light c_0, the Planck constant h and the Boltzmann constant k_B.

$$\Theta_{\text{vib}} = \frac{hc_0\tilde{\nu}}{k_B} \tag{48}$$

The term acoustic dispersion describes the phenomenon of the frequency dependency of $f_{\text{vib}}(\omega)$. With increasing sound frequencies[9] some vibrational modes may not be able to follow the energy exchange finally causing periodic compression and subsequent dilatation. In terms of sound propagation, those modes are no longer relevant, even if they are thermally excited. In order to correctly calculate the adiabatic exponent of complex gas mixtures, Eq. (46) must be adjusted to

$$\gamma(T,\omega) = 1 + \frac{2}{f_{\text{trans}} + \sum\limits_{i=1}^{k} \chi_i \cdot \left(f_{\text{rot}} + \sum\limits_{m=1}^{n} f_{\text{vib}}(T) \cdot \epsilon_{\text{relax},i,\nu_m}(T,\omega)\right)} \tag{49}$$

The sum $\sum_{i=1}^{k}$ takes into account every species within the measurement matrix, where the individual volume ratios of the individual species are considered as χ_i. The vibrational states ν_m of the molecule i and their respective relaxational efficiencies are considered by $\sum_{m=1}^{n} \epsilon_{\text{relax},i,\nu_m}$. The relaxation efficiency accounts for acoustic dispersion ($\epsilon_{\text{relax},i,\nu_m} = 1$: no acoustic dispersion; $\epsilon_{\text{relax},i,\nu_m} = 0$: maximal acoustic dispersion). The following section explains why molecular relaxation plays another significant role in photoacoustic signal generation. For a more theoretical profound derivation of the phenomenon of molecular relaxation processes refer to literature [136–138].

---

[9]Regarding AM-PAS, the sound frequency equals the frequency of light modulation.
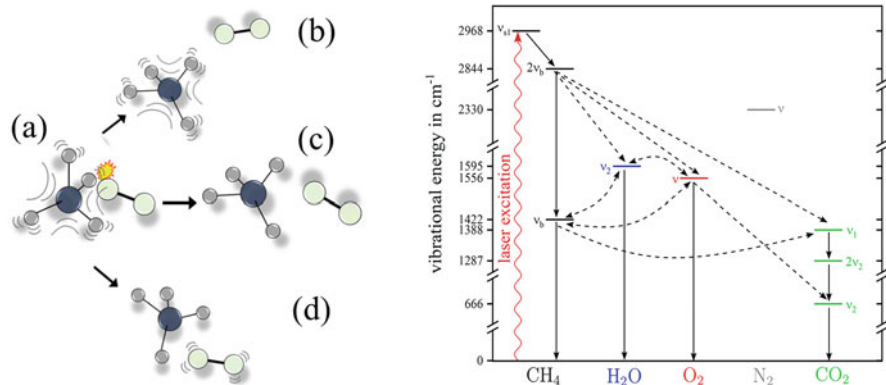
Fig. 12 Schematic representation of non-radiative relaxation processes (left) and a complete Jablonsky diagram (right) showing all relaxational routes regarding the near-IR detection of CH_4 in a mixture further containing H_2O, O_2, N_2, and CO_2. The left diagram displays all possibilities that may occur while collision of a CH_4 molecule with any other molecule (**a**). These include intramolecular energy transfer (**b**), VT relaxation (**c**), and VV relaxation (**d**). On the right side, the solid arrows indicate intramolecular relaxation, while the dashed arrows represent intermolecular energy transitions

4.3.2 Non-radiative Molecular Relaxation

A major challenge when calibrating photoacoustic gas sensors against environmental influences is the effect of non-radiative molecular relaxation. If a vibrationally excited molecule collides with another molecule, some part of (VV relaxation) if not all vibrational energy (VT relaxation) of prior photonic excitation may be released as translational energy into the system. VV relaxations cover intramolecular and intermolecular energy exchange. In the latter case, part of the energy is transferred to the collisional partner. A simplified illustration of possible energy transitions during molecular collision is depicted on the left side of Fig. 12, while the Jablonsky diagram on the right shows the concrete example of NIR CH_4 detection in a complex gas matrix containing H_2O, O_2, N_2, and CO_2.

In the case of 100% relaxation, all vibrational states actively involved in the overall relaxation process are capable of releasing their vibronic energy prior to de novo light absorption. The relaxation efficiency ϵ_{relax} of an individual energy state ν is defined as

$$\epsilon_{relax,\nu} = \frac{1}{\sqrt{1 + \left(\omega k_\nu^{-1}\right)^2}} \tag{50}$$

with ω being the angular frequency of laser modulation and k_ν the non-radiative relaxation rate of ν, i.e. the reciprocal relaxation time τ_ν. While fast relaxation rates result in 100% relaxation, i.e., $\epsilon_{relax,\ \nu} = 1$, slower rates may cause delayed

relaxation, i.e., $\epsilon_{\text{relax}, \nu} < 1$, leading to PA signal loss as slowly relaxing vibrational states cannot be completely depopulated before a new cycle of absorption begins. The number of VV transitions scales with the number of different species composing the gas sample. Such transitions tend to increase the complexity of the relaxation cascade, thus considerably complicating an analytical description of the underlying processes. As is discussed in [6] in detail, literature in this regard often utilizes oversimplified assumptions. More recently, however, analytical approaches have been reported to adequately deal with relaxational effects by considering all molecular collision reactions involved in the respective relaxation process, yielding a theoretically derived PA signal [24, 55, 121].[10] Their calculations show excellent agreement with the measured data, verifying the fundamental mathematical correlations presented by Hunter et al. in 1974 [139].

With CoNRad (an algorithm to compute the collision-based non-radiative efficiency and phase lag of energy relaxation on a molecular level) a more sophisticated approach was introduced in 2022 by Müller et al. [6]. In this work, the capability of CoNRad to compensate for relaxational-induced signal alterations in the concrete case of NIR methane detection was demonstrated. The potential of CoNRad to predict the relaxation-dependent PA signal for different sensor setups employing other acoustic transducers than a microphone, e.g., a QTF, and detecting different analytes was also shown exemplarily in [6]. The direct comparison of the measurement results regarding QEPAS-based carbon monoxide detection from [121] with the theoretical calculations obtained from CoNRad showed excellent agreement. Utilizing this algorithmic approach in combination with a method to calculate or empirically determine the resonance characteristics of the PAC as well as a spectral analysis of the sample may significantly increase the robustness, resilience, and reliability of PA sensors.

5 Selected Applications: Photoacoustic Spectroscopy in Breath Analysis

This section discusses potential biomarkers found in human breath as well as their detection by means of photoacoustic spectroscopy. A more detailed discussion on the term "biomarker" for breath analysis is provided in the chapter *Physio-Metabolic Monitoring via Breath Employing Real-Time Mass Spectrometry: Importance, Challenges, Potentials and Pitfalls* within this book. Table 2 lists potential and already approved (e.g., NO) biomarker molecules, which have been detected by means of photoacoustic spectroscopy. Since until today only a few BA studies have been performed using PAS as a detection method, studies that are still in the laboratory phase but aim to apply their research in the field of breath analysis have

---

[10]By the example of the Jablonsky diagram depicted in Fig. 12, 50 different collision reactions have to be considered.

Table 2 Summary of potential biomarker species and associated diseases, which have been measured by means of photoacoustic spectroscopy

Biomarker	Disease	References
Ammonia	Liver or kidney anomalies	[35, 140–148]
Ethylene	Oxidative stress: lipid peroxidation	[125, 142, 143, 145, 146, 149–152]
Acetone	Metabolic processes, obesity, children with epileptic seizures (ketogenic diet), acute decompensated heart failure	[25, 118, 153–160]
Methane	Sugar malabsorption	[105, 161–164]
Nitric oxide	Lung disease, asthma	[165–169]
Carbon monoxide	Jaundice	[63, 106, 170–172]
Hydrogen cyanide	Cystic fibrosis	[173]
Nitrous oxide	Partial gastrectomy, atrophic gastritis	[174, 175]

been listed as well. Hence, care has been taken to highlight the technology readiness level of the PAS studies discussed within the following subsections.

5.1 The Human Volatilome Regarding Breath Analysis

The human volatilome comprises all volatile metabolites as well as other volatile organic and inorganic compounds originating from humans, i.e., saliva, sweat, urine, stool, blood, and exhaled breath. Thus, more than 870 volatile organic compounds have been identified in breath samples [176]. The origin of the VOCs can thereby be endogenous, i.e., arising in the body, or exogenous, i.e., originating from the environment. Biomarkers are usually endogenous species that either result from normal metabolic processes or reveal an imbalance, which may indicate a disease or a systemic dysfunction. Since breath sampling is non-invasive, breath analysis is considered patient friendly and hence preferable for medical diagnosis. As already listed in Table 1, human exhaled breath contains primarily nitrogen (74%V), oxygen (14–16%V), carbon dioxide (4–5%V), water vapor (2.9–5%V), and argon (1%V) [102–104], while VOCs with clinically relevant information are quite low concentrated. The actual concentrations depend on the patient's age, medical condition, and individual metabolism. In this context, the volume ratio of different potential biomarkers ranges from the pptV to the lower ppmV range. Therefore, it is of crucial relevance to quantify specific biomarkers as accurately as possible in order to generate reliable diagnostic data.

5.2 Breathborne Biomarkers and Photoacoustic Spectroscopy

Ammonia

Ammonia is present in all body fluids and originates from protein metabolism processes. As a potential biomarker, ammonia is of growing interest as it is comparatively easy to measure with a typical concentration in breath of 0.25–2.9 ppm [140]. However, the sampling should be conducted rather nasally than orally as studies have revealed ammonia to be produced by enzymes in the oral cavity, too [141]. NH_3 is associated with liver or kidney anomalies, as it cannot be properly filtered out of the blood in case of hypofunction. Since ammonia is volatile, some of the NH_3 is released into the exhaled breath through alveolar exchanges. Applying amplitude modulated PAS, ammonia is often monitored together with ethylene (see below), since both molecules can be excited with a CO_2 laser (spectral range approx. 9.2–10.8 μm). Further references reports PA NH_3 detection limits in the lower ppbV or even sub-ppbV range [35, 142–148].

As an example, Mitrayana et al. compared the ammonia content of healthy people to patients suffering from a liver disease. On average, they discovered that the NH_3 concentration in the breath of the patients (3.27 ppmV) was about 2 ppmV higher than in the breath of healthy people (1.34 ppmV) [144]. Wang et al. used a tunable NIR fiber laser at 1,522.44 nm to photoacoustically detect the ammonia content in exhaled breath of dialysis patients before and after treatment noticing a reduction of NH_3 concentration by about 1.5 ppmV on average [177]. Recently, Li et al. [35] analyzed the breath of eight healthy volunteers using BF-QEPAS reaching a detection limit of 9.5 ppbV with an integration time of 3 ms.

Ethylene

Ethylene is a potential biomarker mainly associated with oxidative stress (OS). OS is caused by an imbalance of free radicals (oxidative process) and antioxidant processes, which may induce cellular damage or dysfunction. Hence, OS is directly related to physiological or biochemical events. Through lipid peroxidation (LP), i.e., the oxidative degradation of lipids, a radical chain reaction is initiated, causing lipids in the cell membrane to degrade the cell. Diseases associated with OS, as a consequence of LP, are cancer, atherosclerosis, stroke, rheumatoid arthritis, neurodegeneration and diabetes, to name only a few [178]. Besides ethane and pentane, ethylene is a stable end product of LP which can be photoacoustically detected with a CO_2 laser down to the pptV range [149]. Based on the list of possible diseases caused by LP, the determination of ethylene content in breath has a wide range of clinical applications [125, 142, 143, 145, 146, 149–152].

Petrus et al. studied the ethylene concentrations in the breath of lung cancer patients as a direct consequence of smoking before and after chemotherapy. While healthy people are reported to exhale ethylene concentrations between 10 and 25 ppbV, lung cancer patients were identified to exhale up to 480 ppbV [151]. Cristescu et al. monitored the ethylene levels induced by LP in patients undergoing cardiac surgery in real-time with a detection limit of 300 pptV [149]. In other studies, Petrus et al. showed that the breath ethylene content could

be associated with type 2 diabetes. Again, the ethylene content increases significantly as a result of OS. Accordingly, the ethylene content of diabetics was about one order of magnitude higher than compared to non-diabetics [142, 143]. Popa et al. demonstrated breath ethylene to originate generally endogenously by comparing nasal and oral samples before and after brushing with toothpaste/baking soda, obtaining no significant differences [125].

Acetone

Like other ketones, acetone is formed in the liver during fat metabolism by the breakdown of fatty acids, passed to the lungs via the bloodstream, and finally exhaled alveolarly. Besides fat metabolism monitoring, acetone is also used to identify the maximum performance of athletes by determining the anaerobic threshold [153]. However, acetone as a biomarker is often associated with type 1 diabetes, although no clear evidence for a reliable relation has been found so far [154]. Even though it has been shown that the breath acetone content is linearly correlated with the blood glucose level [155], the acetone concentrations in type 1 diabetes vary substantially and therefore cannot completely replace the common blood glucose tests. Nevertheless, acetone is regarded to be a useful target analyte for monitoring ketogenic diets. Thus, monitoring acetone levels can not only help in overcoming obesity [156] but also support children with epileptic seizures on their ketogenic diet [118, 157]. Besides, the clinical relevance of acetone as a biomarker became emphasized in studies by Samara et al. reporting an increased acetone and pentane level among patients with acute decompensated heart failure [158]. Among healthy adults, the mean acetone content is about 500 ppbV [159].

In view of photoacoustic detection, Tyas et al. used a CO_2 laser to compare the acetone content of diabetes Mellitus patients with that of healthy persons, and achieved a detection limit of 30 ppbV [160]. As a low-cost alternative, Weigl et al. developed a measurement system based on a modulated UV LED and reported a detection limit of 20 ppbV under laboratory conditions [25].

Methane

Methane is formed during the metabolism of bacteria in the gut. About 20% of thus generated methane diffuses into the blood and is emitted by breath with an abundance of 3–8 ppmV [105, 161]. In the case of sugar malabsorption (SM), methane serves as a biomarker. As a consequence of SM bloating, cramps, diarrhea, and other symptoms of irritable bowel syndrome may occur in the intestine. It might also interfere with other nutrient intake processes [161].

From the photoacoustic point of view, Lassen et al. follow an approach with a pulsed MIR-OPO between 3.1 and 3.5 μm achieving a methane detection limit of 0.2 ppbV at 100 s integration time [162]. Similarly, using a MIR-OPO but with QEPAS technique, Petersen et al. reached a detection limit of 32 ppbV under laboratory conditions [163]. By means of pig and rat models, Szucs et al. were able to photoacoustically detect methane within a concentration range between 12 and 90 ppmV [164].

Nitric Oxide

Nitric oxide is involved in many processes in the respiratory system and is used as a biomarker for the detection and monitoring of lung disease or asthma, since NO levels are increased in such pathologic states [165]. According to the 2017 NICE Asthma Guidelines, the critical level is 40 ppbV among adults and 35 ppbV among children [166].

Using a QCL emitting at 5.26 μm, where no spectral cross-sensitivities toward water or CO_2 have to be expected, Dong et al. achieved a detection limit of 4.9 ppbV with 1 s integration time measuring synthetic gas mixtures [167]. Similarly, with a QCL at 5.26 μm as well as an integration time of 1 s, Wu et al. reported a detection limit of 7 ppbV by exploiting a differential photoacoustic cell approach (refer to Sect. 3.2.4) [168]. However, this sensor has not yet been tested for real breath samples. Gondal et al. used a Q-switched Nd:YAG laser at the fifth harmonic to reach the strong UV absorption band of NO between 200 and 250 nm [169]. By means of three different PA cells, they investigated the parametric dependence on cell geometry, NO gas pressure, buffer gas including He, Ar, and N_2 as well as laser pulse energy. Finally, they determined the highest sensitivity when using three acoustic filters and argon as buffer gas, achieving detection limits for the 3 PACs of 41, 11, and 20 ppbV, respectively. Again, this setup was only used in the laboratory.

Carbon Monoxide

Increased carbon monoxide levels in exhaled air among neonates may indicate jaundice. In general, exhaled CO is a potential biomarker for oxidative stress (see above), chronic respiratory disease, or exposure due to air pollution [170]. The median CO level, depending on smoking or non-smoking persons, is 16.4 ppm and 1.3 ppmV, respectively [106].

In their laboratory, Dong et al. developed a QEPAS-based sensor system using a 4.65 μm QCL with a detection limit of 2 ppbV (1 s integration time) [63]. Meanwhile, Zhou et al. reached a detection limit of 1.1 ppbV with a QCL-based system, too. In studies of breath samples from non-smokers and smokers, a significant increase of about 2 ppmV CO content was observed [171]. In an experimental comparison between QEPAS and photothermal spectroscopy (PTS), Pinto et al. obtained a detection limit of 6 and 15 ppbV (QEPAS/PTS) in the laboratory. Therefore, they realized compact QEPAS and PTS detection modules assembled as a gas sensor system for CO that stimulates the fundamental mode at 4.6 μm with a distributed feedback QCL [172].

Further Potential Biomarker Species

Hydrogen cyanide is produced by the *Pseudomonas aeruginosa* bacterium, which causes the fatal respiratory disease cystic fibrosis (CF). Neerincx et al. developed a mid-IR laser PAS system using clinical isolates from CF patients. They identified that the HCN concentration increases as soon as the P. aeruginosa bacterium reaches its stationary phase [173].

N_2O is an indicator of bacterial growth in the stomach due to the reduction of gastric acidity. Accordingly, the N_2O content in exhalate in healthy people amounts

to approx. 0.8 ppm V and up twofold in patients with partial gastrectomy or atrophic gastritis, respectively [174]. Bayrakli developed a portable QEPAS system based on a 4.474 μm QCL, which is used to determine the N_2O content in breath with a minimum detection limit of 2 ppbV (100 s integration time) [175].

6 Summary and Outlook

Breath analysis is an emerging technology, which has proven its high potential for modern, non-invasive, and fast diagnostics in the last decades. However, this technique is still struggling to find its way into the everyday routine of clinics let alone the doctoral office or the consumer market. Photoacoustic spectroscopy is a highly promising and innovative technique, which can contribute to paving the way for breath analysis to advance from bench to bed or market.

Illuminating all facets of photoacoustic spectroscopy, the chapter introduces a fundamental understanding of the physical principles this sensor technique exploits. To be able to grasp the potential for an application in breath analysis, a comprehensive overview of various photoacoustic setups including their pros and cons is presented. Besides, it is demonstrated that in terms of sensitivity, PAS achieves the required limits of detection in breath analysis for several biomarkers. Since selectivity is an even greater challenge than sensitivity in breath analysis, care must be taken regarding spectral and non-spectral cross-sensitivities. Especially the latter one is often neglected or oversimplified leading to unreliable sensor readings within changing gas matrices. Therefore, one section of this chapter is dedicated to discussing potential cross-sensitivities when PAS is applied in breath analysis. In the future, digital twins of PA sensors may provide the means to compensate for such cross-sensitivities even in the case of complex and varying measurement conditions. Furthermore, by providing an overview and a discussion of the recent achievements of photoacoustic spectroscopy in the field of breath analysis, the potential of PAS is highlighted once more.

With the current development of novel, less expensive, more reliable and higher output power providing light sources, PAS is gaining more and more momentum toward market readiness. Using application-tailored photoacoustic setups and considering the spectral and non-spectral cross sensitivities during sensor calibration will be the key for compact and reliable photoacoustic sensors that are ready for breath analysis and further applications.

References

1. Pauling L, Robinson AB, Teranishi R, Cary P (1971) Quantitative analysis of urine vapor and breath by gas-liquid partition chromatography. Proc Natl Acad Sci U S A 68(10):2374–2376. https://doi.org/10.1073/pnas.68.10.2374
2. Pereira J et al (2015) Breath analysis as a potential and non-invasive frontier in disease diagnosis: an overview. Metabolites 5(1):3–55. https://doi.org/10.3390/metabo5010003
3. Lawal O, Ahmed WM, Nijsen TME, Goodacre R, Fowler SJ (2017) Exhaled breath analysis: a review of 'breath-taking' methods for off-line analysis. Metabolomics 13(10):1–16. https://doi.org/10.1007/s11306-017-1241-8
4. Bruderer T et al (2019) On-line analysis of exhaled breath. Chem Rev 119(19):10803–10828. https://doi.org/10.1021/acs.chemrev.9b00005
5. Bell AG (1880) On the production and reproduction of sound by light. Am J Sci s3-20(118): 305–324. https://doi.org/10.2475/ajs.s3-20.118.305
6. Müller M et al (2022) An algorithmic approach to compute the effect of non-radiative relaxation processes in photoacoustic spectroscopy. Photoacoustics:100371. https://doi.org/10.1016/j.pacs.2022.100371
7. Sigrist MW, Bernegger S, Meyer PL (1989) Atmospheric and exhaust air monitoring by laser photoacoustic spectroscopy. In: Photoacoustic, photothermal and photochemical processes in gases, pp 173–211
8. Harren FJM, Cristescu SM (2019) Photoacoustic spectroscopy in trace gas monitoring. In: Encyclopedia of analytical chemistry. Wiley, pp 1–29
9. Dumitras DC, Petrus M, Bratu A-M, Popa C (2020) Applications of near infrared photoacoustic spectroscopy for analysis of human respiration: a review. Molecules 25(7): 1728. https://doi.org/10.3390/molecules25071728
10. Besson J-P (2006) Photoacoustic spectroscopy for multi-gas sensing using near infrared lasers. ÉCOLE POLYTECHNIQUE FÉDÉRALE DE LAUSANNE
11. Hollas MJ (2004) Modern spektroskopy.4th edn. Wiley, New York
12. Demtröder W (2011) Laserspektroskopie 1. Springer, Berlin
13. Viegerov ML (1938) Eine Methode der Gasanalyse, beruhend auf der optisch-akustischen Tyndall-Röntgenerscheinung. Dokl Akad Nauk SSSR 19:687–688
14. Kerr EL, Atwood JG (1968) The laser illuminated absorptivity spectrophone: a method for measurement of weak absorptivity in gases at laser wavelengths. Appl Opt 7(5):915. https://doi.org/10.1364/AO.7.000915
15. Weiner ER (2013) Applications of environmental aquatic chemistry: a practical guide. CRC Press/Taylor & Francis Group
16. Hess P (1983) Resonant photoacoustic spectroscopy, pp 1–32
17. Weigl S (2020) Development of a sensor system for human breath acetone analysis based on photoacoustic spectroscopy dissertation. University of Regensburg
18. Miklós A, Hess P, Bozóki Z (2001) Application of acoustic resonators in photoacoustic trace gas analysis and metrology. Rev Sci Instrum 72(4):1937–1955. https://doi.org/10.1063/1.1353198
19. Trusler M (1991) Physical acoustics and metrology of fluids. CRC Press
20. Liu K et al (2010) Trace gas detection based on off-beam quartz enhanced photoacoustic spectroscopy: optimization and performance evaluation. Rev Sci Instrum 81(10). https://doi.org/10.1063/1.3480553
21. Baumann B, Kost B, Wolff M, Groning H (2008) Modeling and numerical investigation of photoacoustic resonators. In: Modelling and simulation. I-Tech Education and Publishing, p 13
22. Rück T (2017) Development, characterization and miniaturization of a trace gas detection system for NO_2 in air based on photoacoustic spectroscopy. University of Regensburg
23. Kreuzer LB (1977) The physics of signal generation and detection. In: Optoacoustic spectroscopy and detection. Elsevier, pp 1–25

24. Pangerl J, Müller M, Rück T, Weigl S, Bierl R (2022) Characterizing a sensitive compact mid-infrared photoacoustic sensor for methane, ethane and acetylene detection considering changing ambient parameters and bulk composition (N_2, O_2 and H_2O). Sensors Actuators B Chem 352:130962. https://doi.org/10.1016/j.snb.2021.130962

25. Weigl S, Feldmeier F, Bierl R, Matysik FM (2020) Photoacoustic detection of acetone in N_2 and synthetic air using a high power UV LED. Sensors Actuators B Chem 316(December 2019):128109. https://doi.org/10.1016/j.snb.2020.128109

26. Weigl S, Wittmann E, Rück T, Bierl R, Matysik FM (2021) Effects of ambient parameters and cross-sensitivities from O_2, CO_2 and H_2O on the photoacoustic detection of acetone in the UV region. Sensors Actuators B Chem 328:129001. https://doi.org/10.1016/j.snb.2020.129001

27. Sampaolo A et al (2016) Improved tuning fork for terahertz quartz-enhanced photoacoustic spectroscopy. Sensors (Switzerland) 16(4):1–8. https://doi.org/10.3390/s16040439

28. Li Z et al (2022) Highly sensitive sphere-tube coupled photoacoustic cell suitable for detection of a variety of trace gases: NO_2 as an example. Sensors 22(1). https://doi.org/10.3390/s22010281

29. Shang Z, Wu H, Li S, Tittel FK, Dong L (2022) Elliptical-tube off-beam quartz-enhanced photoacoustic spectroscopy. Appl Phys Lett 120(17). https://doi.org/10.1063/5.0086697

30. Li S et al (2022) Compact quartz-enhanced photoacoustic sensor for ppb-level ambient NO_2 detection by use of a high-power laser diode and a grooved tuning fork. Photoacoustics 25(2):100325. https://doi.org/10.1016/j.pacs.2021.100325

31. Rück T, Bierl R, Matysik F-MM (2017) Low-cost photoacoustic NO_2 trace gas monitoring at the pptV-level. Sensors Actuators A Phys 263:501–509. https://doi.org/10.1016/j.sna.2017.06.036

32. Rück T, Bierl R, Matysik FM (2018) NO_2 trace gas monitoring in air using off-beam quartz enhanced photoacoustic spectroscopy (QEPAS) and interference studies towards CO_2, H_2O and acoustic noise. Sensors Actuators B Chem 255(2):2462–2471. https://doi.org/10.1016/j.snb.2017.09.039

33. Breitegger P, Schweighofer B, Wegleiter H, Knoll M, Lang B, Bergmann A (2020) Towards low-cost QEPAS sensors for nitrogen dioxide detection. Photoacoustics 18(March):100169. https://doi.org/10.1016/j.pacs.2020.100169

34. Li S et al (2019) Piezo-enhanced acoustic detection module for mid-infrared trace gas sensing using a grooved quartz tuning fork. Opt Express 27(24):35267. https://doi.org/10.1364/oe.27.035267

35. Li B, Feng C, Wu H, Jia S, Dong L (2022) Calibration-free mid-infrared exhaled breath sensor based on BF-QEPAS for real-time ammonia measurements at ppb level. Sensors Actuators B Chem 358(February):131510. https://doi.org/10.1016/j.snb.2022.131510

36. Silva LG et al (2022) Photoacoustic detection of ammonia exhaled by individuals with chronic kidney disease. Lasers Med Sci 37(2):983–991. https://doi.org/10.1007/s10103-021-03342-w

37. Ilke M, Bauer R, Lengden M (2020) A calibration-free methodology for resonantly enhanced photoacoustic spectroscopy using quantum cascade lasers. IEEE Sensors J 20(18):10530–10538. https://doi.org/10.1109/JSEN.2020.2964279

38. Gong Z et al (2021) Ppb-level detection of methane based on an optimized T-type photoacoustic cell and a NIR diode laser. Photoacoustics 21(December 2020):100216. https://doi.org/10.1016/j.pacs.2020.100216

39. Gong Z, Chen K, Chen Y, Mei L, Yu Q (2019) Integration of T-type half-open photoacoustic cell and fiber-optic acoustic sensor for trace gas detection. Opt Express 27(13):18222. https://doi.org/10.1364/oe.27.018222

40. Alahmari S, Kang XW, Hippler M (2019) Diode laser photoacoustic spectroscopy of CO_2, H_2S and O_2 in a differential Helmholtz resonator for trace gas analysis in the biosciences and petrochemistry. Anal Bioanal Chem 411(17):3777–3787. https://doi.org/10.1007/s00216-019-01877-0

41. Lin H et al (2020) Ultra-compact QEPAS acoustic detection module with acoustic wave confinement. Infrared Phys Technol 106(December 2019):103278. https://doi.org/10.1016/j.infrared.2020.103278
42. Ma Y et al (2015) Multi-quartz-enhanced photoacoustic spectroscopy. Appl Phys Lett 107(2): 1–4. https://doi.org/10.1063/1.4927057
43. Chen K et al (2019) Highly sensitive photoacoustic gas sensor based on multiple reflections on the cell wall. Sensors Actuators A Phys 290:119–124. https://doi.org/10.1016/j.sna.2019.03.014
44. Ma Y et al (2022) Quartz tuning forks resonance frequency matching for laser spectroscopy sensing. Photoacoustics 25:100329. https://doi.org/10.1016/j.pacs.2022.100329
45. Hu L et al (2020) Quartz-enhanced photoacoustic spectroscopic methane sensor system using a quartz tuning fork-embedded, double-pass and off-beam configuration. Photoacoustics 18 (March):100174. https://doi.org/10.1016/j.pacs.2020.100174
46. Zhang M et al (2020) Miniaturized multi-pass cell based photoacoustic gas sensor for parts-per-billion level acetylene detection. Sensors Actuators A Phys 308. https://doi.org/10.1016/j.sna.2020.112013
47. Zhang B et al (2020) High-sensitivity photoacoustic gas detector by employing multi-pass cell and fiber-optic microphone. Opt Express 28(5):6618. https://doi.org/10.1364/oe.382310
48. Lin H et al (2021) Ppb-level gas detection using on-beam quartz-enhanced photoacoustic spectroscopy based on a 28 kHz tuning fork. Photoacoustics 25:2022. https://doi.org/10.1016/j.pacs.2021.100321
49. Qiao S et al (2021) Multi-pass quartz-enhanced photoacoustic spectroscopy-based trace gas sensing. Opt Lett 46(5):977. https://doi.org/10.1364/ol.418520
50. Wu H et al (2017) Beat frequency quartz-enhanced photoacoustic spectroscopy for fast and calibration-free continuous trace-gas monitoring. Nat Commun 8(May). https://doi.org/10.1038/ncomms15331
51. Krzempek K et al (2018) Multi-pass cell-assisted photoacoustic/photothermal spectroscopy of gases using quantum cascade laser excitation and heterodyne interferometric signal detection. Appl Phys B Lasers Opt 124(5):1–6. https://doi.org/10.1007/s00340-018-6941-x
52. Hayden J, Giglio M, Sampaolo A, Spagnolo V, Lendl B (2022) Mid-infrared intracavity quartz-enhanced photoacoustic spectroscopy with pptv – level sensitivity using a T-shaped custom tuning fork. Photoacoustics 25(October 2021):0–5. https://doi.org/10.1016/j.pacs.2022.100330
53. Hofstetter D, Beck M, Faist J, Nägele M, Sigrist MW (2001) Photoacoustic spectroscopy with quantum cascade distributed-feedback lasers. Opt Lett 26(12):887–889. https://doi.org/10.1364/ol.26.000887
54. Wojtas J, Gluszek A, Hudzikowski A, Tittel FK (2017) Mid-infrared trace gas sensor technology based on intracavity quartz-enhanced photoacoustic spectroscopy. Sensors (Switzerland) 17(3). https://doi.org/10.3390/s17030513
55. Sgobba F et al (2022) Compact and portable quartz-enhanced photoacoustic spectroscopy sensor for carbon monoxide environmental monitoring in urban areas. Photoacoustics 25: 100318. https://doi.org/10.1016/j.pacs.2021.100318
56. Pan Y et al (2019) Cavity-enhanced photoacoustic sensor based on a whispering-gallery-mode diode laser. Atmos Meas Tech 12(3):1905–1911. https://doi.org/10.5194/amt-12-1905-2019
57. Chen K et al (2020) Highly sensitive photoacoustic multi-gas analyzer combined with mid-infrared broadband source and near-infrared laser. Opt Lasers Eng 124(April 2019). https://doi.org/10.1016/j.optlaseng.2019.105844
58. Ma F et al (2021) Detection of trace C_2H_2 in N_2 buffer gas with cantilever-enhanced photoacoustic spectrometer. Optik (Stuttg) 232(January):166525. https://doi.org/10.1016/j.ijleo.2021.166525
59. Karhu J, Hieta T, Manoocheri F, Vainio M, Ikonen E (2021) LED-based photoacoustic NO_2 sensor with a sub-ppb detection limit. ACS Sensors 6(9):3303–3307. https://doi.org/10.1021/acssensors.1c01073

60. Rey JM, Romer C, Gianella M, Sigrist MW (2010) Near-infrared resonant photoacoustic gas measurement using simultaneous dual-frequency excitation. Appl Phys B Lasers Opt 100(1): 189–194. https://doi.org/10.1007/s00340-010-3994-x

61. Gassner S et al (2022) Anodically bonded photoacoustic transducer: an approach towards wafer-level optical gas sensors. Sensors 22(2):1–12. https://doi.org/10.3390/s22020685

62. Mikkonen T, Hieta T, Genty G, Toivonen J (2022) Sensitive multi-species photoacoustic gas detection based on mid-infrared supercontinuum source and miniature multipass cell. Phys Chem Chem Phys 24(32):19481–19487. https://doi.org/10.1039/D2CP01731H

63. Dong L, Lewicki R, Liu K, Buerki PR, Weida MJ, Tittel FK (2012) Ultra-sensitive carbon monoxide detection by using EC-QCL based quartz-enhanced photoacoustic spectroscopy. Appl Phys B Lasers Opt 107(2):275–283. https://doi.org/10.1007/s00340-012-4949-1

64. Liu L et al (2022) Design and structural optimization of T-resonators for highly sensitive photoacoustic trace gas detection. Opt Laser Technol 148(December 2021):107695. https://doi.org/10.1016/j.optlastec.2021.107695

65. Cristescu SM, Persijn ST, Te Lintel Hekkert S, Harren FJM (2008) Laser-based systems for trace gas detection in life sciences. Appl Phys B Lasers Opt 92(3 Special Issue):343–349. https://doi.org/10.1007/s00340-008-3127-y

66. Sherstov IV, Kolker DB (2020) Photoacoustic methane gas analyser based on a 3.3-μm optical parametric oscillator. Quantum Electron 50(11):1063–1067. https://doi.org/10.1070/qel17316

67. Miklós A, Ng J, Hess P, Kung AH (2005) Application of a wavelength-amplitude double-modulation method in photoacoustic detection using a pulsed optical parametric oscillator. J Phys IV 125:579–581. https://doi.org/10.1051/jp4:2005125133

68. Huang E, Dowling DR, Whelan T, Spiesberger JL (2003) High-sensitivity photoacoustic leak testing. J Acoust Soc Am 114(4):1926–1933. https://doi.org/10.1121/1.1605386

69. Mitrayana D, Apriyanto K, Satriawan M (2020) CO_2 laser photoacoustic spectrometer for measuring acetone in the breath of lung cancer patients. Biosensors 10(6). https://doi.org/10.3390/BIOS10060055

70. Zhang Q, Chang J, Wang Q, Wang Z, Wang F, Qin Z (2018) Acousto-optic Q-switched fiber laser-based intra-cavity photoacoustic spectroscopy for trace gas detection. Sensors (Switzerland) 18(1). https://doi.org/10.3390/s18010042

71. Li L, Thursby G, Stewart G, Uttamchandani D (2010) MEMS scanning mirror used as an laser external modulator for photoacoustic spectroscopy. In: 2010 international conference on optical MEMS and nanophotonics, pp 117–118. https://doi.org/10.1109/OMEMS.2010.5672157

72. Li L et al (2011) Absorption line profile recovery based on TDLS and MEMS micro-mirror for photoacoustic gas sensing. Guang Pu Xue Yu Guang Pu Fen Xi/Spectroscopy Spectr Anal 31(7):1814–1818. https://doi.org/10.3964/j.issn.1000-0593(2011)07-1814-05

73. Rück T, Bierl R, Matysik FM (2017) Development and characterization of a laboratory setup for photoacoustic NO_2 determination based on the excitation of electronic 2B2 and 2B1 states using a low-cost semiconductor laser. Sensors Actuators A Phys 258(2):193–200. https://doi.org/10.1016/j.sna.2017.03.024

74. Romann A, Sigrist MW (2002) Photoacoustic gas sensing employing fundamental and frequency-doubled radiation of a continuously tunable high-pressure CO_2 laser. Appl Phys B Lasers Opt 75(2–3):377–383. https://doi.org/10.1007/s00340-002-0987-4

75. Cheng H et al (2021) Simultaneous detection of CH and CO based on cantilever-enhanced photoacoustic spectroscopy. IEEE Trans Instrum Meas 70(c):1–9. https://doi.org/10.1109/TIM.2021.3080377

76. Pan H, Wang Q, Zhang C, Li Z, Shan P, Ma Z (2021) High-sensitivity acetylene detection system using ellipsoid multi-pass cell (EMPC) based on the opposite dual optical source. Infrared Phys Technol 118(August):1–9. https://doi.org/10.1016/j.infrared.2021.103874

77. Cui R, Wu H, Dong L, Chen W, Tittel FK (2021) Multiple-sound-source-excitation quartz-enhanced photoacoustic spectroscopy based on a single-line spot pattern multi-pass cell. Appl Phys Lett 118(16):161101. https://doi.org/10.1063/5.0047963

78. Wang Z et al (2022) Doubly resonant sub-ppt photoacoustic gas detection with eight decades dynamic range. Photoacoustics 27(11):100387. https://doi.org/10.1016/j.pacs.2022.100387

79. Borri S et al (2014) Intracavity quartz-enhanced photoacoustic sensor. Appl Phys Lett 104(9): 091114. https://doi.org/10.1063/1.4867268

80. Qiao Y et al (2022) Sensitivity enhanced NIR photoacoustic CO detection with SF6 promoting vibrational to translational relaxation process. Photoacoustics 25. https://doi.org/10.1016/j.pacs.2022.100334

81. Sadiek I, Mikkonen T, Vainio M, Toivonen J, Foltynowicz A (2018) Optical frequency comb photoacoustic spectroscopy. Phys Chem Chem Phys 20(44):27849–27855. https://doi.org/10.1039/C8CP05666H

82. Karhu J et al (2019) Broadband photoacoustic spectroscopy of $^{14}CH_4$ with a high-power mid-infrared optical frequency comb. Opt Lett 44(5):1142. https://doi.org/10.1364/OL.44.001142

83. Wildi T, Voumard T, Brasch V, Yilmaz G, Herr T (2020) Photo-acoustic dual-frequency comb spectroscopy. Nat Commun 11(1):4164. https://doi.org/10.1038/s41467-020-17908-9

84. Hofmann M, Bierl R, Rueck T (2012) Implementation of a dual-phase lock-in amplifier on a TMS320C5515 digital signal processor. In: 2012 5th European DSP education and research conference (EDERC). IEEE, pp 20–24. https://doi.org/10.1109/EDERC.2012.6532217

85. Liu W, Wang L, Li L, Liu J, Liu FQ, Wang Z (2011) Fast simultaneous measurement of multigases using quantum cascade laser photoacoustic spectroscopy. Appl Phys B Lasers Opt 103(3):743–747. https://doi.org/10.1007/s00340-010-4298-x

86. Bruhns H, Marianovich A, Wolff M (2014) Photoacoustic spectroscopy using a MEMS microphone with inter-IC sound digital output. Int J Thermophys 35(12):2292–2301. https://doi.org/10.1007/s10765-014-1690-5

87. Lang B et al (2020) Molecular relaxation effects on vibrational water vapor photoacoustic spectroscopy in air. Appl Phys B Lasers Opt 126(4):1–18. https://doi.org/10.1007/s00340-020-7409-3

88. Bozóki Z, Pogány A, Szabó G (2011) Photoacoustic instruments for practical applications: present, potentials, and future challenges. Appl Spectrosc Rev 46(1):1–37. https://doi.org/10.1080/05704928.2010.520178

89. Spagnolo V, Dong L, Kosterev AA, Thomazy D, Doty JH, Tittel FK (2011) Modulation cancellation method (MOCAM) in modulation spectroscopy. In: Optical sensors 2011; and photonic crystal fibers V, vol 8073, p 807313. https://doi.org/10.1117/12.886272

90. Xu-Kun Y et al (2015) Design and optimization of off-beam NO_2 QEPAS sensor by use of E-MOCAM with a high power blue laser diode. Acta Phys Sin 64(13):130701. https://doi.org/10.7498/aps.64.130701

91. Zhang L et al (2022) Advances in differential photoacoustic spectroscopy for trace gas detection. Microw Opt Technol Lett (February):1–10. https://doi.org/10.1002/mop.33228

92. Keller A et al (2005) Open photoacoustic sensor as smoke detector. Sensors Actuators B Chem 104(1):1–7. https://doi.org/10.1016/j.snb.2004.03.013

93. Rousseau R, Ayache D, Trzpil W, Bahriz M, Vicet A (2021) Passive electrical damping of a quartz tuning fork as a path to fast resonance tracking in qepas. Sensors 21(15). https://doi.org/10.3390/s21155056

94. Rousseau R, Maurin N, Trzpil W, Bahriz M, Vicet A (2019) Quartz tuning fork resonance tracking and application in quartz enhanced photoacoustics spectroscopy. Sensors (Switzerland) 19(24). https://doi.org/10.3390/s19245565

95. Russell DA (2000) On the sound field radiated by a tuning fork. Am J Phys 68(12):1139–1145. https://doi.org/10.1119/1.1286661

96. Zhang X et al (2022) Detectors for gas-phase photoacoustic spectroscopy: a review. Microw Opt Technol Lett (March). https://doi.org/10.1002/mop.33246

97. Patimisco P et al (2016) Analysis of the electro-elastic properties of custom quartz tuning forks for optoacoustic gas sensing. Sensors Actuators B Chem 227:539–546. https://doi.org/10.1016/j.snb.2015.12.096

98. Elefante A et al (2019) Dual-gas quartz-enhanced photoacoustic sensor for simultaneous detection of methane/nitrous oxide and water vapor. Anal Chem 91(20):12866–12873. https://doi.org/10.1021/acs.analchem.9b02709

99. Calasso IG, Sigrist MW (1999) Selection criteria for microphones used in pulsed nonresonant gas-phase photoacoustics. Rev Sci Instrum 70(12):4569–4578. https://doi.org/10.1063/1.1150114

100. Giglio M, Patimisco P, Sampaolo A, Scamarcio G, Tittel FK, Spagnolo V (2016) Allan deviation plot as a tool for quartz-enhanced photoacoustic sensors noise analysis. IEEE Trans Ultrason Ferroelectr Freq Control 63(4):555–560. https://doi.org/10.1109/TUFFC.2015.2495013

101. Sampaolo A et al (2022) Quartz-enhanced photoacoustic spectroscopy for multi-gas detection: a review. Anal Chim Acta 1202:338894. https://doi.org/10.1016/j.aca.2021.338894

102. Wojtas J, Bielecki Z, Stacewicz T, Mikołajczyk J, Nowakowski M (2012) Ultrasensitive laser spectroscopy for breath analysis. Opto-Electronics Rev 20(1):26–39. https://doi.org/10.2478/s11772-012-0011-4

103. Zhao D, Miller D, Xian X, Tsow F, Forzani ES (2014) A novel real-time carbon dioxide analyzer for health and environmental applications. Sensors Actuators B Chem 195:171–176. https://doi.org/10.1016/j.snb.2013.12.110

104. Mansour E et al (2020) Measurement of temperature and relative humidity in exhaled breath. Sensors Actuators B Chem 304:127371. https://doi.org/10.1016/j.snb.2019.127371

105. Moskalenko KL, Nadezhdinskii AI, Adamovskaya IA (1996) Human breath trace gas content study by tunable diode laser spectroscopy technique. Infrared Phys Technol 37(1):181–192. https://doi.org/10.1016/1350-4495(95)00097-6

106. Cunnington AJ, Hormbrey P (2002) Breath analysis to detect recent exposure to carbon monoxide. Postgrad Med J 78(918):233–237. https://doi.org/10.1136/pmj.78.918.233

107. Rezaie A et al (2017) Hydrogen and methane-based breath testing in gastrointestinal disorders: the North American consensus. Am J Gastroenterol 112(5):775–784. https://doi.org/10.1038/ajg.2017.46

108. Tittel FK (2010) Current status of midinfrared quantum and interband cascade lasers for clinical breath analysis. Opt Eng 49(11):111123. https://doi.org/10.1117/1.3498768

109. Davies S, Spanel P, Smith D (1997) Quantitative analysis of ammonia on the breath of patients in end-stage renal failure. Kidney Int 52(1):223–228. https://doi.org/10.1038/ki.1997.324

110. Enderby B, Lenney W, Brady M, Emmett C, Ŝpanêl P, Smith D (2009) Concentrations of some metabolites in the breath of healthy children aged 7-18 years measured using selected ion flow tube mass spectrometry (SIFT-MS). J Breath Res 3(3). https://doi.org/10.1088/1752-7155/3/3/036001

111. Turner C, Španěl P, Smith D (2006) A longitudinal study of breath isoprene in healthy volunteers using selected ion flow tube mass spectrometry (SIFT-MS). Physiol Meas 27(1):13–22. https://doi.org/10.1088/0967-3334/27/1/002

112. Alkhouri N et al (2015) Isoprene in the exhaled breath is a novel biomarker for advanced fibrosis in patients with chronic liver disease: a pilot study. Clin Transl Gastroenterol 6(9). https://doi.org/10.1038/ctg.2015.40

113. Diskin AM, Španěl P, Smith D (2003) Time variation of ammonia, acetone, isoprene and ethanol in breath: a quantitative SIFT-MS study over 30 days. Physiol Meas 24(1):107–119. https://doi.org/10.1088/0967-3334/24/1/308

114. Turner C, Španěl P, Smith D (2006) A longitudinal study of methanol in the exhaled breath of 30 healthy volunteers using selected ion flow tube mass spectrometry, SIFT-MS. Physiol Meas 27(7):637–648. https://doi.org/10.1088/0967-3334/27/7/007

115. Lourenço C, Turner C (2014) Breath analysis in disease diagnosis: methodological considerations and applications. Metabolites 4(2):465–498. https://doi.org/10.3390/metabo4020465

116. Studer SM et al (2001) Patterns and significance of exhaled-breath biomarkers in lung transplant recipients with acute allograft rejection. J Heart Lung Transplant 20(11):1158–1166. https://doi.org/10.1016/S1053-2498(01)00343-6

117. Sehnert SS, Jiang L, Burdick JF, Risby TH (2002) Breath biomarkers for detection of human liver diseases: preliminary study. Biomarkers 7(2):174–187. https://doi.org/10.1080/13547500110118184

118. Musa-Veloso K et al (2006) Breath acetone predicts plasma ketone bodies in children with epilepsy on a ketogenic diet. Nutrition 22(1):1–8. https://doi.org/10.1016/j.nut.2005.04.008

119. Giglio M et al (2020) Broadband detection of methane and nitrous oxide using a distributed-feedback quantum cascade laser array and quartz-enhanced photoacoustic sensing. Photoacoustics 17(December 2019):100159. https://doi.org/10.1016/j.pacs.2019.100159

120. Yin X et al (2021) Near-infrared laser photoacoustic gas sensor for simultaneous detection of CO and H_2S. Opt Express 29(21):34258. https://doi.org/10.1364/oe.441698

121. Hayden J, Baumgartner B, Lendl B (2020) Anomalous humidity dependence in photoacoustic spectroscopy of CO explained by kinetic cooling. Appl Sci 10(3). https://doi.org/10.3390/app10030843

122. Wang G, Zhang T, Jiang Y, He S (2022) Compact photoacoustic spectrophone for simultaneously monitoring the concentrations of dichloromethane and trichloromethane with a single acoustic resonator. Opt Express 30(5):7053. https://doi.org/10.1364/oe.450685

123. Sampaolo A et al (2019) Methane, ethane and propane detection using a compact quartz enhanced photoacoustic sensor and a single interband cascade laser. Sensors Actuators B Chem 282:952–960. https://doi.org/10.1016/j.snb.2018.11.132

124. Maurin N et al (2020) First clinical evaluation of a quartz enhanced photo-acoustic CO sensor for human breath analysis. Sensors Actuators B Chem 319(April):4–11. https://doi.org/10.1016/j.snb.2020.128247

125. Popa C, Bratu AM, Petrus M (2018) A comparative photoacoustic study of multi gases from human respiration: mouth breathing vs. nasal breathing. Microchem J 139:196–202. https://doi.org/10.1016/j.microc.2018.02.030

126. Al Fischer D, Smith GD (2018) Can ozone be used to calibrate aerosol photoacoustic spectrometers? Atmos Meas Tech 11(12):6419–6427. https://doi.org/10.5194/amt-11-6419-2018

127. Cotterell MI, Orr-Ewing AJ, Szpek K, Haywood JM, Langridge JM (2019) The impact of bath gas composition on the calibration of photoacoustic spectrometers with ozone at discrete visible wavelengths spanning the Chappuis band. Atmos Meas Tech 12(4):2371–2385. https://doi.org/10.5194/amt-12-2371-2019

128. Menduni G et al (2022) High-concentration methane and ethane QEPAS detection employing partial least squares regression to filter out energy relaxation dependence on gas matrix composition. Photoacoustics 26(March). https://doi.org/10.1016/j.pacs.2022.100349

129. Zifarelli A et al (2020) Partial least-squares regression as a tool to retrieve gas concentrations in mixtures detected using quartz-enhanced photoacoustic spectroscopy. Anal Chem 92(16):11035–11043. https://doi.org/10.1021/acs.analchem.0c00075

130. Sampaolo A et al (2020) Quartz-enhanced photoacoustic spectroscopy for hydrocarbon trace gas detection and petroleum exploration. Fuel 277:118118. https://doi.org/10.1016/j.fuel.2020.118118

131. Dumitras DC, Dutu DC, Matei C, Magureanu AM, Petrus M, Popa C (2007) Laser photoacoustic spectroscopy: principles, instrumentation, and characterization. J Optoelectron Adv Mater 9(12):3655–3701

132. Loh A, Wolff M (2020) Multivariate analysis of photoacoustic spectra for the detection of short-chained hydrocarbon isotopologues. Molecules 25(9). https://doi.org/10.3390/molecules25092266

133. Saalberg Y, Wolff M (2018) Multivariate analysis as a tool to identify concentrations from strongly overlapping gas spectra. Sensors (Switzerland) 18(5). https://doi.org/10.3390/s18051562

134. Schindler W, Haisch C, Beck HA, Niessner R, Jacob E, Rothe D (2004) A photoacoustic sensor system for time resolved quantification of diesel soot emissions. SAE Trans 113:483–490. [Online]. http://www.jstor.org/stable/44740775

135. Sherstov IV, Vasiliev VA, Goncharenko AM, Zenov KG, Pustovalova RV, Karapuzikov AI (2016) Method for measuring the resonant frequency of photoacoustic detector in the real-time mode. Instrum Exp Tech 59(5):749–753. https://doi.org/10.1134/S0020441216050079
136. Herzfeld KF, Litovitz TA (1959) Absorption and dispersion of ultrasonic waves. Academic Press
137. Bhatia AB (1967) Ltrasonic absorption: an introduction to the theory of sound absorption and dispersion in gases, liquids and solids. Oxford University Press
138. Zuckerwar AJ (2002) Handbook of the speed of sound in real gases. Academic Press
139. Hunter TF, Rumbles D, Stock MG (1974) Photophysical processes in the vapour-phase measured by the optic-acoustic effect. Part 1—the model and apparatus for the study of radiationless processes. J Chem Soc, Faraday Trans 2 70:1010–1021. https://doi.org/10.1039/F29747001010
140. Wang C, Sahay P (2009) Breath analysis using laser spectroscopic techniques: breath biomarkers, spectral fingerprints, and detection limits. Sensors 9(10):8230–8262. https://doi.org/10.3390/s91008230
141. Španěl P, Smith D (2018) What is the real utility of breath ammonia concentration measurements in medicine and physiology? J Breath Res 12(2):0–12. https://doi.org/10.1088/1752-7163/aa907f
142. Petrus M, Bratu AM, Popa C (2017) Spectroscopic analysis of breath ethylene and oxidative stress relation with glycaemic status in type 2 diabetes. Opt Quant Electron 49(1):1–12. https://doi.org/10.1007/s11082-016-0837-y
143. Petrus M, Popa C, Bratu A-M (2021) Organic volatile compounds used in type 2 diabetes. In: Type 2 diabetes – from pathophysiology to cyber systems. IntechOpen, p 13
144. Mitrayana M, Ma'arif MA, Wasono MAJ, Ikhsan MR, Satriawan M (2020) Application of the CO_2 laser photoacoustic spectroscopy in detecting ammonia gas (NH3) in liver disease patient's breath. Key Eng Mater 840:399–405. https://doi.org/10.4028/www.scientific.net/kem.840.399
145. Popa C et al (2011) Ethylene and ammonia traces measurements from the patients' breath with renal failure via LPAS method. Appl Phys B Lasers Opt 105(3):669–674. https://doi.org/10.1007/s00340-011-4716-8
146. Popa C, Petrus M, Bratu AM (2015) Ammonia and ethylene biomarkers in the respiration of the people with schizophrenia using photoacoustic spectroscopy. J Biomed Opt 20(5):057006. https://doi.org/10.1117/1.JBO.20.5.057006
147. Kistenev YV et al (2015) Screening of patients with bronchopulmonary diseases using methods of infrared laser photoacoustic spectroscopy and principal component analysis. J Biomed Opt 20(6):065001. https://doi.org/10.1117/1.jbo.20.6.065001
148. Shang Z et al (2022) Quartz-enhanced photoacoustic NH_3 sensor exploiting a large-prong-spacing quartz tuning fork and an optical fiber amplifier for biomedical applications. Photoacoustics 26:3–10. https://doi.org/10.1016/j.pacs.2022.100363
149. Cristescu SM et al (2014) Real-time monitoring of endogenous lipid peroxidation by exhaled ethylene in patients undergoing cardiac surgery. Am J Physiol Lung Cell Mol Physiol 307(7):L509–L515. https://doi.org/10.1152/ajplung.00168.2014
150. Dumitras DC et al (2008) Measurements of ethylene concentration by laser photoacoustic techniques with applications at breath analysis. Rom Reports Phys 60(3):593–602
151. Petrus M, Bratu AM, Serbanescu D (2015) Laser spectroscopy method for non-invasive analysis of breath in pulmonary disease. Rom Reports Phys 67(4):1545–1557
152. Petrus M, Bratu AM, Popa C (2017) Spectroscopic study of dietary effects on volatile breath biomarkers. Rom Reports Phys 69(609):1–12
153. Schubert R et al (2012) Metabolic monitoring and assessment of anaerobic threshold by means of breath biomarkers. Metabolomics 8(6):1069–1080. https://doi.org/10.1007/s11306-012-0408-6

154. Smith D, Španěl P, Fryer AA, Hanna F, Ferns GAA (2011) Can volatile compounds in exhaled breath be used to monitor control in diabetes mellitus? J Breath Res 5(2). https://doi.org/10.1088/1752-7155/5/2/022001

155. Walton C et al (2014) The use of a portable breath analysis device in monitoring type 1 diabetes patients in a hypoglycaemic clamp: validation with SIFT-MS data. J Breath Res 8(3). https://doi.org/10.1088/1752-7155/8/3/037108

156. Prabhakar A et al (2015) Acetone as biomarker for ketosis buildup capability – a study in healthy individuals under combined high fat and starvation diets. Nutr J 14(1). https://doi.org/10.1186/s12937-015-0028-x

157. Musa-Veloso K, Likhodii SS, Cunnane SC (2002) Breath acetone is a reliable indicator of ketosis in adults consuming ketogenic meals. Am J Clin Nutr 76(1):65–70. https://doi.org/10.1093/ajcn/76.1.65

158. Samara MA et al (2013) Single exhaled breath metabolomic analysis identifies unique breathprint in patients with acute decompensated heart failure. J Am Coll Cardiol 61(13):1463–1464. https://doi.org/10.1016/j.jacc.2012.12.033

159. Schwarz K et al (2009) Breath acetone – aspects of normal physiology related to age and gender as determined in a PTR-MS study. J Breath Res 3(2). https://doi.org/10.1088/1752-7155/3/2/027003

160. Tyas FH, Nikita JG, Apriyanto DK, Amin MN (2018) The performance of CO_2 laser photoacoustic spectrometer in concentration acetone detection as biomarker for diabetes mellitus type 2. J Phys Conf Ser 1011(1). https://doi.org/10.1088/1742-6596/1011/1/012056

161. De Lacy Costello BPJ, Ledochowski M, Ratcliffe NM (2013) The importance of methane breath testing: a review. J Breath Res 7(2). https://doi.org/10.1088/1752-7155/7/2/024001

162. Lassen M, Christensen JB, Balslev-Harder D, Petersen JC (2021) Isotopic gas analysis by means of mid-infrared photoacoustic spectroscopy targeting human exhaled air. Appl Opt 60(10):2907. https://doi.org/10.1364/ao.418291

163. Petersen JC, Lamard L, Feng Y, Focant J-F, Peremans A, Lassen M (2017) Quartz-enhanced photoacoustic spectroscopy as a platform for non-invasive trace gas analyser targeting breath analysis [online], pp 3–7. http://arxiv.org/abs/1704.07442

164. Szucs S et al (2019) Detection of intestinal tissue perfusion by real-time breath methane analysis in rat and pig models of mesenteric circulatory distress. Crit Care Med 47(5):e403–e411. https://doi.org/10.1097/CCM.0000000000003659

165. Dillon WC, Hampl V, Shultz PJ, Rubins JB, Archer SL (1996) Origins of breath nitric oxide in humans. Chest 110(4):930–938. https://doi.org/10.1378/chest.110.4.930

166. The National Institute for Health and Care Excellence (NICE) (2017) Asthma: diagnosis, monitoring and chronic asthma management. NICE Guid (November):1–38. [Online]. www.nice.org.uk/guidance/ng80

167. Dong L, Spagnolo V, Lewicki R, Tittel FK (2011) Ppb-level detection of nitric oxide using an external cavity quantum cascade laser based QEPAS sensor. Opt Express 19(24):24037. https://doi.org/10.1364/oe.19.024037

168. Wu H et al (2019) Ppb-level nitric oxide photoacoustic sensor based on a mid-IR quantum cascade laser operating at 52°C. Sensors Actuators B Chem 290:426–433. https://doi.org/10.1016/j.snb.2019.04.007

169. Gondal MA, Khalil AAI, Al-Suliman N (2012) High sensitive detection of nitric oxide using laser induced photoacoustic spectroscopy at 213 nm. Appl Opt 51(23):5724–5734. https://doi.org/10.1364/AO.51.005724

170. Ryter SW (2020) Exhaled carbon monoxide. In: Breathborne biomarkers and the human volatilome. Elsevier, pp 93–107

171. Zhou S et al (2019) An adaptive Kalman filtering algorithm based on back-propagation (BP) neural network applied for simultaneously detection of exhaled CO and N_2O. Spectrochim Acta – Part A Mol Biomol Spectrosc 223:117332. https://doi.org/10.1016/j.saa.2019.117332

172. Pinto D et al (2021) Parts-per-billion detection of carbon monoxide: a comparison between quartz-enhanced photoacoustic and photothermal spectroscopy. Photoacoustics 22(December 2020):100244. https://doi.org/10.1016/j.pacs.2021.100244
173. Neerincx AH et al (2015) Real-time monitoring of hydrogen cyanide (HCN) and ammonia (NH$_3$) emitted by Pseudomonas aeruginosa. J Breath Res 9(2). https://doi.org/10.1088/1752-7155/9/2/027102
174. Mitsui T, Kondo T (2004) Increased breath nitrous oxide after ingesting nitrate in patients with atrophic gastritis and partial gastrectomy. Clin Chim Acta 345(1–2):129–133. https://doi.org/10.1016/j.cccn.2004.03.011
175. Bayrakli I (2021) A portable N$_2$O sensor based on quartz-enhanced photoacoustic spectroscopy with a distributed-feedback quantum cascade laser for medical and atmospheric applications. Opt Quant Electron 53(11). https://doi.org/10.1007/s11082-021-03324-w
176. De Lacy Costello B et al (2014) A review of the volatiles from the healthy human body. J Breath Res 8(1). https://doi.org/10.1088/1752-7155/8/1/014001
177. Wang JW, Xie H, Liang LR, Zhang W, Peng W, Yu QX (2012) Tunable fiber laser based photoacoustic spectrometer for breath ammonia analysis during hemodialysis. Laser Phys 22(1):327–330. https://doi.org/10.1134/s1054660x12010227
178. Fang YZ, Yang S, Wu G (2002) Free radicals, antioxidants, and nutrition. Nutrition 18(10):872–879. https://doi.org/10.1016/S0899-9007(02)00916-4

Advances of Semiconductor Gas Sensing Materials, Structures, and Algorithms for Breath Analysis

Pavel Nosovitskiy, Gennadiy Nosovitskiy, Kiran Nandigam, Ravie Abozaid, and Suzanne Karan

Contents

―――――――――――――――

P. Nosovitskiy (✉)
Naperville, IL, USA

G. Nosovitskiy
Walnut Creek, CA, USA

K. Nandigam
Atlanta, GA, USA

R. Abozaid and S. Karan
University of Rochester Medical Center, Rochester, NY, USA

Abstract This chapter discusses sensor-array-based devices for breath analysis highlighting electronic noses as a prominent example. The sections within the chapter examine material design advances to demonstrate progress in materials selection and innovative sensor structures. In sum, these advances have contributed to a significant increase in the surface ratio of sensors. This has led to a growth in the number of active sites available for sensors to detect particles within the surrounding environment. Besides, a discussion of parametric resonance and excitation applied to sensor-based breath analysis devices is presented as both a hardware and software improvement. Current sensors have the potential to become more relevant and reliable for clinical diagnosis by utilizing parametric resonance. An analysis of a review on the development of carbon nanomaterials concludes the chapter by discussing the current challenges relating to sensor array devices, machine learning algorithms, and the application of breath analysis as a whole. A further emphasis is placed on the fact that parametric resonance can serve as a smart algorithm to meet those challenges.

Keywords Algorithms · Breath analysis · Carbon nanomaterials · Clinical diagnosis · Electronic noses · Parametric resonance · Sensor array devices · Sensor material design · Sensor structure · Sensor surface ratio

Abbreviations

1D	One-dimensional
2D	Two-dimensional
3D	Three-dimensional
ANN	Artificial neural networks
ANOVA	Analysis of variance
BAW	Bulk acoustic wave
BP	Black phosphorus
CNN	Convolutional neural networks
CNT	Carbon nanotubes
DFA	Discriminant function analysis
E-nose	Electronic nose
GC-MS	Gas chromatography-mass spectrometry
GEBT	Gastric emptying breath test
GLSR	Generalized least squares regression
GS	Graphene sheets
hBN	Hexagonal boron nitride
IMS	Ion mobility spectroscopy
KNN	K-nearest neighbor
LDA	Linear discriminant analysis
MEMS	Micro-electromechanical
MLR	Multiple linear regression
MOF	Metal organic frameworks
MOS	Metal oxide semiconductor

MWCNT	Multi-walled carbon nanotubes
MXene	Transition metal carbides/nitrides
NP	Nanoparticles
NS	Nanostructures
PCA	Principal component analysis
PLSR	Partial least squares regression
ppb	Parts per billion
ppm	Parts per million
ppt	Parts per trillion
PTR-MS	Proton transfer reaction mass spectrometry
QCM	Quartz crystal microbalances
QD	Quantum dots
RNN	Recurrent neural network
SAW	Surface acoustic wave
SDA	Stepwise discriminant analysis
SIFT-MS	Selective ion flow tube mass spectroscopy
SVM	Support vector machines
SWCNT	Single-walled carbon nanotubes
TMD	Transitional metal chalcogenides
US EPA	United States Environmental Protection Agency
UV	Ultraviolet
VOC	Volatile organic compound

1 Introduction

A person's nose detects particles in the air and transmits the information to the brain. The brain then calls upon neurons to assemble as a specialized group of elements, perform a coordinated action, such as remember or react to the smell, and separate once the task is complete. Returning to their origins, the neurons wait to be called on again for the same or a different task. A parallel can be drawn in using electronic noses or sensor arrays to measure volatile organic compounds (VOCs) in exhaled breath. In contrast to applying individual sensors to specific, targeted VOCs, this cross-reactive approach mimics natural processes such as smell, sight, and sound.

By using both hardware and software components to create a breathprint [1], sensor arrays collect particles from the surrounding environment, analyze the data gathered, and record the results for display, storage, and classification as illustrated in Fig. 1. Metal oxide semiconductor (MOS) sensors continue to dominate the hardware of sensor arrays [2]. The sensing process begins with the ambient particles being absorbed by the sensor array. At first, a sensitive material layer is exposed to the target gas. The interaction between the sensing layer and the target gas results in some physical properties of the material being altered. These include mass, surface potential, conductivity, dielectric constant, and optical absorbance. In turn, this is
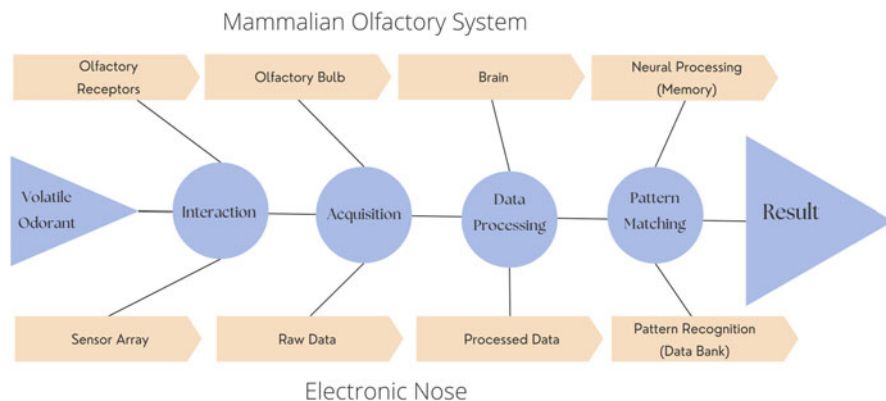
Fig. 1 Schematic comparison of olfactory system and an electronic nose after [1]

converted into the parameter of an electronic device, such as resistance, capacitance, or transconductance, using a basic sensor. The basic sensor is coupled to an electronic circuit to establish signals, such as voltage, that are a function of the concentration of the target gas or gases [3]. Following the sensing stage, the signal is amplified, filtered, and digitized for use in later stages of data analysis [4]. The obtained data is then preprocessed following the requirements of the pattern recognition algorithm once sufficient data has been obtained from the processed signals. Finally, the sensed signal is classified during the pattern recognition stage and displayed, stored, or transmitted as required [5].

On the software side, machine learning algorithms are heavily deployed to distinguish, classify, and store the digital signatures produced by the hardware component. Machine learning is widely used since it can process and comprehend large amounts of data, calibrate gas sensor arrays, and provide accurate recognition and classification results. There are several commonly used tools for pattern recognition algorithms, including linear discriminant analysis (LDA) [6], discriminant function analysis (DFA) [7], stepwise discriminant analysis (SDA) [8], partial least squares regression (PLSR) [9, 10], generalized least squares regression (GLSR) [11, 12], multiple linear regression (MLR) [13], principal component analysis (PCA) [7, 14], support vector machines (SVMs) [15, 16], artificial neural networks (ANNs) [17, 18], and deep learning [5].

Breath analysis is an emerging method to diagnose disease by detecting changes within the VOCs of exhaled breath. In addition to providing the advantage of being noninvasive and direct, this method has the potential to advance the development of predictive, preventive, personalized, and participatory medicine [19]. Sensors and sensor arrays can be applied to breath analysis to provide point-of-care instruments characterized by low fabrication and operation costs and intuitive, low-power, portable operation – a significant advantage over optical and mass spectrometry [20, 21].

For breath analysis, increasing information resources, such as maps of disease-related VOCs to their sources [22], and databases such as the US EPA CompTox
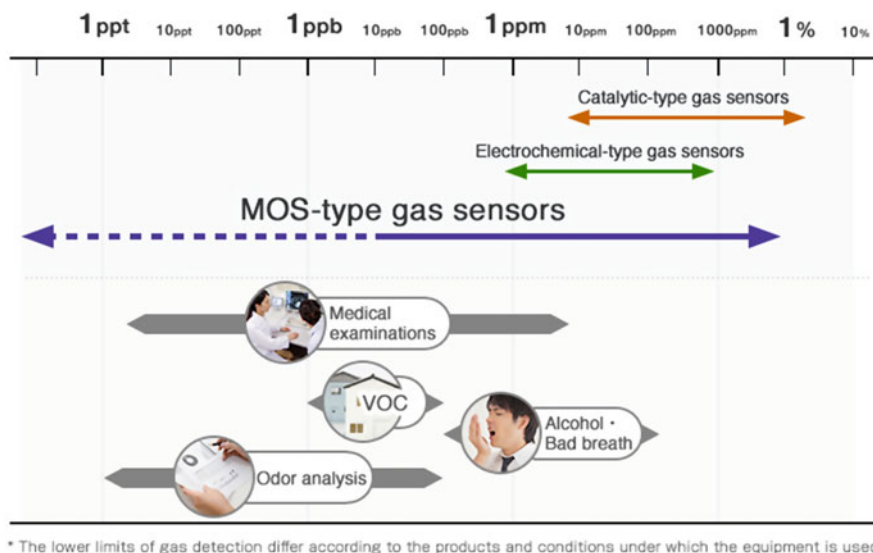
Fig. 2 Sensitivity ranges for types of gas sensors and sensing applications [24]. Permission granted by Figaro, Inc.

Chemicals Dashboard [23], a collection of ~1,178 triaged volatile compounds documented in the gas phase of human breath, allow for sensor development, including the selection of sensing layers, the implementation of sampling methods, and the development of machine learning models using validated datasets.

There is a significant challenge for breath sensors to have a sufficiently low detection limit that can distinguish and accurately detect the constituents of the human breath. Sensors have a limit of detection, illustrated by Fig. 2, defined as the point at which a signal no longer exhibits a predictable linear pattern and is hence classified as noise. A parametrically excited system, or the concept of parametric resonance applied to a system, offers a framework for transforming what is considered noise into signal under non-linear conditions.

The systematic study of non-linear problems and parametrically excited systems dates back to the mid-nineteenth century, with the contributions of Mathieu [25], Rayleigh [24], Stoker [26], and Nayfeh [27] as significant milestones. They created intuitive concepts, such as self-excited systems, forced oscillations, parametric pumps, and non-linear restoring forces, and backed them with rigorous mathematical proofs. In recent studies aimed at understanding and utilizing parametric resonance, especially in resonant micro-electromechanical systems, the possibility of applying parametric excitation in gravimetric sensing [28], chemical sensing [29], inertial sensing [30], and scanning tunneling microscopy [31] has been explored. A previous demonstration of attogram mass sensitivity through frequency resolution enhancement in a parametrically excited mass sensor provides inspiration for parametric control [32]. Further, parametric resonance is widely observed in quantum physics, cosmology, optomechanics, and cellular biology. Among the research topics studied

are the scattering and memory effects of two particles in the context of quantum field theory, the self-induced parametric resonance of collective neutrinos, and the evolution of entanglement in the dynamical Casimir effect [33]. The same algorithms used to solve parametric resonance problems are the basis of particle accelerators and mass spectrometers. By using parametric control, extremely sensitive detection of mass change can be achieved.

The next part of this chapter discusses sensor-array-based devices, highlighting electronic noses as an example. Further sections examine material design advances to demonstrate progress in materials selection and structure of MOS gas sensors. In sum, these advances have contributed to a significant increase in the surface ratio of sensors, increasing the number of active sites available for sensors to detect particles within the surrounding environment. There will be a discussion of parametric resonance and excitation applied to sensor-based breath analysis devices as both a hardware and software improvement. Current sensors can potentially become more relevant and reliable for clinical diagnosis by utilizing parametric resonance. An analysis of a review on the development of carbon nanomaterials concludes the chapter by discussing the current challenges relating to sensor array devices, machine learning algorithms, and the application of breath analysis. A further emphasis is placed on the fact that parametric resonance can serve as a smart algorithm to meet those challenges.

2 Sensor Arrays

Since the late 1990s, an "electronic nose," or e-nose, has been defined as a device containing a multi-sensor array capable of detecting more than one chemical component [34]. Today, electronic nose devices, like sensor arrays for breath analysis, consist of a hardware component, the sensor array, and a software component, machine learning algorithms. Devices of this nature are commercially available and widely used to study various diseases via breath in medicine [35] and in other fields such as agriculture [36], food [37], water [37], and security systems [36].

The following companies dominate the space with their devices: Electronic Sensor Technology zNose [38], AirSense Analytics PEN [39], Electronic Nose Co. [40], Sensigent Cyranose [41], FOODsniffer [42], EN PTY E-Nose Mk4 [43], Alpha MOS Heracles Neo [44], RoboScientific Model 307 [45], Aryballe NeOse Pro [46], Odotech MultiNose [47], Figaro Engineering gas sensors [48], and the eNose Company AeoNose [49]. In addition to their applications, these devices differ according to the machine learning algorithms utilized, the sensor types employed, and the number of sensors included. Sensigent's Cyranose, for example, contains 32 gas sensors that utilize PCA, KNNs, and SVMs to detect and analyze a wide variety of gases. It is one of the most discussed e-noses in research and is used for medical purposes, including breath analysis and air quality monitoring [5].

In recent research, attention has been directed toward the multivariable response principle [50]. The idea is to create a sensor material with multiple response

mechanisms to different gases, a multivariable transducer, and data analysis. Transducers with multivariable capabilities can distinguish between gas responses and provide independent outputs [51]. These outputs are then quantified and classified via data analytics.

2.1 Data Analytics of Sensor Arrays

Machine learning algorithms constitute the software component of e-noses and sensor array devices. Machine learning entails collecting the data, selecting the optimal model and parameters, training the model on the collected data, and evaluating the results. Presented below are the most widely used data analysis algorithms. Furthermore, linear regression, t-test, and ANOVA are employed.

Principal component analysis (PCA) is an unsupervised tool for linearly decreasing the dataset's dimensionality. Despite rotation, it retains the variance structure of the data. High-dimensional data is represented in a new lower-dimensional subspace, spanned by the principal components of the largest variance in the original variables. Principal components are known as eigenvectors of the data covariance matrix. The largest eigenvalue and its corresponding eigenvector exhibit the greatest variation, hence making the greatest contribution between dimensions [5]. Linear discriminant analysis (LDA) is a dimensionality reduction technique that employs linear transformations. LDA is a supervised method that maximizes class discrimination while considering class labels in contrast to PCA [5]. Support vector machines (SVMs) are commonly utilized in regression and classification problems [52, 53]. They have many applications in linear and non-linear binary classification problems as a supervised learning technique. SVMs are used to identify a best-fitting hyperplane (i.e., decision boundary) that helps distinguish between data points [5].

Artificial neural networks (ANNs) are based on the principles of biological neural networks. They are typically designed as fully connected multilayer networks. Depending on the task to be carried out, the number of hidden layers may vary [5]. Hidden layers are activated based on the input layer and the weights between the input and hidden layers [54]. Similarly, the hidden layers and their weights determine the activation of the output layer. It is essential to mention that the activation functions of individual neurons are the gates of ANNs, and without them, any network would behave like a linear regression model. Although there are linear functions, non-linear activations are generally employed to assist the network in learning complex data structures and complex functional mappings for making accurate predictions. Choosing non-linear functions is also advantageous because they are more suitable for use in backpropagation [5]. An array of gas sensors must use a paradigm that can combine the individual sensor outputs and provide an integrated identification and classification result. It is important to note that sensor fusion enables e-noses and sensor-array-based devices to make decisions with minimal error. ANNs incorporate the capability of connecting the outputs of different sensors [55]. Therefore, several ANNs are utilized in sensor fusion, such as quick-prop learning algorithms and multilayer perceptron incorporated with standard backpropagation, cascade correlation, and radial basis functions [56].

As a relatively new phenomenon, deep learning refers to the ability of a machine to detect and classify information within a raw dataset automatically. Deep neural networks are a recent extension of artificial neural networks and have been successfully utilized in various academic and industrial applications [57]. The use of convolutional neural networks (CNNs) has been prevalent. CNNs are generally constructed as layered structures consisting of an input layer, several convolutional layers, pooling layers, non-linear activation layers, fully connected layers, and an output layer. Unlike conventional feature-based pattern recognition algorithms, the CNN technique automatically identifies and extracts features, so the input data does not need to be preprocessed [58]. Another example based on deep learning is using convolutional recurrent neural networks (consisting of both CNNs and RNNs) to perform fast gas recognition [59]. *A more detailed description of data analytics used for breath analysis can be found in the chapter* **"Offline breath analysis: standardization of breath sampling and analysis using mass spectrometry and innovative algorithms."**

2.2   Types of Gas Sensors

The hardware component of sensor arrays, such as e-noses, differs in the types of sensors included. For the application of breath analysis, the most common types of sensors include chemo-resistive sensors (metal oxide, conducting polymer), electro-acoustic sensors (surface acoustic wave, quartz crystal microbalance), electrochemical sensors (potentiometric, amperometric, conductometric), and optical sensors (colorimetric) [60–70].

Gas sensors based on metal oxide semiconductors are widely used since they show good performance in detecting volatile compounds. A MOS gas sensor is an example of a chemo-resistor whose operating principle is based on a change in conductance due to an interaction between the gas and the sensing surface of the metal oxide film, typically through oxygen ions adsorbed on the surface. They possess a high sensitivity, in the order of ppb [71]. Compared with standard gas chromatography and mass spectrometry methods, MOS gas sensors are more straightforward, easier to implement, can be miniaturized, have low power consumption, and are less costly to manufacture [72]. However, they often exhibit instability at the particle/polymer interface. Due to the morphology and structure of the sensing materials, these types of sensors are susceptible to drift phenomena and other external factors such as temperature and humidity. A further disadvantage is their slow recovery time, making them unsuitable for applications where rapid changes in the measurement occur due to continuous fluctuations in the surroundings [73].

The electro-acoustic and piezoelectric sensors work based on the propagation of sound waves created by a piezoelectric material in a multilayer structure. Depending on the type of sensor, acoustic waves may travel on the surface of the sensor, such as surface acoustic wave (SAW) sensors [64], or inside of the sensor, such as bulk acoustic waves (BAW) or quartz crystal microbalances (QCM) [65–67]. As a result

of their small size, sensitivity, low cost, and ability to detect nearly all gases, BAW and SAW sensors are frequently used in e-noses and sensor-array-based devices [74]. The BAW sensor consists of a thin disk of quartz patterned with gold electrodes on both sides. An acoustic wave travels through the crystal when a potential difference between the electrodes is applied. The stability of the crystal allows the measurement of tiny frequency changes [73]. Another advantage of the BAW sensor is its low cost, simplicity, and robustness. However, these sensors are not effective in liquid media [5]. The SAW sensor is derived from the BAW device. This device operates at a high frequency to achieve its high sensitivity. On the other hand, the signal-to-noise ratio is poor because of the high operating frequency [75].

A sensitive coating is present on the surface of a quartz crystal microbalance (QCM) sensor [76]. The selective barrier on the crystal surface captures the released gas from the environment, increasing the total mass. Subsequently, the resonant frequency decreases due to the mass change on the surface of the QCM. As a result, QCM sensors determine small changes on the sensor's surface by measuring frequency changes on the quartz crystal resonator [77]. QCM sensors can operate in both gaseous and liquid environments [78]. With the assistance of sensitive biosensors, they can detect matter as small as a nanogram [79]. Furthermore, QCM sensors are highly adaptable. These sensors can be modified to detect entire cells or only a single-molecule monolayer [80]. Molecularly imprinted polymers (MIPs) [81], polished gold films [82], biomimetic peptide-based materials [83], multi-wall carbon nanotubes [84, 85], and calixarenes [86] are used to coat the surface layers in QCM sensors.

A typical electrochemical gas sensor consists of at least two electrodes and an electrochemical cell. Traditional electrochemical approaches include cyclic voltammetry, amperometry, potentiometry, impedance spectroscopy, and field-effect transistor-based techniques [87]. A gas sample may flow directly into the cell or pass through specific diffusion barriers; hence, if the gas sample reacts with the cell electrodes, the resulting electrochemical reaction can cause either a change in the electrode potential (potentiometric sensor) or an electric current to flow through the cell (amperometric sensor). Overall performance and the transduction method are dependent on the surface layout connecting the sensing element and the sample [88].

Compactness, immunity to electromagnetic interference, and rapid performance make optical sensors attractive [76]. The measurement of fluorescence, optical layer thickness, dye response, light polarization, and absorbance by optical sensors is used to detect environmental odors [89]. Optical sensors are classified according to their ability to detect objects based on color differences, such as colorimetric sensors, and light differences, such as fluorescence sensors. Colorimetric sensors consist of thin films of chemically responsive dyes. Using fluorescent sensors, which are more sensitive than colorimetric sensors, samples are identified by their fluorescent light emission [5]. Optical gas sensing is usually more sensitive, selective, and stable than non-optical methods. These advantages usually come at the cost of more technical complexity and, therefore, more significant miniaturization issues and higher costs. There are only a few commercial gas sensors based on optical principles [90].

As a result of using specific sensing techniques, there are many advantages and disadvantages regarding response and recovery times, sensitivity, detection range,

operating limitations, physical size, costs, and other limitations associated with individual sensor types [73]. For example, chemo-resistors can be used for low-power sensor arrays [91], but for the application of breath analysis using MOS sensors can be challenging, as the signal relating to a compound of interest might be buried by background noise due to significant humidity fluctuations [92]. However, similar to QCM sensors that can be modified through changes in their surface layer coatings, semiconductor-based gas sensors offer similar potential. While several types of gas sensors have been discussed thus far, this chapter focuses on the materials and structures available for improving the sensing layer of metal oxide semiconductor-based sensors utilized in breath analysis. Other types of sensors, such as photoacoustic or optical sensors, are discussed in other chapters of this book.

3 Metal Oxide Semiconductor Gas Sensors

The ability to control metal oxide semiconductors' physical and chemical properties forms the basis of many modern materials and devices. Many chemical and structural characteristics influence the functional properties of MOSs, such as their chemical composition, structural defects, morphology, grain size, and specific surface area [71]. Thus, not only are MOSs one of the most diverse classes of materials, but they also come with additional advantages such as low cost, ease of use, simple fabrication, and commercialization [93].

3.1 Sensor Hardware Components

It is pertinent to review the structure of MOS gas sensors before addressing the optimization of their physical and chemical properties. Pictured in Fig. 3, the typical MOS gas sensor consists of the gas sensing layer, the heater coil, the electrode line, the electrode, the tubular ceramic, and a mesh covering the sensing element.
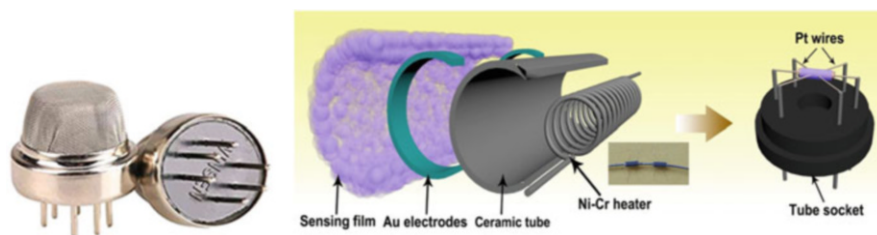
Fig. 3 Picture of a commercial metal oxide VOC gas sensor (Winsen MQ138) and interior components [94, 95]. Permission granted by John Wiley and Sons, Inc., and under the terms of the Creative Commons Attribution 4.0

By interacting with the environment, the gas sensing layer senses the variation in concentrations of gases and generates a change in electrical resistance. The sensing element is burned in to increase its sensitivity and efficiency via the heater coil. The typical operating temperature ranges from 150 to 450°C. Nickel-chromium is frequently used because it has a high melting point and can remain heated without melting. Most conventional designs print the heater on the bottom of the substrate, while the electrode is printed on top. The electrode line efficiently transmits the tiny currents generated by the sensing element. Wires made of platinum transport electrons. An electrode provides a connection between the output of the sensing layer and the electrode line, enabling the output current to flow to the required terminal. The conductivity of gold makes it ideal for this purpose since it is well known to be a good conductor. A tubular ceramic composed of aluminum oxide sits between the heater coil and the gas sensing layer to maintain the burn-in effect necessary for a high-efficiency output current. Finally, a metal mesh prevents dust particles from entering the setup and reduces damage to the gas sensing layer caused by corrosive particles [94].

In recent years, digital sensor platforms have integrated analog and digital electronics, a micro hotplate, and sensing elements onto a single dye [95]. In addition to utilizing more advanced signal processing circuitry in the digital domain, they incorporate a digital interface that simplifies integration into different applications since the output signal is directly used without further processing [96].

3.2 Sensing Mechanism of the Sensing Layer

The charge carrier affects the sensing mechanism in the sensing layer of MOS materials. P-type, in which the charges are holes, and n-type, in which the charges are electrons, are the two main types of charge carriers. For n-type semiconductors, the presence of reducing gases in the sensing layer increases the conductivity, and if the gas is oxidizing, the conductivity decreases. The opposite is true for p-type materials [71].

3.3 Sensor Quality Characteristics

Gas sensors are typically evaluated based on the following characteristics: sensitivity, selectivity, stability, working temperatures, response time, recovery time, and detection limit [97].

The sensitivity of a material refers to a change in its physical or chemical properties when exposed to the gas. This parameter is determined by the ratio of the resistance of the sensor to that of air in the presence of an oxidizing gas; however, when a reductive gas is present, the ratio is the opposite [2, 98]. Selectivity refers to the ability of a semiconductor layer to distinguish between a group of target gases or a single gas within a gas mixture [97]. The stability or reproducibility of gas sensors

is their ability to provide repeatable measurements over time. Preheating at temperatures above the sensor's operating temperature improves the stability of the sensitive layers [71].

In general, the response time is defined as the time it takes for a sensor to reach 90% of the total response after exposure to the target gas. The recovery time is the time it takes for a sensor to return to 90% of its baseline signal after removing a target gas. The detection limit refers to the minimum concentration of gas detected by the sensing layer [71].

3.4 Sensor Hardware Optimizations

Researchers are currently investigating multiple ways to improve MOS gas sensors' physical and chemical properties to enhance their performance. Illustrated in Fig. 4, these include the choice of semiconductor materials for the sensing layer, particle size reduction, nanostructures (NSs), synthesis in different morphologies, and the formation of heterostructures from (nano)composites and polymers. In addition, surface modification techniques such as doping and UV light activation have shown to be effective in improving the performance of MOS gas sensors [100, 101]. Core-shell nanostructures and metal organic frameworks (MOFs) provide examples of how material, morphological, and surface modifications can be combined. The resulting MOS gas sensors are characterized by improved selectivity, sensitivity, and the ability to operate at low temperatures and in high relative humidity conditions [99]. A description of each of these pathways follows.

3.4.1 Sensing Layer Materials

Effective performance of sensing material design consists of a substantial exposed surface for interaction with gas molecules, sufficient active sites for binding these
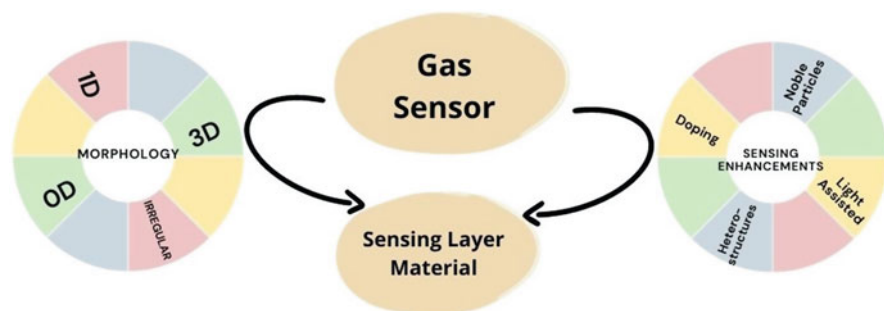
Fig. 4 Sensing layer material, different morphologies, and common strategies to enhance sensing properties of gas sensors after [99]

molecules, the ability to convert these binding events into detectable signals, and an adequate recovery time, i.e., releasing bound molecules and returning to a baseline for subsequent measurements.

Various metal oxides are used as sensing materials in semiconductor gas sensors, such as tin dioxide (SnO_2), zinc oxide (ZnO), indium oxide (In_2O_3), tungsten trioxide (WO_3), cadmium oxide (CdO), titanium dioxide (TiO_2), and others [102–104]. Such materials target most gases. Additionally, carbon-based materials, such as single-wall/multi-wall nanotubes and graphene, along with metal chalcogenides, target nitrogen oxide, nitrogen dioxide, and ammonia [105]. The most popular materials continue to be SnO_2 and TiO_2 due to their manufacturing characteristics, low cost, chemical stability, mechanical strength, heat resistance, and adhesion to various surfaces [71].

Advances in nanomaterials are highlighted by examples such as Das et al., who prepared a sensor of barium hexaferrite oxide nanoparticles ($BaFe_{12}O_{19}$) [106] for detecting trace ammonia vapor in human exhalation with a biomarker of kidney disease; Aghaei et al., who demonstrated the use of graphene-like carbon boron nitride (BC_6N) as a high-performance volatile organic compound (VOC) sensor [107] for human breath analysis; and Zhang et al., who comprehensively introduced semiconductor gas sensors made from two-dimensional materials for disease diagnosis [108].

The sensing layer in gas sensors continues to attract dominant attention [99] as researchers demonstrate the advantage of low-cost composite nano-dimensional materials in the design of simple human breath gas sensor devices [109]. More examples pertaining to breath analysis are further highlighted in Sect. 3.7.

3.4.2   Reduction of Grain Size

An extremely effective way to enhance the gas sensing properties, such as stability, sensitivity, selectivity, and response time, of MOS gas sensors is to reduce grain size to the nanoscale. Grain boundary barriers hinder the sensor's conductivity the most in the presence of gas. In contrast, the sensitivity of the sensing material is independent of the grain boundaries, but it is controlled by the grain size (D) as pictured in Fig. 5. Due to the cross-sectional area and the boundary barriers at the grain boundary, the conductivity increases for grains with $D \geq 2\,L$, where L is the size of the charge depletion layer. If, however, $D < 2\,L$, the grain size determines the sensitivity of the sensing material as conduction channels between the grains become distorted, and conductivity decreases drastically. These results indicate that the grains' morphology and aspect ratio (D/L) also significantly influence gas sensor performance [71].

Fig. 5 Schematic model of the effect of grain size on the sensitivity of semiconductor metal oxide gas sensors. (**a**) $D >> 2L$. (**b**) $D \geq 2L$. (**c**) $D < 2L$ [110]. Permission granted by the terms of the Creative Commons Attribution 4.0
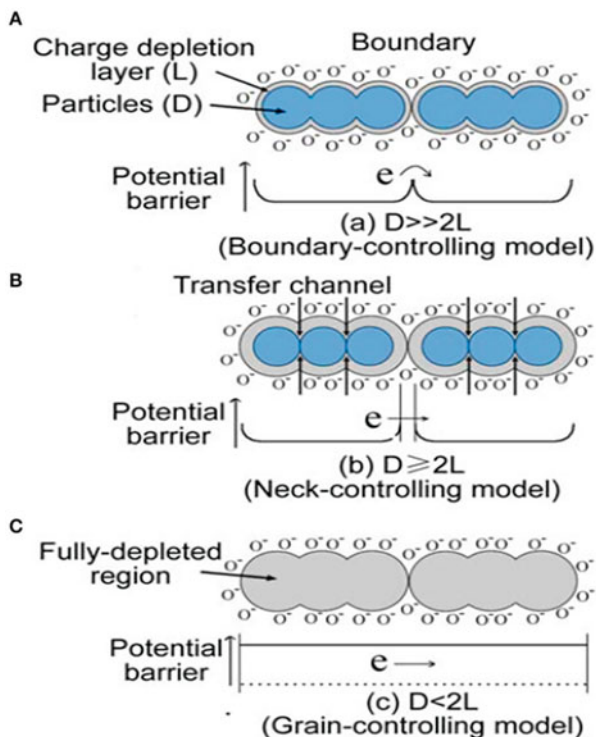
3.4.3 Effects of Morphology

Illustrated by Fig. 6, the research trend in MOS gas sensors is the emergence of sensors that utilize hierarchical nanostructures (NSs) instead of sensors based on thin films. A range of high aspect ratio nanomaterials have been successfully fabricated, ranging from zero-dimensional (0D) quantum dots (QDs) and nanoparticles (NPs) to one-dimensional (1D) nanorods, nanotubes, and nanowires, to two-dimensional (2D) nanosheets, to 3D core-shell nanostructures, such as nanoflowers and nanocubes. Microstructure and morphology determine surface area, active site quantity, and gas diffusion channels [109].

Nanomaterials with grain sizes less than 10 nm, including QDs, are classified as 0D nanomaterials. Using their unsaturated bonds and high surface energies, QDs present a promising solution for lowering the operating temperature of MOS gas sensors to room temperature [110–112].

Compared to other 1D nanomaterials, nanotubes, such as nanowires, nanofibers, and nanorods, have a large surface area and an open porous structure that makes them particularly noteworthy [113, 114]. The formation of meso- and nanosized pores on various nanotube surfaces during the synthesis process can significantly
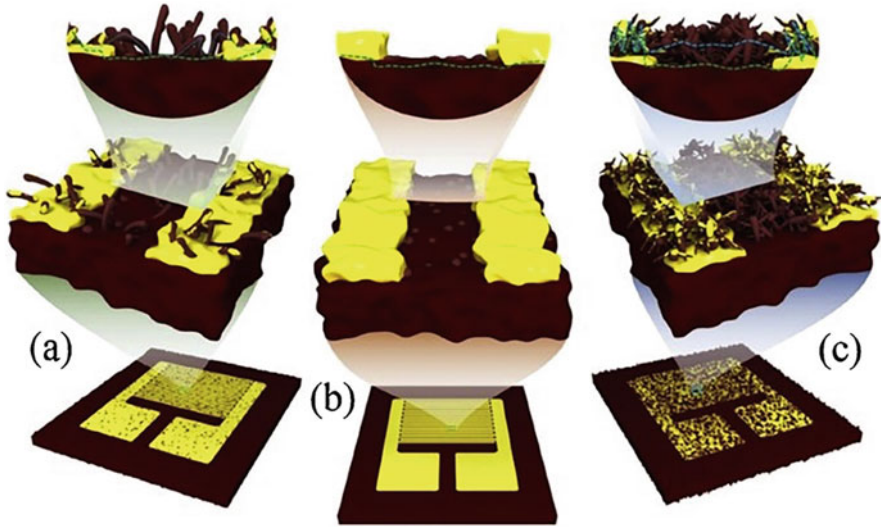
Fig. 6 Models and equivalent circuits of the (**a**) thin film, (**b**) submicron-rod, and (**c**) submicron tree Cu_2O sensors [111]. Permission granted by Elsevier

improve the gas sensing performance by increasing the penetration of the target gas into the deepest parts of the sensing device [109].

2D materials have attracted attention for gas sensing applications in recent years due to their high electron conductivity and excellent mechanical durability [114, 115]. Graphene is a 2D monolayer of bonded carbon atoms that exhibits high electron mobility at room temperature. Its unique structure makes every carbon atom a surface atom, leading to electron transport that is highly responsive to molecules adsorbed on the surface [116, 117]. Compared with carbon nanotubes (CNTs), graphene's sheet-like structure is more conducive to the deposition and stabilization of nanoparticles (metals or metal oxides). It can be easily integrated into sensor devices [76]. Carbon nanotubes (CNTs) consist of a seamless cylinder formed by wrapping graphene sheets in the axial direction. CNTs fall into two categories: single-walled CNTs (SWCNTs), formed of one sheet when all atoms behave as surface atoms, or multi-walled CNTs (MWCNTs), formed of several sheets where only atoms in the outermost layer contribute to sensor response [118]. Carbon nanotubes possess good mechanical and chemical stability, have a high surface-to-volume ratio, and have excellent electronic properties, making them suitable for gas sensing applications [119]. Commercialization, however, is hampered by a variety of technological barriers. They are costly to synthesize due to the difficulty of growing continuous, defect-free nanotubes. CNTs exhibit slow response and recovery due to their material's adsorption and desorption processes [120].

Due to graphene's popularity as a 2D material for gas sensing, analogs have been developed, including transitional metal chalcogenides (TMDs), hexagonal boron nitride (hBN), black phosphorus (BP), and transition metal carbides/nitrides

(MXene family of materials) [119]. The single-layer architecture of these 2D structures allows gas molecules to make complete contact with their surfaces [51]. The band gap value of TMDs is more suitable for practical device applications than that of graphene [121]. Most of the investigation has been conducted on disulfides, which have shown excellent gas sensing properties in terms of high sensitivity, fast response rates, and good stability. Many recent studies have focused on the use of MXenes for gas sensors [122].

Furthermore, the ability of 3D nanostructured devices to be made into layers of porous thin films composed of different materials can potentially be exploited to create a single sensor that can detect a wide range of sensing targets [123]. In such sensors, the most significant flaw is the reaction between water vapor molecules and oxygen ions on the MOS surface, resulting in less reactive hydroxyl groups and decreasing sensing performance [124, 125]. This obstacle may be overcome by increasing the operating temperature and doping with NiO and CuO [125–127].

3.4.4   Polymers

Conducting polymers are advantageous as gas sensing materials because they operate at room temperature, have good mechanical properties, and can be easily synthesized [51]. Oxidation reduces the lifetime of gas sensors based on conducting polymers (9–18 months) compared to metal oxide sensors, preventing widespread adoption. Conducting polymers have nevertheless been widely investigated for the development of sensor arrays [76, 119]. An electronic nose composed of polypyrrole gas sensors is one example [128]. It can discriminate between methanol, ethanol, acetone, 2-butanone, and 2-pentanone. Another example is the electronic nose developed by NASA's Jet Propulsion Laboratory at Caltech (JPL ENose) to monitor air quality in space stations [129, 130]. Conducting polymers enable the detection of redox-active gases, such as NH_3, NO_2, and some organic vapors; however, they have difficulty detecting volatile organic compounds (VOCs) [51].

As with heterostructures, the conductivity of conducting polymers can be further enhanced by nanostructuring and the formation of composites of two polymers (conducting and insulating), such as polypyrrole and ethanol [131]. Conducting polymer composites with metal oxides, particularly nanoparticles such as SnO_2 or TiO_2, have been developed for CO gas detection [132]. Other functional materials, such as carbon nanotubes [133] and graphene [134], have been incorporated into composite structures with conducting polymers. By using conducting polymer nanocomposite sensors, flexible multisensory platforms can be designed, manufactured, and integrated at a relatively low cost into smart textiles or radiofrequency identification tags [51].

3.4.5 Doping and Light Activation

Even at the nanoscale, surface modifications of metal oxides through doping and light activation remain viable approaches to improving the performance of MOS gas sensors.

The doping approach has proven to be an effective method of overcoming the drawbacks of pure MOS gas sensing materials [135]. In general, transition metals such as Fe, Cr, Al, Ni, Tb, Co, Fe, Sn, and Ce and noble metals such as Au, Pt, and Pd have been used as dopants in nanostructured metal oxide semiconductors. Dopants are used in gas sensors to increase the activity and modify the sensing material's resistance by changing its surface's chemical environment [93]. When a metal and semiconductor are in contact, electron transfer occurs, and a barrier layer (high resistance area) forms around the metal nanoparticle. A metal nanoparticle/nanocluster, therefore, represents an electronegative surface. When exposed to gas or vapor, the area with high resistance becomes an area of high conductance, significantly enhancing the sensing performance. In addition, the dopants provide improved stability, selectivity, response time, reproducibility, and a reduction in sensor operating temperature. Lastly, some studies have demonstrated that the type of metallic dopant can influence the type of target gas that can be detected. High-valence dopants, such as Sn, W, and Nb, produce sensors with an excellent response to reducing gases [51, 71, 93].

The exposure of MOS gas sensors to ultraviolet light improves their sensing capability. It is possible, for example, to reduce the gas sensor's operating temperature requirement to room temperature. Upon exposure to ultraviolet light, the material's conductivity is improved due to the photogenerated electrons or holes, which increase the concentration of free carriers at the surface. The electrons emitted from UV light are responsible for promoting chemical reactions between the targeted gas molecules and the adsorbed oxygen ions. The result is that the targeted gas molecules show a high and rapid response [71].

3.5 Combining Sensor Hardware Optimizations: Core-Shell Nanostructure and MOFs

Core-shell nanostructures and metal organic frameworks (MOFs) demonstrate possible advancements when combining material selection, morphology, design, and surface modification techniques.

The core-shell structure refers to heterogeneous nanoparticles (NPs) formed from two or more materials. One nanomaterial forms the core at the center, and the other material or materials form the shell located around the core [71]. Core-shell nanostructures may be classified as nanocomposites, but in contrast to nanocomposites with uniform structures, core-shell NPs typically exhibit an apparent separation between the core and the shell [136]. As new functional materials,

these structures possess unique properties, such as providing more active sites for electrochemical reactions compared to uniform nanostructures [137, 138]. For instance, SnO_2 and TiO_2 core-shell nanostructures have been fabricated in different ways, such as using noble metals (Au, Ag, Pt, and Pd) as cores and MOSs (TiO_2, SnO_2, NiO, and WO_3) as shells. In comparison with pure metal oxide nanostructures and nanocomposites of metal oxides with noble metals, the core-shell structures display superior sensing properties [139].

MOFs are a novel class of crystalline and porous functional materials comprised of strong bonds between metal ions and organic ligands [140]. Pyrolysis or calcination converts these precursor structures into diverse metal oxide sensor nanostructures and nanocomposites [141]. The following characteristics of MOFs make them an attractive candidate for gas sensing applications. Their high surface area and permanent porosity provide numerous active sites, enhancing sensitivity and selectivity. A second advantage is their ability to be tailored in terms of pore size, shape, and surface environment. Third, MOFs are highly recyclable and regenerable as they possess excellent reversibility for the desorption and adsorption of target molecules. Finally, they can operate at or near room temperature [142].

3.6 Sensor Fabrication Process

As a final point, the manufacturing process itself plays an essential role in sensor performance. The interface circuitry design, diagramed in Fig. 7, will differ depending on whether the gas sensor interface is hybrid or monolithic.

Integration is traditionally achieved using a multi-chip approach in which the sensor and circuitry are designed and fabricated on separate chips. The two-chip solution, also known as the hybrid approach, enables independent adjustment and optimization of the gas sensor and the interface circuitry. As a result, design and manufacturing processes are more flexible, leading to shorter development cycles.
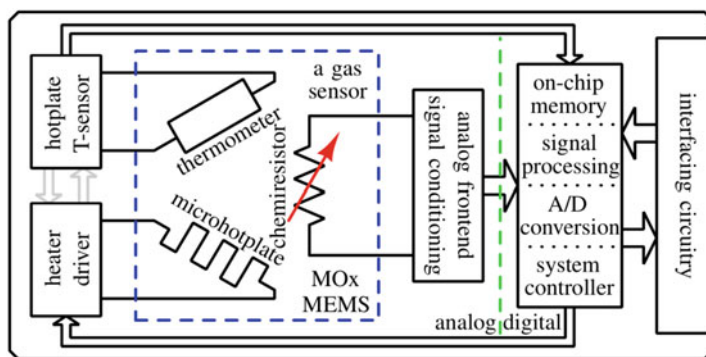
Fig. 7 Chemo-resistive metal oxide gas sensor model and interface circuitry [53]. Permission granted by the terms of the Creative Commons Attribution 4.0

However, the parasitic capacitances and inductances associated with long bonding wires and interconnections between the two chips are undesirable, as they add to the noise and degrade the signal. In addition, the hybrid approach is less robust and more costly than a single-chip implementation, particularly when considering high volume production [51].

The monolithic approach is a relatively new and more advanced approach that combines the design and fabrication of the sensor and interface circuitry on a single substrate. The single-chip solution enhances the gas sensor's performance by reducing its size, power consumption, and noise. In addition, it is both more cost-efficient and more commercially attractive when unit volumes are high. There is, however, the issue of a lengthy and costly development process. Moreover, a potential fault in the nearby circuitry or sensor can cause the chip to fail [51].

3.7   MOS Sensors in Breath Analysis

Common methods for monitoring breath biomarkers include gas chromatography-mass spectrometry (GC-MS) [143], currently the gold standard, selective ion flow tube mass spectrometry (SIFT-MS), proton transfer reaction mass spectrometry (PTR-MS), ion mobility spectroscopy (IMS) [144], and several other sensitive techniques [145–148]. Biomarkers for certain diseases include acetone, ammonia, hydrogen, methane, and isoprene. For example, as a biomarker for diabetes, the normal range for acetone gas concentration is 300–900 ppb (parts per billion), while the symptomatic range is above 1,800 ppb [149]. Elevated concentrations of isoprene gas indicate renal disease at concentrations ranging from 57 to 329.8 ppb, while the normal range is from 28 to144 ppb [150]. In the absence of alcohol or fruit consumption, ethanol, at concentrations above 2,848 ppb in the exhaled breath, is discussed to indicate lung cancer, with normal concentrations ranging from 96 to 2,848 ppb [151].

Biomarker reference ranges provide guidance for gas sensor material and design to establish relevance. For example, a ZnO nanorod sensor demonstrated a detection limit of 1,000 ppb for ethanol [152]. Using nanoneedles based on V_2O_5, Hakim et al. achieved a detection limit of 941 ppb when measuring acetone [153]. A hybrid of graphene and SnO_2 was used to measure formaldehyde and reached a detection limit of 20 ppb [154]. Choi et al. showed that a sensor comprised of Pt-WO_3 nanoflowers can detect 1,000 ppb of H_2S gas [155]. A single crystal polypyrrole sensor demonstrated a detection limit of 0.05 ppb at room temperature [156].

To date only five breath tests have received necessary regulatory approval and are in clinical practice [21, 157]. The first is the urea-^{13}C breath test for detection, diagnosis, and eradication of a *Helicobacter pylori* infection in the gastrointestinal tract developed by Otsuka America Pharmaceutical Inc. in 1996. The second is the nitrogen oxide, NO, breath test for monitoring asthma therapy and test for FeNO developed by Aerocrine AB in 2003. The third is the Heartsbreath test for monitoring heart transplant rejection developed by Menssana Research Inc. in 2004. The fourth is the gastric emptying breath test, GEBT, using ^{13}C-Spirulina, developed by

Cairn Diagnostics in 2015. Lastly, the LiMAx test with intravenous ^{13}C-methacetin to monitor the progression of liver disease was developed by Humedics GmbH in 2016–2017. Currently, there is no single breath test that can diagnose a disease as a stand-alone test [21].

The continued aggregation of connections among sensor material types, clinical diagnosis, gas concentration ranges for diseased and non-diseased states, differences in sensor morphology, target gases, sensor operating temperatures, sensitivity, and response time, as exemplified by sources such as US EPA CompTox Chemicals Dashboard [23], is paramount for the advancement of human breath analysis. Making such information available and easily accessible is key.

4   The Sensor's Output and Role of Resonance

One of the most challenging components of a MOS gas sensor is the interfacing circuitry. In order to produce an accurate output signal, the signal processing unit must compensate for the drift in the baseline resistance of the sensing element as well as handle the precision and dynamic range of the gas sensing element [51].

The most straightforward circuit scheme for this challenge involves a resistance-to-voltage conversion utilizing either a resistive voltage divider or a Wheatstone bridge. These methods are not optimal if complete integration is needed since they require either a large resistor bank circuit or variable resistors to cover a wide range and match the sensing material resistance [51]. Additionally, the output of the sensor is commonly interpreted in linear terms, where the limit of detection denotes the point at which a signal ceases to behave predictably and is therefore classified as noise.

Resistance-to-frequency conversion is an alternative to resistance-to-voltage conversion. It is relatively simple to compress the large dynamic range by using a logarithmic converter; however, this inevitably compromises the accuracy of the measurement [51]. A more complex method of analyzing the output signal is to apply non-linear dynamic theory, such as the concept of parametric resonance. Consequently, complexity increases, but accuracy remains unaffected, selectivity is maintained, relationships above the detection limit are preserved, and noise from below the detection limit is transformed into a signal.

Classically, resonance is defined as the amplitude build-up of oscillations caused by direct stimulation of a system at a specified input frequency. Resonant amplification does not, however, refer only to direct excitation [158]. Parametric resonance is a resonant phenomenon [159]. It is caused by a periodic fluctuation in at least one of the system parameters, resulting in an internal build-up of energy instead of an externally forced response as with a mass-spring-damper system [27]. As an example, consider a base-excited pendulum. Using intuition, one can envision the possibility of large angular motions in this system under resonant, horizontal excitation of the pivot. In addition, there are vertical base excitations, which can cause time-varying stiffness and large angular deflections under certain amplitude/frequency

conditions. These vertical excitations seem strange at first glance, but one must consider that as a child, they might have used analogous changes in their effective length to create large-amplitude motions on playground swings [160].

In 1831, Michael Faraday first observed this peculiar vibration phenomenon after observing a vertically oscillating cylinder on the surface of a fluid with a half-frequency of excitation [161]. Mathieu [25] initiated the study of the underlying mathematics, and Floquet and Hill built on it [162, 163]. Lord Rayleigh (J. Strutt) conducted additional experimental studies in the 1880s utilizing vibrating strings and a wave propagation apparatus [24, 164]. Studies of parametric resonance have traditionally centered around its control and prevention of structural failure since increasing oscillation amplitude, en route to chaos, could accumulate to significantly greater amplitudes than direct resonance [27, 165, 166]. Today, increasing attention and research show that parametric resonance can be an efficient amplifier for a given transducer.

Further, passive approaches have been developed to overcome the critical initiation threshold excitation amplitude that otherwise limits the onset of this phenomenon. This principle has been demonstrated by micro-electromechanical (MEMS) gyroscopes, mass sensors, and vibration energy harvesting [167–169]. Therefore, parametric resonance offers potential advantages such as amplification, noise suppression, and high sensitivity with selectivity.

The unique instability phenomenon of parametric resonance is governed by the Mathieu function [27]:

$$\ddot{y}(t) + [\delta - 2\varepsilon \cos(2t)] \, y(t) = 0$$

where δ and ε are generic parameters relating to the square of the natural frequency and the parametric excitation amplitude, respectively. An instability chart, also known as the Strutt diagram, pictured in Fig. 8, can be plotted from δ and ε (also known as a and q) to illustrate the regions where parametric resonance can be activated [158]. Notably, parametric excitations can yield large-amplitude responses or parametric resonances if the excitation frequency satisfies the condition $\omega = 2\omega_0/n$, where n is a positive integer greater than or equal to unity [171]. When applying this analysis to a gas, each amplitude response will be unique due to the varying molecular weight of the gas. Thus, gas mixtures can further be broken down into its constituent parts. The resulting information looks much like the output of a gas chromatographer or a mass spectrometer. Furthermore, as a system, read gas or gas mixture, traverses from a stable region to an unstable region, as shown by the line with ten points in Fig. 8, the associated calculations not only identify whether a resulting solution, read output, is stable or unstable, but also provides guidance on how to move the system from one region to another.

Tracking resonant frequency shifts of micro/nano-oscillators is an established technology with chemical and biological sensing applications. Mass change is detected by measuring the frequency shift of the stability boundary of the first-order parametric resonance tongue [172–174], which is directly related to the shift of
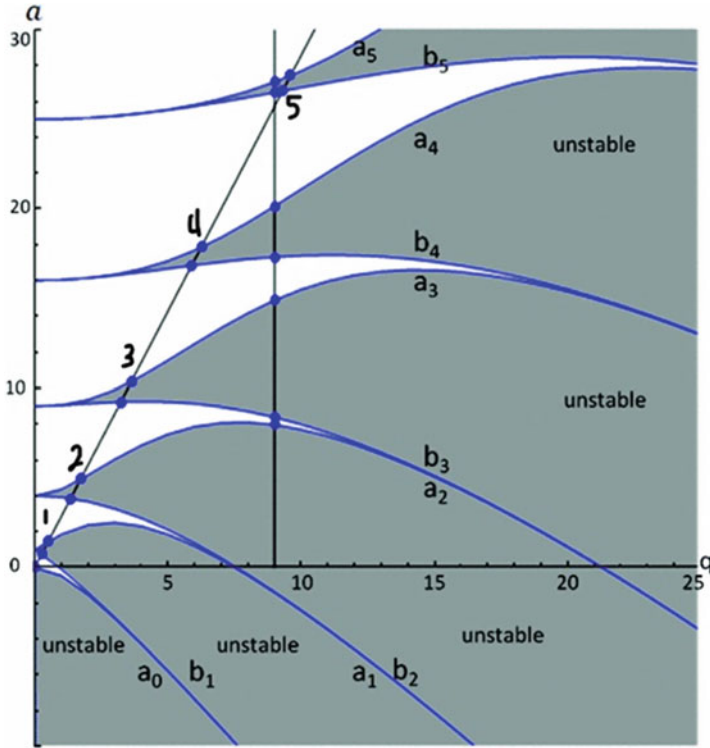
Fig. 8 Strutt diagram illustrating stability and instability regions for Mathieu's equation with plotted solutions of varying parameters demonstrating not only whether the solution is stable and unstable but also the concept of moving from one solution to the next, after [170]. s = stable, u = unstable, colored curves = boundaries between stable and unstable, line with ten points, numbered 1–5, represents a particular system with ten different parameter changes. Permission granted by Samuel Lereah

the resonator's natural frequency. The transition at the boundary is very sharp, making small frequency changes readily observable with high resolution [171].

There are various transduction mechanisms for parametric excitation, including electrostatic, electromagnetic, piezoelectric, and optical actuation [32]. Piezoelectric parametric excitation applies a periodic voltage to an external shear piezoelectric element to modulate its total stiffness, corresponding to a resonant device's periodic base excitation [29, 175]. The alternation of the polarity of the current and the magnetic field in electromagnetic parametric excitation may cause a direct or parametric Lorentz force to be generated in a MEMS device [167, 176, 177]. The thermal effect introduced by a laser beam can also affect the time-varying impedance of the silicon disk oscillator, creating a parametric amplification effect when the optical pump drive phase is selected properly [178].

The overarching point is that if a model meeting the prerequisites for utilizing Mathieu's equation is developed, an example pictured in Fig. 9, such a model can be

Mechanical System

Electrical System

Mechanical kinetic energy:

$$T_T = \tfrac{1}{2} m\, y'^2$$

Mechanical potential energies:

$$U_S = \tfrac{1}{2} k\, y^2$$

$$U_G = m\, g\, y$$

Mechanical damping force:

$$F_d = d\, y'$$

Electrical kinetic energy:

$$T_L = \tfrac{1}{2} L\, q'^2$$

Electrical potential energies:

$$U_C = \tfrac{1}{2}\tfrac{1}{C}\, q^2$$

$$U_B = U_0\, q$$

Electrical damping voltage:

$$V_d = R\, q'$$
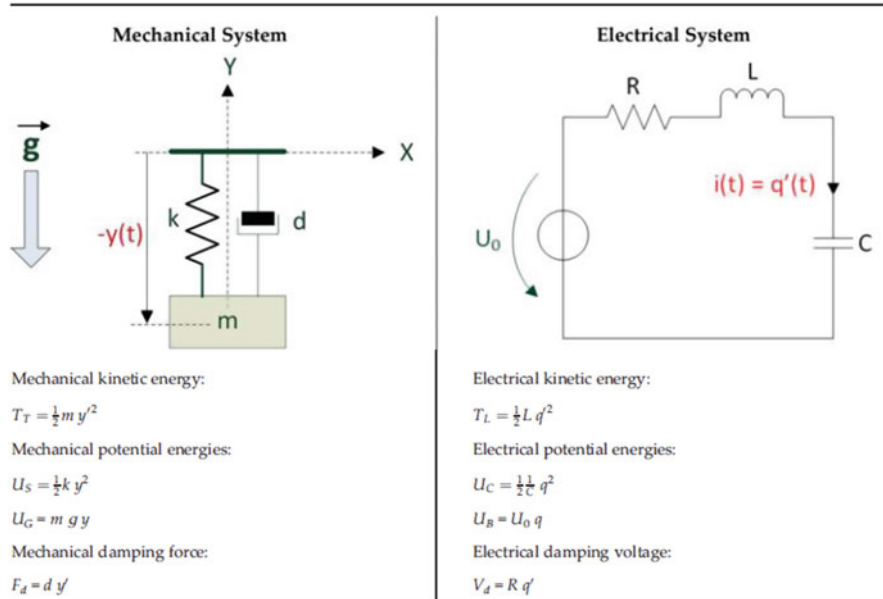
Fig. 9 Examples of physical equations for mechanical and electrical systems which can be modeled by Mathieu's equation [179]. Permission granted by the terms of the Creative Commons Attribution 4.0

implemented to significantly improve the sensitivity and selectivity of a sensor. Understanding the combination of parameters that produce stable and unstable solutions is paramount, as is knowing how to move from a region with unstable solutions to one with stable solutions and vice versa. Fortunately, given the specific case of gas sensors, there are several avenues for developing such models and deploying the notion of parametric resonance. With this approach, one can create a sensitive and selective sensor that provides outputs in real time and under ambient conditions.

Furthermore, the manufacturing of a particular design or the use of a particular material is not necessary. Following the multivariable response principle, the exploitation of parametric resonance operates as an algorithm-based, "smart" transducer that can provide individual inputs for various gas responses. In addition to being compatible with existing commercial sensors, it can also be used with new advanced sensors. The combination of such characteristics is particularly attractive for breath analysis. The following review on carbon nanotube sensors for breath analysis highlights the most recent development in materials and design of gas sensors and how applying the concept of parametric resonance can lead to even more significant improvements and benefits.
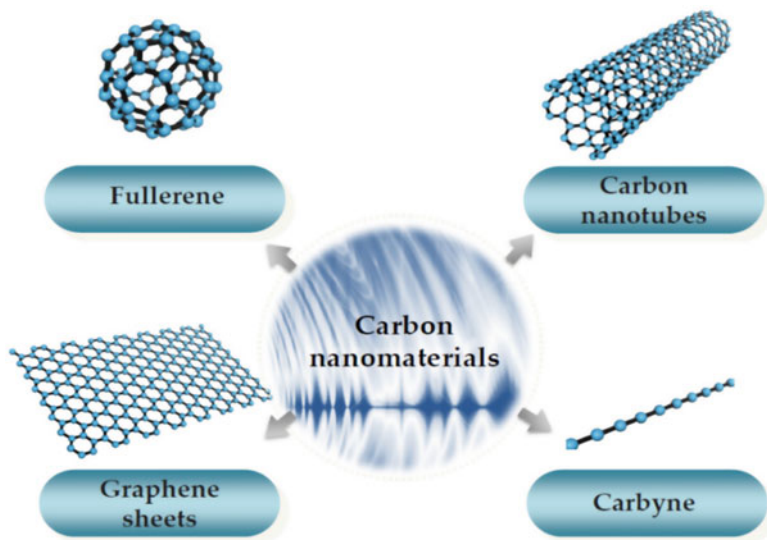
Fig. 10 Examples of carbon nanomaterials [180]. Permission granted by the terms of the Creative Commons Attribution 4.0

5 Advances in Carbon Nanomaterials and Application of Parametric Resonance

During the past several decades, the rapid development of nanotechnology observation instruments led to the discovery and investigation of various carbon nanomaterials, pictured in Fig. 10, including carbon nanotubes (CNTs) [179, 181, 182], graphene sheets (GSs) [180], and carbine [183]. For carbon nanomaterial properties, the representative one-dimensional (1D) CNTs and two-dimensional (2D) GSs exhibit superior mechanical, thermal, electrical, and optical properties almost equally [184–190]. Due to their exceptionally high electronic conductivities, CNTs and GSs have been applied to transistors [186], nanoelectronics [187], and supercapacitors [188]. In addition to being utilized as sensing elements in biosensors [191–193], strain sensors [194–196], and gas sensors [51, 197, 198], CNTs and GSs are also used in nano-mass and nano-force sensors [199].

Mechanical resonators are used as inertial balances to detect an otherwise too tiny mass by measuring the oscillation frequency shifts [200]. Silicon-based mass sensors using the same approach have also been investigated [28, 201–212]. Compared to carbon nanomaterials, silicon-based mass sensors are limited by their relatively lower material properties and larger cross section [199]. The CNT/GS-based nano-mass sensors have been the subject of many experimental and theoretical investigations, demonstrating a much higher sensitivity ($>10^{-21}$ g) than silicon-based mass sensors [213–222].

In general, the resonant frequency shift, which is related to the mass or force of the resonator, is determined by frequency-based vibration analysis in nano-mass and nano-force sensors. By adding additional mass or extra force to a nano-sensor system, the resonant frequency of the resonator changes, and the accurate measurement of the resonant frequency variation can precisely determine the additional mass or the unknown additional force [215, 218, 223, 224].

For a nano-mass sensor system in natural vibration, the typical governing equation of vibrational motion for determining its fundamental frequency can be given as:

$$[M]\ddot{y} + [K]\{y\} = \{0\}$$

where $[M]$ and $[K]$ denote the mass and stiffness matrices of the analytical system and $\{y\}$ and $\ddot{y}$ are the displacement and acceleration vectors, respectively [199].

The mechanism of the nano-mass sensor is the following: the fundamental frequency, f, of the sensor system without attached mass is calculated if the dimensions (e.g., thickness, diameter, length, and width) and density of the resonator related to the mass matrix $[M]$ and the material properties of the resonator (e.g., Young's modulus, shear modulus, and Poisson's ratio), related to stiffness matrix $[K]$, are known. A tiny mass with a mass matrix of $[\Delta M]$ is then added to the resonator to generate a different mass matrix $[M + \Delta M]$ of the total sensor system and determine a new fundamental frequency, f_0. The frequency shift, $\Delta f = f_0 - f$, is then calculated. Following repeated repetitions of this process, a correlation curve is established between the additional mass and the frequency shift of the total sensor system, allowing one to measure a tiny unknown mass. However, when the tiny mass becomes so small that the frequency shift is no longer discernible, the nano-mass sensor is considered to have reached its detection limit [199].

In the governing equation of a nano-force sensor system for detecting unknown external forces, a loading vector $\{F\}$ is added on the right side of the same equation, shown as

$$[M]\ddot{y} + [K]\{y\} = \{F\}$$

A similar approach is utilized up to a point where the nano-force sensor reaches its limit of detection.

This exemplary review of carbon nanomaterials presents the theoretical models for nano-mass and nano-force sensors based on vibration analysis, highlighting that when studying the vibrational behavior of CNTs and GSs, the densities should be determined simultaneously with Young's modulus, shear modulus, and thickness. Citing recent studies of carbon nanomaterial-based (CNTs) [225–242], GS [243–255], and carbyne [256–258] nano-mass sensors, minimum sensitivities of 10^{-23} g, 10^{-24} to 10^{-22} g, and 10^{-26} to 10^{-23} g, respectively, have been achieved. The authors conclude that such sensors should be studied further by vibration analysis, though due to the small size and weight of carbon nanomaterials, the real-time application of nano-testing techniques is complex. Hence, they call for new methods

and approaches to be developed so that measurement uncertainty is reduced, and testing accuracy is improved [199].

The example of nano-mass and nano-force sensors based on carbon nanomaterials described above immediately catches the eye because the typical governing equation for the detection mechanism and the discussion on setting up the mass and stiffness matrices closely matches Mathieu's equation and the setup of its coefficients. Unlike direct resonance, described by the vibration analysis in the review, parametric resonance increases both the response amplitude and the frequency bandwidth with decreased damping. Therefore, parametric resonance circumvents the dilemma of balancing resonant amplification with frequency bandwidth, enabling analysis beyond the detection limit for classical resonators. Furthermore, the application of parametric resonance is agnostic as to whether the sensors are carbon nanomaterial-based or silicon-based. In both cases, sensor performance will be enhanced. Aside from the ease of designing elements with the required features, utilizing this phenomenon under ambient pressures and temperatures makes it even more appealing, especially for breath analysis. Therefore, the call for new real-time approaches and methods can be answered by applying the concept of parametric resonance and analyzing a similar equation differently.

6 Conclusion

Of the more than 870 types of VOCs found in human breath, those most widely studied include ammonia, acetone, isoprene, nitric oxide, and hydrogen sulfide. Detecting VOC concentrations in the breath accurately is challenging, and the typical range of endogenous VOCs, as measured by GC-MS technology, is 1–5,000 ppb (parts per billion). In this regard, sensors and sensor-based devices used to diagnose diseases through exhaled breath must meet such low detection limits while accurately separating the numerous VOCs present before being trusted in point-of-care and clinical settings. These devices must also perform in conditions such as high humidity, at room temperature, deliver results in real time or as close to real time as possible, and present information in an understandable form. Applying sensors and sensor-based devices to analyze human breath poses additional challenges. These challenges include distinguishing and measuring endogenous versus exogenous compounds, capturing exhaled breath from the nose instead of the mouth, analyzing alveolar breath versus dead space air, and considering influences such as diet, age, gender, pregnancy status, exercise, and smoking. Furthermore, how breath samples are analyzed – offline versus online, direct versus stored – affects the measured results. With the advancement of breath analysis, it has become evident that basing diagnosis on a single VOC (with the notable exception of NO for asthma) is usually unreliable. Hence, current research is shifting from targeted analysis to non-specific analysis of exhaled breath. Consequently, single sensors are being substituted for sensor arrays, and sensors that react to multiple compounds are being developed.

This chapter primarily discussed using metal oxide semiconductor gas sensors for breath analysis, exemplified by sensor array devices such as electronic noses. Typically, such devices consist of a hardware component, the sensor array, and a software component, machine learning and pattern recognition algorithms. Thus, a review of materials, structures, and advancements in techniques to increase the amount of reactive active sites has been presented. MOS gas sensors remain at the forefront of the development of simple, repeatable, reproducible, reliable, real-time, lightweight, hand-held devices that are inexpensive, particularly for breath analysis. The utilization of nanomaterials and nanostructures represents the next generation of gas sensors. Such techniques increase the surface area, thereby lowering detection limits and improving sensitivity by orders of magnitude over semiconductor sensors. Their nuances have also been discussed in this chapter. Lastly, parametric resonance, a method for dealing with non-linear dynamics below a sensor's detection limit, has been presented, reviewed, and illustrated. The application of parametric resonance can serve as a "smart algorithm" to enable sensors and sensor arrays to meet and exceed the collection of requirements and challenges posed by breath analysis for disease diagnosis.

References

1. Pennazza G, Santonico M (2019) Introduction. Breathprinting: what, why, how. In: Breath analysis. Elsevier, pp 1–11. https://doi.org/10.1016/B978-0-12-814562-3.00001-1
2. Wang C, Yin L, Zhang L, Xiang D, Gao R (2010) Metal oxide gas sensors: sensitivity and influencing factors. Sensors 10(3). https://doi.org/10.3390/s100302088
3. Haick H, Vishinkin R, di Natale C, Marco S (2020) Sensor systems. In: Breathborne bio-markers and the human volatilome. Elsevier, pp 201–220. https://doi.org/10.1016/B978-0-12-819967-1.00013-X
4. Pallás-Areny R, Webster JG (2000) Sensors and signal conditioning.2nd edn. Wiley, New York
5. Karakaya D, Ulucan O, Turkan M (2020) Electronic nose and its applications: a survey. Int J Autom Comput 17(2):179–209. https://doi.org/10.1007/s11633-019-1212-9
6. McLachlan GJ (2005) Discriminant analysis and statistical pattern recognition. Wiley, New York
7. Duda RO, Hart PE, Stork DG (2000) Pattern classification.2nd edn. Wiley, New York
8. Tian X, Wang J, Cui S (2013) Analysis of pork adulteration in minced mutton using electronic nose of metal oxide sensors. J Food Eng 119(4). https://doi.org/10.1016/j.jfoodeng.2013.07.004
9. Vinzi VE, Chin WW, Henseler J, Wang HW (2010) Handbook of partial least squares. https://doi.org/10.1007/978-3-540-32827-8
10. Aguilera T, Lozano J, Paredes JA, Álvarez FJ, Suárez JI (2012) Electronic nose based on independent component analysis combined with partial least squares and artificial neural networks for wine prediction. Sensors (Switzerland) 12(6). https://doi.org/10.3390/s120608055
11. Amemiya T (1985) Advanced econometrics.1st edn. Harvard University Press, Cambridge
12. Giungato P, Laiola E, Nicolardi V (2017) Evaluation of industrial roasting degree of coffee beans by using an electronic nose and a stepwise backward selection of predictors. Food Anal Methods 10(10). https://doi.org/10.1007/s12161-017-0909-z

13. Baskar C, Nesakumar N, Balaguru Rayappan JB, Doraipandian M (2017) A framework for analysing E-nose data based on fuzzy set multiple linear regression: paddy quality assessment. Sens Actuators A Phys 267. https://doi.org/10.1016/j.sna.2017.10.020

14. Jolliffe I (2011) Principal component analysis. In: Lovric M (ed) International encyclopedia of statistical science. Springer, Berlin, pp 1094–1096. https://doi.org/10.1007/978-3-642-04898-2_455

15. Wang L (2005) Support vector machines: theory and applications.1st edn. Springer, Berlin

16. Laref R, Losson E, Sava A, Adjallah K, Siadat M (2018) A comparison between SVM and PLS for E-nose based gas concentration monitoring. In: Proceedings of the IEEE international conference on industrial technology. https://doi.org/10.1109/ICIT.2018.8352372

17. Zurada JM (1992) Introduction to artificial neural systems. West Publishing House, St. Paul

18. Zhang L, Tian F (2014) Performance study of multilayer perceptrons in a low-cost electronic nose. IEEE Trans Instrum Meas 63(7). https://doi.org/10.1109/TIM.2014.2298691

19. Hood L, Friend SH (2011) Predictive, personalized, preventive, participatory (P4) cancer medicine. Nat Rev Clin Oncol 8(3). https://doi.org/10.1038/nrclinonc.2010.227

20. di Natale C, Paolesse R, Martinelli E, Capuano R (2014) Solid-state gas sensors for breath analysis: a review. Anal Chim Acta 824. https://doi.org/10.1016/j.aca.2014.03.014

21. Bruderer T et al (2019) On-line analysis of exhaled breath. Chem Rev 119(19):10803–10828. https://doi.org/10.1021/acs.chemrev.9b00005

22. Broza YY, Vishinkin R, Barash O, Nakhleh MK, Haick H (2018) Synergy between nanomaterials and volatile organic compounds for non-invasive medical evaluation. Chem Soc Rev 47(13). https://doi.org/10.1039/c8cs00317c

23. Williams AJ et al (2017) The CompTox chemistry dashboard: a community data resource for environmental chemistry. J Chem 9(1):61. https://doi.org/10.1186/s13321-017-0247-6

24. Rayleigh L (1887) XVII. On the maintenance of vibrations by forces of double frequency, and on the propagation of waves through a medium endowed with a periodic structure. Lond Edinb Dublin Philos Mag J Sci 24(147). https://doi.org/10.1080/14786448708628074

25. Mathieu É (1868) Mémoire sur le mouvement vibratoire d'une membrane de forme elliptique. J Math Pures Appl 13:137–203. [online]. http://eudml.org/doc/234720

26. Stoker JJ (1992) Nonlinear vibrations in mechanical and electrical systems. Wiley, New York

27. Nayfeh AH, Mook DT (1995) Nonlinear oscillations. Wiley, New York

28. Zhang W, Turner KL (2005) Application of parametric resonance amplification in a single-crystal silicon micro-oscillator based mass sensor. Sens Actuators A Phys 122(1 Spec. Iss). https://doi.org/10.1016/j.sna.2004.12.033

29. Li LL, Holthoff EL, Shaw LA, Burgner CB, Turner KL (2014) Noise squeezing controlled parametric bifurcation tracking of MIP-coated microbeam MEMS sensor for TNT explosive gas sensing. J Microelectromech Syst 23(5). https://doi.org/10.1109/JMEMS.2014.2310206

30. Kacem N, Hentz S, Baguet S, Dufour R (2011) Forced large amplitude periodic vibrations of non-linear Mathieu resonators for microgyroscope applications. Int J Non Linear Mech 46(10). https://doi.org/10.1016/j.ijnonlinmec.2011.07.008

31. Turner KL, Miller SA, Hartwell PG, MacDonald NC, Strogatz SH, Adams SG (1998) Five parametric resonances in a microelectromechanical system. Nature 396(6707). https://doi.org/10.1038/24122

32. Bhushan B (ed) (2016) Encyclopedia of nanotechnology. Springer, Dordrecht. https://doi.org/10.1007/978-94-017-9780-1

33. Bachelor DL (2020) The effects of noise on parametrically excited systems with nonlinear damping

34. Craven MA, Gardner JW, Bartlett PN (1996) Electronic noses – development and future prospects. TrAC – Trends Analyt Chem 15(9). https://doi.org/10.1016/S0165-9936(96)00061-1

35. Friedrich MJ (2009) Scientists seek to sniff out diseases. JAMA 301(6). https://doi.org/10.1001/jama.2009.90

36. Pobkrut T, Eamsa-Ard T, Kerdcharoen T (2016) Sensor drone for aerial odor mapping for agriculture and security services. In: 13th international conference on electrical engineering/electronics, computer, telecommunications and information technology (ECTI-CON). IEEE, pp 1–5. https://doi.org/10.1109/ECTICon.2016.7561340

37. Rocha Á, Serrhini M, Felgueiras C (2017) Europe and MENA cooperation advances in information and communication technologies. Springer, Cham. https://doi.org/10.1007/978-3-319-46568-5

38. Electronic Sensor Technology, Inc. (2022). https://www.estcal.com. Accessed 25 June 2022

39. AIRSENSE Analytics (2022). https://airsense.com/en. Accessed 25 June 2022

40. Electronic Nose Co., LTD (2022). http://e-nose.asia/index.php?lang=en. Accessed 25 June 2022

41. Sensigent (2022). https://www.sensigent.com. Accessed 25 June 2022

42. FOODsniffer (2022). http://www.myfoodsniffer.com/. Accessed 25 June 2022

43. E-Nose Pty Ltd (2022). http://www.e-nose.info/about.html. Accessed 25 June 2022

44. Alpha MOS (2022). www.alpha-mos.com. Accessed 25 June 2022

45. RoboScientific (2022). http://www.roboscientific.com. Accessed 25 June 2022

46. Aryballe (2022). http://www.aryballe.com. Accessed 25 June 2022

47. Odotech (2022). http://www.odotech.com/en/. Accessed 25 June 2022

48. Figaro MOS-type gas sensors. www.figarosensor.com/technicalinfo/semicondoctor.html. Accessed 20 May 2022

49. The eNose Company (2022). https://www.enose.nl. Accessed 25 June 2022

50. Potyrailo RA (2016) Correction: multivariable sensors for ubiquitous monitoring of gases in the era of internet of things and industrial internet (Chem. Rev. (2016) 116: 19 (11877–11923) DOI: 10.1021/acs.chemrev.6b00187). Chem Rev 116(23). https://doi.org/10.1021/acs.chemrev.6b00741

51. Nikolic MV, Milovanovic V, Vasiljevic ZZ, Stamenkovic Z (2020) Semiconductor gas sensors: materials, technology, design, and application. Sensors 20(22):6694. https://doi.org/10.3390/s20226694

52. Burges CJC (1998) A tutorial on support vector machines for pattern recognition. Data Min Knowl Disc 2(2). https://doi.org/10.1023/A:1009715923555

53. Goudjil M, Koudil M, Bedda M, Ghoggali N (2018) A novel active learning method using SVM for text classification. Int J Autom Comput 15(3). https://doi.org/10.1007/s11633-015-0912-z

54. Jain AK, Mao J, Mohiuddin KM (1996) Artificial neural networks: a tutorial. Computer 29(3). https://doi.org/10.1109/2.485891

55. Mendez MR (2016) Electronic noses and tongues in food science.1st edn. Academic Press, London

56. Faceli K, de Carvalho ACPLF, Rezende SO (2004) Combining intelligent techniques for sensor fusion. Appl Intell 20(3). https://doi.org/10.1023/B:APIN.0000021413.05467.20

57. Lecun Y, Bengio Y, Hinton G (2015) Deep learning. Nature 521(7553). https://doi.org/10.1038/nature14539

58. Qi PF, Meng QH, Zeng M (2017) A CNN-based simplified data processing method for electronic noses. In: 2017 ISOCS/IEEE international symposium on olfaction and electronic nose (ISOEN). IEEE, pp 1–3. https://doi.org/10.1109/ISOEN.2017.7968887

59. Zhang H, Ye W, Zhao X, Teng RKF, Pan X (2018) A novel convolutional recurrent neural network based algorithm for fast gas recognition in electronic nose system. In: 2018 IEEE international conference on electron devices and solid state circuits (EDSSC), pp 1–2. https://doi.org/10.1109/EDSSC.2018.8487105

60. Cho JH, Kim YW, Na KJ, Jeon GJ (2008) Wireless electronic nose system for real-time quantitative analysis of gas mixtures using micro-gas sensor array and neuro-fuzzy network. Sensors Actuators B Chem 134(1). https://doi.org/10.1016/j.snb.2008.04.019

61. Righettoni M, Tricoli A, Pratsinis SE (2010) Si: WO3 sensors for highly selective detection of acetone for easy diagnosis of diabetes by breath analysis. Anal Chem 82(9). https://doi.org/10.1021/ac902695n

62. Chiu SW, Tang KT (2013) Towards a chemiresistive sensor-integrated electronic nose: a review. Sensors (Switzerland) 13(10). https://doi.org/10.3390/s131014214

63. Peng G et al (2009) Diagnosing lung cancer in exhaled breath using gold nanoparticles. Nat Nanotechnol 4(10). https://doi.org/10.1038/nnano.2009.235

64. Chen X et al (2005) A non-invasive detection of lung cancer combined virtual gas sensors array with imaging recognition technique. In: Annual international conference of the IEEE engineering in medicine and biology – proceedings, vol 7. https://doi.org/10.1109/iembs.2005.1615826

65. Bartolazzi A et al (2010) A sensor array and GC study about VOCs and cancer cells. Sensors Actuators B Chem 146(2). https://doi.org/10.1016/j.snb.2009.11.046

66. Pennazza G et al (2008) Application of a quartz microbalance based gas sensor array for the study of halitosis. J Breath Res 2(1). https://doi.org/10.1088/1752-7155/2/1/017009

67. di Natale C et al (2003) Lung cancer identification by the analysis of breath by means of an array of non-selective gas sensors. Biosens Bioelectron 18(10). https://doi.org/10.1016/S0956-5663(03)00086-1

68. Mondal SP, Dutta PK, Hunter GW, Ward BJ, Laskowski D, Dweik RA (2011) Development of high sensitivity potentiometric NOx sensor and its application to breath analysis. Sensors Actuators B Chem 158(1). https://doi.org/10.1016/j.snb.2011.05.063

69. Mazzone PJ et al (2007) Diagnosis of lung cancer by the analysis of exhaled breath with a colorimetric sensor array. Thorax 62(7). https://doi.org/10.1136/thx.2006.072892

70. Janzen MC, Ponder JB, Bailey DP, Ingison CK, Suslick KS (2006) Colorimetric sensor arrays for volatile organic compounds. Anal Chem 78(11). https://doi.org/10.1021/ac052111s

71. Saruhan B, Lontio Fomekong R, Nahirniak S (2021) Review: influences of semiconductor metal oxide properties on gas sensing characteristics. Front Sens 2. https://doi.org/10.3389/fsens.2021.657931

72. Povarov VG, Lopatnikov AI, Geibo DS, Bulatova AV, Razgonyaev AO (2013) Use of semiconductor oxide films for the detection of volatile organic compounds in the gas phase. J Anal Chem 68(4). https://doi.org/10.1134/S1061934813040084

73. D'Amico A, Ferri G, Zompanti A (2019) Sensor systems for breathprinting: a review of the current technologies for exhaled breath analysis based on a sensor array with the aim of integrating them in a standard and shared procedure. Breath Anal:49–79. Elsevier. https://doi.org/10.1016/B978-0-12-814562-3.00004-7

74. Sberveglieri G (2012) Gas sensors: principles, operation and developments. Springer. https://doi.org/10.1007/978-94-011-2737-0

75. Cheeke JDN, Wang Z (1999) Acoustic wave gas sensors. Sensors Actuators B Chem 59(2). https://doi.org/10.1016/S0925-4005(99)00212-9

76. Arshak K, Moore E, Lyons GM, Harris J, Clifford S (2004) A review of gas sensors employed in electronic nose applications. Sens Rev 24(2). https://doi.org/10.1108/02602280410525977

77. Huang X, Bai Q, Hu J, Hou D (2017) A practical model of quartz crystal microbalance in actual applications. Sensors (Switzerland) 17(8). https://doi.org/10.3390/s17081785

78. Turner NW, Bloxham M, Piletsky SA, Whitcombe MJ, Chianella I (2017) The use of a quartz crystal microbalance as an analytical tool to monitor particle/surface and particle/particle interactions under dry ambient and pressurized conditions: a study using common inhaler components. Analyst 142(1). https://doi.org/10.1039/c6an01572g

79. Thies JW, Kuhn P, Thürmann B, Dübel S, Dietzel A (2017) Microfluidic quartz-crystal-microbalance (QCM) sensors with specialized immunoassays for extended measurement range and improved reusability. Microelectron Eng 179. https://doi.org/10.1016/j.mee.2017.04.023

80. Yan Y et al (2012) Polyaniline-modified quartz crystal microbalance sensor for detection of formic acid gas. Water Air Soil Pollut 223(3). https://doi.org/10.1007/s11270-011-0943-1

81. Jha SK, Hayashi K (2015) A quick responding quartz crystal microbalance sensor array based on molecular imprinted polyacrylic acids coating for selective identification of aldehydes in body odor. Talanta 134. https://doi.org/10.1016/j.talanta.2014.09.049

82. Wasilewski T, Szulczyński B, Wojciechowski M, Kamysz W, Gębicki J (2019) A highly selective biosensor based on peptide directly derived from the harmOBP7 aldehyde binding site. Sensors (Switzerland) 19(19). https://doi.org/10.3390/s19194284

83. Sankaran S, Panigrahi S, Mallik S (2011) Olfactory receptor based piezoelectric biosensors for detection of alcohols related to food safety applications. Sensors Actuators B Chem 155(1). https://doi.org/10.1016/j.snb.2010.08.003

84. Zhang Y, Yu K, Xu R, Jiang D, Luo L, Zhu Z (2005) Quartz crystal microbalance coated with carbon nanotube films used as humidity sensor. Sens Actuators A Phys 120(1). https://doi.org/10.1016/j.sna.2004.11.032

85. Qi P, Zhao C, Wang R, Fei T, Zhang T (2018) High-performance QCM humidity sensors using acidized-multiwalled carbon nanotubes as sensing film. IEEE Sensors J 18(13). https://doi.org/10.1109/JSEN.2018.2839110

86. Koshets IA, Kazantseva ZI, Shirshov YM, Cherenok SA, Kalchenko VI (2005) Calixarene films as sensitive coatings for QCM-based gas sensors. Sensors Actuators B Chem 106(1 Spec. Iss). https://doi.org/10.1016/j.snb.2004.05.054

87. Capone S et al (2003) Solid state gas sensors: state of the art and future activities. ChemInform 35

88. Jordan LR, Hauser PC (1997) Electrochemical for acetylene. Anal Chem 69(14). https://doi.org/10.1021/ac9700585

89. Laffort P (1989) Models for describing intensity interactions in odor mixtures: a reappraisal. In: Laing DG, Cam WS, McBride RL, Ache BW (eds) Perception of complex smells and tastes, pp 205–223

90. Liu X, Cheng S, Liu H, Hu S, Zhang D, Ning H (2012) A survey on gas sensing technology. Sensors (Switzerland) 12(7). https://doi.org/10.3390/s120709635

91. Machado RF et al (2005) Detection of lung cancer by sensor array analyses of exhaled breath. Am J Respir Crit Care Med 171(11). https://doi.org/10.1164/rccm.200409-1184OC

92. Pennazza G et al (2013) Electronic nose and GC-MS analysis of volatile compounds in tuber magnatum Pico: evaluation of different storage conditions. Food Chem 136(2). https://doi.org/10.1016/j.foodchem.2012.08.086

93. Drmosh QA, Olanrewaju Alade I, Qamar M, Akbar S (2021) Zinc oxide-based acetone gas sensors for breath analysis: a review. Chem Asian J 16(12):1519–1538. https://doi.org/10.1002/asia.202100303

94. (2022) Introduction to gas sensors: construction types and working principles. https://components101.com/articles/introduction-to-gas-sensors-types-working-and-applications. Accessed 25 June 2022

95. Briand D, Courbat J (2013) Micromachined semiconductor gas sensors. Semiconduct Gas Sensor. https://doi.org/10.1533/9780857098665.2.220

96. Rüffer D, Hoehne F, Bühler J (2018) New digital metal-oxide (MOx) sensor platform. Sensors (Switzerland) 18(4). https://doi.org/10.3390/s18041052

97. Bochenkov VE, Sergeev GB (2010) Sensitivity, selectivity, and stability of gas-sensitive metal-oxide nanostructures. In: Umar A, Hang YB (eds) Metal oxide nanostructures and their applications. American Scientific Publishers, Valencia

98. Huang J, Wan Q (2009) Gas sensors based on semiconducting metal oxide one-dimensional nanostructures. Sensors 9(12). https://doi.org/10.3390/s91209903

99. Wang H et al (2021) Gas sensing materials roadmap. J Phys Condens Matter 33(30):303001. https://doi.org/10.1088/1361-648X/abf477

100. Dong C, Zhao R, Yao L, Ran Y, Zhang X, Wang Y (2020) A review on WO3 based gas sensors: morphology control and enhanced sensing properties. J Alloys Compd 820:153194. https://doi.org/10.1016/j.jallcom.2019.153194

101. Kim DH, Jang JS, Koo WT, Choi SJ, Kim SJ, Kim ID (2018) Hierarchically interconnected porosity control of catalyst-loaded WO3 nanofiber scaffold: superior acetone sensing layers for exhaled breath analysis. Sensors Actuators B Chem 259. https://doi.org/10.1016/j.snb.2017.12.051

102. Xu Y et al (2020) Highly sensitive and selective detection of acetone based on platinum sensitized porous tungsten oxide nanospheres. Sensors Actuators B Chem 307. https://doi.org/10.1016/j.snb.2019.127616

103. Liu W, Gu D, Zhang JW, Li XG, Rumyantseva MN, Gaskov AM (2021) ZnSe/NiO heterostructure-based chemiresistive-type sensors for low-concentration NO_2 detection. Rare Metals 40(6). https://doi.org/10.1007/s12598-020-01564-5

104. Wagner T, Haffer S, Weinberger C, Klaus D, Tiemann M (2013) Mesoporous materials as gas sensors. Chem Soc Rev 42(9). https://doi.org/10.1039/c2cs35379b

105. Yoon J-W, Lee J-H (2017) Toward breath analysis on a chip for disease diagnosis using semiconductor-based chemiresistors: recent progress and future perspectives. Lab Chip 17(21):3537–3557. https://doi.org/10.1039/C7LC00810D

106. Das T, Das S, Karmakar M, Chakraborty S, Saha D, Pal M (2020) Novel barium hexaferrite based highly selective and stable trace ammonia sensor for detection of renal disease by exhaled breath analysis. Sensors Actuators B Chem 325. https://doi.org/10.1016/j.snb.2020.128765

107. Aghaei SM, Aasi A, Farhangdoust S, Panchapakesan B (2021) Graphene-like BC6N nanosheets are potential candidates for detection of volatile organic compounds (VOCs) in human breath: a DFT study. Appl Surf Sci 536. https://doi.org/10.1016/j.apsusc.2020.147756

108. Zhang L, Khan K, Zou J, Zhang H, Li Y (2019) Recent advances in emerging 2D material-based gas sensors: potential in disease diagnosis. Adv Mater Interfaces 6(22). https://doi.org/10.1002/admi.201901329

109. Nasiri N, Clarke C (2019) Nanostructured gas sensors for medical and health applications: low to high dimensional materials. Biosensors (Basel) 9(1):43. https://doi.org/10.3390/bios9010043

110. Liu H et al (2014) Physically flexible, rapid-response gas sensor based on colloidal quantum dot solids. Adv Mater 26(17). https://doi.org/10.1002/adma.201304366

111. Li L, Gu L, Lou Z, Fan Z, Shen G (2017) ZnO quantum dot decorated Zn_2SnO_4 nanowire heterojunction photodetectors with drastic performance enhancement and flexible ultraviolet image sensors. ACS Nano 11(4). https://doi.org/10.1021/acsnano.7b00749

112. Pan J, Li J, Yan Z, Zhou B, Wu H, Xiong X (2013) SnO_2@CdS nanowire-quantum dots heterostructures: tailoring optical properties of SnO_2 for enhanced photodetection and photocatalysis. Nanoscale 5(7). https://doi.org/10.1039/c3nr34096a

113. Romo-Herrera JM, Terrones M, Terrones H, Dag S, Meunier V (2007) Covalent 2D and 3D networks from 1D nanostructures: designing new materials. Nano Lett 7(3). https://doi.org/10.1021/nl0622202

114. Alenezi MR, Henley SJ, Emerson NG, Silva SRP (2014) From 1D and 2D ZnO nanostructures to 3D hierarchical structures with enhanced gas sensing properties. Nanoscale 6(1). https://doi.org/10.1039/c3nr04519f

115. Tan H, Fan Y, Zhou Y, Chen Q, Xu W, Warner JH (2016) Ultrathin 2D photodetectors utilizing chemical vapor deposition grown WS2 with graphene electrodes. ACS Nano 10(8). https://doi.org/10.1021/acsnano.6b03722

116. Song Z et al (2016) Sensitive room-temperature H2S gas sensors employing SnO_2 quantum wire/reduced graphene oxide nanocomposites. Chem Mater 28(4). https://doi.org/10.1021/acs.chemmater.5b04850

117. Hu N et al (2014) Ultrafast and sensitive room temperature NH3 gas sensors based on chemically reduced graphene oxide. Nanotechnology 25(2). https://doi.org/10.1088/0957-4484/25/2/025502

118. Mittal M, Kumar A (2014) Carbon nanotube (CNT) gas sensors for emissions from fossil fuel burning. Sensors Actuators B Chem 203. https://doi.org/10.1016/j.snb.2014.05.080

119. Dai J et al (2020) Printed gas sensors. Chem Soc Rev 49(6). https://doi.org/10.1039/c9cs00459a
120. Yeow JTW, Wang Y (2009) A review of carbon nanotubes-based gas sensors. J Sensor 2009. https://doi.org/10.1155/2009/493904
121. Neri G (2017) Thin 2D: the new dimensionality in gas sensing. Chemosensors 5(3). https://doi.org/10.3390/chemosensors5030021
122. Lee E, Kim D-J (2020) Review – recent exploration of two-dimensional MXenes for gas sensing: from a theoretical to an experimental view. J Electrochem Soc 167(3). https://doi.org/10.1149/2.0152003jes
123. Moon HG et al (2013) Extremely sensitive and selective NO probe based on villi-like WO 3 nanostructures for application to exhaled breath analyzers. ACS Appl Mater Interfaces 5(21). https://doi.org/10.1021/am402456s
124. Tricoli A, Righettoni M, Pratsinis SE (2009) Minimal cross-sensitivity to humidity during ethanol detection by SnO_2-TiO_2 solid solutions. Nanotechnology 20(31). https://doi.org/10.1088/0957-4484/20/31/315502
125. Bârsan N, Weimar U (2003) Understanding the fundamental principles of metal oxide based gas sensors; the example of CO sensing with SnO_2 sensors in the presence of humidity. J Phys Condens Matter 15(20). https://doi.org/10.1088/0953-8984/15/20/201
126. Kim HR, Haensch A, Kim ID, Barsan N, Weimar U, Lee JH (2011) The role of NiO doping in reducing the impact of humidity on the performance of SnO_2-based gas sensors: synthesis strategies, and phenomenological and spectroscopic studies. Adv Funct Mater 21(23). https://doi.org/10.1002/adfm.201101154
127. Choi KI, Kim HJ, Kang YC, Lee JH (2014) Ultraselective and ultrasensitive detection of H2S in highly humid atmosphere using CuO-loaded SnO_2 hollow spheres for real-time diagnosis of halitosis. Sensors Actuators B Chem 194. https://doi.org/10.1016/j.snb.2013.12.111
128. Šetka M, Drbohlavová J, Hubálek J (2017) Nanostructured polypyrrole-based ammonia and volatile organic compound sensors. Sensors (Switzerland) 17(3). https://doi.org/10.3390/s17030562
129. Ryan MA, Shevade AV, Zhou H, Homer ML (2004) Polymer-carbon black composite sensors in an electronic nose for air-quality monitoring. MRS Bull 29(10). https://doi.org/10.1557/mrs2004.208
130. Shevade AV et al (2007) Development of the third generation JPL electronic nose for international space station technology demonstration. SAE Trans J Aerosp. https://doi.org/10.4271/2007-01-3149
131. Gangopadhyay R, De A (2001) Conducting polymer composites: novel materials for gas sensing. Sensors Actuators B Chem 77(1–2). https://doi.org/10.1016/S0925-4005(01)00719-5
132. Ram MK, Yavuz Ö, Lahsangah V, Aldissi M (2005) CO gas sensing from ultrathin nano-composite conducting polymer film. Sensors Actuators B Chem 106(2). https://doi.org/10.1016/j.snb.2004.09.027
133. Sharma S, Hussain S, Singh S, Islam SS (2014) MWCNT-conducting polymer composite based ammonia gas sensors: a new approach for complete recovery process. Sensors Actuators B Chem 194. https://doi.org/10.1016/j.snb.2013.12.050
134. Lei W, Si W, Xu Y, Gu Z, Hao Q (2014) Conducting polymer composites with graphene for use in chemical sensors and biosensors. Microchim Acta 181(7–8). https://doi.org/10.1007/s00604-014-1160-6
135. Chang CJ, Lin CY, Chen JK, Hsu MH (2014) Ce-doped ZnO nanorods based low operation temperature NO_2 gas sensors. Ceram Int 40(7 Part B). https://doi.org/10.1016/j.ceramint.2014.03.080
136. Khatami M, Alijani HQ, Nejad MS, Varma RS (2018) Core@shell nanoparticles: greener synthesis using natural plant products. Appl Sci (Switzerland) 8(3). https://doi.org/10.3390/app8030411

137. Majhi SM et al (2018) Au@NiO core-shell nanoparticles as a p-type gas sensor: novel synthesis, characterization, and their gas sensing properties with sensing mechanism. Sensors Actuators B Chem 268. https://doi.org/10.1016/j.snb.2018.04.119

138. Zhang X et al (2019) ZIF-8 derived hierarchical hollow ZnO nanocages with quantum dots for sensitive ethanol gas detection. Sensors Actuators B Chem 289. https://doi.org/10.1016/j.snb.2019.03.090

139. Rai P, Majhi SM, Yu YT, Lee JH (2015) Noble metal@metal oxide semiconductor core@shell nano-architectures as a new platform for gas sensor applications. RSC Adv 5(93). https://doi.org/10.1039/c5ra14322e

140. Wang XF, Song XZ, Sun KM, Cheng L, Ma W (2018) MOFs-derived porous nanomaterials for gas sensing. Polyhedron 152. https://doi.org/10.1016/j.poly.2018.06.037

141. Zhang D, Yang Z, Yu S, Mi Q, Pan Q (2020) Diversiform metal oxide-based hybrid nanostructures for gas sensing with versatile prospects. Coord Chem Rev 413. https://doi.org/10.1016/j.ccr.2020.213272

142. Li HY, Zhao SN, Zang SQ, Li J (2020) Functional metal-organic frameworks as effective sensors of gases and volatile compounds. Chem Soc Rev 49(17). https://doi.org/10.1039/c9cs00778d

143. Henderson B et al (2021) The peppermint breath test benchmark for PTR-MS and SIFT-MS. J Breath Res 15(4). https://doi.org/10.1088/1752-7163/ac1fcf

144. Agapiou A, Amann A, Mochalski P, Statheropoulos M, Thomas CLP (2015) Trace detection of endogenous human volatile organic compounds for search, rescue and emergency applications. TrAC – Trend Analyt Chem 66. https://doi.org/10.1016/j.trac.2014.11.018

145. King J et al (2012) Measurement of endogenous acetone and isoprene in exhaled breath during sleep. Physiol Meas 33(3). https://doi.org/10.1088/0967-3334/33/3/413

146. Amann A et al (2014) The human volatilome: volatile organic compounds (VOCs) in exhaled breath, skin emanations, urine, feces and saliva. J Breath Res 8(3). https://doi.org/10.1088/1752-7155/8/3/034001

147. Saasa V, Malwela T, Beukes M, Mokgotho M, Liu C-P, Mwakikunga B (2018) Sensing technologies for detection of acetone in human breath for diabetes diagnosis and monitoring. Diagnostics 8(1). https://doi.org/10.3390/diagnostics8010012

148. Bretos I, Jiménez R, Ricote J, Calzada ML (2018) Low-temperature crystallization of solution-derived metal oxide thin films assisted by chemical processes. Chem Soc Rev 47(2). https://doi.org/10.1039/c6cs00917d

149. Sui LL et al (2015) Construction of three-dimensional flower-like α-MoO3with hierarchical structure for highly selective triethylamine sensor. Sensors Actuators B Chem 208. https://doi.org/10.1016/j.snb.2014.10.138

150. Grabowska-Polanowska B et al (2013) Detection of potential chronic kidney disease markers in breath using gas chromatography with mass-spectral detection coupled with thermal desorption method. J Chromatogr A 1301. https://doi.org/10.1016/j.chroma.2013.05.012

151. Dweik RA et al (2011) An official ATS clinical practice guideline: interpretation of exhaled nitric oxide levels (FENO) for clinical applications. Am J Respir Crit Care Med 184(5). https://doi.org/10.1164/rccm.9120-11ST

152. Shankar P, Rayappan JBB (2017) Room temperature ethanol sensing properties of ZnO nanorods prepared using an electrospinning technique. J Mater Chem C Mater 5(41). https://doi.org/10.1039/c7tc03771f

153. Hakim SA, Liu Y, Zakharova GS, Chen W (2015) Synthesis of vanadium pentoxide nanoneedles by physical vapour deposition and their highly sensitive behavior towards acetone at room temperature. RSC Adv 5(30). https://doi.org/10.1039/c4ra16564k

154. Bo Z, Yuan M, Mao S, Chen X, Yan J, Cen K (2018) Decoration of vertical graphene with tin dioxide nanoparticles for highly sensitive room temperature formaldehyde sensing. Sensors Actuators B Chem 256. https://doi.org/10.1016/j.snb.2017.10.043

155. Choi SJ, Ku KH, Kim BJ, Kim ID (2016) Novel templating route using Pt infiltrated block copolymer microparticles for catalytic Pt functionalized macroporous WO3 nanofibers and its

application in breath pattern recognition. ACS Sens 1(9). https://doi.org/10.1021/acssensors.6b00422

156. Yan Y, Zhang M, Moon CH, Su HC, Myung NV, Haberer ED (2016) Viral-templated gold/polypyrrole nanopeapods for an ammonia gas sensor. Nanotechnology 27(32). https://doi.org/10.1088/0957-4484/27/32/325502

157. Modak AS (2022) Why have only a handful of breath tests made the transition from R&D to clinical practice?

158. Jia Y, Du S, Seshia AA (2016) Twenty-eight orders of parametric resonance in a microelectromechanical device for multi-band vibration energy harvesting. Sci Rep 6(1): 30167. https://doi.org/10.1038/srep30167

159. Daqaq MF, Bode D (2011) Exploring the parametric amplification phenomenon for energy harvesting. Proceed Inst Mech Eng Part I: J Syst Control Eng 225(4). https://doi.org/10.1177/2041304110401145

160. Rhoads JF, Guo C, Fedder GK (2015) Parametrically excited micro- and nanosystems. In: Resonant MEMS: fundamentals, implementation and application, pp 73–95. https://doi.org/10.1002/9783527676330.ch4

161. Faraday M (1837) On a peculiar class of acoustical figures; and on certain forms assumed by groups of particles upon vibrating elastic surfaces. In: Abstracts of the papers printed in the Philosophical Transactions of the Royal Society of London, vol 3. The Royal Society, London. https://doi.org/10.1098/rspl.1830.0024

162. Floquet G (1883) Sur les équations différentielles linéaires à coefficients périodiques. Annales scientifiques de l'École normale supérieure 12. https://doi.org/10.24033/asens.220

163. Hill GW (1886) On the part of the motion of the lunar perigee which is a function of the mean motions of the sun and moon. Acta Mathematica 8(1). https://doi.org/10.1007/BF02417081

164. Rayleigh L (1883) XXXIII. On maintained vibrations. Lond Edinb Dublin Philos Mag J Sci 15(94). https://doi.org/10.1080/14786448308627342

165. Tondl A, Ruijgrok T, Verhulst F, Nabergoj R (2000) Autoparametric resonance in mechanical systems. In: Autoparametric resonance in mechanical systems. Cambridge University Press

166. Fossen TI, Nijmeijer H (2012) Parametric resonance in dynamical systems. Springer. https://doi.org/10.1007/978-1-4614-1043-0

167. Requa MV, Turner KL (2006) Electromechanically driven and sensed parametric resonance in silicon microcantilevers. Appl Phys Lett 88(26). https://doi.org/10.1063/1.2216033

168. Oropeza-Ramos LA, Turner KL (2005) Parametric resonance amplification in a MEMGyroscope. In: Proceedings of IEEE sensors, vol 2005. https://doi.org/10.1109/ICSENS.2005.1597785

169. Jia Y, Yan J, Soga K, Seshia AA (2014) A parametrically excited vibration energy harvester. J Intell Mater Syst Struct 25(3). https://doi.org/10.1177/1045389X13491637

170. S. (https://math.stackexchange.com/users/232891/slereah). Arbitrary factors for the (modified) Mathieu equation [online]. https://math.stackexchange.com/q/1515145

171. Moran K, Burgner C, Shaw S, Turner K (2013) A review of parametric resonance in microelectromechanical systems. Nonlinear Theory Appl IEICE 4(3):198–224. https://doi.org/10.1587/nolta.4.198

172. Zhang W, Baskaran R, Turner KL (2002) Effect of cubic nonlinearity on auto-parametrically amplified resonant MEMS mass sensor. Sens Actuators A Phys 102(1–2). https://doi.org/10.1016/S0924-4247(02)00299-6

173. Zhang W, Turner KL (2005) Frequency-tuning for control of parametrically resonant mass sensors. J Vac Sci Technol A 23(4). https://doi.org/10.1116/1.1924717

174. Yie Z, Zielke MA, Burgner CB, Turner KL (2011) Comparison of parametric and linear mass detection in the presence of detection noise. J Micromech Microeng 21(2). https://doi.org/10.1088/0960-1317/21/2/025027

175. Kaajakari V, Lal A (2004) Parametric excitation of circular micromachined polycrystalline silicon disks. Appl Phys Lett 85(17). https://doi.org/10.1063/1.1807951

176. Thompson MJ, Horsley DA (2010) Lorentz force mems magnetometer. In: 2010 solid-state, actuators, and microsystems workshop technical digest, pp 45–48. https://doi.org/10.31438/trf.hh2010.12

177. Rhoads JF, Kumar V, Shaw SW, Turner KL (2013) The non-linear dynamics of electromagnetically actuated microbeam resonators with purely parametric excitations. Int J Non Linear Mech 55. https://doi.org/10.1016/j.ijnonlinmec.2013.04.003

178. Zalalutdinov M et al (2001) Optically pumped parametric amplification for micromechanical oscillators. Appl Phys Lett 78(20). https://doi.org/10.1063/1.1371248

179. Iijima S, Ichihashi T (1993) Single-shell carbon nanotubes of 1-nm diameter. Nature 363(6430). https://doi.org/10.1038/363603a0

180. Novoselov KS et al (2004) Electric field in atomically thin carbon films. Science (1979) 306(5696). https://doi.org/10.1126/science.1102896

181. Oberlin A, Endo M, Koyama T (1976) Filamentous growth of carbon through benzene decomposition. J Cryst Growth 32(3). https://doi.org/10.1016/0022-0248(76)90115-9

182. Iijima S (1991) Helical microtubules of graphitic carbon. Nature 354(6348). https://doi.org/10.1038/354056a0

183. Heimann RB, Kleiman J, Salansky NM (1983) A unified structural approach to linear carbon polytypes. Nature 306(5939). https://doi.org/10.1038/306164a0

184. Shokrieh MM, Rafiee R (2010) A review of the mechanical properties of isolated carbon nanotubes and carbon nanotube composites. Mech Compos Mater 46(2). https://doi.org/10.1007/s11029-010-9135-0

185. Kumar A, Sharma K, Dixit AR (2019) A review of the mechanical and thermal properties of graphene and its hybrid polymer nanocomposites for structural applications. J Mater Sci 54(8). https://doi.org/10.1007/s10853-018-03244-3

186. Sun DM, Liu C, Ren WC, Cheng HM (2013) A review of carbon nanotube- and graphene-based flexible thin-film transistors. Small 9(8). https://doi.org/10.1002/smll.201203154

187. Che Y, Chen H, Gui H, Liu J, Liu B, Zhou C (2014) Review of carbon nanotube nanoelectronics and macroelectronics. Semicond Sci Technol 29(7). https://doi.org/10.1088/0268-1242/29/7/073001

188. Yang Z, Tian J, Yin Z, Cui C, Qian W, Wei F (2019) Carbon nanotube- and graphene-based nanomaterials and applications in high-voltage supercapacitor: a review. Carbon 141. https://doi.org/10.1016/j.carbon.2018.10.010

189. Kumanek B, Janas D (2019) Thermal conductivity of carbon nanotube networks: a review. J Mater Sci 54(10). https://doi.org/10.1007/s10853-019-03368-0

190. Yamashita S (2012) A tutorial on nonlinear photonic applications of carbon nanotube and graphene. J Lightwave Technol 30(4). https://doi.org/10.1109/JLT.2011.2172574

191. Wang J (2005) Carbon-nanotube based electrochemical biosensors: a review. Electroanalysis 17(1). https://doi.org/10.1002/elan.200403113

192. Fam DWH, Palaniappan A, Tok AIY, Liedberg B, Moochhala SM (2011) A review on technological aspects influencing commercialization of carbon nanotube sensors. Sensors Actuators B Chem 157(1). https://doi.org/10.1016/j.snb.2011.03.040

193. Castillo-Henríquez L, Brenes-Acuña M, Castro-Rojas A, Cordero-Salmerón R, Lopretti-Correa M, Vega-Baudrit JR (2020) Biosensors for the detection of bacterial and viral clinical pathogens. Sensors (Switzerland) 20(23). https://doi.org/10.3390/s20236926

194. Mahar B, Laslau C, Yip R, Sun Y (2007) Development of carbon nanotube-based sensors – a review. IEEE Sensors J 7(2). https://doi.org/10.1109/JSEN.2006.886863

195. Li C, Thostenson ET, Chou TW (2008) Sensors and actuators based on carbon nanotubes and their composites: a review. Compos Sci Technol 68(6). https://doi.org/10.1016/j.compscitech.2008.01.006

196. Her SC, Hsu WC (2020) Strain and temperature sensitivities along with mechanical properties of CNT Buckypaper sensors. Sensors (Switzerland) 20(11). https://doi.org/10.3390/s20113067

197. Zhang X, Cui H, Gui Y, Tang J (2017) Mechanism and application of carbon nanotube sensors in SF6 decomposed production detection: a review. Nanoscale Res Lett 12(1). https://doi.org/10.1186/s11671-017-1945-8

198. Pandhi T, Chandnani A, Subbaraman H, Estrada D (2020) A review of inkjet printed graphene and carbon nanotubes based gas sensors. Sensors (Switzerland) 20(19). https://doi.org/10.3390/s20195642

199. Shi J-X, Lei X-W, Natsuki T (2021) Review on carbon nanomaterials-based nano-mass and nano-force sensors by theoretical analysis of vibration behavior. Sensors 21(5):1907. https://doi.org/10.3390/s21051907

200. Sauerbrey G (1959) Verwendung von Schwingquarzen zur Wägung dünner Schichten und zur Mikrowägung. Z Phys 155(2). https://doi.org/10.1007/BF01337937

201. Davis ZJ et al (2003) Monolithic integration of mass sensing nano-cantilevers with CMOS circuitry. Sens Actuators A Phys 105(3). https://doi.org/10.1016/S0924-4247(03)00208-5

202. Ono T, Li X, Miyashita H, Esashi M (2003) Mass sensing of adsorbed molecules in sub-picogram sample with ultrathin silicon resonator. Rev Sci Instrum 74(3). https://doi.org/10.1063/1.1536262

203. Forsen E et al (2005) Ultrasensitive mass sensor fully integrated with complementary metal-oxide-semiconductor circuitry. Appl Phys Lett 87(4). https://doi.org/10.1063/1.1999838

204. Naik AK, Hanay MS, Hiebert WK, Feng XL, Roukes ML (2009) Towards single-molecule nanomechanical mass spectrometry. Nat Nanotechnol 4(7). https://doi.org/10.1038/nnano.2009.152

205. Barton RA, Ilic B, Verbridge SS, Cipriany BR, Parpia JM, Craighead HG (2010) Fabrication of a nanomechanical mass sensor containing a nanofluidic channel. Nano Lett 10(6). https://doi.org/10.1021/nl100193g

206. Gil-Santos E et al (2010) Nanomechanical mass sensing and stiffness spectrometry based on two-dimensional vibrations of resonant nanowires. Nat Nanotechnol 5(9). https://doi.org/10.1038/nnano.2010.151

207. Hanay MS et al (2012) Single-protein nanomechanical mass spectrometry in real time. Nat Nanotechnol 7(9). https://doi.org/10.1038/nnano.2012.119

208. Wasisto HS, Merzsch S, Waag A, Uhde E, Salthammer T, Peiner E (2013) Airborne engineered nanoparticle mass sensor based on a silicon resonant cantilever. Sensors Actuators B Chem 180. https://doi.org/10.1016/j.snb.2012.04.003

209. Olcum S, Cermak N, Wasserman SC, Manalis SR (2015) High-speed multiple-mode mass-sensing resolves dynamic nanoscale mass distributions. Nat Commun 6. https://doi.org/10.1038/ncomms8070

210. Hanay MS, Kelber SI, O'Connell CD, Mulvaney P, Sader JE, Roukes ML (2015) Inertial imaging with nanomechanical systems. Nat Nanotechnol 10(4). https://doi.org/10.1038/nnano.2015.32

211. Cermak N et al (2016) High-throughput measurement of single-cell growth rates using serial microfluidic mass sensor arrays. Nat Biotechnol 34(10). https://doi.org/10.1038/nbt.3666

212. Sader JE, Hanay MS, Neumann AP, Roukes ML (2018) Mass spectrometry using nanomechanical systems: beyond the point-mass approximation. Nano Lett 18(3). https://doi.org/10.1021/acs.nanolett.7b04301

213. Bunch JS et al (2007) Electromechanical resonators from graphene sheets. Science (1979) 315(5811). https://doi.org/10.1126/science.1136836

214. Jensen K, Kim K, Zettl A (2008) An atomic-resolution nanomechanical mass sensor. Nat Nanotechnol 3(9). https://doi.org/10.1038/nnano.2008.200

215. Eom K, Park HS, Yoon DS, Kwon T (2011) Nanomechanical resonators and their applications in biological/chemical detection: nanomechanics principles. Phys Rep 503(4–5). https://doi.org/10.1016/j.physrep.2011.03.002

216. Chaste J, Eichler A, Moser J, Ceballos G, Rurali R, Bachtold A (2012) A nanomechanical mass sensor with yoctogram resolution. Nat Nanotechnol 7(5). https://doi.org/10.1038/nnano.2012.42

217. Chen HJ, di Zhu K (2014) Graphene-based nanoresonator with applications in optical transistor and mass sensing. Sensors (Switzerland) 14(9). https://doi.org/10.3390/s140916740

218. Wang Q, Arash B (2014) A review on applications of carbon nanotubes and graphenes as nano-resonator sensors. Comput Mater Sci 82. https://doi.org/10.1016/j.commatsci.2013.10.010

219. Asadi E, Askari H, Behrad Khamesee M, Khajepour A (2017) High frequency nano electromagnetic self-powered sensor: concept, modelling and analysis. Measurement (Lond) 107. https://doi.org/10.1016/j.measurement.2017.04.019

220. Duan K, Li L, Hu Y, Wang X (2017) Pillared graphene as an ultra-high sensitivity mass sensor. Sci Rep 7(1). https://doi.org/10.1038/s41598-017-14182-6

221. Kwon SH, Kim HJ, Choi WS, Kang H (2018) Development and performance analysis of carbon nanowall-based mass sensor. J Nanosci Nanotechnol 18(9). https://doi.org/10.1166/jnn.2018.15699

222. Ricci F, Cuairan MT, Conangla GP, Schell AW, Quidant R (2019) Accurate mass measurement of a levitated nanomechanical resonator for precision force-sensing. Nano Lett 19(10). https://doi.org/10.1021/acs.nanolett.9b00082

223. Hierold C, Jungen A, Stampfer C, Helbling T (2007) Nano electromechanical sensors based on carbon nanotubes. Sensors Actuators A Phys 136(1). https://doi.org/10.1016/j.sna.2007.02.007

224. Li CY, Chou TW (2004) Strain and pressure sensing using single-walled carbon nanotubes. Nanotechnology 15(11). https://doi.org/10.1088/0957-4484/15/11/021

225. Wu DH, Chien WT, Chen CS, Chen HH (2006) Resonant frequency analysis of fixed-free single-walled carbon nanotube-based mass sensor. Sens Actuators A Phys 126(1). https://doi.org/10.1016/j.sna.2005.10.005

226. Li Y, Qiu X, Yang F, Wang XS, Yin Y (2008) Ultra-high sensitivity of super carbon-nanotube-based mass and strain sensors. Nanotechnology 19(16). https://doi.org/10.1088/0957-4484/19/16/165502

227. Chowdhury R, Adhikari S, Mitchell J (2009) Vibrating carbon nanotube based bio-sensors. Physica E Low Dimens Syst Nanostruct 42(2). https://doi.org/10.1016/j.physe.2009.09.007

228. Georgantzinos SK, Anifantis NK (2010) Carbon nanotube-based resonant nanomechanical sensors: a computational investigation of their behavior. Physica E Low Dimens Syst Nanostruct 42(5). https://doi.org/10.1016/j.physe.2010.02.002

229. Joshi AY, Harsha SP, Sharma SC (2010) Vibration signature analysis of single walled carbon nanotube based nanomechanical sensors. Physica E Low Dimens Syst Nanostruct 42(8). https://doi.org/10.1016/j.physe.2010.03.033

230. Cho SH, Choi MS, Kang DK, Lee JH, Kim CW (2015) Analysis on mass sensing characteristics of SWCNT-based nano-mechanical resonators using continuum mechanics based finite element analysis. J Mech Sci Technol 29(11). https://doi.org/10.1007/s12206-015-1027-8

231. Lee HL, Hsu JC, Chang WJ (2010) Frequency shift of carbon-nanotube-based mass sensor using nonlocal elasticity theory. Nanoscale Res Lett 5(11). https://doi.org/10.1007/s11671-010-9709-8

232. Aydogdu M, Filiz S (2011) Modeling carbon nanotube-based mass sensors using axial vibration and nonlocal elasticity. Physica E Low Dimens Syst Nanostruct 43(6). https://doi.org/10.1016/j.physe.2011.02.006

233. Mehdipour I, Barari A, Domairry G (2011) Application of a cantilevered SWCNT with mass at the tip as a nanomechanical sensor. Comput Mater Sci 50(6). https://doi.org/10.1016/j.commatsci.2011.01.025

234. Shen ZB, Tang GJ, Zhang L, Li XF (2012) Vibration of double-walled carbon nanotube based nanomechanical sensor with initial axial stress. Comput Mater Sci 58. https://doi.org/10.1016/j.commatsci.2012.02.011

235. Shen ZB, Li DK, Li D, Tang GJ (2012) Frequency shift of a nanomechanical sensor carrying a nanoparticle using nonlocal Timoshenko beam theory. J Mech Sci Technol 26(5). https://doi.org/10.1007/s12206-012-0338-2

236. Natsuki T, Matsuyama N, Shi JX, Ni QQ (2014) Vibration analysis of nanomechanical mass sensor using carbon nanotubes under axial tensile loads. Appl Phys A Mater Sci Process 116(3). https://doi.org/10.1007/s00339-014-8289-3

237. Natsuki T, Matsuyama N, Ni QQ (2015) Vibration analysis of carbon nanotube-based resonator using nonlocal elasticity theory. Appl Phys A Mater Sci Process 120(4). https://doi.org/10.1007/s00339-015-9398-3

238. Bouchaala A, Nayfeh AH, Younis MI (2016) Frequency shifts of micro and nano cantilever beam resonators due to added masses. J Dyn Syst Meas Control, Trans ASME 138(9). https://doi.org/10.1115/1.4033075

239. Eltaher MA, Agwa MA (2016) Analysis of size-dependent mechanical properties of CNTs mass sensor using energy equivalent model. Sens Actuators A Phys 246. https://doi.org/10.1016/j.sna.2016.05.009

240. Eltaher MA, Agwa MA, Mahmoud FF (2016) Nanobeam sensor for measuring a zeptogram mass. Int J Mech Mater Des 12(2). https://doi.org/10.1007/s10999-015-9302-5

241. Ghaffari SS, Ceballes S, Abdelkefi A (2019) Effects of thermal loads representations on the dynamics and characteristics of carbon nanotubes-based mass sensors. Smart Mater Struct 28(7). https://doi.org/10.1088/1361-665X/ab1e25

242. Ghaffari SS, Ceballes S, Abdelkefi A (2020) Nonlinear dynamical responses of forced carbon nanotube-based mass sensors under the influence of thermal loadings. Nonlinear Dyn 100(2). https://doi.org/10.1007/s11071-020-05565-y

243. Tsiamaki AS, Georgantzinos SK, Anifantis NK (2014) Monolayer graphene resonators for mass detection: a structural mechanics feasibility study. Sens Actuators A Phys 217. https://doi.org/10.1016/j.sna.2014.06.015

244. Xu C, Rong D, Tong Z, Zhou Z, Hu J, Deng Z (2020) Analytical modeling of a magnetically affected cantilever nanoplate-based mass detector. Superlattice Microst 137. https://doi.org/10.1016/j.spmi.2019.106338

245. Xu C, Qu J, Rong D, Zhou Z, Leung AYT (2021) Theory and modeling of a novel class of nanoplate-based mass sensors with corner point supports. Thin-Walled Struct 159. https://doi.org/10.1016/j.tws.2020.107306

246. Natsuki T, Shi JX, Ni QQ (2013) Vibration analysis of nanomechanical mass sensor using double-layered graphene sheets resonators. J Appl Phys 114(9). https://doi.org/10.1063/1.4820522

247. Lei XW, Natsuki T, Shi JX, Ni QQ (2013) An atomic-resolution nanomechanical mass sensor based on circular monolayer graphene sheet: theoretical analysis of vibrational properties. J Appl Phys 113(15). https://doi.org/10.1063/1.4802438

248. Shen ZB, Tang HL, Li DK, Tang GJ (2012) Vibration of single-layered graphene sheet-based nanomechanical sensor via nonlocal Kirchhoff plate theory. Comput Mater Sci 61. https://doi.org/10.1016/j.commatsci.2012.04.003

249. Lee HL, Yang YC, Chang WJ (2013) Mass detection using a graphene-based nanomechanical resonator. Jpn J Appl Phys 52(2). https://doi.org/10.7567/JJAP.52.025101

250. Jalali SK, Naei MH, Pugno NM (2015) A mixed approach for studying size effects and connecting interactions of planar nano structures as resonant mass sensors. Microsyst Technol 21(11). https://doi.org/10.1007/s00542-014-2362-x

251. Zhou SM, Sheng LP, Shen ZB (2014) Transverse vibration of circular graphene sheet-based mass sensor via nonlocal Kirchhoff plate theory. Comput Mater Sci 86. https://doi.org/10.1016/j.commatsci.2014.01.031

252. Natsuki T (2015) Theoretical analysis of vibration frequency of graphene sheets used as nanomechanical mass sensor. Electronics (Switzerland) 4(4). https://doi.org/10.3390/electronics4040723

253. Natsuki T, Yiwada A, Natsuki J (2017) Influence of temperature on vibrational frequency of graphene sheet used as nano-scale sensing. C (Basel) 3(4). https://doi.org/10.3390/c3010004

254. Shen ZB, Jiang RW, Zhang L, Tang GJ (2018) Nonlocal galerkin strip transfer function method for vibration of double-layered graphene mass sensor. Acta Mechanica Solida Sinica 31(1). https://doi.org/10.1007/s10338-018-0003-0

255. Li H, Wang X, Wang H, Chen J (2020) The nonlocal frequency behavior of nanomechanical mass sensors based on the multi-directional vibrations of a buckled nanoribbon. Appl Math Model 77. https://doi.org/10.1016/j.apm.2019.09.023
256. Liu M, Artyukhov VI, Lee H, Xu F, Yakobson BI (2013) Carbyne from first principles: chain of c atoms, a nanorod or a nanorope. ACS Nano 7(11). https://doi.org/10.1021/nn404177r
257. Shi JX, Liu Y, Shimoda M (2015) Vibration analysis of a carbyne-based resonator in nano-mechanical mass sensors. J Phys D Appl Phys 48(11). https://doi.org/10.1088/0022-3727/48/11/115303
258. Agwa MA, Eltaher MA (2016) Vibration of a carbyne nanomechanical mass sensor with surface effect. Appl Phys A Mater Sci Process 122(4). https://doi.org/10.1007/s00339-016-9934-9

Breath Analysis as Part of Pulmonary Function Diagnostics

Meike Aufderhaar

Contents

Abstract Modern methods of pulmonary function diagnosis include spirometry, body plethysmography and a variety of other common tests used to assess a patient's respiratory status. Additional procedures such as different forms of blood gas analysis applications are available and can be supplemented by an analysis of

M. Aufderhaar (✉)
Niederlauer, Germany

expiratory carbon dioxide in the form of capnometry or capnovolumetry. In the field of exhaled breath components analysis, measurement of the fraction of exhaled nitrogen oxide has proven to be an additional means of supporting the diagnostic process. The aforementioned lung function tests form the basis for further breath tests since they allow other biomarkers, e.g., certain volatile organic compounds, to be interpreted in the physiological context. Hence, the lung function tests provide important additional information for the correct interpretation of the breath tests.

Keywords Blood gas analysis · Capnovolumetry · FeNO · Pulmonary function test

Abbreviations

ARTP	Association for Respiratory Technology & Physiology
ATS	American Thoracic Society
BGA	Blood gas analysis
BTPS	Body temperature, pressure, saturated with water vapour
CO	Carbon oxide
CO_2	Carbon dioxide
COPD	Chronic obstructive pulmonary disease
CPET	Cardio pulmonary exercise test
DLCO	Diffusion capacity of the lung for carbon monoxide
DLNO	Diffusing capacity of the lung for nitric oxide
DLO	Diffusing capacity of the lung for oxygen
ECG	Electrocardiogram
ERS	European Respiratory Society
ERV	Expiratory reserve volume
FeNO	Fractional exhaled nitric oxide
$FeNO_{50}$	Fractional exhaled nitric oxide, measured at a flow of 50 ml/s
FEV1	Forced expiratory volume in 1 s
FOT	Forced oscillation technique
FRC	Functional residual capacity
FVC	Forced vital capacity
GOLD	Global initiative for chronic obstructive lung disease
H^+	Hydron
Hb	Haemoglobin
HCO_3^-	Standard bicarbonate
ICS	Inhaled corticosteroids
IOS	Impulse oscillometry
IRV	Inspiratory reserve volume
LED	Light emitting diode
LCI	Lung clearance index
NO	Nitric oxide
O_2	Oxygen

pCO_2	Partial pressure of carbon dioxide
P0.1	Mouth closure pressure at 0.1 seconds
$PaCO_2$	Arterial partial pressure of carbon dioxide
PaO_2	Arterial partial pressure of oxygen
PEF	Peak expiratory flow
PE_{max}	Maximal static expiratory pressure
PI_{max}	Maximal static inspiratory pressure
pO_2	Partial pressure of oxygen
ppb	Parts per billion
RER	Respiratory exchange ratio
RV	Residual volume
TLC	Total lung capacity
TGV	Thoracic gas volume
TLCO	Transfer factor of the lung for carbon monoxide
SaO_2	Arterial oxygen saturation
SF_6	Sulphur hexafluoride
SpO_2	Pulse oximetry oxygen saturation
SNIP	Sniff Nasal inspiratory pressure
VC	Vital capacity
VT	Tidal volume
VCO_2	Carbon dioxide output
VO_2	Oxygen uptake
VO_2max	Maximum oxygen uptake

1 Introduction

Additionally to the composition of the expired gas that is subject of the volatile organic compound analysis, lung function diagnostic has traditionally been inflicted with the mechanics of breathing. Pressure, flow and volume are the measurable mechanical variables that can be used to characterize the lung function and model it.

Lung diseases are on the rise worldwide. They have increased disproportionately in relation to other diseases in internal medicine and are of significant importance in terms of morbidity, mortality and also health related expenses [1]. Infamous examples are chronic obstructive pulmonary disease (COPD) and asthma. COPD is one of the leading causes of death in both developing and developed countries. Approximately 170 million people suffer from this lung disease which has a strong impact on the quality of life of those affected [2–4]. It is characterized by a non-reversible airflow limitation which usually progresses over time. The lung tissue reacts with an abnormal inflammatory response to exogenous noxious particles, resulting, for example, from cigarette smoking or air pollution [5]. Asthma is one of the most common chronic diseases that can occur at any age. The disease is characterized by chronic inflammation and increased sensitivity of the bronchi to inhaled substances

and stimuli. Consequently, airway obstruction can occur [6]. In contrast to COPD, in asthma the obstruction is usually reversible if the trigger substances are avoided. According to different estimates, about 235 to more than 300 million people worldwide are affected by bronchial asthma [2, 6].

More than 175 years ago, in the year 1846, John Hutchinson introduced an apparatus to the world that should become the gold standard of diagnosing lung function. He framed the important terms still in use today, spirometer and vital capacity [7]. Early spirometers were closed systems with a diving bell inside a water tank that changed its height depending on the volume the patient was breathing into the system via a tube. The change of height could be directly measured [7]. Since then, great advances in sensor technology and diagnostics have been achieved to further refine the diagnostic of lung function. The use of the parameter describing the forced expiratory volume in 1 s, FEV1, was proposed in 1947. The first peak flow meter has been created in 1959. The flow-volume-curve that is utilized today to depict spirometry results became famous in its current form in the late 1950s to the early 1960s [7].

Methods such as spirometry and body plethysmography have since then become established standards for the first assessment of lung function and lung function deficiencies. However, as these rather mechanical methods are not within the objective of this book, they shall only be briefly mentioned here. The exact procedures are described in detail and extensively in other publications. For detailed procedural information, among others, guidelines from the American Thoracic Society (ATS), European Respiratory Society (ERS) and Association for Respiratory Technology & Physiology (ARTP) are available. Some diagnostic procedures of the area of lung function assessment make use of the gases that participate in the natural gas exchange, such as, for example, oxygen, carbon dioxide and nitrogen, which does not participate in the respiratory exchange to a notable amount but is present in the ambient air. These methods such as single-breath diffusion measurement and the nitrogen washout procedure will also be described in the following chapters. As these gases are present in the human blood, blood gas analysis is also considered a part of lung function diagnostics.

Though breath analysis is usually known for revealing systemic issues by detecting the volatile blood compounds emitted via the lungs in the exhaled breath, blood gas analysis can work vice versa. Emphasis shall be put on the development on newer measurement techniques of exhaled breath compounds. Foremost, lots of research has been conducted in the last years on capnometry and capnovolumetry, respectively, to assess obstructive conditions and matters of gas exchange in mammalian lungs. A recent approach has been to analyse the fractional exhaled nitrogen monoxide (FeNO), which has proven useful in the diagnostic and monitoring of asthma.

Summarizing, this chapter provides an overview of rather seldom mentioned techniques in breath analysis related literature including body plethysmography or spirometry but furthermore discusses methods of analysing the gas exchange functionality of highly abundant gases like oxygen in the lungs. Those techniques provide vital information over the functionality of a patient's or test person's lung,

which must be accounted for as well in modern breath analysis. Finally, modern measurement techniques like capnovolumetry or FeNO, tackling diseases like asthma or COPD, will be closing the chapter.

## 2 Modern Lung Function Diagnostic

Breath is a mixture of gas consisting of the gases present in ambient air, mainly nitrogen, oxygen carbon dioxide and traces of argon. Additionally, it can contain all kinds of environmentally present pollutants and organic compounds. Those substances are characterized as exogenous. Metabolic, endogenous compounds such as isoprene and acetone can be found in exhaled breath as well.

Breathing patterns and posture during measurements have a high impact on the measurement results. Hypoventilation or hyperventilation induce haemodynamic changes that alter the expiratory patterns of the gas mixture. Similar effects can occur after deep inhalation or forcefully executed exhalations [8]. Therefore, for many diagnostic approaches, standard breathing patterns have been agreed upon. In others, standard breathing patterns have yet to be developed and introduced for better comparability of different studies.

Pulmonary functions tests are used to diagnose and assess mainly airway obstruction in terms of severity and prognosis. Age, height, sex and ethnicity influence lung function and must be taken into account in the respective context [9]. If the analysis of volatile organic compounds requires a defined and standardized breathing manoeuvre from a patient, it might be sensible to perform a pulmonary function test beforehand to assess the patient's ability to cope and meet the required standards. Limitations of the lung function could influence the assessment of the volatile organic compounds analysis. Results of pulmonary function tests should then be taken into account when evaluating the results. The state-of-the-art methods of lung function diagnostic will be briefly presented in this chapter.

2.1 Spirometry

Spirometry is currently considered to be the gold standard of lung function diagnostics and is the most widely used pulmonary function test in clinical practice and primary care [2, 7, 10, 11]. It is often used to get a first impression of the patient's respiratory health and essential to respiratory disease diagnosis and management [7, 12]. Spirometry can be used to determine various volumes of the lungs, including tidal volume (VT), inspiratory and expiratory reserve volume (IRV, ERV) and vital capacity (VC), as shown in Fig. 1. A whole-body plethysmography measurement is necessary to determine the residual volume (RV) that remains in the lungs even after an exhalation performed under maximum effort. Total lung capacity (TLC) can therefore only be determined via plethysmography [13, 14]. To measure dynamic
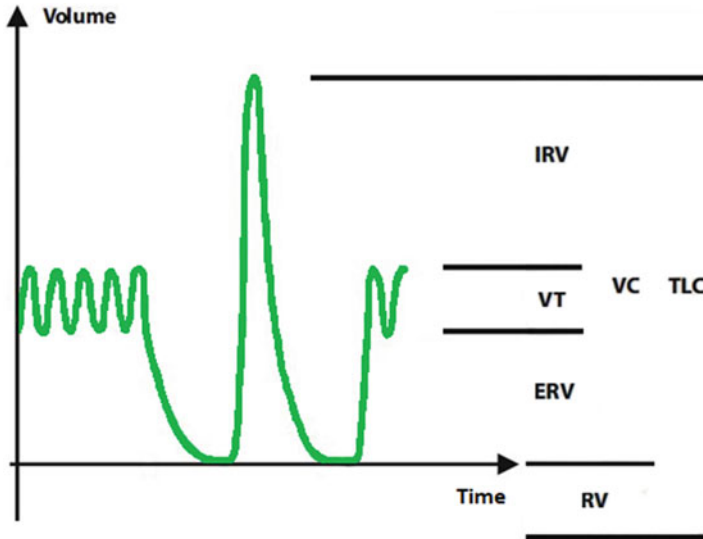
Fig. 1 Spirogram, representation of inhaled and exhaled volume over time

breathing parameters, a Tiffeneau test is performed to determine the forced expiratory volume in 1 s (FEV1), the peak expiratory flow (PEF) and the forced vital capacity (FVC) [14]. In the forced manoeuvre, the patient's cooperation is essential for obtaining usable measurement results. Spirometry aids physician in the diagnostic of the severity of a condition and is often used as a monitoring tool for regular check-ups in various lung diseases, such as COPD, asthma or cystic fibrosis [15].

Early spirometers consisted of a closed tube system with a diving bell in which a float changed its height depending on inhalation and exhalation. This change in height is displayed over time with the help of a recorder [14]. Modern spirometers measure the flow rate during inspiration and expiration and determine the respiratory volumes by mathematical integration of the determined flow. Thus, in addition to the spirogram, a flow-volume curve can be obtained, which can be used to better assess dynamic breathing parameters [16].

Turbines, pneumotachographs or ultrasonic sensors are used for spirometry measurement. The ultrasonic measurement method is considered the most accurate because no secondary parameters such as pressure drop or rotational speed need to be measured and it is calibration-free. Two diagonally opposed ultrasonic transducers, which penetrate the respiratory flow at a defined angle, measure the difference in transit time of two signals. In the process, one signal is accelerated and the other is slowed down. Gas properties, temperature and humidity are the same in both measurement directions and have no influence on the measurement. The measured transit time difference is proportional to the respiratory flow, which is integrated to the volume. Spirometers that directly co-determine temperature and humidity perform the BTPS (body temperature, pressure, saturated with water vapour) correction of the values obtained internally during the measurement [17].

One of the important limitations of spirometry to consider is its inability to represent the condition of the peripheral airways as each of those only contributes little to the cumulative flow that is measured at the mouth. Therefore, spirometry is less sensitive in detecting peripheral airway changes compared to other measurement techniques such as, for example, the forced oscillation technique [7, 18]. Additionally, the spirometry measurement relies on forced expiratory manoeuvres and therefore does not represent the state of the lung function during normal tidal breathing [7].

In order to investigate the applicability and reliability of spirometers, especially in children and elderly people, several studies have been conducted in recent years. There is disagreement about the age at which valid results can be obtained with spirometry [7]. The current guidelines of the ATS suggest that spirometry could be performed from 2.5 years of age [17]. The British Association for Respiratory Technology & Physiology states that often spirometry can be successfully performed from the age of 3 years [16] and prediction equations have been published by Quanjer et al. for the age range from 3 to 95 [9]. Lo et al. found in their study that quality spirometry could be achieved in children as young as 5 years of age [19], whereas Lundberg et al. believe it still to be a challenge at 6 years of age, although it is possible to obtain valid data [10]. For elderly patients, Melo et al. found that the majority of them are able to perform a valid spirometry measurement if no cognitive deficits are present. Other comorbidities were not an obstacle [11].

To investigate various lung diseases such as asthma, COPD or cystic fibrosis in detail and to assess patients' condition post stem cell and lung transplantation, the use of home spirometry has been studied [7]. Home measurements have correlated with measurements performed at a clinic, as Noth et al. proved recently. Home spirometry offers great potential as it is easy to perform for cooperative patients. Having a spirometry device as home, patients can provide frequent measurements to contribute to earlier detection of disease progression or acute exacerbations [20].

2.2   Body Plethysmography

In contrast to spirometry, a body plethysmography measurement requires a much higher level of equipment. Consequently, it is able to provide additional information. Residual volume and airway resistance can be determined. Knowing the residual volume, the thoracic gas volume (TGV) can also be determined. The additional time required is low. For those reasons, the whole-body plethysmography (comprising a spirometry measurement) is regarded as the gold standard for advanced pulmonary function testing [21, 22]. The body plethysmograph is an airtight cabin that includes a spirometry sensor that is equipped with a shutter. The measurement is largely independent of patient cooperation and not physically strenuous. The patient's tidal breathing is measured continuously due to ventilation-related volume changes or compression/decompression, the pressure is measured continuously and displayed as a so-called breathing loop, representing flow over shift volume, as shown in Fig. 2.

Fig. 2 Resistance curves, representation of flow over shift volume. 1 normal curve of a healthy individual, 2 curve of a present obstruction
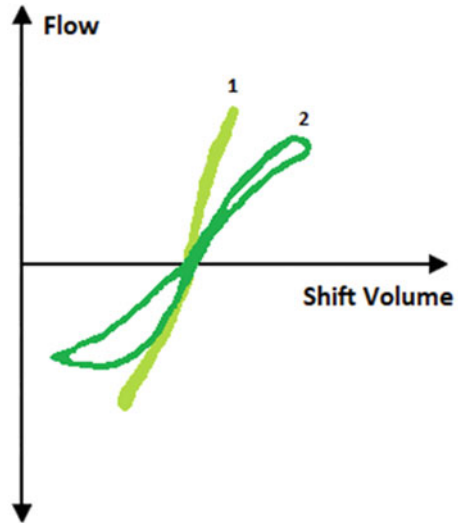
The specific airway resistance is an expression of the work of breathing determined by a straight line through the breathing loop [23].

The measurement of thoracic gas volume is based on Boyle and Mariotte's law of physics, according to which the product of pressure and volume is constant. The lung volume at a particular time in the respiratory cycle (e.g. the thoracic gas volume at the end of normal expiration/resting breathing) can be calculated by automatically closing the shutter for a short time at the end-expiratory peak of tidal breathing, when the alveolar pressure closely approximates the pressure at the mouthpiece. The patient is asked to continue to breathe frustratingly against the shutter. The actual airway resistance can be calculated by putting the specific airway resistance into relation to the lung volume [16, 23, 24].

The basic assumption of the body plethysmography measurement is the isothermal behaviour of the changes of pressure and volume inside the cabin. However, it is not entirely clear to what extent heat may be lost through the walls during the patient's respiration that causes changes in temperature and humidity inside the plethysmograph. In prolonged measurements, a resulting drift of the signal must be corrected [25]. It is assumed that the pressure changes in the lungs are uniform. Another assumption is the equivalence of the pressure at the mouth and the pressure in the alveoli at the end of expiration. This might not always be the case in airway obstruction because of the time needed to achieve the equilibrium and therefore the total thoracic gas volume might be overestimated [16].

The body plethysmography measurement includes all the volumes in the thoracic cage including trapped gas compartments [14, 22]. Abdominal gas is believed to be negligible although it is not recommended to consume fizzy beverages prior to a measurement [16]. Limiting factors of body plethysmography are the large volume and the immobility of the cabin, which are associated with high costs and regular

maintenance. The manoeuvres required are comparable to those of spirometry in terms of complexity and patient compliance [12, 21].

Gupta et al. recently assessed parameters of spirometry and body plethysmography in the male Indian population. They described that, in contrast to body plethysmography, spirometry could not differentiate between healthy controls and smokers with COPD and they conclusively recommend body plethysmography for the early detection of changes in pulmonary function. Damages to the lung tissue caused by smoking could be reduced when smokers manage to quit timely [4].

Dreher et al. found an alarmingly high prevalence of undiagnosed COPD in a study of patients with acute myocardial infarction undergoing percutaneous coronary intervention. In 80% of the COPD patients of the study, the disease was not treated. They recommend a general pulmonary workup for patients with myocardial infarction and coronary heart disease [26]. These results underline the close connection between pulmonary and cardiac diseases. Body plethysmography could be used for routine screening for COPD. A combination of spirometry and body plethysmography has been found feasible for asthma control in children in a study by Korten et al. No single lung function parameter could indicate a difference between controlled and uncontrolled asthma [27].

Body plethysmography has become an important tool as well in clinical practice as in biomedical research. It can even be used to analyse respiration in non-anaesthetized animals in preclinical studies and enable the observation of effects such as sighing or sniffing [28].

2.3   Occlusion Pressure

The ventilation of the lung is driven by the so-called respiratory pump, which consists of the respiratory centre, nerves and respiratory muscles. By measuring the occlusion pressure maximum respiratory muscle strength and current load can be determined. Just like other muscles the inspiratory muscles are fatigable when overstrained. Since it is not possible to assess the respiratory muscle strength directly, the airway pressure is measured as a surrogate of their output. The respiratory muscle strength is therefore determined by measuring the pressure at the mouth with a closed shutter and with different breathing manoeuvres [16, 24].

To measure the current load (P0.1), the mouth closure pressure is determined 0.1 s after the start of the inspiration during tidal breathing with the shutter closed. The measured pressure is proportional to the inspiratory pressure or pleural pressure [24]. The pressure that is generated by the respiratory muscles is reflected by the maximal static inspiratory pressure (PI_{max}) and maximal static expiratory pressure (PE_{max}). The respiratory muscle strength is dependent on the lung volume during the test because this influences the operating length of the muscle fibres. To measure PI_{max}, the pressure is measured during a forced inspiratory manoeuvre against the shutter. To measure PE_{max}, the pressure is similarly measured during a sustained forceful expiration from total lung volume [16, 24]. P0.1 is also measured with

specialized ventilators in intensive care settings to assess the respiratory drive in ventilated patients before undergoing weaning trials [29]. P0.1 is increased in case of respiratory muscle weakness, for example, in diseases like amyotrophic lateral sclerosis, as recently described by Pinto et al. [30].

Another possibility to assess the inspiratory muscle strength non-invasively is the so-called SNIP test, the Sniff Nasal Inspiratory Pressure. For this test, one nostril is equipped with a catheter connected to a pressure sensor. The duration of a sniff should be less than 0.5 s. This test is simple for patients to perform since sniffing is a natural manoeuvre that does not require special training. Therefore, it is suitable for children from the age of 4 years. Pressure values obtained with the SNIP test usually exceed those of PI_{max}. The common approach to assessing inspiratory muscle strength is to perform both PI_{max} and SNIP measurements [16].

With the occlusion pressure measurement, it is possible to detect limitations of the maximum inspiratory force (capacity), as well as increased strain (load) on the inspiratory muscles. Possible causes can be chronic diseases or acute diseases with reduced maximum inspiratory force or overuse of the inspiratory muscles due to increased load. In the case of larger interindividual deviations, the method is only suitable to a limited extent for determining general degrees of severity. However, it is suitable for assessing the course of the disease if the intraindividual results are stable [16, 24].

2.4 Forced Oscillation Technique

Forced oscillation technique (FOT), or in short oscillometry, provides another non-invasive way to assess the lung function. It can be used in clinical settings such as lung function laboratories and the intensive care unit as well as for field testing or home monitoring. Forced oscillations are brought to the lung by a loudspeaker during the patient's tidal breathing and allow to measure the respiratory system impedance [10, 18, 31–34]. The impulse oscillometry (IOS) is a variant of this technique, where a series of pulses is applied [7, 31, 32, 35].

During tidal breathing, the oscillometry assesses the respiratory impedance, which is comprised of the system's resistance and reactance. Those are measured and displayed as a function of the different applied frequencies. The resistance represents the size and diameter of the airway. Elastic and inert properties of the respiratory system are represented by the reactance [7, 18, 34, 36–38]. The use of multiple waveforms has been described in literature. Either single-frequency sine waves or multi-frequency pressure waves can be applied at the patient's mouth during tidal breathing [7, 10, 32]. The typically applied frequency range is between 5 and 50 Hz, with the majority of publications reporting ranges from 5 to 35 Hz [34, 36–38]. The lower frequencies (5 Hz) are capable of penetrating deep into the

periphery and small airways, whereas mid- to high frequencies only reach the proximal airways [39, 40].

The distribution of resistances, elastances and inertances within the lung is heterogeneous, even for healthy lungs. This explains the frequency dependence. At frequencies decreasing below 5 Hz, the reactance is more negative whereas the resistance increases. When the frequency increases, the elastance decreases, so that the reactance in total becomes less negative. Consequently, at higher frequencies inertance becomes positive [34]. The frequency at which inertance and elastance are equal, so that the reactance becomes zero, is called the resonance frequency [34, 38]. Norm values for the resonance frequency from healthy adults range from 8 to 12 Hz, while children have higher resonance frequencies [34]. Also in lung diseases, where typically a decreased reactance can be seen, while the resistance is increased, the resonance frequency tends to move to higher frequencies.

Oscillometry measurements should be performed before testing methods that require forced breathing manoeuvres and deep breaths (such as spirometry, diffusing capacity or FeNO measurement) are carried out as those are known to have an effect on the lung function and bronchial tonus [34, 41, 42]. The forced oscillation technique is in particular useful to assess the function of the small airways. The function of the large airways is pronounced in spirometry measurements and the gas exchange can be assessed with a diffusion measurement. Therefore, the oscillometry offers a possibility to assess the so-called silent zone in between. The reactance parameters of the oscillometry measurements are found to be far more sensitive than spirometry to assess peripheral airway diseases. It shows mild cases of obstruction much earlier than a spirometry measurement [10, 18, 32, 35, 36, 38, 40, 43].

Cho et al. showed that about 75% of the small airways must be affected from obstruction before changes can be detected by measuring the FEV1 [39]. The forced oscillation technique is also more sensitive to determine bronchoconstriction than spirometry. Oscillation measurement and spirometry are equally able to identify exercise-induced bronchoconstriction [34, 44]. For the monitoring and follow-up programmes for the treatments of diseases like asthma oscillometry might therefore provide supplementary and clinically relevant information as it correlates better with respiratory symptoms [7, 10, 18, 34, 36, 37]. It is also a useful tool to spot rejection reactions after lung transplantation in a very early stage. In spirometry, the effects appear up to 2 weeks later [39].

Forced oscillation technique also proves a suitable alternative for patients that are unable to perform a satisfactory spirometry, especially children or elderly patients. It demands less cooperation of the patient as it only requires tidal breathing but no complex manoeuvres, so it can be performed more easily and quickly. The measurement can be repeated as needed without stressing and exhausting the patient [32–34, 36, 37, 39, 40, 43, 44]. However, the direct correlations between spirometry and oscillometry outcomes have not proven feasible and have been described to be moderate at best [10].

According to Lundblad et al., oscillometry has already become the gold standard in laboratory animal research [43]. Problematic for the clinical use of oscillometry

are the substantial differences of the commercially available devices in measurement duration, frequency content, waveform and intensity of oscillations, and signal processing techniques. Studies from different devices are therefore not extensively comparable [34, 35].

Further standardization is needed to exploit the full potential of the technology. It is important to ensure compliance with criteria for acceptability and reproducibility as for all pulmonary function testing [32, 34]. More studies are necessary to determine normal values for different ethnic groups, equivalent to the normal values of the Global Lung Initiative for spirometry measurements [34].

2.5   Ergo Spirometry/CPET

Ergo spirometry, also known as cardiopulmonary exercise testing, short CPET, is a measurement of the body's performance for the diagnosis of cardiorespiratory diseases, for monitoring during rehabilitation or for training monitoring of athletes, as it allows a full diagnosis of the cardiorespiratory system. The parameter for the maximum oxygen uptake (VO_2max) is considered a suitable means of assessing the fitness status of patients or athletes [14, 46, 47]. Further parameters of interest are the carbon dioxide production and lung ventilation. Different causes of exercise limitation can be evaluated with ergo spirometry as it allows conclusions about the disturbances occurring under stress that resting pulmonary and cardiac function testing cannot reliably predict [48, 49]. In healthy individuals, performance is primarily limited depending on cardiac output [23]. Therefore, CPET also plays an important role in cardiology, for example, in the assessment of patients with severe heart failure for the decision on heart transplantation or to support the optimal programming of a pacemaker [47]. As Stavrou et al. described in a recent review, patients with obstructive sleep apnoea have a reduced aerobic capacity that is associated with a dysfunction of the pulmonary, cardiovascular, neuropsychological and skeletal muscle systems and their interaction. Ergo spirometry could therefore also be useful for early detection of sleep apnoea [49].

A CPET is usually carried out on a treadmill or a bike ergometer, sometimes rotary crank ergometers have been used [14, 23]. The choice of method depends on availability and preference. When using a treadmill, the maximum values can be up to 10% higher compared to those achieved in a test on a cycle ergometer. Ramp or step protocols can be utilized to increase the workload. The ramp protocol is preferred to determine the patient's performance limit as stepwise increases of intensity can lead to artefacts that might be misinterpreted as thresholds [50].

A complete CPET consists of four stages: A resting phase to determine baseline values, a warm-up phase, the workload phase and the recovery phase. The breathing volume, breathing frequency and heart rate are continuously monitored during the exercise test and related to the ergometer workload. During the test, oxygen, carbon dioxide and the flow are directly measured [51]. The latter is used to determine the

respired volume. Additionally, a 12-channel ECG should be recorded. All signals must be precisely synchronized.

For the detection of oxygen during CPET, different types of sensors are available. Biochemical cells offer a fast response time for breath-by-breath analysis. However, their life time is limited and highly dependent on usage and storage conditions. Paramagnetic oxygen sensors can also be used. They are more sensitive to shock, but usually offer a longer lifetime. Zirconium cells, optical spectrometers or chemical cells have also been described to be used for the oxygen measurement [51]. For the detection of carbon dioxide, non-dispersive infrared sensors are utilized, where the infrared absorption of the molecules is measured with a pulsating light beam through a cuvette. Alternatively, chemical cells can be used [51]. For the measurement of the flow during CPET, turbines and pneumotachographs are commonly used. Pneumotachographs offer the advantage of linear behaviour for a large flow range. Light turbines can be scanned by a photo sensor, they must respond immediately to flow changes and must not run after the flow has stopped. Orifice spiroceptors with a thin plastic foil allow the measurement of pressure differences proportional to the respiratory flow as the orifice opening is proportional to the flow. Alternatively, mass flow sensors can be used [51].

During the test, the ventilatory thresholds can be determined. The first ventilatory threshold appears when the organism begins with lactate metabolism, so additional carbon dioxide is produced [14, 50]. The second ventilatory threshold marks the point of the test when the patient starts to hyperventilate. It shows the respiratory compensation point. Individual thresholds are useful to assess the endurance performance and control the intensity to provide training recommendations for preventive and rehabilitative sport. A key advantage for the use of CPET in occupational medicine is the patient's inability to cheat during the exercise test as the ventilatory thresholds are independent of motivation or workload [50]. It is sensible to use data averaging to display the test data. However, a high averaging lowers the resulting maximum values. Therefore, for athletes, a breath-by-breath inspection might be useful to evaluate the true maximum values. Peak oxygen uptake and ventilatory threshold can be severely altered by switching the averaging method [46, 51].

Lie et al. recently investigated the influence of exercise-induced laryngeal obstruction in CPET because the larynx represents an important point of resistance in the airway tree. They described the effect as common and found prolonged inspiratory time, lower breathing frequency, lover ventilation and lower inspiratory flow rate at maximal exercise. Still, most data overlapped so only the inspiratory flow rate could be promising in discriminating patients with an exercise-induced laryngeal obstruction although further investigations are needed to confirm their findings [52].

The usage of filters in a CPET measurement is problematic. Firstly, it will increase the dead space and even more important, because of the long duration of the measurement the filter will eventually become wet from the permanent exposure to exhaled breath, which is saturated with water vapour and might contain saliva and sputum. Therefore, resistance of the filter will rise and thus breathing becomes more difficult for the test subject.

3   Diffusion Measurement Techniques

In lung function diagnostics, a number of procedures have been established in which the lung volume can be determined with the aid of various gases. By the application of external gases, the functional residual capacity (FRC) of the lung can be determined without the need for a body plethysmography measurement. The FRC is defined as the sum of the residual volume and the expiratory reserve volume. It describes the volume that remains in the lungs at end-tidal expiration [22].

Furthermore, the diffusion of gases is an essential part of respiration. Oxygen has to be transported from the air in the lung into the blood and carbon dioxide has to be disposed. Besides ventilation and perfusion, the efficiency of the diffusion is dependent on the surface area of the lungs and membrane thickness. To measure the capability of the respiratory system for diffusion, the diffusion capacity of the lung for carbon monoxide (DLCO) can be determined by measuring the uptake of carbon monoxide from a specific test gas during a phase of breath holding. Decisive for this process are above all the conductivity of the membrane and the ability of the carbon monoxide to bind to haemoglobin. The concentration of haemoglobin also directly affects the gas exchange across the alveolar–capillary membrane [12, 53].

In volatile organic compound analysis, advantage is taken of the fact that the volatile substances pass from the blood into the lungs and are present in the exhaled breath. In the case of diffusion measurement, the approach is vice versa: The diffusion of the tracer gases from the lungs into the tissue is used for diagnostic purposes. Diffusion measurement techniques can be either single-breath or multiple-breath techniques. Nowadays, the single-breath techniques are most widely used [16]. Common tracer gases are helium, methane or carbon monoxide, also nitrogen washout is utilized. In contrast to the body plethysmograph, the diffusion measurement techniques are only able to measure the volume of the ventilated areas of the lung and not the total thoracic gas volume, which includes also gas trapped in non-ventilated areas [16, 22]. The most common diffusion measurement techniques shall be presented in the subsection below.

3.1   Single-Breath Diffusion Measurement and CO Transfer Factor

To measure the diffusion capacity, test systems must have a source to apply the test gas, a measurement method to determine inspired and expired volume and a measurement method to determine carbon monoxide and the tracer gas concentration. Carbon monoxide can easily be measured by infrared or electrochemical analysis [16]. The analysers need to be linear and should have a high accuracy with a recommended sampling rate of 1,000 Hz. A precise alignment of gas concentration signals to the flow signal is crucial [53].

Cross sensitivities of the gas analysers have to be observed and reduced as far as possible. An offset for water vapour and carbon dioxide can be provided by measuring the patient's expiration over some tidal breath cycles before inhalation of the test gas to adjust the concentration signal [53].

For a single-breath diffusion measurement, a test gas that comprises carbon monoxide, helium and ambient air is used. Carbon monoxide has a high affinity to haemoglobin and displaces the oxygen. The similar behaviour to oxygen regarding the diffusion coefficient and rate of reaction with haemoglobin makes carbon monoxide the ideal test gas. It does not naturally occur in the respired air, except for smokers [24]. At lower concentrations, the inhalation of CO is not dangerous. Common test gases for diffusion measurement contain 0.3% carbon monoxide, 21% oxygen, a tracer gas and a balance of nitrogen. Helium or methane are suitable tracer gases because they are relatively insoluble, inert and are not present in the alveolar gas [16, 23, 53]. The most important parameter of this measurement technique is the DLCO. It is dependent on the volume of capillary blood flow, the chemical reaction between carbon monoxide and haemoglobin and the diffusion conductivity of the alveolar membranes. Nowadays, it is therefore common to acknowledge the influence of the different factors by using the term of transfer factor (TLCO) rather than DLCO, albeit the term is still popular and broadly present in literature [24, 53]. Among others, DLCO values are varying with height, age and sex and are also influenced by haemoglobin, lung volume, exercise and body position. A premise of the method is that carbon monoxide and the tracer gas are diluted equally in the lung. However, in diseases such as severe COPD or emphysema this is not the case. The inspired test gas will be distributed primarily in the well ventilated parts of the lungs. Subsequently, the measured diffusion properties will likely be describing the situation in these regions of the lungs [53]. Méndez and Menéndez reported a reduced DLCO in Covid-19 survivors as the disease is associated with diffuse alveolar damage and vascular changes. They acknowledged that it is yet unknown, which clinical variables may be responsible [54].

The measurement of helium dilution with multiple breaths is a well-known method to determine the resting lung volume (FRC) [22]. The helium is equilibrated between the unknown lung volume and the closed measurement system [22]. The system contains a spirometer, a sampling gas pump and analysers for helium and oxygen, as well as a source for oxygen and an absorber for carbon dioxide [16]. Although the test is simple and relatively cheap, this steady-state method for measuring gas uptake during tidal breathing has become less important in clinical practice in recent years [22, 24].

Single-breath diffusion measurement takes less time and has therefore partially replaced the dilution method. In a recent study, Fragoso et al. suggested that the combined measurement of spirometry and DLCO may be sufficient for the evaluation of respiratory diseases, without the need for a body plethysmography measurement [12].

Additionally to DLCO and the originally determined diffusing capacity of the lung for oxygen (DLO), recent studies investigate in the use of the diffusing capacity of the lung for nitric oxide (DLNO) [55]. Radtke et al. compared two commercial

devices capable of determining the combined single-breath diffusion capacities for DLNO and DLCO in one manoeuvre in 35 healthy adults but found substantial differences for DLNO and lamented the absence of an established gold standard, since DLNO has up to now been mainly used in research settings. Despite, its additional value for use in clinical practice should be further evaluated to overcome the current shortcomings that impact the utility of DLNO as a biomarker [55].

3.2 Nitrogen Washout

The nitrogen washout measurement is a relatively new application to determine FRC that has only recently been emerging into commercial diagnostic markets, even though the principle has long been known. Also known under the term Fowler's method, nitrogen is used as an indicator to determine the FRC and the anatomic dead space of the lung [56]. Additionally, the lung clearance index (LCI) can be determined by calculating the quotient of the total expiratory volume and the FRC. Measurements can either be performed with a single breath or multiple ones. Both variants provide information about the functional residual capacity and irregularities in gas distribution in the lungs. The multiple-breath test is believed to be more accurate when it comes to measure absolute lung volumes [22].

For the multiple-breath washout measurement, the patient breathes 100% medical oxygen from a gas bottle. This displaces the nitrogen from the lungs, hence the term "wash out". The volume of the exhaled nitrogen is measured. Because of the inspiration of pure oxygen, nitrogen washout measurements should take place after the measurement of TLCO, otherwise the measurement could be influenced too strongly [16, 22, 56].

The concentration of washed out nitrogen can be measured directly and continuously by fast-responding nitrogen analysers at the mouthpiece [22] or indirectly by using carbon dioxide and oxygen sensors [57]. Air flow at the mouth can be measured with a pneumotachographs or an ultrasound flowmeter. The signal must be corrected for BTPS. The oxygen required for the inspiration is either provided from a tank via an on-demand valve or from a reservoir bag filled with 100% oxygen [22, 57]. The measurement system measures the flow and analyses the amount of nitrogen that is exhaled by the patient after the inspiration of oxygen has started. Exhaled concentrations of gas are plotted against the volume in real time. It is recommended that the system also monitors end-tidal carbon dioxide [16, 22, 57]. The tidal breathing of oxygen is continued until the expired nitrogen concentration becomes less than 1.5%. Healthy subjects will reduce the expired nitrogen concentration typically within 7 min. The actual duration is dependent on whether or not and to what extent an airway obstruction is present [16].

The measurement of FRC with a body plethysmograph and with the nitrogen washout technique shows close agreements for unobstructed lungs. In patients with severe emphysema, the body plethysmography will determine a considerably larger FRC than the nitrogen washout test and the test will typically take longer than 7 min

to achieve nitrogen concentrations of less than 1.5%. This can be explained with the areas of trapped gas that are not or hardly ventilated. Hence, gas mixing in these areas is very slow [16, 22]. Disagreements between the helium dilution technique and the nitrogen washout supposedly result from environmental and methodological differences [22].

The multiple-breath washout and determination of LCI have been investigated in some recent studies regarding cystic fibrosis. Hardaker et al. and Stahl et al. found it useful to detect changes in lung function and early ventilation inhomogeneity at an early stage [58, 59]. Hardaker describes abnormal LCI values in children to be an indicator for lower spirometric lung function in later years and believes the washout technique to be feasible to detect those children [58]. Stahl et al. used sulphur hexafluoride (SF_6) for their study in infants and pre-schoolers with cystic fibrosis to determine the LCI. Because sedation was necessary to ensure cooperation, the nitrogen washout technique could not be used as the inhalation of pure oxygen in this age group can cause alterations in the natural breathing pattern [59]. In a recently published study by Arigliani et al., LCI was determined to detect peripheral lung abnormalities in patients with sickle cell anaemia at an early stage. In comparison to spirometry and body plethysmography, the lung clearance index detected slightly more deviations in patients with sickle cell anaemia [60].

4   Blood Gas Analysis

Blood gas analysis is used to assess the oxygen uptake and ventilation of the lungs and the metabolic situation of the organism. It is used in the emergency room, to assess the risk of surgery, during anaesthesia, in intensive care monitoring, to monitor respiratory parameters in patients with COPD or cystic fibrosis, to monitor the course of cardiopulmonary diseases and to diagnose unexplained tachypnoea and dyspnoea. The change in blood gases can provide indications of the patient's diseases and help to initiate a targeted therapy [16, 61, 62].

Different gases are found in different concentrations in the blood. Some of them are physically dissolved, but chemical bonds also occur. Among the gases dissolved in the blood, the two respiratory gases oxygen and carbon dioxide are of diagnostic interest in lung function diagnostics. Nitrogen also occurs in the blood, but only in low concentrations and exclusively in physically dissolved form [14].

Because of its high informative value, the determination of blood gases is of prime importance for the practice of the lung function diagnostics, even before the measurement of expiratory carbon dioxide and oxygen concentrations [23, 48].

4.1 Parameters of Blood Gas Analysis

Important parameters of the blood gas analysis to assess the efficiency of lung function are partial pressure of oxygen (pO_2), partial pressure of carbon dioxide (pCO_2) and the pH value, representing the potential of hydrogen. To assess the acid–base balance, standard bicarbonate and base excess are also commonly determined [24].

Oxygen is poorly soluble in the blood and is mainly transported in the erythrocytes bound to haemoglobin. About 96–98% of the oxygen is thus chemically bound to the double positive iron ions of the haem group [63, 64]. A haemoglobin molecule can bind up to four oxygen molecules, one to each of its four subunits. These four subunits interact cooperatively so that when the first oxygen molecule attaches, the affinity for oxygen attachment to the other subunits increases [13]. The bonds are reversible, so that the oxygen can easily be released again in an oxygen-deficient environment. The partial pressure of oxygen is therefore decisive for the amount of oxygen that is bound to haemoglobin. The position of the binding curve describes the haemoglobin–oxygen affinity, i.e. the strength of the bond between haemoglobin and oxygen [64, 65]. A balance between oxygen demand and delivery is maintained in the organism [66]. The upper part of the binding curve is almost flat, so even if the pO_2 increases, the SpO_2 does no change much. Thus, the system is able to buffer a drop in pO_2 while keeping the haemoglobin highly saturated with O_2. The lower part of the binding curve is steep, offering the advantage that if the tissue requires larger quantities of O_2, those can be removed from the haemoglobin while keeping pO_2 fairly stable [65].

The pO_2 is used to assess the oxygen uptake of the lungs. It is measured with a polarographic gold or platinum electrode (Clark electrode) and an Ag/AgCl reference electrode in an electrolyte solution, which are connected to a voltage source. The oxygen molecules are reduced at the electrode, which leads to a measurable charge shift that is proportional to the partial pressure of oxygen. Polycrystalline boron-doped diamond is being discussed as a new, promising electrode material because it shows a pronounced linear behaviour between current and dissolved oxygen molecules. The normal value for pO_2 is between 72 and 100 mmHg (9.6–13.3 kPa) [62, 63].

For carbon dioxide, the physical solubility in the blood is greater than that of oxygen. At the same time, however, the arteriovenous partial pressure difference is lower, so that only a small part of the carbon dioxide from the tissue is physically dissolved in the blood. Instead, the majority is chemically bound and transported as bicarbonate by reacting with water in the erythrocytes to form carbonic acid. The carbonic acid dissociates to form protons and the carbonate residue, which diffuses back out of the erythrocytes in exchange for chlorine ions. In the capillaries of the lungs, this process is reversed. The carbonate residues diffuse back into the erythrocytes where they react with the protons buffered by haemoglobin to form carbonic acid, which in turn dissociates to form water and carbon dioxide, which is exhaled [14, 63]. The pCO_2 reflects the ratio of carbon dioxide production to carbon dioxide

elimination. pCO_2 is measured using a Severinghaus electrode, a pH electrode in a bicarbonate solution, which is considered the gold standard for clinical blood gas analysis. The selection of the molecules takes place via a gas-permeable membrane around the electrode. The diffusing carbon dioxide leads to a change in the concentration of the H^+ ions and thus to a change in the measured difference in potential. A slight drawback of the Severinghaus electrode is the long response time of more than a minute due to the slow carbon dioxide diffusion. The normal value for pCO_2 is between 35 and 46 mmHg (4.7–6.0 kPa) [16, 62, 63].

The pH value can influence all physiological processes. Analysis is done with a pH electrode [16], an ion selective glass membrane that is permeable for the H^+ ions and a silver wire. The potential difference that can be measured with a voltmeter is proportional to the hydrogen ion concentration. The normal value for blood pH is between 7.35 and 7.45, on average approximately 7.4 [14, 16].

Standard bicarbonate (HCO_3^-) is the main buffer system for physiological processes. It is dependent on the pCO_2 and calculated via the Henderson–Hasselbach equation related to the standard bicarbonate concentration at a pCO_2 of 40 mmHg at 37°C. This eliminates the effects of respiratory acidosis or alkalosis. The normal value for standard bicarbonate is between 22 and 26 mmol/l [16]. The base excess describes the amount of the buffer bases or acids that is necessary to titrate 1 l of blood to the standard values of pH 7.4 at pCO_2 5.3 kPa (40 mmHg) and 37°C [16]. The normal range lies between −2 and +2 mmol/l.

The percentage of haemoglobin saturated with oxygen is called oxygen saturation (SaO_2) [16]. It can be determined with a photometric oximetry and the calculation of the concentration via Lambert–Beer's law. The normal value SaO_2 is between 94% and 98% [16, 64]. With a normal arterial value, saturation reaches a saturation plateau at 97% [14]. Haemoglobin can also be determined with a photometric measurement. Normal values range from 11 to 18 g/dl with the mean value being about 15 g/dl [14].

The aim of lung function diagnostics is to analyse how well the organism is supplied with oxygen and able to eliminate the metabolic waste product carbon dioxide. Therefore, blood gas analysis is regarded as an important part of the lung function diagnostic. With blood gas analysis, the result and efficiency of the lung function can be assessed by displaying the amount of the blood gases oxygen and carbon dioxide [24]. In the clinical practice, the invasive blood gas analysis represents the state of the art and will be presented in the following. Some approaches have been made to determine blood gas values in a non-invasive way, such as transcutaneous blood gas measurement and capnometry.

4.2   Invasive Determination of Blood Gases

Blood samples for the invasive determination can be taken arterial, venous or from capillaries. The analysis of arterial blood is considered to be the gold standard for blood gas analysis [16, 24, 67]. Indwelling arterial catheters can be used in intensive

care setting where frequent blood gas samples are required [16]. Arterial puncture can be painful for the patient [16, 68] and carries some risks for the patient, like the general risk of infection, the possibility of a major vascular injury and haematoma formation. Arterial blood sampling can therefore only be performed by qualified and trained personnel. The notation of PaO_2 and $PaCO_2$ instead of pO_2 and pCO_2 is used to indicate the arterial measurement. Venous blood gas analyses can be performed faster and safer. Taking a venous blood sample is less painful for the patient, although, venous blood is not well suited because the venous blood gases are significantly dependent on the metabolism of a subject [24]. A compromise regarding simplicity and safety is the usage of arterialized capillary blood, which has been proven to be sufficient for routine examinations to determine pH, pCO_2 and pO_2 [16, 23]. Puncture of the hyperaemised earlobe is patient-friendly, especially if frequent samples are necessary to closely monitor the blood gases. With this method, comparable biochemical parameters can be determined as with the arterial blood gas analysis [68]. The capillary sample contains mostly blood from the arterioles and to a lesser extent from the venule side because of the differences in blood pressure [16]. However, capillary blood samples have no validity in shock states with reduced peripheral perfusion [23, 24].

Difficulties in the measurement are the small sample volumes and the volatilization of the gases with advancing time. Therefore, the analysis of the collected blood samples is usually done in close proximity to the patient. Invasive blood gas measurement is time-consuming and the results cannot be determined in real time. Modern analysers can analyse the blood samples for the desired parameters within a few minutes. For each measurement, a sufficient amount of blood must be taken from the patient for analysis. During follow-up visits in the hospital, the analysis must be repeated frequently, depending on the patient's condition [69]. For all methods of taking invasive blood gas samples, possible complication include bleeding to tissue, formation of thrombus, damage of peripheral nerves or a vasovagal responses of the patient. Additionally, the risk of infection must be taken into account [16].

Blood gas levels are influenced by many other factors. The altitude of the measurement site has a major influence, as the air pressure and thus also the partial pressure of oxygen decreases with increasing altitude above sea level. The arterial pO_2 decreases accordingly while the pCO_2 in the blood remains largely constant. Only at high altitudes compensatory hyperventilation can occur due to the lack of oxygen which can lead to a lowering of the pCO_2 [70]. In addition, arterial blood gas levels fluctuate by up to 8 mmHg (1.07 kPa) over the course of a day. The pCO_2 also increases slightly overnight during sleep [71]. With increasing age, the pO_2 decreases. Changes in diffusion conditions at the alveolar membrane may be responsible for this [72]. However, the loss of uniform lung elasticity with age and the altered proportion of diaphragmatic and chest wall breathing may also lead to greater distribution abnormalities that limit oxygen uptake [73]. In obese patients, ventilation is complicated by increased extra pulmonary airway resistance. There is a drop in oxygen pressure and hypoxaemia, as well as an increase in pCO_2 due to retention of carbon dioxide [74].

Because of their diverse applicability, blood gas values continue to be a subject of interest in many research fields. Calvo et al. have recently demonstrated that arterial blood gas values show significant correlations to pulmonary function tests in patients with amyotrophic lateral sclerosis and thus recommended blood gas analysis as a substitute for pulmonary function tests. According to their findings, standard bicarbonate, base excess and pCO_2 could be early predictors of respiratory failure [75]. In a study with Covid-19 patients, Elezagic et al. found venous pCO_2 values to be significantly higher and pO_2 and SaO_2 to be significantly lower in positive tested patients compared to patients who tested negative for SARS-CoV-2. They recommend to use these parameters in symptomatic patients to early identify signs of hypoxia and to prevent development of respiratory failure [76]. Bezuidenhout et al. assessed arterial blood gas and acid–base patterns in Covid-19 patients in an intensive care unit. They observed alkalaemia in the majority of patients and that a higher pH and lower pO_2 were significantly associated with patient survival [77].

4.3 Non-invasive Determination of Blood Gases

Compared to arterial blood gas analysis, the analysis of capillary blood is perceived as more comfortable by patients, but by definition also belongs to the invasive procedure, since the skin must still be pierced with a needle. Transcutaneous measurement of blood gases has been thoroughly investigated in the last decades. Additionally, pulse oximetry is a common procedure to measure SpO_2 and estimate pO_2 without conducting a complete blood gas analysis.

4.3.1 Transcutaneous Blood Gas Monitoring

There are only a few approaches for the non-invasive determination of blood gases so far. One possibility is the transcutaneous determination of the carbon dioxide partial pressure. For this, local hyperthermia is induced [48]. The skin is heated to approximately 43–45°C under a special electrode in order to increase the permeability of the tissue. This increases local perfusion and arterializes the capillary blood of the skin [78]. The carbon dioxide diffuses from the capillaries through the tissue and through the semi-permeable membrane of the electrode [62]. This electrode is a modified version of the Severinghaus electrode [69]. The Severinghaus electrode is a pH electrode with a buffer of sodium hydrogen carbonate. The carbon dioxide diffusing in through the membrane influences the chemical equilibrium of the carbonic acid reaction. The ions of the solution, on the other hand, cannot penetrate the membrane. The pH value of the solution consequently changes according to the concentration of the carbon dioxide. There is a logarithmic relationship between the two quantities [79]. Transcutaneous measurements need longer measurement times and do not provide blood gas values instantly [62]. After a short warm-up time, the transcutaneous carbon dioxide partial pressure can be read in real time. The

measured values can also be recorded continuously over a longer period of time [23, 67, 69, 80].

The transcutaneous determination of the carbon dioxide partial pressure is established in some medical specialities, in others it is doubted. The values determined in this way correlate more or less well with the measured arterial values. Good agreement with directly measured arterial values is only found in infants [48]. An overestimation of the transcutaneous pCO_2 is likely because of the cellular metabolic production [62]. In a study of 22 healthy volunteers, Bertram et al. compared the transcutaneous measurement with a capillary blood gas analysis while the subjects were hyperventilating. They found the comparability of the readings of the healthy volunteers acceptable, but did not rule out a change in severely ill patients [81]. Kelly and Klim investigated the accuracy of transcutaneous measurement in non-invasively ventilated patients. Based on their results, they did not recommend the use of transcutaneous pCO_2 as a substitute for arterial pCO_2 [80]. Rosier et al. also found insufficient agreement in their studies of patients with severe brain injury to use transcutaneous pCO_2 to infer arterial partial pressure of carbon dioxide [69]. The results of transcutaneous carbon dioxide measurement can also be influenced by age-related changes in skin blood flow, metabolism and skin thickness. A study on elderly patients by Janssens et al. nevertheless showed a very high correlation between transcutaneous measured carbon dioxide and the carbon dioxide partial pressure of an arterial blood gas analysis [78]. In a more recent study, Galetin et al. recommend to use transcutaneous measurement of the pCO_2 during and after bronchoscopy in analgosedation in patients with COPD because of the induced alveolar hypoventilation and hypercapnia from the procedure [82]. Saruhan et al. evaluated the measurement of transcutaneous pCO_2 in patients with sepsis and septic shock. In patients with sepsis, it may be used as less invasive method for continuous measurement. However, in patients with septic shock the assessment of transcutaneous pCO_2 appears to be questionable [83]. Transcutaneous measurement of pCO_2 during electrophysiological catheter ablation procedures has been investigated by Weinmann et al. and proven feasible during the conscious sedation of the procedure. They reported good correlation to arterial and venous blood gas samples [84]. A recent study of van Wijk et al. observed the course of transcutaneous measured pCO_2 in mechanically ventilated children under general anaesthesia. They too reported good agreement to the arterial measured values for pCO_2 [67].

Transcutaneous determination of oxygen partial pressure is also possible with a similar method. In contrast to pCO_2, pO_2 is likely to be underestimated by the transcutaneous measurement because of the oxygen consumption of the superficial tissue [62]. Originally, the method was used in vascular surgery to assess diseases of the blood vessels [85]. Janssen's study of elderly patients showed that although there was a significant correlation between the transcutaneous oxygen values and the partial pressures of oxygen in the blood gas analysis, the high variability of the measured values precluded clinical application [78]. Saruhan et al. concluded after their study, that transcutaneous measured pO_2 is not reliable in patients with sepsis or in septic shock [83]. Van Wijk et al. found transcutaneous pO_2 to be only accurate in ventilated children under 6 months of age [67]. Miniaturized polydimethylsiloxane

based oxygen sensors are currently under investigation as a possible alternative to conventional transcutaneous devices [62].

4.3.2 Pulse Oximetry

For non-invasive determination of oxygen saturation, a photometric measurement with a pulse oximeter can be conducted. This is a spectrophotometric method for the non-invasive, continuous measurement of the arterial oxygen saturation of the blood. It allows to continuously measure the saturation and pulse rate on a finger, toe or the earlobe by sending two wavelengths of red and infrared light (typically 660 and 940 nm) through the tissue to a photodetector. Healthy people have an arterial oxygen saturation of about 94%–98%. The clinically relevant saturation range is between 70% and 90%. At a low saturation value, pulse oximeters have a lower accuracy than at high saturations. Below 70%, only the trend information of the measurement result is retained. The continuous measurement is particularly useful in anaesthesia as well as in emergency and intensive care medicine in order to quickly detect disturbances in oxygen uptake and oxygen distribution [16, 23, 48, 64, 76].

For a valid pulse oximetry, the measurement site must be well perfused. The amount of light absorption is dependent on the haemoglobin saturated with oxygen. Deoxygenation changes the colour of the blood from reddish to bluish. The pulse oximeter measures this colour change. When broadband light is sent through a haemoglobin bond, the individual electromagnetic wave frequencies are absorbed to different degrees. Absorption depends on concentration, thickness and material properties. Haemoglobin behaves like an optical filter that only allows red and near-infrared light to shine through. The ratio of the two main components of haemoglobin, oxyhaemoglobin and reduced haemoglobin, is measured [64].

The common technology is the use of light-emitting diodes (LED) for pulse oximetry with two wavelengths. They offer high light intensity with low heat generation and narrow spectral content. The disadvantage is deviations from the desired average wavelength, which can be up to ±15 nm due to production and temperature. The wavelengths 600 and 940 nm are advantageous because the extinction curves of oxyhaemoglobin and reduced haemoglobin differ greatly and stable LEDs exist for these ranges [64]. Since the received red and infrared signals are usually strongly disturbed, signal processing is required. Filtering and averaging are used to improve the represented values. Relative movements between the patient and the sensor cause movement artefacts. With a finger clip sensor, slightest hand movements or shaking influences the shape of the plethysmogram. Scattered light from external light sources absorbed by the detector can also alter the measured saturation value and readings are influenced by nail polish, artificial nails or skin pigmentation [16, 64]. As Sjoding et al. pointed out, there is a significant racial bias in pulse oximetry. In their study, black patients had a higher frequency of silent hypoxaemia that could not be detected with pulse oximetry. They see the cause in the original development of pulse oximetry in a homogeneous population without racial

diversity and warn that oxygen administration based on pulse oximetry may put black patients at increased risk of hypoxaemia [86].

It is important to note that pulse oximetry will overestimate oxygen saturation values in patients with acute poisoning from carbon monoxide as the measurement technique does not allow to distinguish between haemoglobin saturated with oxygen and haemoglobin bound to carbon monoxide (carboxyhaemoglobin) [16]. Carboxyhaemoglobin is on average around 2% of total haemoglobin, but can be up to 15% in smokers. Car exhaust fumes, industrial emissions and fire accidents can also cause carboxyhaemoglobin to rise [64]. As Dünnwald et al. recently reported in a review of pulse oximetry in acclimatization to high altitude, measurement of SpO_2 levels becomes more difficult with increasing height. The technical characteristics of the device must allow for the respective altitude and operating temperature [87].

A new and promising development regarding home use is the possibility of modern smartphones or wearables, like smartwatches, to measure SpO_2 with reportedly high accuracy. During silent hypoxia, which occurs, for example, in Covid-19 patients, the need for hospitalization can be identified faster and before worsening of symptoms [76, 88, 89].

5 Expiratory Carbon Dioxide

Another approach for the non-invasive determination of the carbon dioxide partial pressure is the determination of the expiratory carbon dioxide fraction. Various authors have dealt with capnometry in different publications and compared end-tidal carbon dioxide values with arterial blood gases. Though the accuracy of the end-tidal pCO_2 is not comparable to the arterial determination because of gas admixtures from the alveolar dead space, they correlate clearly with the $PaCO_2$. The mean difference is between 2 and 5 mmHg [62]. The measurement and monitoring of the partial pressure of exhaled carbon dioxide during tidal breathing has been utilized for a long time to monitor respiration. It can be regarded as the most commonly used breath biomarker [8].

The graphical representation of the expired carbon dioxide concentration is called capnography. The course of the concentration can be plotted either against time or the expired volume. A sensor measures the carbon dioxide concentration of the expired air to record the capnogram. The measurement of capnography takes place during tidal breathing, whereby the courses of the carbon dioxide concentration can be recorded and displayed in real time. Changes in the pattern indicate complications regarding circulation or breathing [8, 90]. In various lung dysfunctions, the resulting capnograms differ from those of healthy individuals.

For the analysis of volatile organic compounds the monitoring of expired carbon dioxide is particularly suited for controlled sampling of breath [8]. It shows a clear respiratory phase profile and allows the distinction between alveolar and non-alveolar gas. In clinical practice, carbon dioxide is detected with commercially

available capnometers with high sampling frequencies [8]. In the following section, the principles and the milestones of capnometry and capnovolumetry will be addressed.

5.1   Capnometry

Capnography, the plotting of expired CO_2 over exhalation time, has been used for some time in intensive care medicine and anaesthesia in addition to the pure measurement of end-tidal CO_2 partial pressure. It has already been used there as an aid for intubation control and for monitoring the position of the tube, e.g. during transport. It can also be used to assess the patient's ventilation status or the effectiveness of resuscitation. Advantages are the capability for continuous analysis and the breath-by-breath resolution. In this context, capnometry or capnography is an important indicator of the patient's respiratory status for doctors and nurses. Pulse oximetry measurement of blood oxygen saturation, unlike capnometry, is slow to respond to changes in pulmonary ventilation; it primarily describes oxygenation. The measurement of end-tidal CO_2 content, on the other hand, primarily describes ventilation. Therefore, capnography would indicate apnoea immediately, while pulse oximetry would still indicate high saturation levels in the blood for a few minutes [8, 91–94] [108].

For a capnogram, the course of the CO_2 concentration over the time axis is usually recorded over the duration of multiple breaths. In this way, the inspiratory and expiratory courses are recorded continuously. The capnogram shows characteristic phases: the phases of anatomical dead space, mixed air volume and alveolar plateau, as shown in Fig. 3. The end-tidal concentration most closely mirrors the alveolar gas [8, 23].

These phases are important for the standardization of other measurement methods for respiratory gas analysis. Capnometry can be used to determine at which point in time alveolar gas is available for sampling. In the end-tidal gas mixture, blood borne volatiles are present in higher proportions and end-tidal samples contain lower amounts of impurities from the dead space [8].

In the dead space phase, air is first exhaled that was predominantly in the air-conducting airways and was not in contact with the alveoli. The CO_2 concentration in this section is therefore negligible and corresponds approximately to the concentration of the ambient air. In the mixed air phase, the CO_2 content increases almost linearly. The proportion of alveolar volume in the exhaled air increases steadily in this phase. The alveolar plateau represents air from the alveoli involved in the gas exchange [95, 96]. The end-tidal CO_2 level is determined at the end of the alveolar plateau. The end-tidal CO_2 level is thought to be representative of the concentration of CO_2 in the alveolar gas. However, due to the admixture of gas from the alveolar dead space, it is somewhat lower than the actual alveolar CO_2 content. The alveolar dead space includes the portions of the alveoli that do not
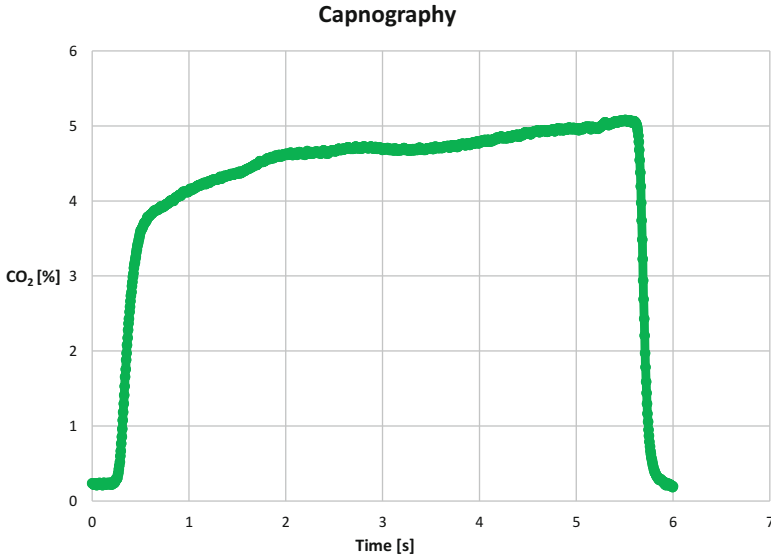
Fig. 3 Exemplary capnogram representing carbon dioxide over time

participate in gas exchange due to poor circulation or ventilation. Therefore, end-tidal concentrations are not identical to the alveolar concentrations [8].

Ventilation disorders change the shape of the capnogram and mixed air and alveolar air phases are no longer separable from each other. The rise of the mixed air phase is less steep depending on the severity of the impairment and the shape of the alveolar plateau changes to a so-called shark fin [23]. In 1949, Fowler first described that the respiratory phases were clearly distinguishable in healthy subjects whereas in patients with asthma or emphysema, there were greater deviations and the phases could not always be clearly delineated [97]. Smidt and Worth later confirmed the diagnostic value of the gas washout curves [98]. Capnography has since been assessed for the diagnosis of airway obstruction and emphysema. The deformation of the CO_2 time curve indicates emphysema [99] and shows correlations to spirometry parameters [100]. The slope of the plateau of the curve and the angle between the rise phases of the CO_2 time curve are suitable for the diagnostic differentiation of patients with airway obstruction from healthy subjects. Correlations of the plateau slope of the capnograms with the FEV1 value have been reported [100–102].

There are various methods for determining expired CO_2. Selective CO_2 sensors use non-dispersive infrared absorption or mass spectrometry. In the non-dispersive infrared absorption measurement method, a photodetector measures the amount of infrared light absorbed. The CO_2 molecules absorb specific wavelengths of infrared light, specifically wavelengths of 4.256 µm. The absorption is proportional to the CO_2 concentration. For the measurement, the infrared light penetrates a cuvette with the gas to be analysed and hits the detector. A filter allows only a narrow spectrum from the spectrum of the light source to pass through, which is effectively absorbed

by the molecules of the gas under investigation. A second detector with a separate infrared filter that is not influenced by the measuring gas serves as a reference. Since many gases absorb in the infrared range, the water vapour contained in the air, for example, influences the measurement due to the spectral proximity of the absorption characteristics to each other. Infrared sensors have short response times, long lifetimes and low power consumption [91, 103]. Mass spectrometry is technically more complex and expensive, but it enables very precise detection of the partial volumes of all gas components with a high temporal resolution. The molecules of the gas to be analysed are ionized, accelerated in an electric field and deflected by a magnetic field. The individual components of the gas separate according to their charge and molecular masses and are registered by a detector [63, 91].

Depending on the design, it is more favourable to use either the main or the secondary flow method. Hygienic aspects must also be taken into account when analysing respiratory gases. With the side stream method, the pump for suction must be particularly protected against contamination. The condensation of water vapour in the system must also be prevented. In contrast to the main stream method, in the side stream method only a part of the expired gas mixture is extracted and passed on to a sensor [8]. The measured values are then extrapolated accordingly. This method is flexible and can easily be adapted to different positions of the patient (e.g. when used in anaesthesia), but also offers many critical points where gas leaks can occur [94]. A disadvantage of this method is the delay between actual expiration and the actual gas analysis, which can be up to several milliseconds. In addition, mixing of expiratory gases from several breaths can occur in the suction system, especially with small breath volumes and high breathing frequencies [91]. If the volume of breaths is too small, air may even be extracted and evaluated exclusively from the anatomical dead space [104]. An advantage over the main stream method is the usually lower weight of the sensors [94].

The fields of application of capnometry are manifold and still subject of research. Sandroni et al. suggest to employ continuous capnography during cardiac arrest to monitor the quality of cardiopulmonary resuscitation in addition to confirming correct placement of the endotracheal tube. A sudden rise of end-tidal CO_2 could suggest the return of spontaneous circulation [105]. In a recent study by Leonova et al. to assess changes of heart rate regulation in patients with myocardial infarction, capnometry was used to avoid adverse events during cardiorespiratory training sessions. The fraction of end-tidal CO_2 was determined to exclude hyperventilation syndrome by adjusting the depth of breathing if necessary [106]. Williams et al. investigated the use of end-tidal CO_2 in the monitoring of ventilated infants to reduce the magnitude of difference in CO_2 levels that can lead to cerebral injury. The continuous measurement of end-tidal CO_2 was associated with a reduction of CO_2 abnormalities [90]. Ostacher et al. evaluated the use of capnometry for a guided respiratory intervention in patients with posttraumatic stress disorders, which has already been successfully applied in patients with panic disorders. A lower end-tidal CO_2 value has been reported to be a marker of panic-related respiratory dysfunction. Therefore, feedback on end-tidal CO_2 and respiratory rate is given to the patient in real time in order to increase the end-tidal CO_2 while decreasing the breathing

frequency. Ostacher et al. described the intervention as safe and well-tolerated by patients during home use. Symptoms improved and posttraumatic stress disorder scores persistently decreased in the majority of participants [107].

5.2 Capnovolumetry

Capnovolumetry or volumetric capnography is the measurement of CO_2 expired per breath as a function of expired volume. The course of this measurement can be displayed graphically as a volumetric capnogram. For this purpose, a CO_2 sensor measures the exhaled CO_2 and software integrates the measured respiratory flow value to display the concentration over the volume. The measurement is carried out during tidal breathing and the expiratory curves can be displayed in real time.

The capnogram is also called a volumetric capnogram when plotted against volume. With a volumetric capnogram, in contrast to the plotting of a CO_2 time curve, only the expiratory component is recorded. Figure 4 shows the volumetric capnogram that can be divided into four characteristic phases [15, 108]:

- Phase I: The flat course of the capnogram up to the beginning of the first slope represents the volume from the anatomical dead space, the air-conducting airways. In this section, there is hardly any CO_2 present in the exhaled air.
- Phase II: The first slope of the capnogram represents a mixed volume, the CO_2 concentration increases sharply, while the proportion of alveolar volume in the exhaled air increases steadily and less and less dead space air is contained.
- Phase III: The plateau phase of the capnogram shows a flat slope. In this section, air is predominantly expired from the alveoli with the same CO_2 concentration.
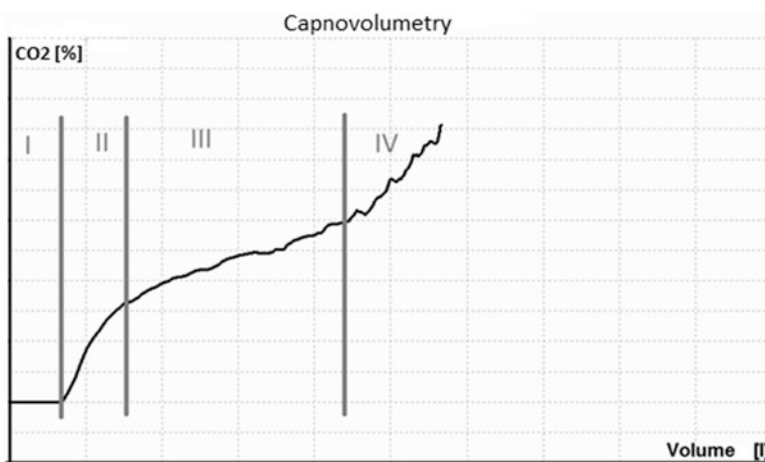

Fig. 4 Schematic volumetric capnogram showing the four phases of expiration

- Phase IV: A renewed steep rise in CO_2 concentration can be explained by the collapse of the alveoli at the end of expiration. This phase is not pronounced in all capnograms.

With healthy subjects and resting breathing that is not too slow, often only the first three phases are recognizable and can be clearly distinguished from each other. Ideally, phase II follows phase I with a short, steep rise and phase III ideally runs almost flat with a slight slope. In various lung diseases, sometimes large deformations of the capnogram can occur. In the case of obstruction, the plateau of phase III is rising while the inclination of phase II becomes less steep, resulting in a wider angle between the two lines [108, 109].

Since the shape of the volumetric capnogram naturally differs from that of the non-volumetric one, there are different reference values and calculation formulae for different parameters for both shapes. For the angle between phases II and III, the normal range is 100°–110° when plotted against time [94]. For a volumetric capnogram, angles up to 130° are normal for healthy individuals. This deviation of the angle values results mainly from the changes in phase II of the volumetric capnogram compared to the classical capnogram. When plotted against volume, the mixed air phase is recorded as a gradual increase, whereas when plotted against time, it shows an almost vertical course. The reason for this is the large flow velocity at the beginning of expiration, whereby the volume of the anatomical dead space is usually exhaled very quickly. In contrast to the plot over time, the plot over volume was found to reduce the dependence of the curve on respiratory rate [110]. However, in a recent study by Klütsch et al., dead space volumes and the slope of phase III were found to be significantly dependent on the respiratory volume [111].

The various dead spaces that can be derived from the course of the CO_2 volume curve were frequently considered to distinguish patients with emphysema from asthmatics [101]. Most attention was given to the Bohr dead space and the threshold dead space, which are the largest and smallest dead spaces that can be determined. For emphysema diagnosis, significant differences have been demonstrated from a healthy control group when the Bohr dead space was related to the previously inspired volume [112]. The threshold dead space most clearly reflected the changes after bronchospasmolysis in children with asthma [113].

Following the promising approaches of CO_2-time curves for diagnostic purposes, approaches have been made to use the volumetric capnogram for diagnostic purposes. The use of capnography in the diagnostic of COPD has been suggested frequently. The different progressions of the slopes of the CO_2 curves were regarded promising to distinguish between healthy and obstructed individuals [15, 101, 102, 108, 110, 114, 115]. Therefore, in addition to the methods of capnography, capnovolumetry seems to be extremely promising for the diagnosis of ventilatory disorders of the lung. Jarenbäck et al. created an artificial efficiency index in their 2018 study to express the efficiency of the breath in the elimination of CO_2 that they found to be aiding in the diagnostic and grading of COPD [109]. Klütsch et al. recommend capnovolumetry especially in already suspected COPD [111]. This is in accordance with the findings of Kellerer et al., who found only a moderate potential

for the recognition of airway obstruction and an increased diagnostic accuracy with the severity of airway obstruction [116]. Conclusively, capnovolumetry can support the diagnostic of obstructive airway diseases, while basic anamnestic information should be taken into account [115].

In contrast to spirometry, capnovolumetry offers the advantages to be an easy and effortless test that requires minimal patient cooperation and minimal maintenance, making it a suitable test for children, home use or point of care diagnostics [15, 109, 111, 115, 116]. However, both measurements do not assess the same elements, as Parazzi et al. pointed out. While spirometry aids in assessing the degree of airway obstruction, the capnovolumetry reflects the alveolar ventilation inhomogeneity [15]. Parazzi et al. have compared spirometry and capnovolumetry in patients with cystic fibrosis before, during and after a treadmill exercise test. They concluded that capnovolumetry can also be useful as a complementary tool for the monitoring of the pulmonary status of patients with cystic fibrosis [15].

So far, the method of capnovolumetry is still used rather experimentally and has not yet been established as a standard in lung function diagnostics. Additionally, it has been investigated in veterinary medicine in different animals. In addition to previous studies on calves [91] and horses [117], Tolnai et al. investigated the potential to assess the shape and parameters in rats and confirmed the value for the study of ventilation-perfusion mismatches [118].

6 Fraction Exhaled Nitric Oxide

In the human body and the respiratory system, nitric oxide (NO) takes part in various processes. It plays an important role as vasodilator, bronchodilator, neurotransmitter and inflammatory mediator [119]. NO diffuses through the cell membranes and is evidently present in the exhaled breath, where it can be measured and analysed as fraction exhaled nitric oxide (FeNO). Nitric oxide and thus FeNO values in exhaled breath are increased in the case of mucosal inflammation, especially in eosinophilic asthma [8, 119–122].

Nitric oxide has first been observed in exhaled breath in 1991 [122, 123]. It shows its highest concentrations at the beginning of the exhalation, since NO production is highest in the upper airways and nasal cavity. Elevated values have been found in acute airway inflammation and asthma. Diagnostic use of FeNO measurement to assess asthma has first been possible after comprehensive studies had evaluated the flow dependency of the measured FeNO concentrations. The most commonly used parameter is $FeNO_{50}$, which describes the present concentration of NO as part per billion (ppb). The index 50 is added to indicate that measurement took place at a recommended flow of 50 ml/s [8].

6.1 FeNO Measuring Technology

The first devices to measure FeNO were stationary chemiluminescence devices, which measure NO indirectly when light is generated in a chemical reaction between NO and ozone [120, 122]. They offer fast response times and accurate detection limits from 0.1 to 0.5 ppb in a wide range of flow rates. The use of chemiluminescence instruments for routine clinical applications is limited because of the high costs. The chemical reaction converters and other components have to be checked and maintained regularly. Because of the occurrence of drift, chemiluminescence instruments have to be calibrated daily [122].

Electrochemical sensors can be integrated in lightweight handheld devices [120, 122]. The concentration of NO is measured with an electrical signal like the current in a large detection range from 5 ppb up to 300 ppb with a high accuracy of 5 ppb up to 300 ppb in less than 10 s. The electrochemical sensor has to be changed after a specified period of 1–2 years. The analysers are exclusively used to measure the FeNO value at a flow of 50 ml/s (FeNO$_{50}$), which is considered to be suitable for routine clinical practice [122]. Further options to measure FeNO are smart solid-state microsensors or laser-based NO sensors. The optical sensors are able to detect low levels of NO in the range of ppb. The change of light intensity due to the absorption by NO is measured. These laser-based analysers do not need consumables and require minimal maintenance [122].

In a recent study, Korn et al. compared three different commercially available FeNO devices and found that measured concentrations were statistically equivalent and the measurements were highly accepted by the patients [120]. FeNO measurement is a simple and safe non-invasive method to assess airway inflammation quantitatively [119–121]. Important to note is that devices of different manufacturers are as of yet not interchangeable [120, 122]. Until further standardization is reached, patients should always be measured with the same device type.

6.2 FeNO Measurement in Asthma

For the diagnosis of asthma, treatment decisions have traditionally been based on assessing airflow obstruction, frequency of occurrence of symptoms and the frequency of exacerbations. With the development of the FeNO measurement, a point of care test has been developed which is promising to support the diagnostic pathway and treatment decisions for asthma [120, 121]. However, because asthma is a heterogeneous disease, a clinical diagnosis cannot be made with a single test [119]. There are different types of asthma and FeNO is associated with eosinophilic airway inflammation. FeNO values have been found to be high in subjects with eosinophilic asthma, therefore it can be used as a biomarker in the process of diagnosing asthma as an eosinophilic or non-eosinophilic asthma [119, 121,

123]. If asthma is not caused by eosinophilic inflammation, FeNO values can be inconspicuous [119].

Rather than reference values, cut points are recommended by the ATS when evaluating FeNO values [119]. FeNO value above 50 ppb in adults and above 35 ppb in children indicates an eosinophilic inflammation of the respiratory system, especially if accompanied by symptoms, and responsiveness to inhaled corticosteroids (ICS) is likely [8, 119]. Values below 25 ppb and 20 ppb in children are in general considered low and eosinophilic inflammation and responsiveness to corticosteroids are less likely [119]. In the presence of nonspecific respiratory symptoms but with low FeNO values an eosinophilic airway inflammation is unlikely, as is the responsiveness to ICS [119]. FeNO values between 25 ppb and 50 ppb and for children between 20 ppb and 35 ppb must be interpreted cautiously [119, 121]. Because of the wide ranges there is an overlap between mean FeNO values in healthy and asthmatic subjects [119]. Values can even be normal in subjects with asthma [122]. Allergen exposure should be taken into account when higher FeNO levels are detected [119]. Reference values have limited application in practice. The derived values from a normal population are unlikely to offer cut points in patients with airways diseases [119]. The personal FeNO values might be most useful to establish a baseline to evaluate the treatment with anti-inflammatory drugs [119, 122]. FeNO values are influenced by a variety of factors. Men have slightly higher values than women and values increase with age [119, 122]. Body height and pre-existing conditions like allergic sensitization or smoking influence the values [8, 119]. FeNO levels are lower in smokers [119] but have also been observed to increase after exposure to electronic cigarette aerosol with and without nicotine in a recent study by Antoniewicz et al. [40].

Treatment decisions for the usage of ICS in asthma can be supported by using FeNO as a biomarker. The measured FeNO value can predict the likelihood of corticosteroid responsiveness [119]. The inflammatory response of the airways following changes in dosage can be monitored [119, 120, 122, 123]. Low FeNO values in asymptomatic patients can be an indicator to reduce the dose of ICS [119]. A high FeNO value in asthmatic patients is associated with a higher risk of exacerbation [120, 122, 123]. Additionally, FeNO measurement is also suitable to verify the patient's adherence to anti-inflammatory medication [119, 123]. Persistently high FeNO values might be an indication for poor adherence to prescribed ICS therapy [119] as inhalation of ICS decreases FeNO values [121], but they return to their baseline level when the patient does not continue the regular intake of the medication. Therefore, it is possible to assess the patients' compliance in taking the prescribed medication [8].

FeNO does not directly correlate with lung function parameters in asthma, but has been observed to correlate with acute hyper responsiveness [121, 123]. FeNO values have been observed to decline correspondingly to a decreasing FEV1 in provocation challenges [8, 121, 122]. It is suggested, that after bronchodilation a decrease in FEV1 simultaneously to an increase of FeNO values might hint to the involvement of more proximal airways while a decrease in FEV1 and FeNO indicates the involvement of peripheral airways. Further evidence is needed to verify this thesis.

After its verification, FeNO could be used as a pulmonary function test after bronchodilation to identify the site of obstruction [8].

In patients with a chronic inflammatory airway disease like eosinophilic asthma, it is recommended to use FeNO measurements as an additional tool to usual care [121], because conventional lung function tests are not associated directly with airway inflammation [119]. Including FeNO in asthma management at an early stage leads to an increased sensitivity and specificity. Both quality of care and expected costs are improved. With additional FeNO measurements, the probability for light exacerbations and the necessity for the use of ICS were reduced [124, 125]. Asthma diagnosis can be supported by spirometry and FeNO in adults and paediatric patients above the age of 5 years, as recommended in asthma guidelines. FeNO testing has been proven to be successful in this age group. However, while patients at the age of 5 years had a low success rate of only 17%, at the age of 8 years, 80% were able to perform a valid FeNO measurement. Therefore, in general practice, it is recommended to apply FeNO testing in patients above the age of 8 years [19].

6.3 FeNO Measurement in Other Diseases

The use of FeNO measurements has been studied in numerous other diseases and elevated levels have not been entirely specific to asthma [121, 122]. In addition to occurring in eosinophilic asthma, high levels of FeNO have also been found in patients with bronchiectasis, viral respiratory tract infections, systemic lupus erythematosus and liver cirrhosis. FeNO values have also been elevated in cases of acute lung allograft rejection [122, 123]. Different diseases such as cystic fibrosis, HIV infection and pulmonary hypertension have been reported to be associated with low FeNO values [119, 122, 123].

Cystic fibrosis is a congenital metabolic disease, in which lung tissue is progressively deteriorated. In the assessment and monitoring of the disease, spirometry is the most frequently applied method. But as pointed out earlier, sensitivity of spirometry for the detection of early lung changes is rather poor and challenging in young age groups [58]. Additionally, capnovolumetry and also FeNO can be used to assess the status and progression of cystic fibrosis [15]. In cystic fibrosis, which is associated with chronic airway inflammation and accompanying increased mucus production, FeNO values have been found to be reduced [8, 123]. The low levels are related to a missing enzyme, the nitric oxide synthase, which is normally present in the epithelium of the airways [119].

Many patients show symptoms and features of asthma and COPD [119]. In COPD, FeNO values have not yet been studied as thoroughly as in asthma. Smokers and ex-smokers have generally lower FeNO values than non-smoker. In the case of COPD, this leads to a more problematic interpretation of the patients' FeNO values. They have not been found to correlate with the GOLD (Global Initiative for Chronic Obstructive Lung Disease) stages of COPD, although they increase during

exacerbations [8, 123]. Treatment with ICS and active smoking decrease the NO-concentrations inside the alveolar walls. This is believed to be an additional reason for the large variabilities of FeNO values in different patients with COPD. For the follow-up of individual COPD patients FeNO measurement could be beneficial, since increasing values could be an early prediction of exacerbations. However, for patients with persisting airway obstructions it can be difficult to generate the FeNO specific exhalation flow of 50 ml/s [8].

6.4 FeNO Summary

FeNO has become an exhaled biomarker parameter that has been established in clinical routine use [8]. FeNO appears to be more sensitive in identifying airway inflammation in asthma [7] and has thus been established as a suitable tool to monitor the progress of eosinophilic asthma and to assess adherence to medication. First guidelines on FeNO measurements were published by the ATS in 1999 and updated in 2005 in collaboration with the ERS [8]. Key advantages compared to a standard spirometry measurement are that FeNO measurement does not require forced expiratory manoeuvres, leading to a high patient acceptance. Single measurements can be performed at moderate costs [121]. Although $FeNO_{50}$ is the established standard parameter for a FeNO measurement, an extended analysis can include the measurement of FeNO levels at multiple expiratory flows [8].

FeNO values must always be interpreted in their clinical context [119]. Relevant reference values for FeNO cannot be given. Instead, the concept of limit values is followed. Individuals that regularly perform FeNO measurements can use their personal baseline and best values to monitor changes and trends for comparison and assessment [8, 119]. For the assessment of COPD and cystic fibrosis, FeNO values are only of limited use [8]. Because of the wide range of physiological mechanisms, that affect the NO parameter, it cannot be recommended to use the exhaled NO concentration alone to make a diagnosis. However, it can be a beneficial additional parameter to support diagnoses originating from other measurements and the patient's history [8].

7 Summary and Outlook

Modern methods of pulmonary function diagnosis include spirometry, body plethysmography and a variety of other common tests used to assess a patient's respiratory status. These include determination of occlusion pressure, forced oscillation techniques and cardiopulmonary exercise testing. The analysis of flow, volume, pressure and their relationships to each other provide information about the ventilation of the lungs. Diffusion measurement techniques assess the distribution of the gas in the lungs and provide information about the diffusion capacity. Besides, variants

of invasive and non-invasive blood gas analysis are available to determine the oxygen uptake and the metabolic situation of the organism. Supplementary, analysis of expiratory carbon dioxide in the form of capnometry or capnovolumetry can be used for the determination of the carbon dioxide partial pressure. Furthermore, the measurement of the fraction of exhaled nitrogen oxide has proven to be an additional means of supporting the diagnostic process. All pulmonary function tests suffer to a greater or lesser extent from limitations in terms of their diagnostic value. They are generally more accurate in healthy people than in patients with lung diseases [53]. It is often the combination of different measurement approaches, paying respect to the patients' medical history and possible apparent symptoms that lead to a reliable diagnosis.

For an enhanced understanding of respiratory physiology laboratory and clinical research should be pursued and encouraged. A strong collaboration between researchers and clinicians is inevitable to ensure the development of suitable standards and guidelines for better comparability of clinical results and to assure full and equitable patient treatment. Evidence for routine clinical use must be established for newly developed measurement techniques to realize their full potential. The determination of volatile organic compounds is a promising and beneficial addition to classical lung function diagnostics to optimize patient care. Typical breathing profiles can indicate certain diseases. Non-invasive measurement of exhaled compounds is ideal for serial monitoring of patients without much patient burden. In this context, the combination of information from modern lung function diagnostics and breath analysis of volatile organic compounds can make a valuable contribution to healthcare. However, a challenging mission remains in the detection of the small trace amounts in the expired air. A lot of research is currently performed in this area and it shows potential to become a cornerstone of personalized medicine in the future. It remains to be seen what benefits volatile organic compound analysis will add to the field of respiratory diagnostics to optimize patient care in clinical settings as well as at home.

References

1. Teschler H et al (2010) Die Lage der Pneumologie in Deutschland: Status quo und Blick in die Zukunft*", Georg Thieme Verlag KG Stuttgart
2. van de Hei S et al (2020) Quality of spirometry and related diagnosis in primary care with a focus on clinical use. Prim Care Respir Med 30(22)
3. Steppuhn H et al (2017) 12-Monats-Prävalenz der bekannten chronisch obstruktiven Lungenerkrankung (COPD) in Deutschland. J Health Monit 2(3)
4. Gupta Y et al (2020) Body plethysmography in chronic obstructive pulmonary disease patients: a cross-sectional study. Lung India 5:127–131
5. Celli B et al (2004) Standards for the diagnosis and treatment of patients with COPD: a summary of the ATS/ERS position paper. Eur Respir J 23(6):932–946
6. Steppuhn H et al (2017) 12-Monats-Prävalenz von Asthma bronchiale bei Erwachsenen in Deutschland. Journal of Health Monitoring 2(3)

7. Kouri A et al (2021) Exploring the 175-year history of spirometry and the vital lessons it can teach us today. Eur Respir Rev 30(162)
8. Beauchamp J et al (2020) Breathborn biomarkers and the human volatilome. Elsevier
9. Quanjer P et al (2012) Multi-ethnic reference values for spirometry for the 3–95 year age range: the GLOBAL lung function 2012 equations. Eur Respir J 40(6):1324–1343
10. Lundberg B et al (2020) Agreement between spirometry and impulse oscillometry for lung function assessment in 6-year-old children born extremely preterm and at term. Pediatr Pulmonol 55:2745–2753
11. Melo S et al (2018) Evaluating the extremely elderly at a pulmonary function clinic for the diagnosis of respiratory disease: frequency and technical quality of spirometry. J Bras Pneumol 45(4)
12. Fragoso C et al (2020) Diffusing capacity in normal-for-age spirometry and spirometric impairments, using reference equations from the global lung function initiative. Respir Med 170
13. Faller A, Schünke M (2012) Der Körper des Menschen. Georg Thieme Verlag KG
14. Silbernagl S, Despopoulos A (2012) Taschenatlas Physiologie Georg Thieme Verlag KG
15. Parazzi P et al (2019) Correlation between parameters of volumetric capnography and spirometry during a submaximal exercise protocol on a treadmill in patients with cystic fibrosis and healthy controls. Pulmonology 25(1):21–31
16. Sylvester KP et al (2020) ARTP statement on pulmonary function testing 2020. BMJ Open Respir Res 7
17. Graham B et al (2019) Standardization of spirometry 2019 update: an Official American Thoracic Society and European Respiratory Society Technical Statement. Am J Respir Crit Care Med 200(8)
18. Cottee AM et al (2020) Bronchodilator response assessed by the forced oscillation technique identifies poor asthma control with greater sensitivity than spirometry. Chest J 157(6): 1435–1441
19. Lo D et al (2020) Spirometry and FeNO testing for asthma in children in UK primary care: a prospective observational cohort study of feasibility and acceptability. Br J Gen Pract 70:809–816
20. Noth I et al (2021) Home spirometry in patients with idiopathic pulmonary fibrosis: data from the INMARK trial. Eur Respir J 58
21. Dal Negro R et al (2021) Comparison of consistency, feasibility, and convenience of a novel compact system for assessing lung volumes and carbon monoxide diffusing capacity versus whole body plethysmography. Clinico Econ Outcomes Res 13:637–643
22. Newth C et al (1997) Multiple-breath nitrogen washout techniques: including measurements with patients on ventilators. Eur Respir J 10:2174–2185
23. Ulmer W et al (1986) Die Lungenfunktion, Georg Thieme Verlag KG Stuttgart
24. Bösch D, Criée C (2009) Lungenfunktionsprüfung Springer Medizin Verlag
25. Stucky F et al (2020) Automating the correction of flow integration drift during whole-body plethysmography, Annual international conference of the IEEE Engineering in Medicine & Biology Society, Montréal
26. Dreher M et al (2019) Whole-body plethysmography and blood gas analysis in patients with acute myocardial infarction undergoing percutaneous coronary intervention. Respiration 97: 24–33
27. Korten I et al (2019) Asthma control in children: body plethysmography in addition to spirometry. Pediatr Pulmonol 54(8):1141–1148
28. Sunshine MD, Fuller DD (2021) Automated classification of whole body plethysmography waveforms to quantify breathing patterns. Front Physiol 12
29. Sassoon C, Younes M (2020) Airway occlusion pressure revisited. Am J Respir Crit Care Med 201(9):1027–1028
30. Pinto S et al (2021) Mouth occlusion pressure at 100ms (P0.1) as a respiratory biomarker in amyotrophic lateral sclerosis. Amyotroph Lateral Scler Front Degener 22

31. Soares M et al (2019) Comparison of forced and impulse oscillometry measurements: a clinical population and printed airway model study. Sci Rep 19
32. Wu J et al (2020) Development of quality assurance and quality control guidelines for respiratory oscillometry in clinic studies. Respir Care 65(11)
33. Goldman M (2001) Clinical application of forced oscillation. Pulm Pharmacol Ther 14:341–350
34. King GG et al (2020) Technical standards for respiratory oscillometry. Eur Respir J 55:1900753
35. D'Ascanio M et al (2020) Assessing static lung hyperinflation by whole-body plethysmography, helium dilution, and impulse oscillometry system (IOS) in patients with COPD. Int J Chron Obstruct Pulmon Dis 15:2583–2589
36. Frantz S et al (2012) Impulse oscillometry may be of value in detecting early manifestations of COPD. Respir Med 106:1116–1123
37. Milne S et al (2019) Respiratory system reactance reflects communicating lung volume in chronic obstructive pulmonary disease. J Appl Physiol 126:1223–1231
38. Malmberg L et al (2002) Determinants of respiratory system input impedance and bronchodilator response in healthy Finnish preschool children. Clin Physiol Funct Imaging 22(1): 64–71
39. Cho E et al (2020) Airway oscillometry detects spirometric-silent episodes of acute cellular rejection. Am J Respir Crit Care Med 201(12):1536–1544
40. Antoniewicz L et al (2019) Acute effects of electronic cigarette inhalation on the vasculature and the conducting airways. Cardiovasc Toxicol 19:441–450
41. Olsson K et al (1999) Changes in airway dead space in response to methacholine provocation in normal subjects. Clin Physiol 19:426–432
42. X. Sun et al., "Comparison of capnovolumetry-derived dead space with pulmonary function test in normal adults using histamine provocation.," The Clinical Respiratory Journal, 2014
43. Lundblad L et al (2019) Applications of oscillometry in clinical research and practice. Can J Respir Crit Care Sleep Med 5(1):54–68
44. Seccombe L et al (2019) Exercise-induced bronchoconstriction identified using the forced oscillation technique. Front Physiol 10
45. Dandurand R et al (2019) Comparison of oscillometry devices using active mechanical test loads. ERJ Open Res 5
46. Dumitrescu D, Rosenkranz S (2017) Graphical data display for clinical cardiopulmonary exercise testing. Ann Am Thorac Soc 14(supplement 1):S12–S21
47. Wonisch M et al (2003) Spiroergometrie in der Kardiologie – Klinische Anwendungsmöglichkeiten. Aust J Cardiol 10(10):440–446
48. Löllgen H, Erdmann E (2001) Ergometrie. Springer
49. Stavrou V et al (2018) Brief review: ergospirometry in patients with obstructive sleep apnea syndrome. J Clin Med 7
50. Kindermann W (2004) Anaerobe Schwelle. Deutsche Zeitschrift für Sportmedizin 55(6): 161–162
51. Kroidl R et al (2007) Kursbuch Spiroergometrie. Georg Thieme Verlag KG
52. Lie A et al (2021) Breathing patterns in people with exercise-induced laryngeal obstruction. Physiol Rep 9
53. Graham B et al (2017) 2017 ERS/ATS standards for single-breath carbon monoxide uptake in the lung. Eur Respir J 49
54. Méndez R, Menéndez R (2021) Reduced diffusion capacity in COVID-19 survivors. Ann Am Thorac Soc 18(7)
55. Radtke T et al (2021) Lung diffusing capacity for nitric oxide measured by two commercial devices: a randomised crossover comparison in healthy adults. Eur Respir J Open Res 7
56. Bullock J et al (2001) Physiology Band 578. Lippincott Williams & Wilkins

57. de la Grandville B et al (2019) High inspired oxygen fraction impairs lung volume and ventilation heterogeneity in healthy children: a double-blind randomised controlled trial. Br J Anaesth 122(5):682–691

58. Hardaker K et al (2019) Abnormal preschool lung clearance index (LCI) reflects clinical status and predicts lower spirometry later in childhood in cystic fibrosis. J Cyst Fibros 18:721–727

59. Stahl M et al (2018) Three-center feasibility of lung clearance index in infants and preschool children with cystic fibrosis and other lung diseases. J Cyst Fibros 17:249–255

60. Arigliani M et al (2022) Lung clearance index may detect early peripheral lung disease in sickle cell Anemia. Ann Am Thorac Soc

61. Betz S et al (2017) D – Point of Care – Die präklinische Blutgasanalyse als diagnostisches Tool. Notfall+Rettungsmedizin 20(2):132–140

62. van der Weerd B et al (2016) Trends in electrochemical sensing of blood gases. Springer

63. Gebert G (1987) Physiologie als Grundlage der klinischen Medizin. Schattauer

64. Schöller B (2000) Pulsoximetrie-Fibel. MCC GmbH

65. Madan A (2017) Correlation between the levels of SpO2 and PaO2. Lung India 34:307–308

66. Sarkar M et al (2017) Mechanisms of hypoxemia. Lung India 34:47–60

67. van Wijk J et al (2022) Validation of a new combined transcutaneous tcPCO2 and tcPO2 sensor in children in the operating theatre. Pediatr Anesth 32:429–435

68. Dar K et al (1995) Arterial versus capillary sampling for analysing blood gas pressures. Br Med J 310:24–25

69. Rosier S et al (2014) The accuracy of transcutaneous PCO2 in subjects with severe brain injury: a comparison with end-tidal PCO2. Respir Care 59(8):1242–1247

70. Kann J et al (1967) Das Verhalten der arteriellen Blutgase in verschiedenen Höhen über dem Meeresspiegel und ihre Bedeutung für arbeitsmedizinische Untersuchungen. Int Arch Gewerbepathol Gewerbehyg 23(3):270–280

71. Hertz C, Schumann K (1970) Tagesschwankungen der arteriellen Blutgase. Klin Wochenschr 48(7):399–401

72. Loew P, Thews G (1962) Die Altersabhängigkeit des arteriellen Sauerstoffdruckes bei der berufstätigen Bevölkerung. Klin Wochenschr 40(21):1093–1098

73. Ulmer W, Reichel G (1963) Untersuchungen über die Altersabhängigkeit der alveolären und arteriellen Sauerstoff-und Kohlensäuredrucke. Klin Wochenschr 41(1):1–6

74. Fabel H, Hamm J (1967) Atemmechanik und arterielle Blutgase bei Fettsucht. Beitr Klin Erforsch Tuberk Lungenkr 135(3):298–309

75. Calvo A et al (2021) The role of arterial blood gas analysis (ABG) in Amyotrophic Lateral Sclerosis respiratory monitoring. Neurology 96(15 supplement):4109

76. Elezagic D et al (2020) Venous blood gas analysis in patients with COVID-19 symptoms in the early assessment of virus positivity. J Lab Med 45(1):27–30

77. Bezuidenhout M et al (2021) Correlating arterial blood gas, acid–base and blood pressure abnormalities with outcomes in COVID-19 intensive care patients. Ann Clin Biochem 58(2): 95–101

78. Janssens J et al (2004) Non-invasive (transcutaneous) monitoring of PCO2 (TcPCO2) in older adults. Gerontology 51(3):174–178

79. Severinghaus J, Bradley A (1958) Electrodes for blood pO2 and pCO2 determination. J Appl Physiol 13:515–520

80. Kelly A, Klim S (2011) Agreement between arterial and transcutaneous PCO2 in patients undergoing non-invasive ventilation. Respir Med 105(2):226–229

81. Bertram L et al (2012) Transkutane Kohlenstoffdioxidmessung. Anaesthesist 61(12): 1027–1035

82. Galetin T et al (2021) Hypercapnia in COPD patients undergoing endobronchial ultrasound under local anaesthesia and analgosedation: a prospective controlled study using continuous transcutaneous capnometry. Respiration 100:958–968

83. Saruhan R et al (2021) Comparison of transcutaneous and arterial blood gas analyses in patients with sepsis and septic shock. Turk J Intensive Care 19:111–117

84. Weinmann K et al (2021) Continuous transcutaneous carbon-dioxide monitoring to avoid hypercapnia in complex catheter ablations under conscious sedation. Int J Cardiol 325:69–75

85. Ludwig M et al (2010) Gefäßmedizin in Klinik und Praxis. Georg Thieme Verlag KG

86. Sjoding M et al (2020) Racial bias in pulse oximetry measurement. N Engl J Med 383(25)

87. Dünnwald T et al (2021) The use of pulse oximetry in the assessment of acclimatization to high altitude. Sensors 21

88. Teo J (2020) Early detection of silent hypoxia in Covid-19 pneumonia using smartphone pulse oximetry. J Med Syst 44

89. Luks A, Swenson E (2020) Pulse oximetry for monitoring patients with COVID-19 at home. Ann Am Thorac Soc 17(9):1040–1046

90. Williams E et al (2021) End-tidal capnography monitoring in infants ventilated on the neonatal intensive care unit. J Perinatol 41:1718–1724

91. Reißig S (2007) Validierung der volumetrischen Kapnographie zur Erfassung klinisch inapparenter Lungenfunktionsstörungen beim Kalb. PhD thesis, Freie Universität Berlin

92. Kroegel C, Costabel U (Hrsgg) (2014) Klinische Pneumologie Georg Thieme Verlag KG

93. Potwin J et al (2021) Effects of capnometry monitoring during recovery in the post-anaesthesia care unit: a randomized controlled trial in adults. J Clin Monit Comput

94. D'Mello J, Butani M (2002) Capnography. Indian J Anaesth 46:269–278

95. Verscheure S et al (2016) Volumetric capnography: lessons from the past and current clinical applications. Crit Care 20(184)

96. Muysers K et al (1962) Formanalysen von exspiratorischen Sauerstoff- und Kohlensäuredruckkurven. Klin Wochenschr 40(6):281–285

97. Fowler WS (1949) Lung function studies. III. Uneven pulmonary ventilation in Normal subjects and in patients with pulmonary disease. J Appl Physiol 2:283–289

98. Smidt U, Worth H (1981) Gas mixing in patients. Prog Respir Res 16:86–92

99. Durben G (1986) Zur Prüfung der Abhängigkeit der Form exspiratorischer CO2-Partialdruckkurven vom Grad der Atemwegsobstruktion. PhD thesis, Rheinische Friedrich-Wilhelm-Universität Bonn

100. You B et al (1994) Expiratory capnography in asthma. Eur Respir J 7:318–323

101. Kars AH et al (1997) Dead space and slope indices from the expiratory carbon dioxide tension-volume curve. Eur Respir J 10:1829–1836

102. Krauss B et al (2005) Capnogram shape in obstructive lung disease. Anesth Analg

103. Kroidl R et al (2010) Kursbuch Spiroergometrie. Georg Thieme Verlag KG

104. Trenz C (2007) Klinische Evaluierung der Validität des nichtinvasiven Kapnometrie-Systems Microcap Plus R. PhD thesis, Universitätsklinikum Ulm

105. Sandroni C et al (2018) Capnography during cardiac arrest. Resuscitation 132:73–77

106. Leonova I et al (2021) The biofeedback training, controlled by capnometry is a successful method of rehabilitation after myocardial infarction. Eur Heart J Acute Cardiovasc Care 10

107. Ostacher M et al (2021) Investigation of a capnometry guided respiratory intervention in the treatment of posttraumatic stress disorder. Appl Psychophysiol Biofeedback 46:367–376

108. Ponto S et al (2016) Capnovolumetry as a cooperation free method in the diagnosis and monitoring of COPD. ERS Annual Congress, London

109. Jarenbäck L et al (2018) The efficiency index (EFFi), based on volumetric capnography, may allow for simple diagnosis and grading of COPD. Int J COPD 13:2033–2039

110. Kars AH (1995) Clinical application of capnography in chronic obstructive pulmonary disease. PhD thesis, Erasmus Universität Rotterdam

111. Klütsch K et al (2019) Wertigkeit der Ultraschall-Kapnovolumetrie in der Differentialdiagnose von obstruktiven Atemwegserkrankungen in der klinischen Praxis, DGP Annual Congress, Munich

112. Hoeser C (2007) Zum Einfluss akuter und chronischer bronchopulmonaler Veränderungen auf die Kapnovolumetrie. PhD thesis, Justus-Liebig-Universität Gießen

113. Steiß JO et al (2008) Capnovolumetry: a new tool for lung function testing in children with asthma. Clin Physiol Funct Imaging 28(5):332–336

114. Qi G et al (2014) The ability of volumetric capnography to distinguish between chronic obstructive pulmonary disease patients and normal subjects. Lung 192:661–668
115. Kellerer C et al (2020) Capnovolumetry in combination with clinical history for the diagnosis of asthma and COPD. Prim Care Respir Med 30(32)
116. Kellerer C et al (2019) Diagnostic accuracy of capnovolumetry for the identification of airway obstruction – results of a diagnostic study in ambulatory care. Respir Res 20(92)
117. Herholz C et al (2001) Statistical shape analysis of volumetric capnograms: evaluation of a new approach for the assessment of pulmonary function in horses with chronic obstructive pulmonary disease. J Veterinary Med Ser A 48:75–84
118. Tolnai J et al (2018) Assessment of shape factors and dead space indices by volumetric capnography in rats. Eur Respir J 52
119. Dweik R et al (2011) An official ATS clinical practice guideline: interpretation of exhaled nitric oxide levels (FENO) for clinical applications. Am J Respir Crit Care Med 184:602–615
120. Korn S et al (2020) Measurement of fractional exhaled nitric oxide: comparison of three different analysers. Respiration 99(1)
121. Khatri S et al (2021) Use of fractional exhaled nitric oxide to guide the treatment of asthma. Am J Respir Crit Care Med 204(10):e97–e109
122. Horváth I et al (2017) A European Respiratory Society technical standard: exhaled biomarkers in lung disease. Eur Respir J 49
123. Silkoff PE et al (2005) ATS/ERS recommendations for standardized procedures for the online and offline measurement of exhaled lower respiratory nitric oxide and nasal nitric oxide, 2005. Am J Respir Crit Care Med 171
124. Dick A et al (2018) Cost analysis of FeNO for asthma diagnosis in primary care in Germany. ERS Annual Congress, Paris
125. Wiener et al (2019) Cost analysis of FeNO-based asthma management in primary care in Germany, ERS Annual Congress, Madrid